



École des Ponts  
ParisTech

UNIVERSITÉ —  
— PARIS-EST



Lebanese University  
Faculty of Engineering III

Dissertation presented for the degree of  
**Doctor from Université Paris-Est**

*Field: Geotechnical Engineering*

by

**Layal JRADI**

Doctoral School: Sciences, Ingénierie et Environnement (SIE)

---

***Study of the influence of fine particles on the properties of  
liquefaction of sands***

---

*Draft Thesis*

JURY

M. Pierre BREUL	Referee	Université de Clermont Auvergne
M. Daniel LEVACHER	Referee	Université de Caen
M. Pierre-Yves HICHER	Examiner	Ecole Centrale de Nantes
M. Jean CANOU	Examiner	Ecole des Ponts ParisTech
M. Bassel SEIF EL DINE	Examiner	Lebanese University
M. Jean-Claude DUPLA	PhD Supervisor	Ecole des Ponts ParisTech

## Abstract

---

### Abstract

Since the last 50 years, the study of the phenomenon of liquefaction of saturated sandy soils has been a topic of extensive laboratory research. Most of the earlier research has focused on the liquefaction of clean sands assuming that the presence of fines resists the development of excess pore water pressure as well as the risk of liquefaction. However, natural sand is found in nature under the form of a mixture of sand and fines and, the influence of these fines on the liquefaction risk of this type of material is still unclear. In fact, we could find contradictory results in the literature review of the effect of fine particles on the sand liquefaction phenomenon.

In this context, the main objective of this study is to clarify and quantify the influence of fine particles (plastic and non-plastic) present in a sandy matrix on the initiation and development of the liquefaction phenomenon. We've focused, in particular, on the nature of fine particles (plastic/non-plastic), their proportion in the matrix, the matrix compactness condition and initial stress state (state consolidation). For this purpose, with the aid of a new triaxial servo-hydraulic device, a series of monotonic and cyclic tests were done in order to clarify this effect. Experimental results show that the increase in non-plastic fines increases the resistance to liquefaction of the mixture under both monotonic and cyclic loading. However, this trend is reversed for the mixtures containing plastic fines. Finally a comparison has been established between the behavior of these soils under undrained monotonic and cyclic shearing in terms of evaluation of the initiation of instability phenomenon and other mechanical parameters.

### Résumé

Au cours des 50 dernières années, l'étude du phénomène de liquéfaction de sols sableux saturés a fait l'objet de nombreuses recherches en laboratoire. La plupart de ces recherches antérieures se sont concentrées sur la liquéfaction de sables propres, en supposant que la présence de fines limite le développement de la surpression interstitielle et donc le risque de liquéfaction. Cependant, les sables naturels se trouvent généralement dans la nature sous la forme d'un mélange de sable et de fines et l'influence de ces fines sur le risque de liquéfaction de ce type de matériau n'est toujours pas claire. En effet, on trouve des résultats contradictoires, dans la littérature, sur l'effet des particules fines sur le phénomène de liquéfaction des sables.

## Abstract

---

Dans ce contexte, l'objectif principal de ce travail expérimental est de clarifier et de quantifier l'influence des particules fines présentes au sein d'une matrice sableuse sur l'initiation et le développement du phénomène de liquéfaction. On s'est intéressé, en particulier, à la nature des particules fines (plastique/non-plastique), à leur proportion au sein de la matrice, à l'état de compacité de la matrice et à l'état de contrainte initial (état de consolidation). A cet effet, à l'aide d'un nouveau dispositif triaxial servo-hydraulique, une série d'essais monotones et cycliques ont été effectués afin de clarifier cet effet. Les résultats expérimentaux montrent que l'augmentation de la proportion de fines non plastiques augmente la résistance à la liquéfaction du mélange sous chargements monotone et cyclique. Par contre, cette tendance est inversée pour les mélanges qui contiennent des fines plastiques. Enfin, une comparaison a été établie entre le comportement de ces sols sous cisaillement monotone et cyclique non drainé en termes d'évaluation du déclenchement du phénomène d'instabilité et d'autres paramètres mécaniques.

**NOTATIONS**

$e$	Void ratio	-
$e^g$	Intergranular void ratio	-
$e^{eq}$	Equivalent void ratio	-
$e^f$	Interfine void ratio	-
$I_D$	Density index	-
$I_{Dmat}$	Density index of sand matrix	-
$D_r$	Relative density	-
$D_r^s$	Specific relative density	-
$\Psi$	State parameter	-
$\Psi_0$	Initial state parameter	-
$Q$	Deviator stress	kPa
$q_{inst}$	Deviator stress at initiation of instability	kPa
$p'$	Mean effective stress	kPa
$H$	Stress ratio	-
$\eta_{inst}$	Stress ratio at initiation of instability	-
$\Phi$	Friction angle	°
$\varphi_{inst}$	Instability friction angle	°
$\Phi_{max}$	Maximum friction angle	°
$\Phi_{car}$	Characteristic friction angle	°
$Fc$	Fines content	%
$Fc_{th}$	Threshold fines content	%
$fc$	$Fc/100$	-

## Notations

---

$f_{c_{th}}$	F <sub>c<sub>th</sub></sub> /100	-
$\Delta u$	Excess pore water pressure	kPa
$\varepsilon_a$	Axial deformation	%
$\varepsilon_v$	Volumetric deformation	%
$e_{max}$	Maximum void ratio	-
$e_{min}$	Minimum void ratio	-
$C_u$	Coefficient of uniformity	-
$C_c$	Coefficient of curvature	-
$\rho_s$	Density	g/cm <sup>3</sup>
$b$	Ratio of active fines	-
$V_v$	Volume of voids	-
$V_s$	Volume of solid grains	-

## Table of content

General introduction .....	1
1 Chapter I: Literature review .....	4
1.1 History of liquefaction .....	4
1.2 General overview on the mechanical behavior of sands .....	6
1.2.1 Terminology and definitions .....	6
1.2.2 Localized and Diffused Instabilities.....	10
1.3 Identification of liquefaction phenomenon in the laboratory .....	11
1.3.1 General overview on the behavior of sand under undrained triaxial test .....	11
1.3.2 Chinese criteria for the identification of liquefaction.....	13
1.3.3 Initiation of Instability.....	15
1.4 Specimen preparation methods and their effects on soil behavior .....	17
1.4.1 Overview of specimen preparation methods for sandy soils.....	17
1.4.2 Effect of reconstitution methods on the mechanical behavior of material .....	23
1.4.3 Effect of reconstitution method on the material structure .....	25
1.5 Influence of fines on the behavior of silty sands .....	26
1.5.1 Definitions and influence of different parameters.....	27
1.5.2 Influence of the non-plastic fines content on the initiation of instability .....	33
1.5.3 Influence of the non-plastic fines content on the critical state .....	47
1.5.4 Influence of plastic fines .....	51
1.6 Conclusions on literature review .....	53
2 Chapter II: Materials, experimental protocols and testing setup .....	54
2.1 Characterization of the materials studied.....	54
2.2 Fontainebleau sand .....	54
2.2.1 Silica C500.....	55
2.2.2 Kaolinite Speswhite.....	56

## Table of content

---

2.3	Triaxial testing .....	57
2.3.1	Triaxial device $\Phi$ 100 mm.....	58
2.3.2	Calibration of the cell .....	61
2.4	Homogeneity of mixtures .....	69
2.4.1	Laser granulometry.....	69
2.4.2	Particle size distribution of mixtures .....	70
2.5	Experimental procedure .....	80
2.5.1	Preparation of specimens .....	80
2.5.2	System preparation .....	81
2.5.3	Saturation.....	87
2.5.4	Consolidation.....	88
2.5.5	Shearing.....	89
2.5.6	Measurements and acquisition of data .....	89
2.6	Conclusion .....	89
3	Chapter III: Undrained behavior of sand containing fines under monotonic shear .....	90
3.1	Experimental program .....	90
3.2	Typical results .....	92
3.2.1	Clean sand .....	92
3.2.2	Sand-C500 mixture.....	92
3.2.3	Sand-Speswhite mixture .....	95
3.3	Repeatability .....	95
3.4	Influence of the density index of sand matrix $I_{Dmat}$ .....	98
3.4.1	Sand and non- plastic fines .....	98
3.4.2	Sand and plastic fines .....	100
3.5	Influence of the consolidation stress.....	104
3.5.1	Sand and non-plastic fines.....	104

## Table of content

---

3.5.2	Sand and plastic fines .....	105
3.6	Influence of fines content .....	109
3.6.1	Sand and non-plastic fines.....	109
3.6.2	Sand and plastic fines .....	110
3.6.3	Synthesis of results .....	112
3.7	Influence of type of fines .....	117
3.8	Evaluation of different mechanical parameters .....	120
3.8.1	Maximum friction angle $\Phi'_{\max}$ .....	120
3.8.2	Characteristic angle $\Phi'_{car}$ .....	122
3.9	Analysis of the conditions of initiation of instability .....	123
3.10	Interpretation and discussion of results .....	129
3.11	Evaluation of the liquefaction resistance in terms of other parameters .....	131
3.11.1	Evaluation in terms of intergranular void ratio .....	131
3.11.2	Evaluation in terms of equivalent void ratio .....	134
3.11.3	Estimation of critical fines content based on Westman and Hugill diagram ...	134
4	Chapter IV: Undrained behavior of sand containing fines under cyclic shear.....	139
4.1	Experimental program .....	139
4.2	Typical results .....	141
4.2.1	Clean sand .....	141
4.2.2	Sand-fines mixtures .....	149
4.3	Repeatability test.....	155
4.4	Influence of significant parameters on the behavior of sand-fines mixtures under cyclic loading .....	159
4.4.1	Matrix density index.....	159
4.4.2	Influence of cyclic stress ratio.....	161
4.4.3	Influence of fines content .....	165

## Table of content

---

4.5 Cyclic shear resistance curves .....	167
4.5.1 Case of loose states.....	168
4.5.2 Case of dense states .....	170
4.6 Proposition of a model for predicting the cyclic shear resistance curve based on the fines content .....	176
4.7 Synthesis of behaviors observed under undrained monotonic and cyclic loading (Comparison between monotonic and cyclic behaviors of mixtures) .....	181
4.7.1 Total liquefaction phenomena (case of loose materials).....	181
4.7.2 Cyclic mobility phenomenon (case of dilating mixtures) .....	188
General conclusions and perspectives .....	192
References .....	194
List of figures .....	202
List of tables .....	211



## General introduction

The geotechnical literature describes a very large amount of damages associated with particular and often spectacular ground failures, in which the soil appears to suddenly loose a large part of its shear strength and temporarily flows in a liquid-like manner until re-stabilization of the material in a configuration very different from the initial configuration. These soil failures correspond to a phenomenon known by the generic name of "liquefaction" and are generally observed in the case of saturated sands subjected to rapid, monotonous or cyclic stresses, such as earthquakes, tidal waves, shocks or explosions...

Since the earthquakes of Niigata in Japan and Alaska in the United States in 1964, important research has been initiated and developed on the study of liquefaction phenomena in an attempt to evaluate the susceptibility to liquefaction of saturated sandy sites subjected to earthquakes. Indeed, this subject has been the object of extensive experimental research where most of the earlier research has focused on the liquefaction of clean sands assuming that the presence of fines resists the development of excess pore water pressure as well as the risk of liquefaction. However, as natural sand is frequently found in nature under the form of a mixture of sand and fine particles and based on case histories of actual soils behavior during earthquakes, it has been reported that sands containing fines have shown to liquefy Chang (1982), Koester (1994)... therefore, the presence of silt and clay will in some manner affect the resistance of sand to liquefaction. Unfortunately the influence of these fines on the liquefaction risk of this type of material is still unclear. In fact, we could find contradictory results in the literature review concerning the effect of fine particles on the liquefaction properties of sands.

Researchers have studied the effect of fines on the liquefaction resistance of sands for high values of fines content ranging between 10% and 100%. It is interesting to note that, based on field studies following major earthquakes and the case histories of actual soil behavior during earthquakes, there are some evidence that soils with greater fines content are less likely to liquefy. Okashi (1970) has realized during the 1964 Niigata earthquake that soils with fines content less than 10% are more likely to liquefy. Also, Tokimatsu and Yoshimi (1983) declared in a study of 17 worldwide earthquakes that 50% of liquefied soils had fines content less than 5%. Therefore, it would be very interesting to test soils behavior at very low fines content (below 5%).

In this context, the main objective of this thesis is to clarify and quantify the influence of fine particles (less than 5%) present in a sandy matrix on the initiation and development of the liquefaction phenomenon in order to improve the knowledge of these specific unstable behaviors that are very sensitive to the influence of several parameters and eventually to contribute to the improvement of the methods of evaluation of liquefaction risk of sands containing fines under rapid monotonic and cyclic loading. In order to achieve this objective, an experimental approach has been adopted, with the aid of a new servo-hydraulic triaxial setup we have focused on the study of the influence of the nature of fine particles (plastic/non-plastic), their proportion in the matrix, the matrix compactness condition and initial stress state (state consolidation).

First of all, the behavior under undrained monotonic loading of a reference sand (Fontainebleau sand) and mixtures of Fontainebleau sand and two types of fines (plastic and non-plastic) has been studied. In particular, monotonic loadings have been used for the initiation of instabilities as well as for the ultimate states reached in large deformation, by highlighting the influence of various significant parameters on observed behaviors, in particular the influence of fines content. Then, based on this "framework" of monotonic behavior, we have studied the response of these materials under cyclic shear, trying, as far as possible, to highlight the analogies existing between monotonic and cyclic behavior.

This thesis is composed of four chapters, briefly described as follows:

The first chapter presents a review of the literature on liquefaction phenomenon, in particular the influence of fine particles on the mechanical response of sands. This review has revealed that the presence of fines will in some manner affect the resistance of sand to liquefaction, however, the published studies show no clear conclusion as to in what manner the presence of these fines affect the sands resistance. This is particularly true for the soils containing non-plastic fines. This overview of the literature has helped us to set our objectives and consequently to choose the parameters of our work. Indeed, as we have seen in the literature of this subject that the actual soils that have liquefied during the earthquakes throughout the history contained less than 5% fines, we focused in our study on clarifying the influence of low contents of fine particles ( $Fc \leq 5\%$ ).

The second chapter presents the materials used for this study, as well as the experimental device (Triaxial testing) and the experimental protocol used in our study. In fact, based on the

## General introduction

---

conclusions of the literature review, we have traced our study path and set up our objectives. Therefore, an experimental program has been defined, allowing to focus, in particular, on the nature of fine particles (plastic/non-plastic), their proportion in the matrix, the matrix compactness condition and initial stress state (state consolidation).

The third chapter presents and analyzes the behaviors of sand containing fines observed in the triaxial apparatus under undrained monotonic loading with emphasis on the conditions of the initiation of liquefaction instability. This chapter also presents the influence of fundamental parameters on the mechanical response of sand-fines mixtures.

The fourth chapter presents the results of the undrained cyclic shearing and also focuses on the conditions of initiation of instability. According to the results presented in the two previous chapters, a synthesis of the undrained behaviors under monotonic and cyclic loading is presented emphasizing the analogies between these two types of solicitations.

# 1 Chapter I: Literature review

## 1.1 History of liquefaction

Derived from the Latin verb “liquefacere” which means to dissolve or to weaken, liquefaction is the term used in order to describe the phenomenon of liquefaction that occurs when the shear resistance of soils decreases in response to a monotonic (rapid sediment accumulation, erosion at the toe of a slope...), dynamic (blast, vibration) or cyclic (earthquake, tidal waves) loading at constant volume.

Liquefaction of soils is a phenomenon whereby a saturated or partially saturated soil loses its strength in response to an applied shear stress, usually an earthquake causing it to behave like a liquid.

The phenomenon of liquefaction of sands due to earthquakes has been recorded throughout the history. However it wasn't studied by scientists until the early 1960's. The study on liquefaction of sands started greatly after the Niigata earthquake and the Alaska earthquake of 1964 which caused dramatic damages due to liquefaction. During the Niigata earthquake in Japan 1964, the damages caused by liquefaction were very important (Seed *et al.*, 1967). Approximately 310 buildings constructed of reinforced concrete were damaged, of which 200 were tilted. It should be noted that the soil on which the city rests consists of recent sedimentary deposits, of low relative density, with a shallow water table. Damaged buildings were built on shallow foundations or piles and on a very loose soil layers.

The Alaskan earthquake in 1964 with a magnitude of 8.6, presented huge landslides that took away 9.6 million m<sup>3</sup> of soil where the surface of the ground was completely devastated by displacements.

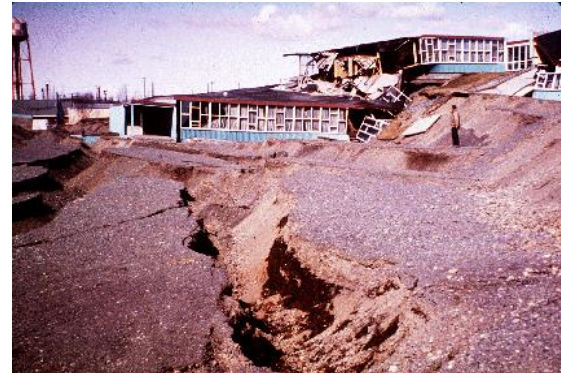
Liquefaction was also a major factor in the destruction in San Francisco's Marina District during the 1989 Loma Prieta earthquake, and in Port of Kobe during the 1995 Great Hanshin earthquake.

More recently liquefaction was largely responsible for extensive damage to residential properties of Christchurch, New Zealand during the 2010 Canterbury earthquake and more

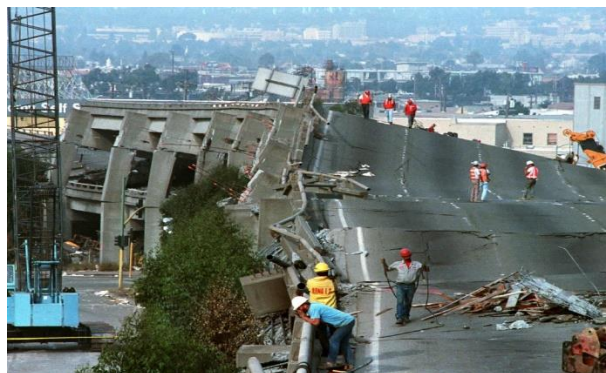
extensively again following the Christchurch earthquakes that followed in early and mid-2011. Road surfaces were forced up by liquefaction, and water and sand flood out of cracks. Moreover, in 2014 in Cephalonia Greece this phenomenon was detected due to an earthquake causing severe damages and road failures. Examples of the consequences of this phenomenon are presented below in figure 1.1.



(a) Niigata, Japan, 1964



(b) Alaska, 1964



(c) San Fransisco, 1989



(d) Port of Kobe, 1995



(e) Christchurch, NewZealand, 2010



(f) Cephalonia, Greece, 2014

**Figure 1.1 - Examples of liquefaction phenomena during earthquakes**

## 1.2 General overview on the mechanical behavior of sands

### 1.2.1 Terminology and definitions

#### 1.2.1.1 Drained and undrained behavior

The drained behavior corresponds to the case where the pore water can drain out of the soil easily under loading causing no change in pore water pressure ( $\Delta u = 0$ ). Therefore, both total and effective stresses in this case are similar due to the fact that the pore water pressure remains equal to a constant value  $u_0$  (hydrostatic pressure), however it must be noted that for drained conditions the drainage of water allows the occurrence of volumetric strains in the soil.

On the other hand, the undrained behavior presents the opposite case where pore water is unable to drain out of the soil. In the undrained condition, the rate of loading is faster than the rate at which the pore water is able to drain out of the soil. As a result, this external loading is taken by the pore water in which it leads to an increase in the pore water pressure ( $u = u_0 + \Delta u$ ). In this case, the definition of effective stresses is introduced where the values of these stresses are much different than those of the total stresses. During undrained loading, the tendency of soil to change volume is maintained, which results in the development of excess pore water pressures

#### 1.2.1.2 Characteristic state

The characteristic state concept has been formulated by Habib and Luong (1978) in order to translate the passage of the volumetric deformations from the contractancy phase to the dilatancy phase. This threshold is characterized by a characteristic friction angle  $\Phi'_{car}$  which characterizes the entanglement capacity of the material. It is defined by the stress level corresponding to a zero irreversible volume deformation rate:

$$\Phi_{car} = \frac{3\eta_{car}}{6 + \eta_{car}}$$

$$\varepsilon_v^p = 0 \text{ at } \eta = \eta_{car} \quad (1.2)$$

The characteristic angle of friction is an intrinsic parameter of the material since it is independent from its density state, the particles size and the followed stress path. The characteristic state thus separates in the  $(q, p')$  plane the domain of the admissible stresses in

the material in two zones corresponding to two types of volumetric behaviors of the soil (figure 1.2).

- a sub-characteristic domain ( $\eta < \eta_{car}$ ) delimited by the characteristic lines LC where the material is contracting.
- an over characteristic domain ( $\eta > \eta_{car}$ ) beyond the LC line and up to the limit of LR failure where the material is dilating.

This can be translated by the following relations

$$\varepsilon_v^p > 0 \text{ for } \eta < \eta_{car}$$

$$\varepsilon_v^p < 0 \text{ for } \eta > \eta_{car}$$

Under undrained conditions, the contractancy and dilatancy mechanism results in a positive or negative excess pore water pressure (EPWP) generation rate. By analogy, the characteristic threshold must, in this case, correspond to the level of stress at which the reversal of EPWP generation direction.

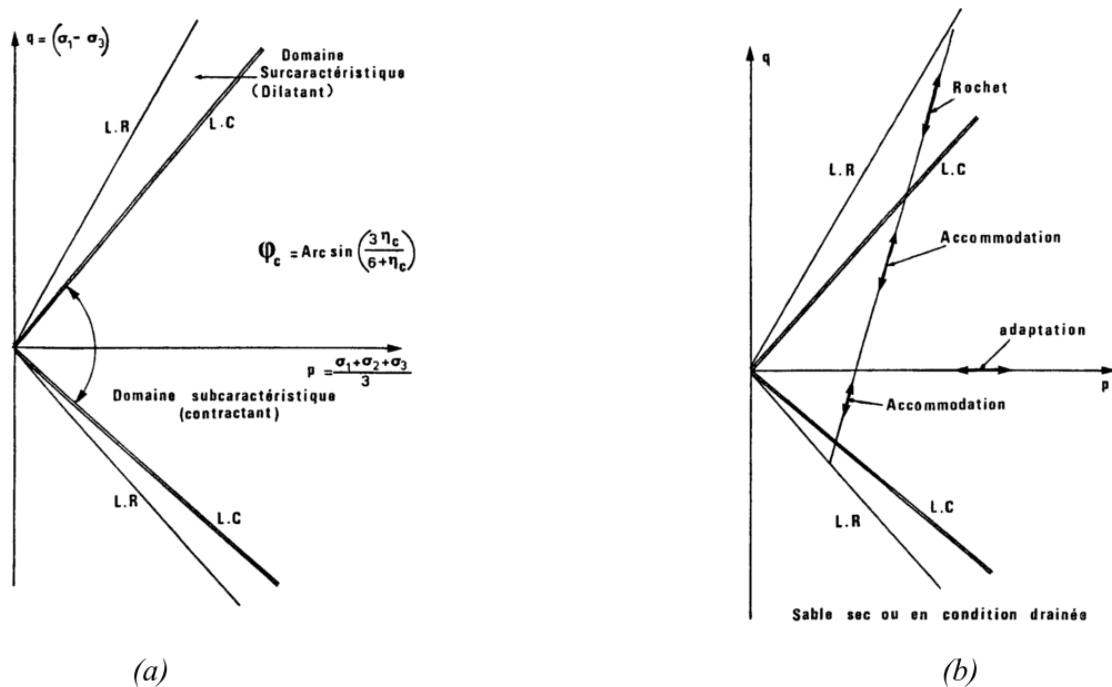


**Figure 1.2 - Characteristic state (Luong 1980)** (a): monotonic behavior; (b) cyclic behavior

### 1.2.1.3 Critical state

Casagrande (1936) conducted the first experimental researches in order to understand the mechanism of volumetric variations and carried out a series of tests on sand using the direct

shear box. Based on the results obtained, he hypothesized that upon shearing a loose sample of sand, it contracts and its volume decreases and approaches a steady state of volume. On the other hand, if the sand is initially dense, its volume grows and tries to reach a stable state in the same way as the loose sand.

At this ultimate state, the value of the void ratio reached is practically identical and constant in both cases, while the material continues to deform at constant volume and shear stress (figure 1.3).

Casagrande has thus developed the concept of the critical void ratio. After that, he has shown that the critical density or critical void ratio varies as a function of the normal stress, and decreases with the increase of the latter. Consequently, this makes it possible to represent the critical points in the plane ( $e$ ,  $\log p'$ ) and to draw the critical state line.

A material whose initial state is located above this line will witness a decrease in its void ratio when subjected to shear stress. As well if it is located below, its void ratio will decrease. The critical state line thus delimits the contracting domain from the dilatant one. Note that the first case is the most critical with respect to liquefaction because the effective stress decreases while in the other case it increases.

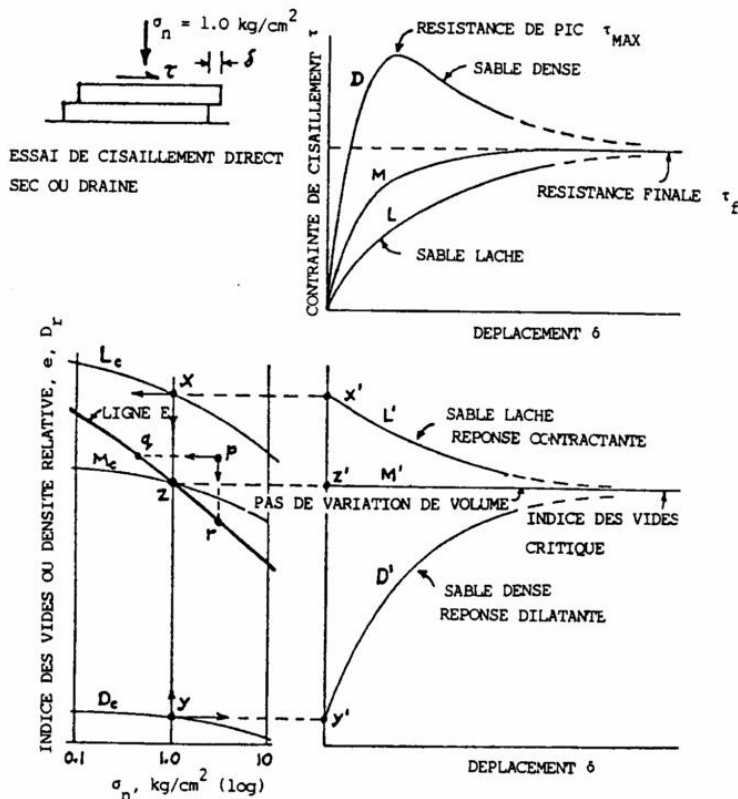


Figure 1.3 - Concept of critical void ratio (Casagrande, 1975)

#### 1.2.1.4 Stability and instability definitions

Granular soils may become unstable even before the stress state reaches failure, this has been observed by Lade (1992) for loose fine sand under undrained conditions, and by Chu *et al.* (1993) for medium loose to dense sand under strain path controlled conditions and by Leong *et al.* (2000) for loose granular fill materials under load controlled undrained condition.

There exists several different definitions for the stability and instability states in the literature review. Lade *et al.* (1988) defined the instability as the inability of the material to sustain or carry a given load including small perturbations of this load. Chu *et al.* (2012) defined the instability as the behavior in which large plastic strains are generated rapidly because of the inability of a soil element to sustain a given load (or stress) or a combination of loads and displacements. Gajo *et al.* (2000) considered that the instability is the state where a small increment in some variables leads to a sudden large increment in other quantities.

The sign of the second order work on the basis of the load condition of stability defined by Hill (1958) is often used to study the stability of granular materials (Darve et Laouafa 2000;

Darve *et al.* 2004; Nicot *et al.* 2007; Daouadji *et al.* 2010; Nicot et Wan 2010; Sawicki et Swidzinski 2010). According to Hill's stability postulate, a material is stable if the second-order work is strictly positive

$$d^2W = d\sigma' d\varepsilon > 0 \quad (1.3)$$

Darve et Laouafa (2000) adopted the definition of stability proposed by Lyapunov (1907) for which the field of applicability is larger than the mechanics of continuum media. He states that: “for a given rate independent material, a stress-strain state ( $\sigma, \varepsilon$ ) for a given strain history is called stable if any “small” change of any admissible loading  $d\mathbf{l}$  leads to a “small” change of the response  $d\mathbf{r}$ .

### 1.2.2 Localized and Diffused Instabilities

It is now recognized that some collapses and instabilities can occur before the Mohr-Coulomb plastic limit criterion is reached. One of these instabilities is the “localized instability”. Many experimental studies have been devoted to the analysis of localized failure with shear band formation. It is well recognized that this failure mode appears in the hardening regime of soil deformation, before reaching the Mohr-Coulomb plastic limit condition (Rice 1976). This instability mode is characterized by the localization of plastic deformation under the form of one or several shear bands. Strain localization has been studied experimentally (Desrues and Viggiani, 2004), theoretically (Bardet, 1990), and numerically (Andrade and Borja, 2006). The widely used theoretical framework for the prediction of strain localization is the localization criterion of Rudnicki and Rice (1975) which corresponds to the vanishing determinant value of the acoustic tensor  $\det(A_{jk})=0$ .

However, since Castro (1969), other experimental research has repeatedly shown collapses strictly inside Mohr-Coulomb surface (Sladen *et al.* 1985, Vaid et Chern 1985, Canou, 1989). Such undrained triaxial compressions tests on loose sands are axially force-controlled and the collapse occurs at  $q$  peak ( $q=\sigma_1 - \sigma_3$ ) (Lade *et al.* 1988). Moreover, it appears that this failure mode is very sudden, with an instantaneous transition from a quasi-static deformation mode to a dynamic one and thus corresponds to a bifurcation of the response of the specimen. A chaotic displacement field without any localization pattern is described (Khoa *et al.* 2006; Darve *et al.* 2007). In order to distinguish this failure mode from the localized one, Darve *et al.* 2004 has called it “diffuse failure”. This type of instability can cause destruction of structures on ground surface as witnessed in San-Fernando in 1971 (see figure 1.4). During the undrained compression tests, diffuse instability can be predicted by Hill's stability postulate.

According to Hill (1958)'s second-order work theory, the necessary condition for the undrained diffuse instability is  $d^2W = d\sigma_{ij}d\varepsilon_{ij} < 0$ .



Figure 1.4 - Diffuse rupture of San Fernando dam, United States 1971

### 1.3 Identification of liquefaction phenomenon in the laboratory

#### 1.3.1 General overview on the behavior of sand under undrained triaxial test

Castro 1969 performed a series of undrained triaxial tests where he distinguished three different behaviors of three sand samples having three different density indexes and tested under the same confining pressure.

##### 1.3.1.1 Liquefaction behavior

In this case, the deviatoric stress curve is characterized by a peak resistance corresponding to a relatively small axial deformation ( $\varepsilon_a = 1\%$ ), followed by a sudden and sharp reduction in the resistance until reaching a residual state called stable state of deformation. The corresponding stress path reveals a peak that migrates left towards the origin until reaching the steady state point. This type of behavior resembles that observed in loose saturated sands that tend to develop a very important pore water pressure. The significant loss of shear strength and the development of large deformations present the characteristics of rupture by liquefaction in nature (see figure 1.5, curve (a)).

### **1.3.1.2 Limited liquefaction behavior**

This case presents an intermediate behavior between total liquefaction and dilatant behavior. The deviator stress records an increase followed by a slight decrease that stabilizes at average deformations before it regains its resistance again. The pore water pressure increases to a level that remains below that of the confining pressure and then it starts to decrease slowly. The stress path migrates to the left and approaches a minimal value of shear strength before it shows a return to the right and rises along the rupture line indicating the appearance of a dilatant behavior. This behavior is typical in medium dense samples (see figure 1.5, curve (b)).

### **1.3.1.3 Dilatant behavior (no occurrence of liquefaction)**

In this case, the shear resistance continues to increase until the end of the test whereas the pore water pressure shows a slight increase followed by an important decrease that might reach negative values. This behavior is related to the high dilatancy of the material where this behavior is usually observed in very dense samples.

Figure 1.5 (c) presents the variations in deviatoric stresses and pore water pressure as a function of the axial strain in addition to the effective stress paths for these three types of responses.

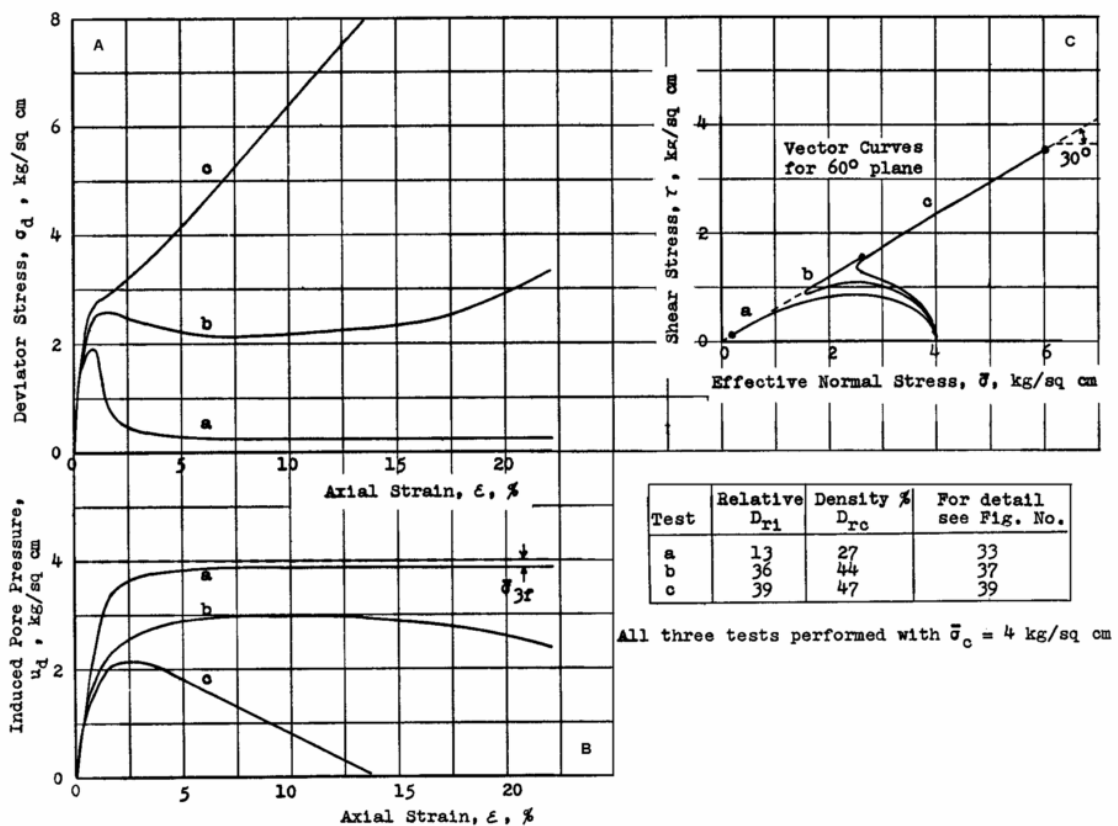


Figure 1.5 - Three types of responses in an undrained triaxial test according to Castro (1969)

### 1.3.2 Chinese criteria for the identification of liquefaction

Based on data from sites where liquefaction was and wasn't observed after earthquakes in China, Wang (1979) developed a criterion for evaluating liquefaction susceptibility of fine-grained soils. He noted that any clayey soil containing less than 15-20% particles by weight smaller than 0.005mm and having a  $W_c/LL$  ratio greater than 0.9 is susceptible to liquefaction (figure 1.6). Seed and Idriss (1982) observed that clayey soils that are susceptible to liquefaction have the following characteristics:

- (1) Percent of particles less than 0.005mm < 15%
- (2) LL < 35
- (3)  $W_c/LL > 0.9$

This was known as the Chinese Criteria due to its origin.

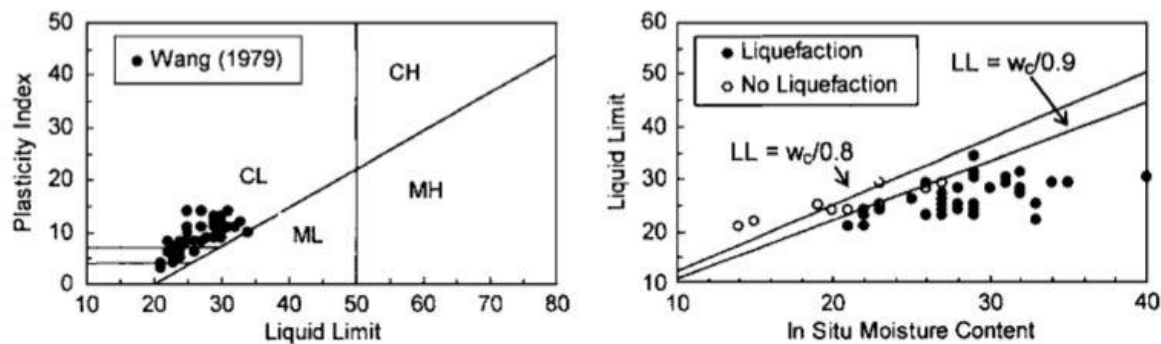


**Figure 1.6 - Data presented by Wang (1979) which led to the development of the Chinese criteria**

Koester (1992) noted that the determination of the LL by means of the fall cone used in the Chinese criteria produces values that are higher than those determined by means of Casagrande.

Moreover, Andrews and Martin (2000) reduced the LL condition for liquefaction susceptibility to values less than 32. Besides, they used 0.002mm as the limit between silt-size and clay-size particles with <10% clay-particles being necessary for a silty or clayey soil to be liquefiable and they dropped the  $w_c/LL$  as a condition in their liquefaction susceptibility.

Boulanger and Idriss (2004) recommended laboratory testing as the best way to evaluate liquefaction susceptibility. They also recommended that the evaluation of the liquefaction potential of silts and clays must be separated into procedures applicable for “sand-like” fine-grained soils that can liquefy and for “clay-like” fine grained soils that can undergo cyclic failure. The plasticity index PI can be used to discriminate between these two categories. Fine grained soils with  $PI < 7$  indicate sand-like response (susceptible to liquefaction), and soils with  $PI \geq 7$  indicate clay-like response. Bray and Sancio’s (2006) observations from recent earthquakes and results of cyclic tests indicate that the Chinese criteria is not reliable for determining the liquefaction susceptibility of fine-grained soils. A good evidence is represented by soils that liquefied during 1994 Northridge, 1999 Koaeli and 1999 Chi-Chi earthquakes where they didn’t meet the clay-size criterion of the Chinese criteria. Hence, Bray and Sancio (2006) have introduced the plasticity index (PI) as an indicator of liquefaction susceptibility where they declared that loose soils with  $PI < 12$  and  $w_c/LL > 0.85$  are susceptible to liquefaction, while loose soils with  $12 < PI < 18$  and  $w_c/LL > 0.8$  are more resistant to liquefaction. Soils with  $PI > 18$  tested at low effective confining stresses weren’t susceptible to liquefaction. Moreover, they noticed that the results of the cyclic testing program provide

insights regarding the effects of confining pressure, initial static shear stress and stress-path on the liquefaction of fine grained soils.

### 1.3.3 Initiation of instability

#### 1.3.3.1 Undrained potential instability zone according to Vaid and Chern (1985)

According to the studies done on two types of sands, Ottawa sand and Mine sand, Vaid and Chern (1985) have shown that there exists a critical effective stress ratio  $\sigma'_1/\sigma'_3$  at which the instability is triggered. This ratio is shown to be independent of the initial state of the sand (before shearing) and therefore this indicated that the liquefaction is initiated at a unique value of critical effective stress ratio. For different effective stress paths, the instability initiation points are collinear and can be joined with a line passing through origin. This line is called the critical stress ratio line.

For this reason, Vaid and Chern (1985) defined a potential instability zone that is located between the critical stress ratio (CSR) line as an inferior limit and the phase transformation (PT) line defined by Ishihara et al. (1975) as a superior limit (figure 1.7). Once the stress state of sand is located in the interior of this zone, the instability is triggered. However, this zone doesn't extend to the origin since it terminates by an approximately horizontal line "ab" whose position varies with the initial relative density of the sand.

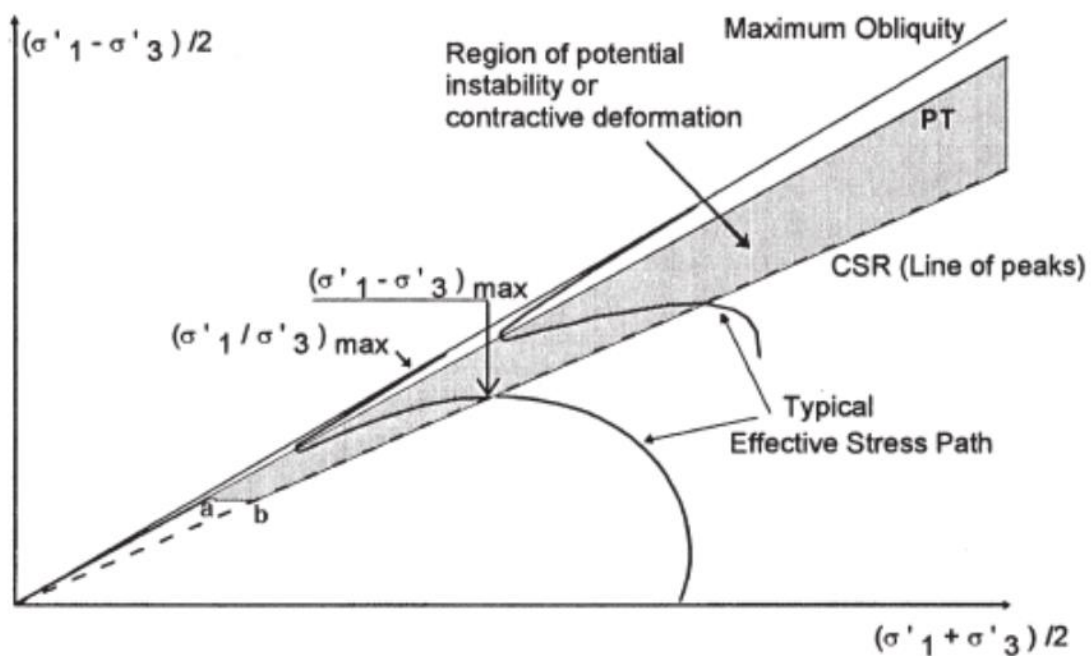


Figure 1.7 - Instability zone defined by Vaid et Chern (1985)

### 1.3.3.2 Collapse surface according to Sladen et al.

Sladen *et al.* (1985) have presented another approach that is called “collapse surface” and it is presented in figure 1.8. They have remarked that the peak shear stresses for three samples having the same void ratio but consolidated at different confining stresses can be joined by a line that passes through the steady state point. This line has been identified as the “collapse line” figure I.8a. Sladen has also observed that at a lower void ratio (higher density) this line will have the same slope but will pass through a higher point on the steady state line in stress space. This observation of the colinearity of peak strengths and that these lines change their positions only with the change in void ratio has introduced the concept of collapse surface in three-dimensional stress-void ratio space (figure 1.8b).

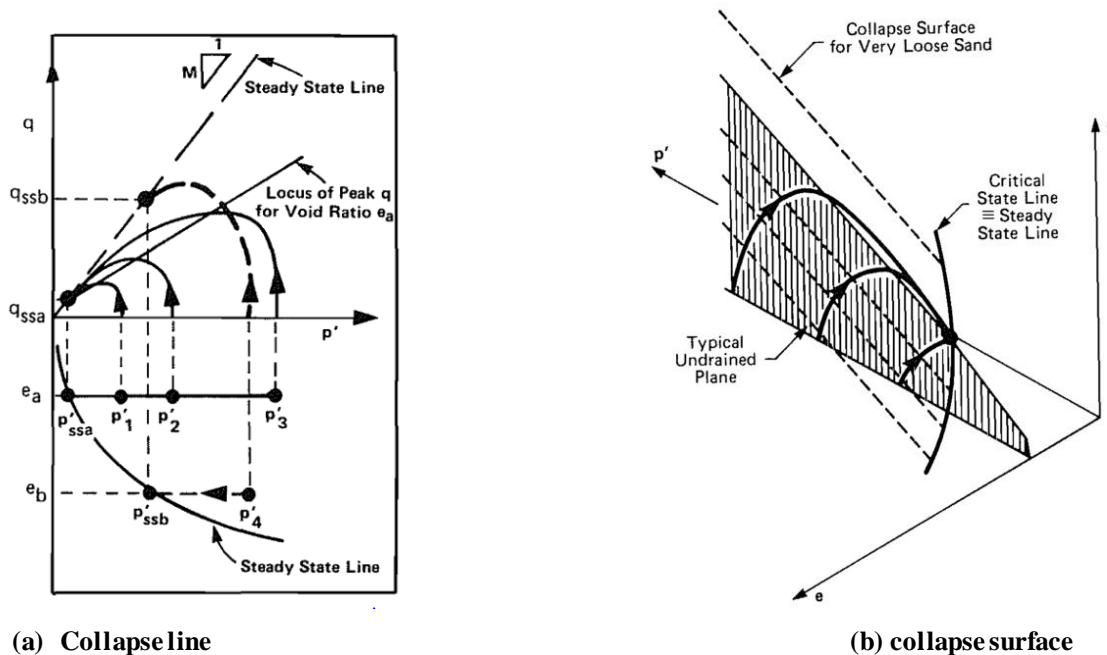
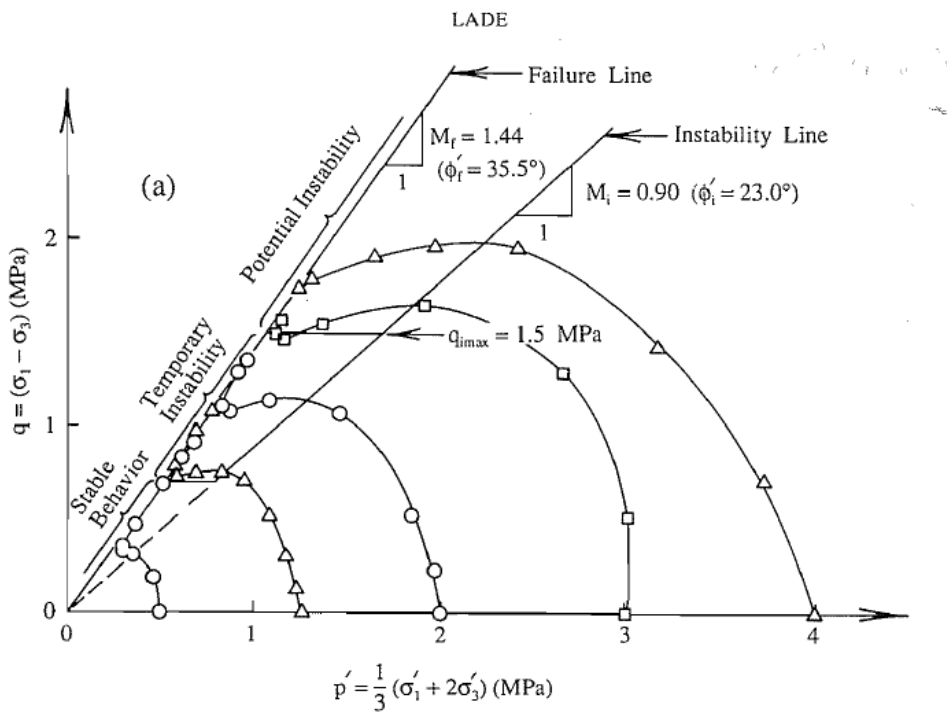


Figure 1.8 - Collapse line and surface according to Sladen (1985)

### 1.3.3.3 Instability line

The effective stress paths from the undrained tests on very loose compressible soil trace the yield surfaces, and determination of the top of one such yield surface is in principle, sufficient to define the instability line. The instability line connects the tops of the yield surfaces and it defines the inferior limit of the potential instability zone, Lade (1992). For very loose sands, the peak resistance is very low and therefore the instability line passes through the stress origin.

Lade (1993) has introduced a small modification to the concept of instability line that has been previously presented. After many investigations, he showed that the instability line passes through the origin of stress plane rather than ultimate state (see figure 1.9). Moreover, he has noticed that the slope of the instability line decreases as the relative density decreases. Furthermore, he divided the potential instability zone into three small zones: potential instability, temporary instability and stable behavior as shown in the figure.



**Figure 1.9 - Instability line and potential instability zone (Lade 1993)**

## 1.4 Specimen preparation methods and their effects on soil behavior

### 1.4.1 Overview of specimen preparation methods for sandy soils

#### 1.4.1.1 Moist tamping (MT) method

Moist tamping (MT) is the oldest sample preparation technique, which mimics the compaction of fills (Lambe, 1951). In the MT method, dry soil is mixed with a small amount of water to facilitate the development of capillarity. The moist soil is then compacted in successive layers within a mold to form the specimen with the desired density (Lambe, 1951). Key advantages of MT method include its simplicity, the wide range of specimen densities, the self-standing nature of the specimen because of capillarity, and no segregation. The

accumulation and compaction of the upper layers, however, tend to densify the bottom layer. Ladd (1977) proposed an under-compaction procedure to minimize over-compaction and ensure uniformity within the specimen. Frost and Park (2003) critically assessed the MT method and found that it could induce over consolidated specimens with a variation in the relative density among layers of up to 15%, which is about twice that of air pluviated specimens.

Some studies have indicated that silty sand specimens reconstituted by the moist tamping method were not able to simulate the stress–strain response of in-situ alluvial deposits (Høeg *et al.*, 2000; Ishihara, 1993; Vaid *et al.*, 1999). Sand specimens made by moist tamping may have the most unstable structure and lower strength under monotonic or cyclic loadings (Kuerbis and Vaid, 1988; Høeg *et al.*, 2000; Frost and Park, 2003; and Yamamuro and Wood, 2004). However, studies by Huang *et al.* (2004) and Huang & Huang (2007) on silty sand specimens prepared by the MT method showed higher strength.

### 1.4.1.2 Air Pluviation (AP) method

In the air pluviation (AP) method, dry soil particles fall through air before they are deposited into a mold from a distance above the top of the soil specimen by a pluviator. The AP method mimics the deposition process of aeolian deposits. The density of the soil specimen is related to the deposition intensity (mass of deposited soil per unit time) and vertical distance between the pluviator and top of the deposited soil. Various air pluviation methods have been proposed, with the major difference in the design of the pluviator. Miura and Toki (1982) developed a multiple sieving pluviation apparatus (MSP) to prepare sand specimens at various densities by controlling the rate of sand discharge, and the concept has been extended to prepare a large volume specimen by Ueng *et al.* (2004). Preparing a silty sand specimen with the AP method can easily cause particle segregation. Lo Presti *et al.* (1992) reported that particle segregation in both vertical and lateral direction can develop. Segregation in the lateral direction forms silt columns below the opening of the pluviator. The dry deposition (DD) method by Yamamuro and Wood (2004) may be considered as a special case of AP, where dry soil is deposited directly on the top of the soil specimen to minimize particle segregation for silty sand. However, Kuerbis and Vaid (1988) pointed out that air pluviated dry silty sands are prone to bulking and thus can result in lower monotonic and cyclic strength. The AP method has been used to prepare dry sand specimens for physical modeling tests (Fretti *et al.*, 1995; Wang and

Lin, 2011). Benahmed (2001) has developed a motorized pluviator that permits to control both the sand flow and the velocity of rising the pluviator and hence the fall height. This apparatus consists essentially of a sand reservoir, a cylindrical body a diffuser and a lift system as illustrated in figure 1.10. this device permits us to have a wide density range that varies between  $ID = 0.05$  (very loose) to 1 (very dense). Recently, Ueng et al. (2004) developed a special pluviator to prepare large saturated sand specimens for 1-g shake table tests by combining air pluviation and water deposition. However, the procedure cannot be used with silty sands, due to particle segregation.

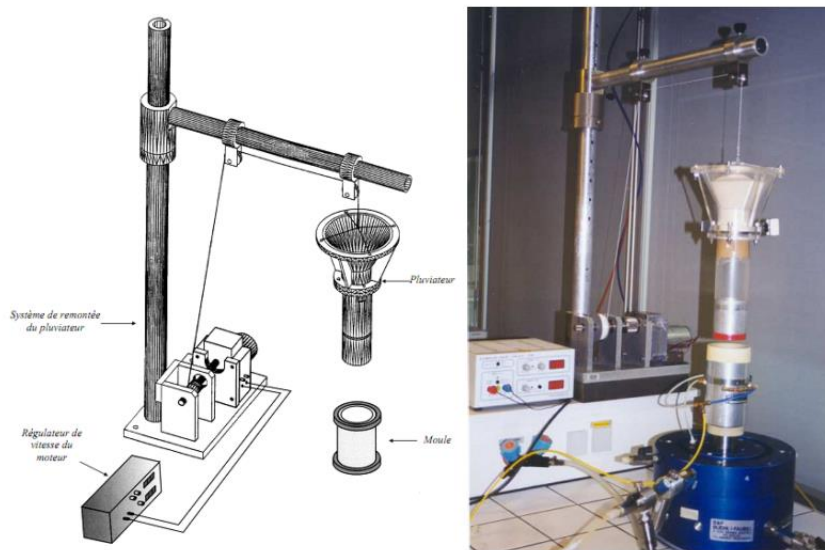


**Figure 1.10 - Pluviator presented by Benahmed (2001)**

#### 1.4.1.3 Water pluviation (WP) method

The water pluviation (WP) or water sedimentation method is similar to the AP method, except that the dry soil particles are pluviated into deaired water. The terminal velocity of the soil particles is significantly reduced in comparison with the AP method, as they pass through a layer of water instead of air. As a result, the WP specimens are generally looser than those created by AP. The WP simulates the process of alluvial deposition, or that of hydraulic fills. For relatively uniform sand, the WP and slurry deposition (SD) methods are more likely to duplicate the strength/dilatancy behavior of in-situ alluvial soils (Oda et al., 1978; Yamamuro and Wood, 2004; Yoshimi et al., 1984). It is also possible to use this technique to prepare large volumes of saturated sandy soils for physical modeling tests. However, for silt or silty sands, the WP method tends to create segregation during the falling process. The SD method,

proposed by Kuerbis and Vaid (1988), is a modified version of WP for reconstituting silty sand specimens. In the SD method, the sand with silt/clay are first thoroughly mixed in deaired water, and then poured into a triaxial specimen mold lined with rubber membrane. The initially loose specimen is densified by tapping the mold or applying a consolidation pressure in the triaxial cell. Kuerbis and Vaid (1988) reported that the SD method is able to produce uniform silty sand specimens and simulate the behavior of natural silty sands. However, Høeg et al. (2000) compared the silty sand specimens prepared by the SD method with undisturbed samples, and concluded that this approach is promising but incapable to reproduce the stress–strain relationships seen with in-situ alluvial soil with fines.

Rahardjo (1989) used the SD method to prepare large specimens of silty sands for calibration chamber tests. A concrete mixer was used to ensure proper blending of sand and silt. After several hours of blending, the specimen was then poured into a mold for consolidation. The cone penetration (CPT) performed in the silty sand specimen prepared by the SD method showed limited success in terms of the uniformity and repeatability of cone tip resistance ( $q_c$ ). In any case, the complexity of the SD method makes it impractical to prepare large size specimens.

#### **1.4.1.4 Mist pluviation (MP) method**

Huang et al. (2015) proposed a new specimen preparation technique for preparing reconstituted silty sand specimens called the mist pluviation (MP) method. The MP method is named based on the process of soil deposition and the medium that the soil falls through. In the MP method, the dry soil particles are dispersed from a pluviator then sequentially pass through air, mist, and water. The mist zone is introduced to mix relatively uniform water droplets with soil particles, and this significantly reduces the size difference of soil and water mixtures and thus potential of particle segregation in the air. A thin water layer on top of the deposited soil mimics the sedimentation process, and saturates the soil without inducing severe particle segregation. A schematic diagram of this approach is shown in figure 1.11. Also the setup of the mist pluviation system and details of the pluviator are shown in figure 1.12.

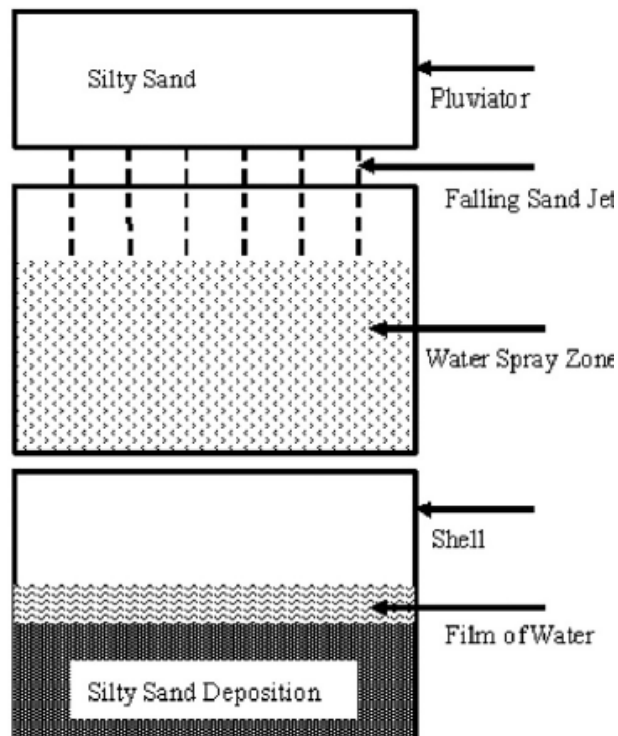


**Figure 1.11- Schematic layout of the mist pluviation method (Huang et al. 2015)**

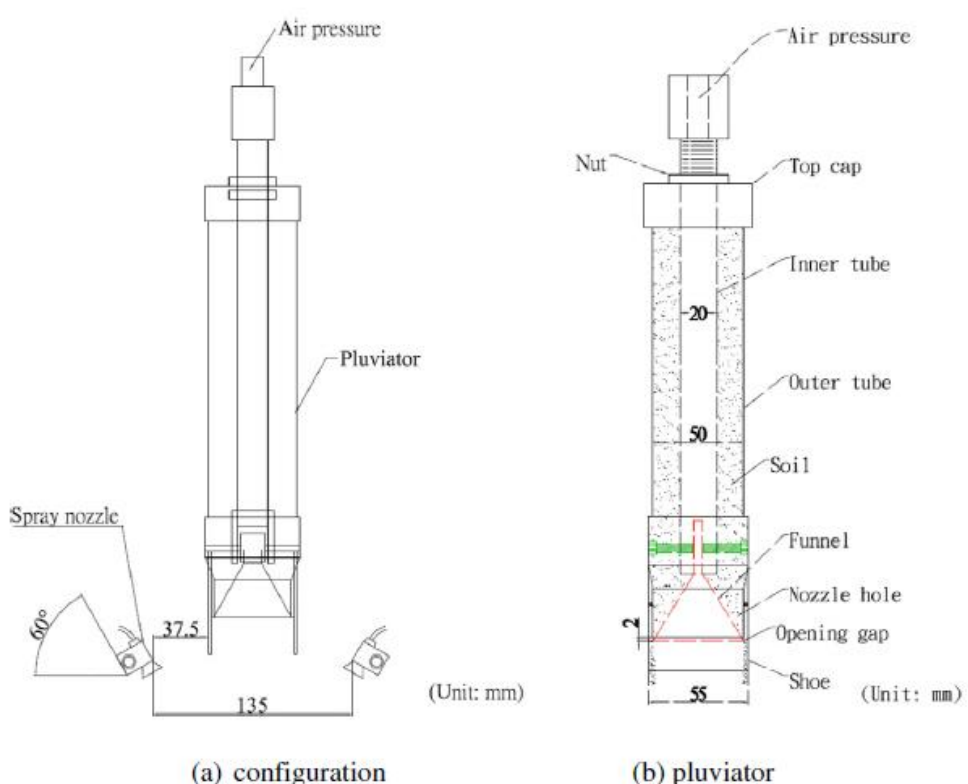


**Figure 1.12 - Configuration of mist pluviation unit and details of pluviator (Huang et al. 2015)**

Huang et al. (2015) performed a series of triaxial tests on a silty fine, Mai Liao sand (MLS) to evaluate the performance of the MP method with regard to homogeneity, repeatability, undrained monotonic compression, and cyclic strength of triaxial specimens with various fines contents Fc. Results show that the MP method can produce macroscopic homogeneous specimens, regardless of the Fc and particle gradations (figure 1.13). Furthermore, the repeatability tests confirm that this method can produce repeatable shear behavior for silty sands (figure 1.14).

The MP specimens have shown dilative, strain-hardening behavior under monotonic undrained triaxial compression while MT specimens at the same initial state showed contractive, strain-softening behavior. Similar dilative behavior had been observed on undisturbed fluvial sands and those reconstituted by water pluviation method which indicates that the MP method has higher potential than other techniques to produce the monotonic shear response similar to that of the WP method, which is the reconstitution technique that best reproduce the response of natural alluvial and hydraulically filled sands.

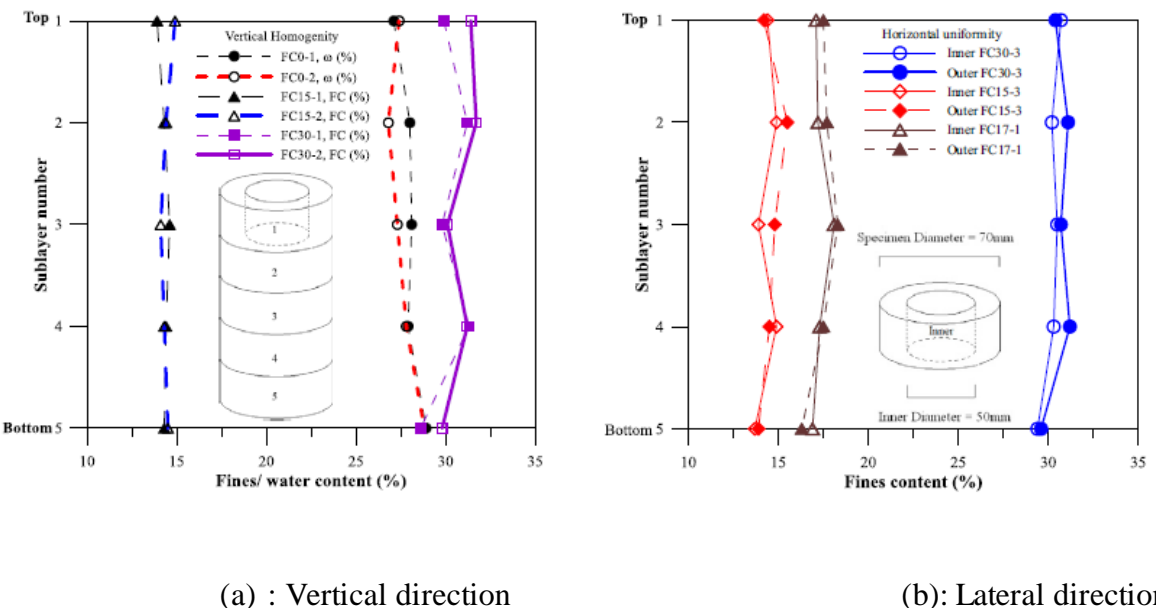
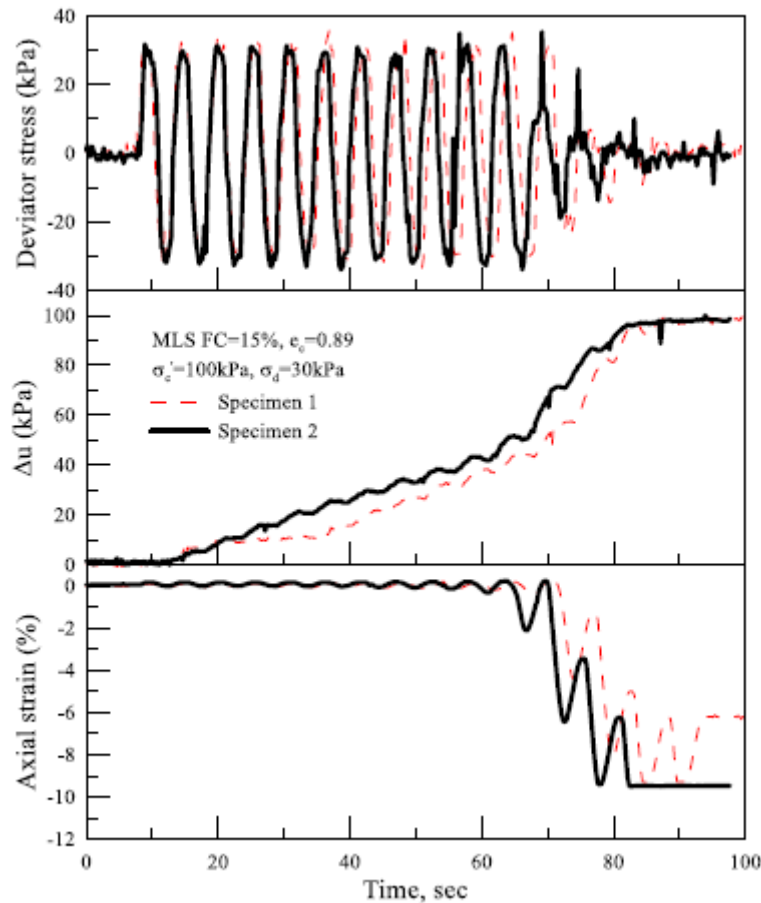


Figure 1.13 - Homogeneity of sample prepared by MP method (Huang et al., 2015)



**Figure 1.14 - Repeatability in cyclic undrained triaxial test (Huang *et al.*, 2015)**

#### 1.4.2 Effect of reconstitution methods on the mechanical behavior of material

In the literature review concerning the influence of the reconstitution mode of sand samples on their behavior, it is obvious, according to many authors, that the reconstitution mode has a significant influence on the cyclic and monotonic shear resistance of sands (Mulilis *et al.* 1975; Tatsuoka *et al.* 1986).

Been and Jefferies (1985) noted that upon reconstitution of sand samples either by wet tamping or pluviation method, the samples show different shear behavior under drained conditions. Moreover, concerning the liquefaction instability Canou (1989) presented preliminary results showing that sand specimens prepared by wet tamping method are more unstable and more susceptible to liquefaction than those prepared by dry pluviation for the same void ratio. The same result was noted by Vaid *et al.* (1999) who confirmed that the wet tamping method favors the initiation of liquefaction compared to that of water pluviation. Benahmed *et al.* (2004) tested the effect of the reconstitution method on the behavior of two

reconstituted samples by wet tamping and dry pluviation. The sand used for the triaxial testing program is Hostun RF sand. Benahmed (2001) observed significant differences showing the strong influence of preparation procedures on corresponding behavior. She noted that wet tamping favors a very contractant and unstable behavior (strain softening) with a liquefaction type of response whereas dry pluviation favors a slightly dilatant and more stable response (strain hardening) (see figure 1.15).

Yamamuro and Wood (2004) investigated the effect of depositional method on the undrained response of silty sands. Undrained triaxial compression tests were performed at an initial effective confining pressure of 25 kPa on Nevada sand containing 20% non-plastic silt content. Figure 1.16 present the results found by Yamamuro and Wood (2004) who have shown that the water pluviation WD method indicated a more volumetrically dilatant or stable response whereas dry methods appeared to exhibit a more contractive or unstable behavior. Moreover, they mentioned that effects were more noticeable at lower densities than higher densities. Juneja and Raghunandan (2010) conducted both drained CD and undrained CU compression tests on samples prepared using pluviation and tamping techniques under both dry and moist conditions. Results showed that samples prepared using tamping technique usually strain softens whereas those prepared by pluviation technique may harden or soften depending on the sample relative density and confining pressures applied during testing.

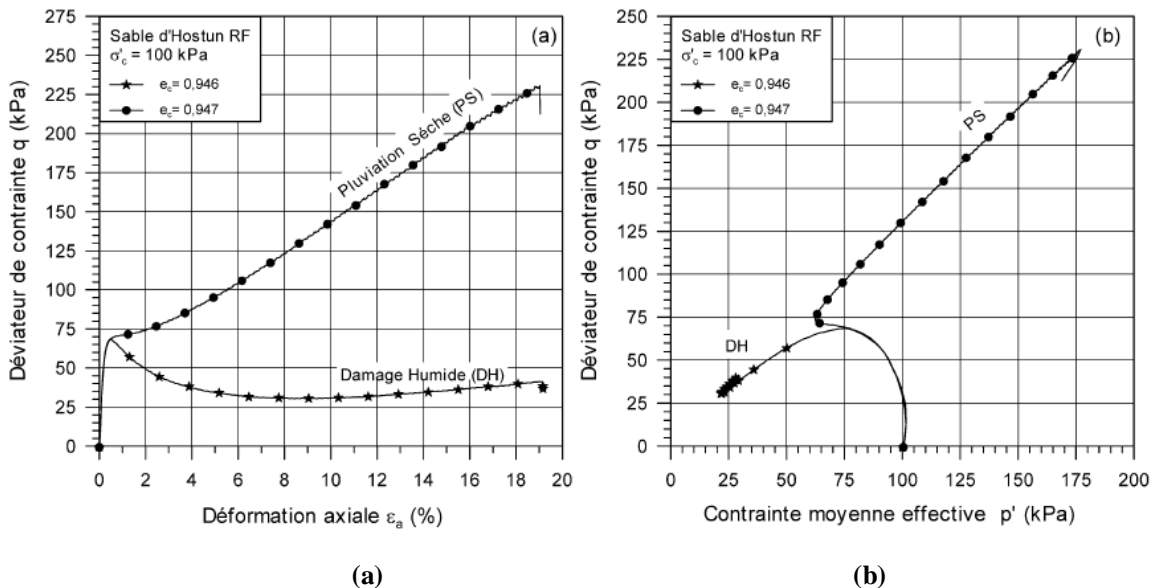


**Figure 1.15 - Influence of the specimen reconstitution procedure on the observed behavior, for a loose state of the sand: (a) shear curves; (b): effective stress paths (Benahmed *et al.* 2004)**

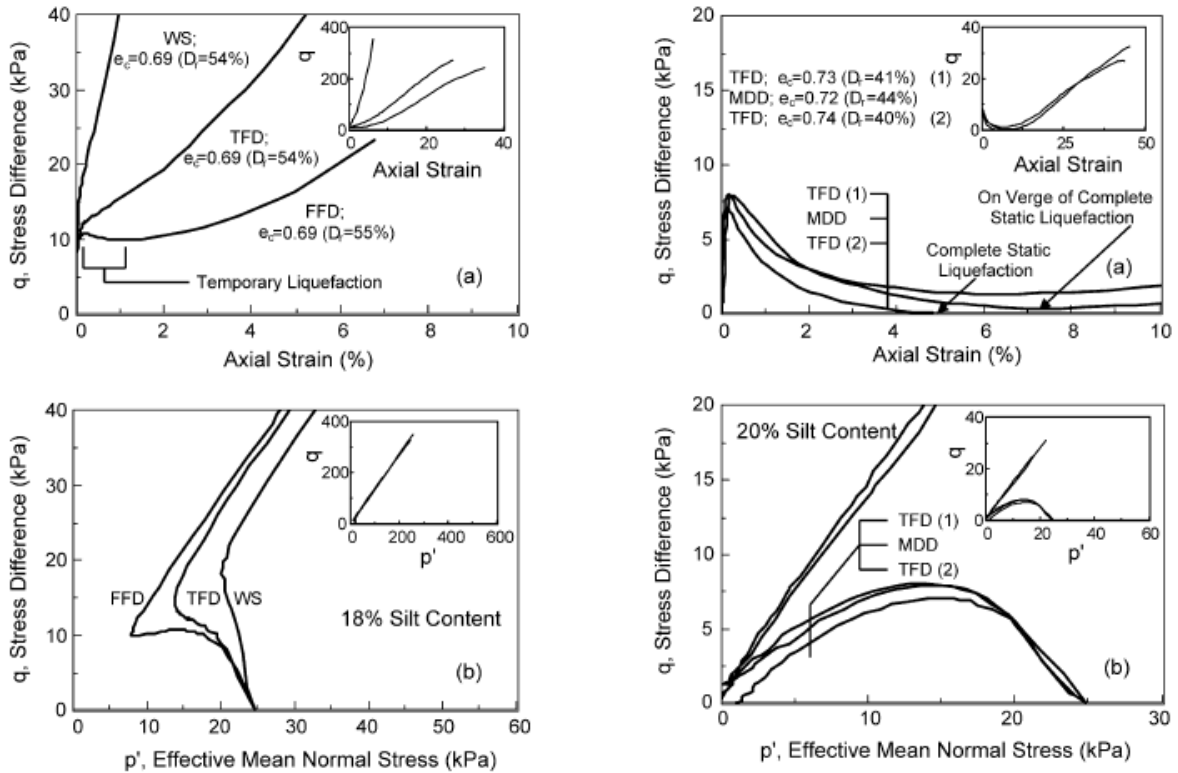


**Figure 1.16 - Undrained triaxial test results for medium and low densities showing the effect of reconstitution methods on the specimen behavior (Yamamuro et Wood 2004)**

#### 1.4.3 Effect of reconstitution method on the material structure

It is widely recognized that the mechanical behavior of soils in general and sands in particular depends to a large extend on the initial state in terms of the void ratio and effective stress state. However, and particularly for sands, the importance of initial structure is rarely referred to. Benahmed *et al.* (2004) studied the effect of the reconstitution method on the microscopic structure of Hostun sand RF. The microscopic observations of the sand structures corresponding to two reconstitution procedures of the samples are presented in figure 1.17. These observations allow to clearly identify two different and well characterized types of arrangements. For wet tamping, an irregular structure is observed, with predominance of aggregates and macropores, whereas for dry pluviation, a more regular and classical single-grained structure is observed, with grains regularly stacked up and without macropores.

Also Yamamuro and Wood (2004) investigated the effect of depositional method on the microscopic grain structures of sand containing non-plastic silt. Specimens were reconstituted using water sedimentation (WS) and dry funnel deposition (DFD) methods. Yamamuro

(2004) observed that specimens that underwent temporary liquefaction (DFD) appeared to have a larger percentage of unstable grain contacts. Whereas specimens exhibiting a stable response (WS) contained more stable grain contacts (see figure 1.18).

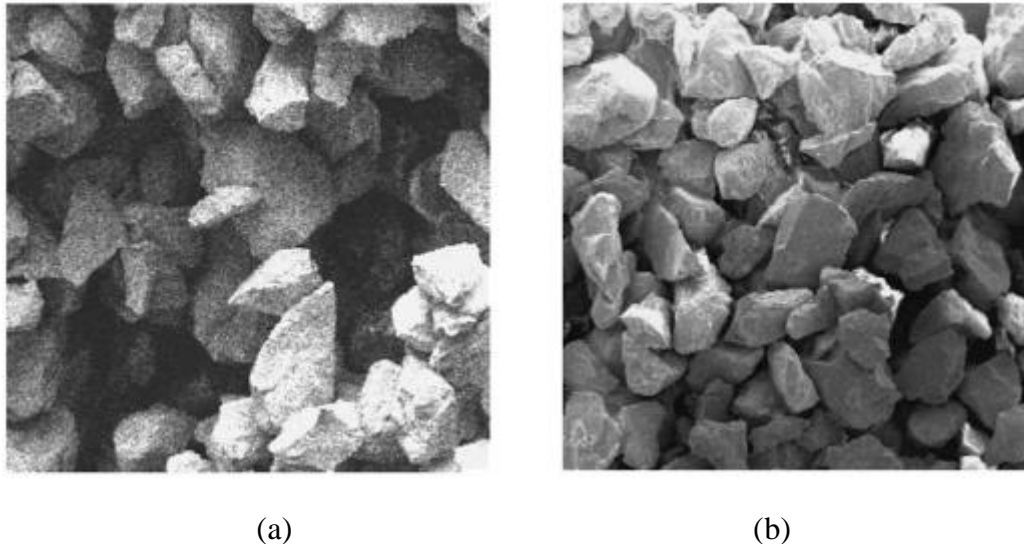


**Figure 1.17 - Microphotographies of Hostun sand RF showing two differentiated structures : (a) aggregates and macropores (wet tamping); (b) regular stack (dry pluviation) (Benahmed *et al.* 2004)**

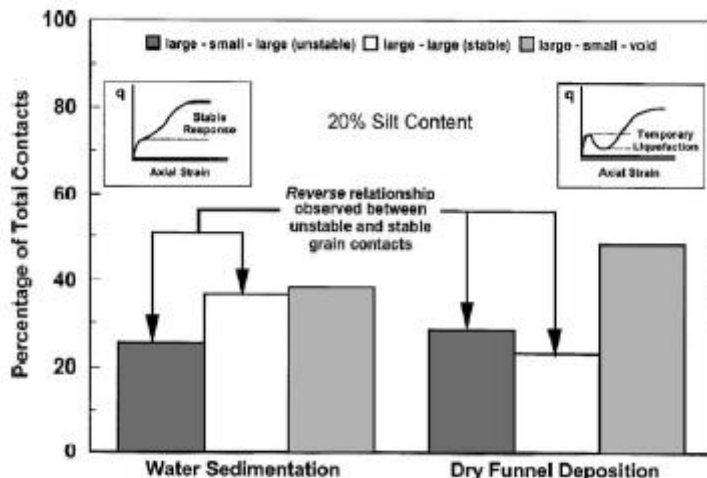


**Figure 1.18 - Comparison of grain contact structure between specimens formed by dry funnel deposition and water sedimentation containing 20% silt (Yamamuro and Wood 2004)**

## 1.5 Influence of fines on the behavior of silty sands

Since the last 50 years, generation of excess pore water pressure (EPWP) and subsequent liquefaction of saturated sandy soils with or without fines has been a topic of extensive laboratory research. Most of the earlier research has focused on the liquefaction of clean sands

assuming that the presence of fines resists the development of pore water pressure. However, natural sand is found in nature under the form of a mixture of sand and fines.

Unfortunately, the liquefaction of this type of material is still unclear and there exist no definite conclusion about it. Besides, we could find contradictory results concerning this subject in the literature review of the effect of fine particles on the sand liquefaction phenomenon. This could be explained due to the fact that these authors have used different types of sand, fines content, densities and confining pressures. Moreover, they have used criteria based on different definitions of liquefaction resistance. For this reason, it is very interesting to study the effect of fine particles on the phenomenon of sand liquefaction.

Although several authors have studied the effect of fines on the liquefaction resistance of sands for high values of fines content that ranges between 10% and 80%, it is interesting to note here that based on field studies following major earthquakes and the case histories of actual soil behavior during earthquakes there are some evidence that soils with greater fines content are less likely to liquefy. Okashi (1970) has realized during the 1964 Niigata earthquake that soils with fines content less than 10% were more likely to liquefy. Also, Tokimatsu and Yoshimi (1983) declared in a study of 17 worldwide earthquakes that 50% of liquefied soils had fines content less than 5%. Therefore, it would be very interesting to study soil behavior at very low fines content (below 5%).

### **1.5.1 Definitions and influence of different parameters**

#### **1.5.1.1 Intergranular void ratio and interfine void ratio**

According to the literature review, many authors have evaluated the effect of fine particles on the liquefaction potential using the concept of intergranular void ratio  $e_s$  and interfines void ratio  $e_f$ .

Based on the analysis of the mechanical behavior of silty sands, Kuerbis *et al.* (1988) were the first who proposed the intergranular void ratio  $e_s$ , where the volume of fine particles is considered as void as long as the fines are simply confined by the voids formed from the sand grains. Consequently, these fine particles do not participate in the shear resistance of the granular structure and the behavior of the mixture is dominated by the sand grains.

Therefore, this theory is applicable in the case where the fines content is less than a certain value that is the limiting fines content or the critical fines content. In other words, the fine

particles are totally confined within the matrix formed by the sand skeleton grains and hence they don't participate or contribute to the shear resistance of the structure. In this case, the intergranular void ratio parameter is more representative than the global void ratio  $e$ .

On the other hand, when the fines content exceeds the limiting or the critical value, the quantity of fine particles is sufficient to establish active contact between each other whereas the sand grains loose contact among each other . The role of fines content becomes more pronounced as their amount increases progressively and those of the sand decrease. In this case, the interfines void ratio  $e_f$  must be taken into consideration.

These two parameters can be simply calculated using the formulas proposed by Thevanayagam (1998). A schematic phase diagram proposed by Thevanayagam is presented in figure 1.19 to clarify the differences between these parameters.

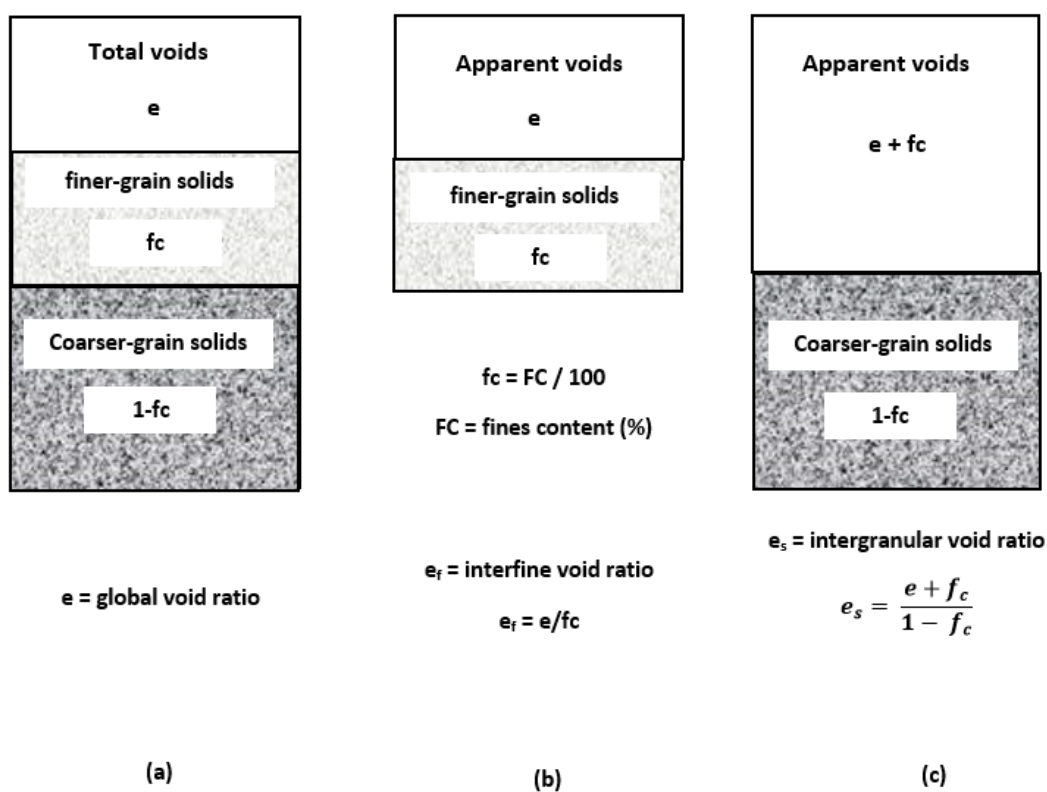


Figure 1.19 - Schematic phase diagrams: (a) silty Sand; (b) silt Matrix ;( c) sand Matrix (Thevanayagam 1998).

We should also mention that the intergranular void ratio is also called sand skeleton void ratio (Polito and Martin II, 2001; Kuerbis *et al.* 1988; Dash and Sitharam, 2011) or granular void ratio (Ni *et al.*, 2004).

### 1.5.1.2 Limiting fines content

It is known for now that the presence of fine particles in a sand deposit affects its general structure. When fines are added to a sand deposit, the latter passes from one phase to the other through a transition point.

Below this point, the soil structure is generally a sand dominated one with silt contained within a sand skeleton and therefore the fine particles are not active and they do not participate in the shear resistance of the material. Whereas beyond this point there are enough fines such that the sand grains loose contact with each other and the soil structure becomes a silt dominated one and hence the mechanical response of the material is dominated by the fine particles. This limiting value is called “fines content threshold”, “limiting fines content” or “critical fines content”. Figure 1.20 shows a schematic diagram presented by Karim *et al.* (2014) that illustrates the effect of adding fines on the behavior of sand.

Limiting fines content (LFC) was first investigated by Polito (1999). Later, Hazirbaba (2005) proposed an approach to estimate LFC using the following equation:

$$LFC = \frac{W_{fines}}{W_{sand} + W_{fines}} = \frac{G_f e_s}{G_f e_s + G_s(1 + e_f)}$$

where  $W_{fines}$  is the weight of fines and  $W_{sand}$  is the weight of sand in a sand-silt mixture. Similarly,  $G_f$ ,  $G_s$ ,  $e_f$  and  $e_s$  stand for specific gravity of fines, specific gravity of sand, maximum index void ratio of fines and maximum index void ratio of sand respectively.

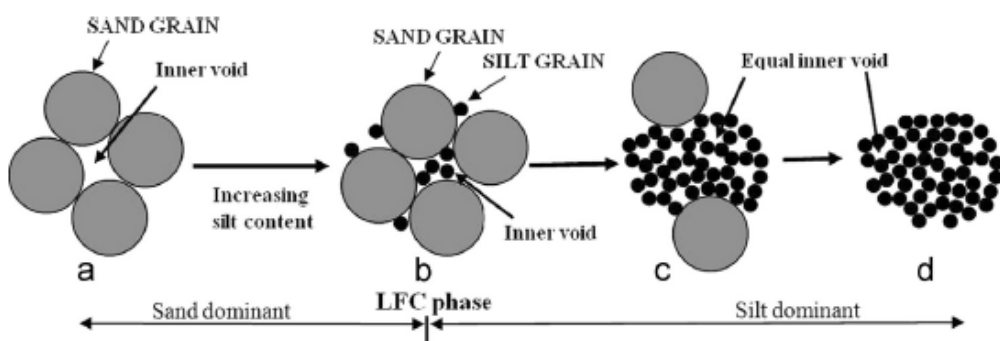


**Figure 1.20 - Schematic diagram demonstrating particle arrangement of sand-silt mixture with the variation of silt content. (Karim *et al.*, 2014)**

### 1.5.1.3 Evolution of specific relative density – maximum and minimum void ratios

Many authors have noted that both the maximum and minimum void ratios present the same type of evolution with the increase in fines content  $F_c$ , (see figure 1.21). These two parameters decrease until the fines content reaches a certain value and then increases progressively (Lade et al., 1998; Polito et Martin II, 2001; Huang et al., 2004; Papadopoulou et Tika, 2008; Belkhatir et al., 2010; Dash et Sitharam 2011).

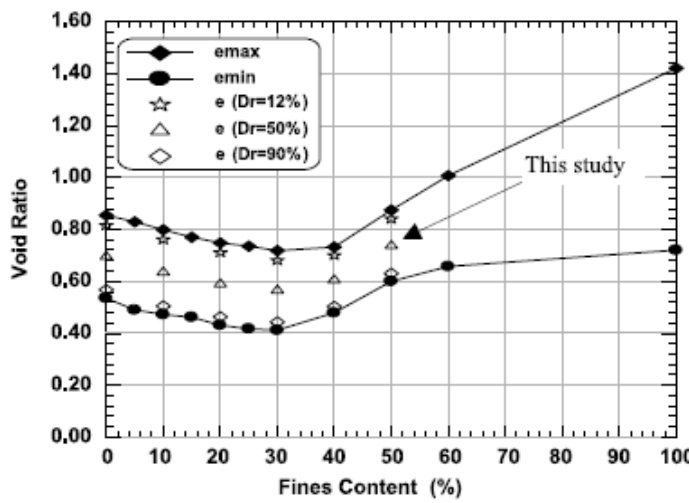


Figure 1.21 - Variation of maximum and minimum void ratios of the sand-silt mixtures. (Belkhatir et al., 2010)

As the maximum and minimum void ratios vary with the variation of fines content, Polito and Martin II (2003) distinguished two parameters: the relative density  $D_r$  using  $e_{min}$  and  $e_{max}$  of clean sand (Eq 1.4), and the specific relative density  $D_r^s$  computed using the  $e_{min}$  and  $e_{max}$  of the mixture (Eq 1.5). It is interesting to note here that many authors have determined the maximum and minimum void ratios for mixtures of sand and fines (for fines contents that reach 80%) using either the American procedure ASTM-4254-91 and ASTM-4253-93 or the French norm NF P94-059 even though that the ASTM limits this method by a fines content up to 15% and the French norm limits it by a fines content equal to 12%. Consequently, we can wonder if these estimations are really correct and, hence, if it is possible for us to compare these results among them since there is an absence of unity between the definitions of these parameters including the density index  $I_D$  of the whole mixture and that of the sand matrix  $I_{Dmat}$ , note that the density index  $I_D$  and the relative density  $D_r$  are identical but  $I_D$  is a decimal value of the density whereas the  $D_r$  is a percentage of the latter. For our study, we are going

to fix the density index of the sand matrix  $I_{Dmat}$ . Also, another question is imposed concerning the state of the sand matrix upon adding large quantities of fines, in other words can we still talk about the effect of fines on the matrix or is it the fines particles who totally control the behavior of the mixture.

$$D_r = \frac{e_{\max(sand)} - e}{e_{\max(sand)} - e_{\min(sand)}} \quad (1.4)$$

$$D_r^s = \frac{e_{\max(mixture)} - e}{e_{\max(mixture)} - e_{\min(mixture)}} \quad (1.5)$$

#### 1.5.1.4 Equivalent intergranular void ratio

(Thevanayagam and Martin 2002) have improved the concept of intergranular void ratio and interfines void ratio. They have presented different possible granular structures of a mixture of sand and fines as illustrated in figure 1.22. These structures can be decomposed into three major categories:

- 1) coarse grain soil mix;
- 2) fine grain soil mix;
- 3) layered soil mix.

The silty sands could be represented by the first category. This category corresponds to the case where the fines content is less than the limiting value and consequently the sand grains control the behavior of the material. This category, according to Thevayanagam and several authors could be subdivided to three sub-categories as follows:

- The fine particles are totally confined in the voids between the sand grains, and consequently don't participate in the resistance of the material. These fine particles are totally inactive. Therefore, for this case the intergranular void ratio best describes the material's state.
- The fine particles are decomposed into two different parts, one of them is found inside the grains matrix that is the inactive part, whereas the second part starts to touch the sand grains and hence becomes active.
- A part of the fines occupy the voids created by the sand grains whereas the other part interlocks between the sand grains and consequently separate them.

- For the last two cases, it is obvious that the fine particles participate in the forces chain and the shear resistance of the material and therefore the intergranular void ratio isn't anymore a reliable factor. In this case and in order to take into consideration the role of the active fines, Thevayanagam et al. (2002) have proposed a new parameter known as the equivalent intergranular void ratio, computed using this formula:

$$e^{eq} = \frac{e + (1 - b)f_c}{1 - (1 - b)f_c}$$

The physical meaning of b is the fraction of fines which actively participates in the force structure. A gradual increase in the contribution of fines in the force structure can be reflected by setting b in the range of 0-1.

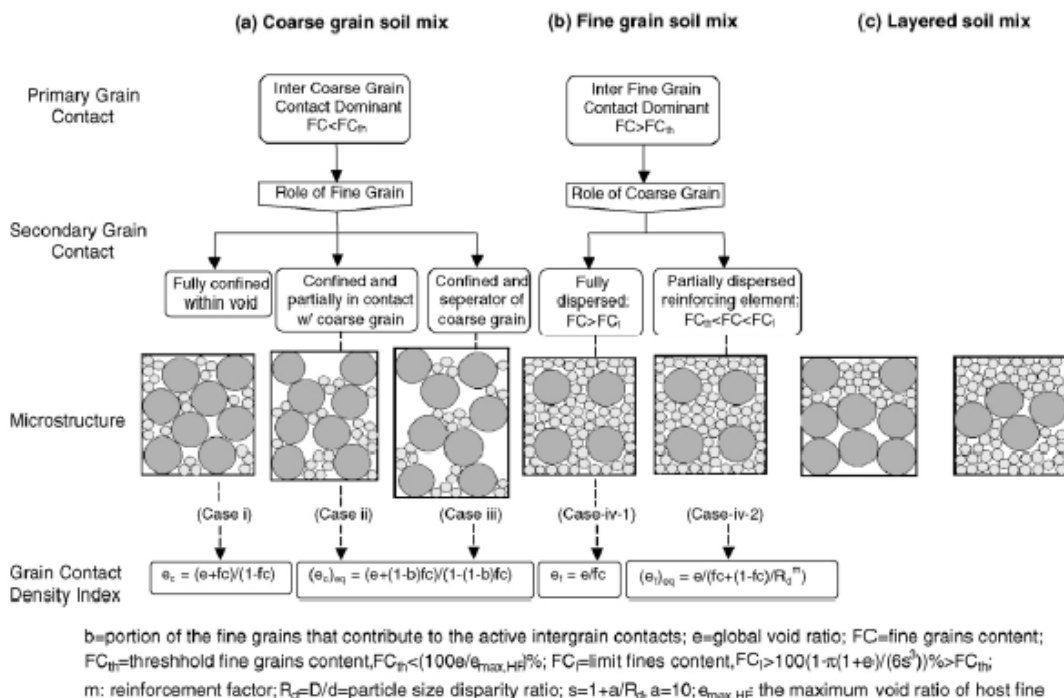


Figure 1.22 - Different granular structures of sand – fines mixture (Thevayanagam & Martin 2002)

The successful application of the equivalent intergranular void ratio have been discussed in the literature by (Thevanayagam 2002) and (Ni et al. 2004).

It is interesting to note that  $e^{eq}$  has also been referred to by different authors under different names such as equivalent granular void ratio, contact index void ratio, equivalent

intergranular contact index and equivalent granular void ratio. For simplicity, the term equivalent granular void ratio will be used.

However, the prediction of the b value, and thus the determination of the equivalent granular void ratio is problematic and controversial. Some researchers assumed b independent of fines content and determined b for a given sand-fines type by a back analysis process (Ni et al. 2004). Thevanayagam and Martin (2002) reported that b=0.35 for Ottawa sand-silt mixture, and Ni et al. (2004) reported b=0.25 for Toyoura sand-silt mixture.

On the other hand, Rahman et al. (2008) has examined the factors affecting the b value based on published work in which that led him to a semi-empirical equation for predicting the b value based on fines size and fines content.

$$b = [1 - \exp(-0.3 \frac{f_c/f_{thre}}{k})] (r \frac{f_c}{f_{thre}})^r \quad (1.6)$$

Where  $k = (1-r^{0.25})$  and  $r=d_{50}/D_{10}$  where  $d_{50}$  is the fines particle diameter at 50% finer and  $D_{10}$  is the sand particle diameter at 10% finer. Thus k and r can be obtained from the grading curves. The other input parameter,  $f_{thre}$ , is the threshold fines content or limiting fines content defined previously.

### **1.5.2 Influence of the non-plastic fines content on the initiation of instability**

According to the literature review, there are different approaches in order to understand the behavior of silty sands, for example: evaluation in terms of global void ratio, intergranular void ratio, equivalent intergranular void ratio, the specific relative density and several other parameters. It is noted that the evaluation of liquefaction differs from one parameter to another, a good evidence has been presented by Karim et al. (2014) who has showed the different cyclic behavior as a function of the evaluating parameter based on published data of several authors (see figure 1.23). However, these results will be explained in detail in the following paragraphs.

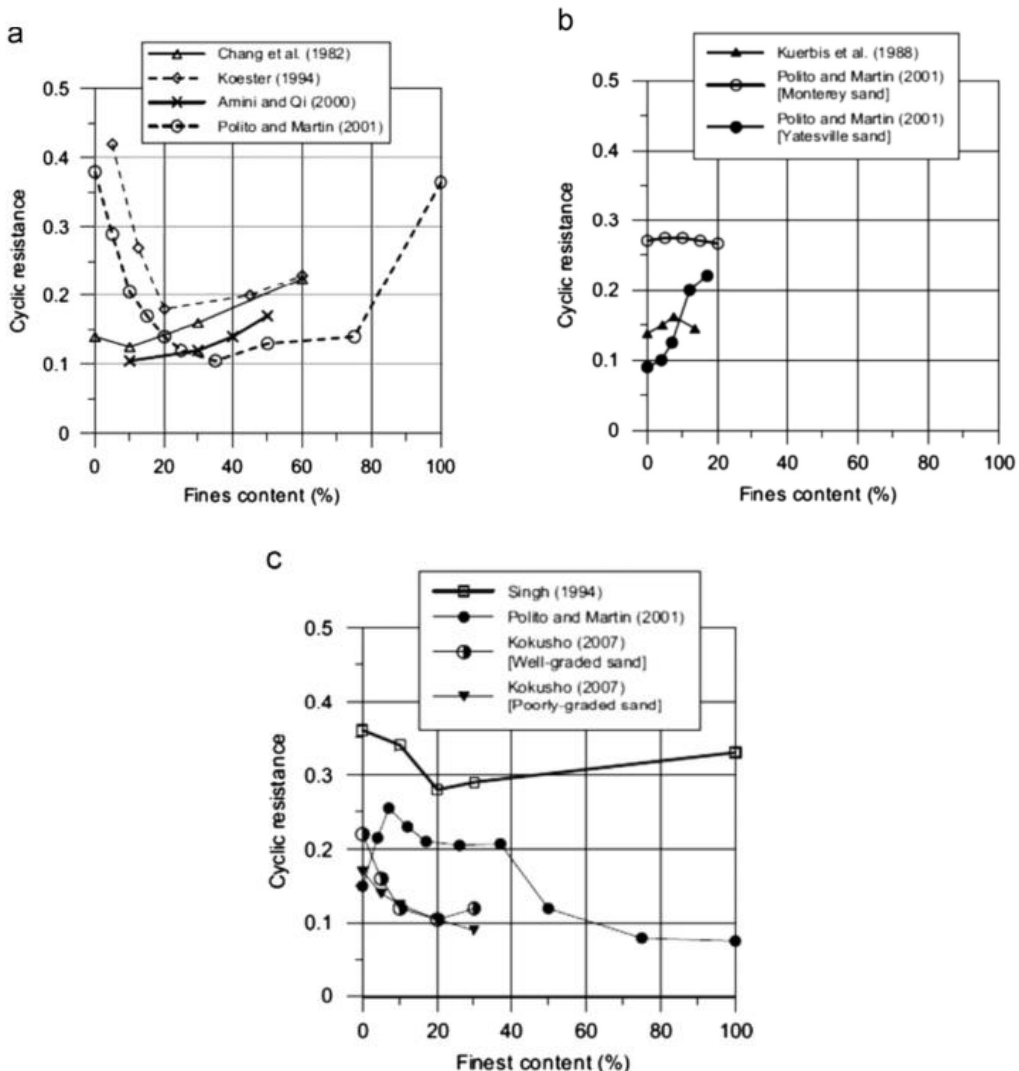


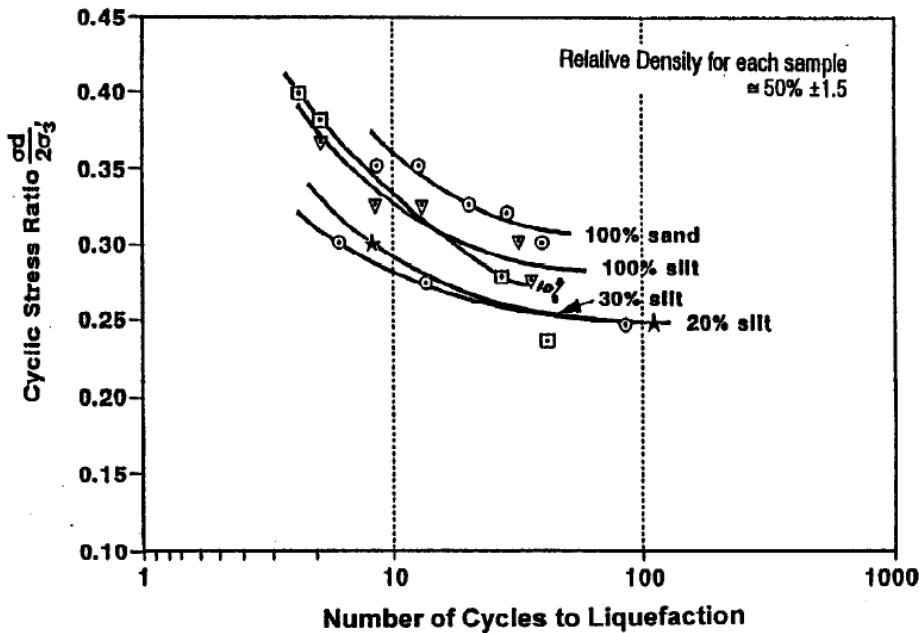
**Figure 1.23 - Results from previous studies on the effect of fines content (fc) on cyclic resistance: (a) studies at constant overall void ratio; (b) studies at constant sand skeleton void ratio; and (c) studies at constant relative density (Karim *et al.*, 2014)**

### 1.5.2.1 Evaluation in terms of global void ratio

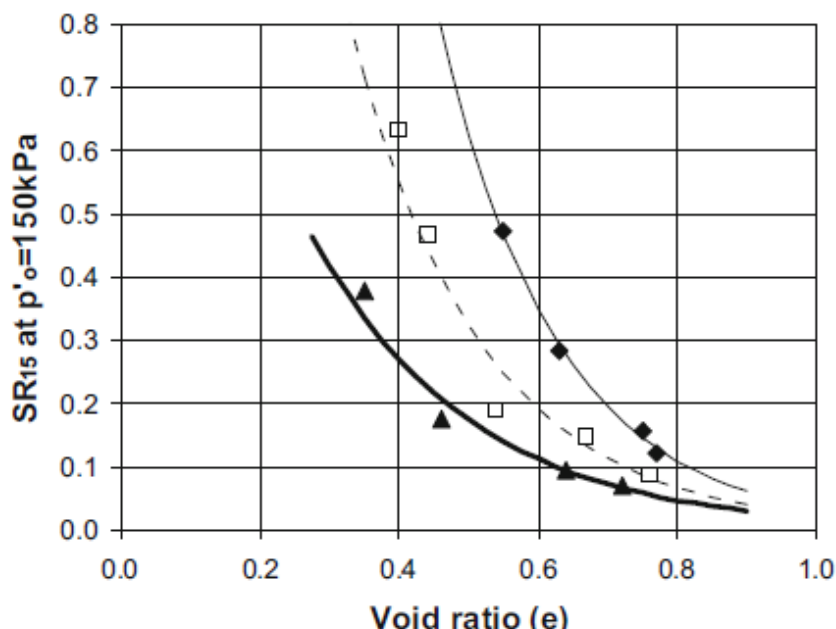
Based on the results obtained by several authors concerning the effect of fines content on the cyclic liquefaction potential, the literature review shows contradictory results concerning this subject.

- Some authors have reported an increase in the cyclic resistance with the increase in fines content (Amini and Qi, 2000; Chang *et al.* 1982, Dezfulian 1982), (figure 1.24a)
- Belkhatir *et al.*, 2010; Stamatopoulos, 2010 and Carraro *et al.*, 2003 have reported a decrease in the cyclic resistance with the increase in fines content, (figure 1.24 b)

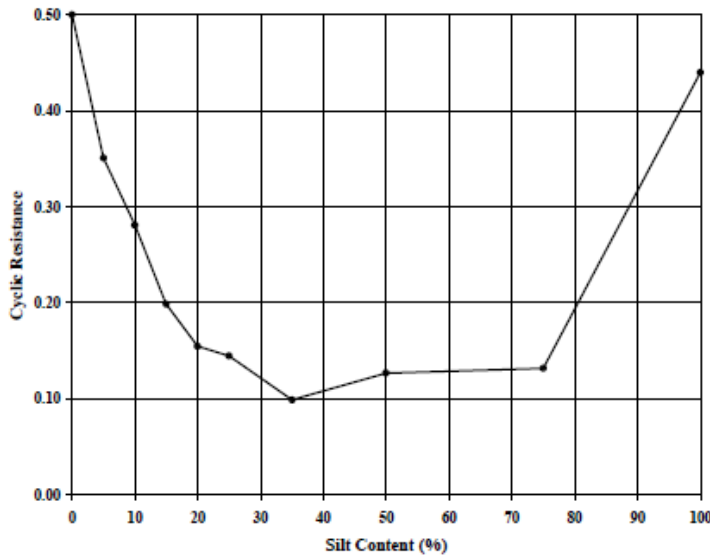
- Several authors have reported a decrease in the resistance until a certain limiting value and then an increase (Koester, 1994; Polito, 1999; Xenaki and Athanasopoulos, 2003; Papadopoulou and Tika, 2008) figure (1.24 c).



(a) Chang et al., (1982)



(b) Stamatopoulos (2010)



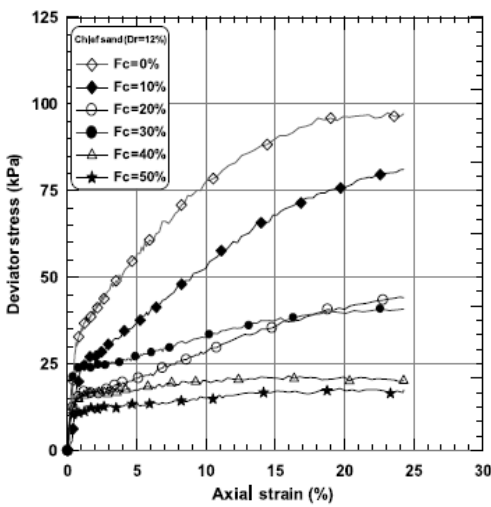
(c) : Polito, (1999)

**Figure 1.24 - Influence of the fines content on the cyclic liquefaction resistance**

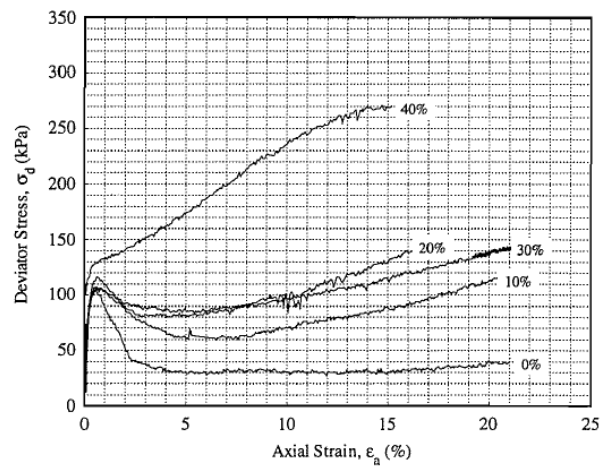
In addition to the cyclic tests, many authors have studied the influence of fines content on the mechanical behavior of silty sands based on static monotonic tests. Belkhatir *et al.* (2010) have noticed a decrease in the deviatoric stress at peak with the increase in fines content up to 50% of fines (see figure 1.25 a). Whereas Pitman *et al.* (1994) have recorded that adding up to 40% of fines makes the silty-sand mixture more resistant (figure 1.25 b). On the other hand, Naeini et Baziar (2004), Yang *et al.* (2006 a) and Dash et Sitharam (2011) have observed that the deviatoric stress at peak decreases until a certain value of fines content is reached, which is the threshold value, and then it increases after that with the addition of fines (figure 1.25 c). This result has been recorded by other researchers that have evaluated liquefaction resistance in terms of other parameters such as pore pressure and instability line. Nguyen (2014) has presented a comparison between 2 groups of tests compared either at constant global void ratio or at constant intergranular void ratio. For the group of tests performed at a constant global void ratio, he presented results of tests with a fines content that ranges between 0% and 20%. He noted that the mechanical response with the variation of fines content is similar for all curves (contractant). Also, he has observed that for fines content of 5% the behavior of the specimen resembles that of a clean sand. Whereas, beyond 10% the shear resistance of the mixture starts to increase with the increase in fines content (figure 1.25 d).

Erten and Maher (1995) and Maheshwari and Patel (2010) have shown that upon increasing the fines content the generation of EPWP increases until the critical fines content value and then it decreases. Papadopoulou and Tika (2008), have reported that the instability line is at first directed downwards and after the fines content exceeds the limiting value it inverts upwards.

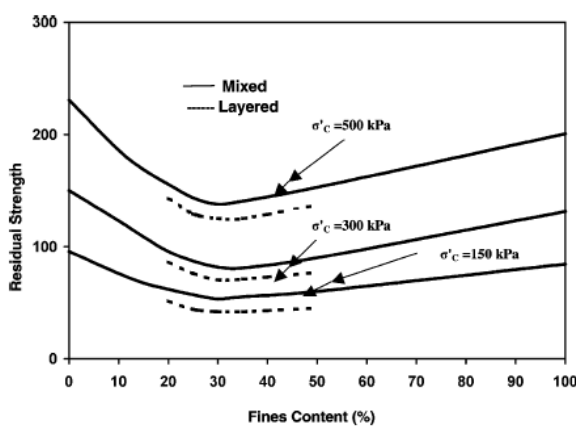
As the global void ratio is not a reliable parameter that detects the mechanical behavior of silty sands, several approaches were used in order to study the behavior of this material.



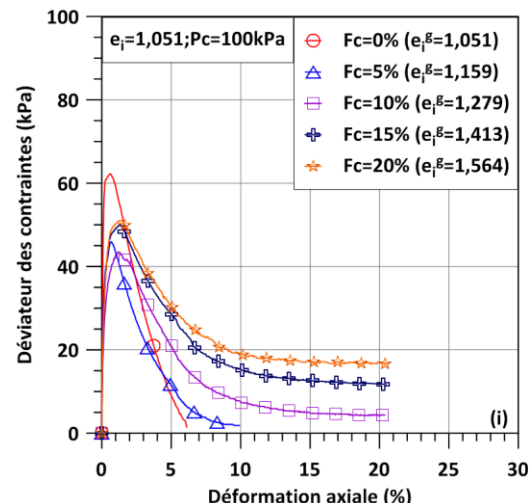
(a) Belkhatir *et al.*, (2010)



(b) Pitman *et al.*, (1994)



(c) Naeini and Baziar, (1994)



(d) Nguyen, (2014)

**Figure 1.25 - Influence of fines content on the static liquefaction resistance**

### 1.5.2.2 Evaluation in terms of specific relative density

Polito et Martin II (2003) have reported that there exist a strong relationship between the specific relative density and the shear resistance at the initiation of instability (see figure 1.26).

Polito (1999) have reported that for soils with silt content below the LSC (limiting silt content) there is a nearly linear relationship between soil specific relative density and cyclic resistance. Below the LSC, the cyclic resistance of the soil is independent of silt content, increasing with the increase in specific relative density. However, above limiting silt content, the cyclic resistance varies with the silt fraction void ratio, increases with the decrease in the silt fraction void ratio and is independent of the amount of sand present (see figure 1.27).

Dash and Sitharam (2011) have tested samples of same relative density with a percentage of fines that vary between 0 and 100% and they observed that the maximum shear stress decreases until the fines content reaches 20% and then becomes constant.

On the other hand, Kuerbis et al. (1988) showed that for a given relative density the cyclic resistance decreases as the fines content increases up to 21%.

Sadrekarimi (2013) has noticed that for  $10\% < FC < 30\%$ ,  $S_u$  (critical)/ $\sigma'_{nc}$  decreases with increasing FC at a given  $D_r$ . However, this trend is reversed for  $FC < 10\%$  and  $FC > 30\%$ , where  $S_u$  (critical)/ $\sigma'_{nc}$  increases with the increase in FC.

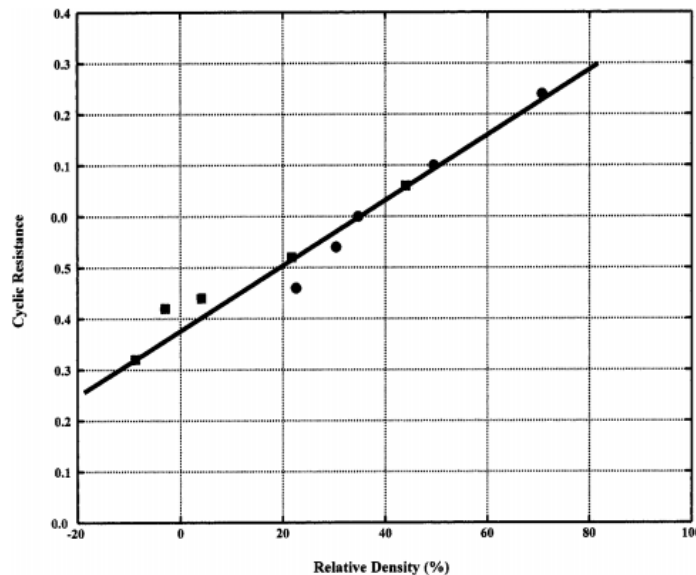
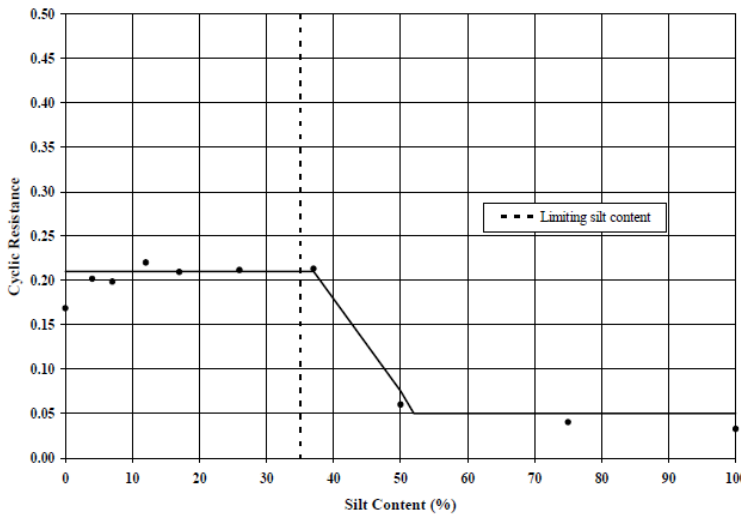


Figure 1.26 - Variation in cyclic resistance with relative density (Polito and Martin II, 2003)



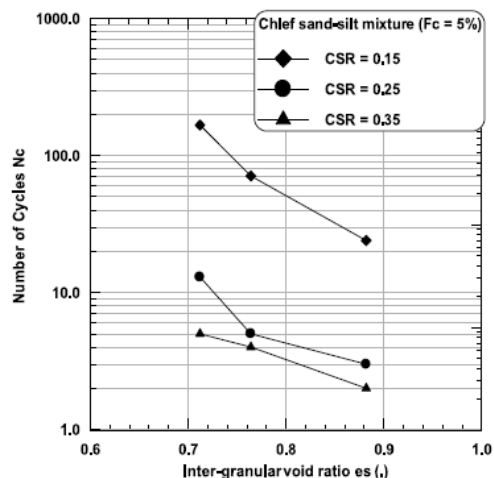
**Figure 1.27 - Variation in cyclic resistance with silt content for Yatesville sand specimens adjusted to 25% soil specific relative density (Polito, 1999)**

### 1.5.2.3 Evaluation in terms of intergranular void ratio

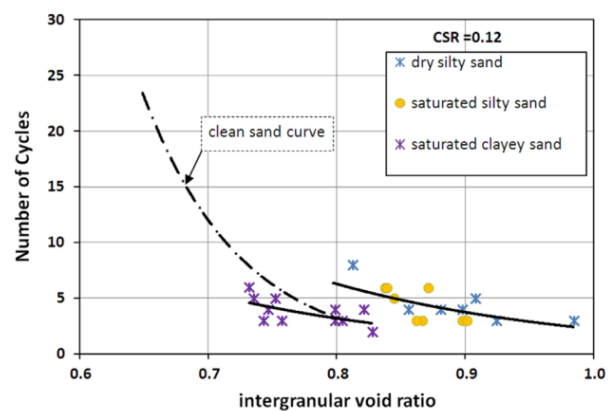
As we mentioned before that authors have evaluated liquefaction phenomenon depending on different parameters, some authors have realized that the intergranular void ratio is a reliable parameter that affects the liquefaction resistance of sands containing fines. Belkhatir *et al.* (2010) and Monkul *et al.* (2015) have observed that the liquefaction resistance decreases with the increase in intergranular void ratio. Actually they related this to the fact that by increasing the fines content in the range of 0-50%, the contact between the sand grains decreases and therefore the intergranular void ratio increases and consequently results in the decrease of the undrained shear strength. These results are shown in figures 1.28a and 1.28b respectively. Also he noted that samples sheared with high cyclic stress ratio CSR are more vulnerable to liquefaction than those sheared with smaller loading level.

On the other hand, Kuerbis *et al.* (1988), Xenaki and Athanasopoulos (2003), Papadopoulou and Tika (2008) and Stamatopoulos (2010) have shown that the cyclic resistance increases with the increase in fines content. Polito (1999) has performed cyclic tests for two different types of sand. He noticed that for a given intergranular void ratio, with the increase in fines percentage, the cyclic resistance of Yatesville sand increases whereas the one of Monterey sand remains constant (figures 1.28c and 1.28d). Ni *et al.* (2004) observed that the deviatoric stress at peak for a constant intergranular void ratio could either increase or decrease whether the fine used is plastic or non-plastic respectively. On the other hand, Benahmed *et al.* (2016) performed a series of monotonic tests on sand-silt mixtures at a constant initial intergranular

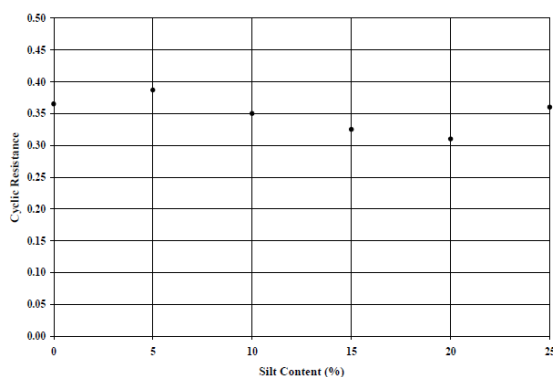
void ratio. They noted that the peak strength decreases for fines content below 5% where the fine particles are considered completely inactive. However, the peak strength starts to increase steadily as the fines content increases from 5 to 15% due to the fact that at higher fines content, the fine particles contribute to the overall chain forces and control the behavior of the soil (figure 1.29). These results are compatible with those obtained by Benghalia *et al.*, (2011) who studied the effect of fines content on the cyclic behavior of Oued Chlef sand at a constant intergranular void ratio for fines content values ranging between 0 and 15%. He noted that the number of cycles to liquefaction decreases with an increase in  $F_c$  to 5% then it increases again and he realized that this effect is more obvious for smaller values of densities (figure 1.30a). Moreover, he noticed that clean sand behaves like a natural sand containing 10% fines for a density index of 0.5. Whereas, clean sand shows a more resistant behavior than sand-fine mixture for a low density index 0.15 (figure 1.30b).



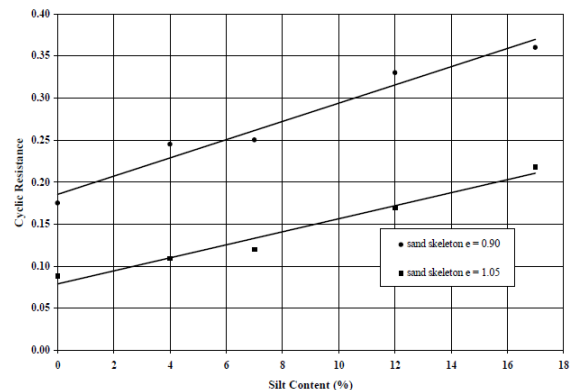
(a) after Belkhatir *et al.*, (2010)



(b) Monkul *et al.*, (2015)



(c) Monterey sand



(d) Yatseville sand

**Figure 1.28: Variation of cyclic resistance as a function of intergranular void ratio**

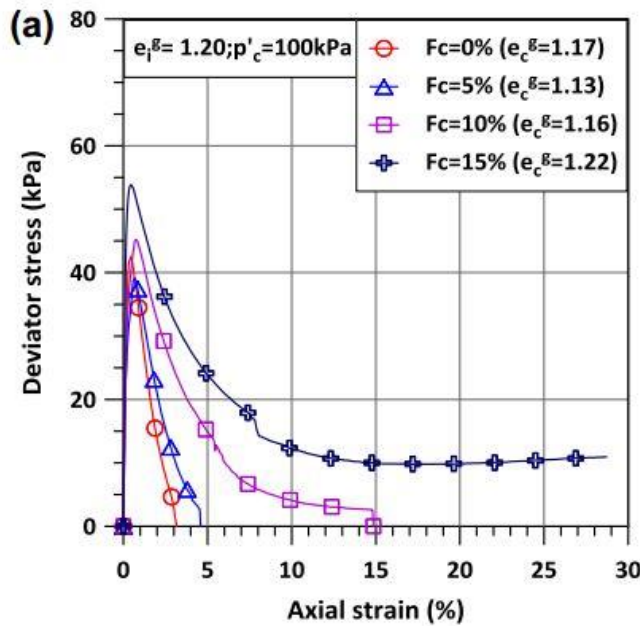


**Figure 1.29 - Effect of fines content on mechanical behavior of sand at constant intergranular void ratio**  
Benahmed et al., (2016)

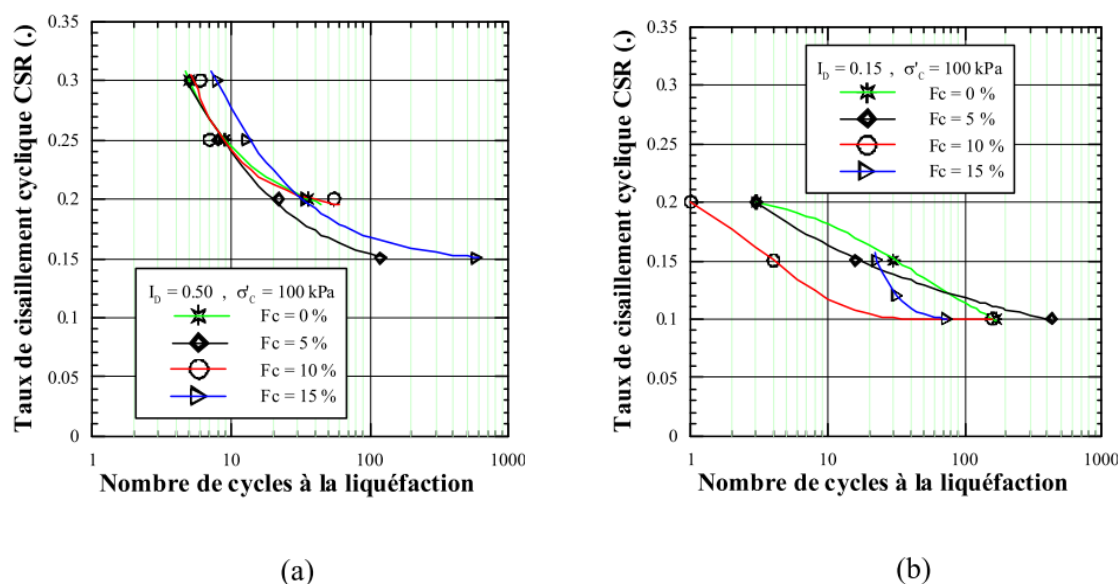


**Figure 1.30 - Influence of fines content on the cyclic shear resistance: (a)  $I_d = 0.5$ ; (b)  $I_d = 0.15$  (Benghalia et al., 2011)**

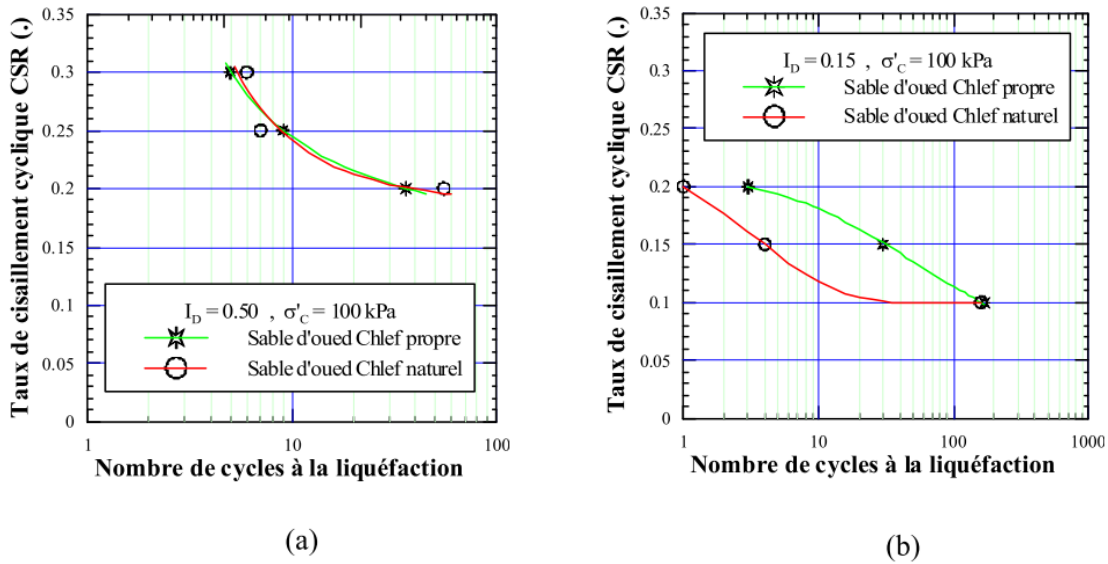


**Figure 1.31 - Influence of density index on the cyclic shear resistance of sand: (a) ID= 0.5; (b) ID= 0.15**  
**(Benghalia et al., 2011)**

#### 1.5.2.4 Evaluation in terms of equivalent granular void ratio

Recent publications show that void ratio may not be a good state parameter for characterizing sand with fines. An alternative state parameter, referred to as the equivalent granular void ratio, has been proposed to resolve this problem.

According to Ni *et al.* (2004) there exists a very good correlation between the shear resistance and the equivalent granular void ratio (figure 1.32a).

Yang *et al.* (2006b) have obtained a linear relationship between the deviatoric stress at peak and the equivalent granular void ratio independent of the percentage of fines up to a value below the limiting fines content (figure 1.32b).

Rahman *et al.* (2008) have interpreted the results obtained by other authors from the literature review and these interpretations have indicated that the equivalent granular void ratio controls the liquefaction resistance independently of any other factors (figure 1.32c).

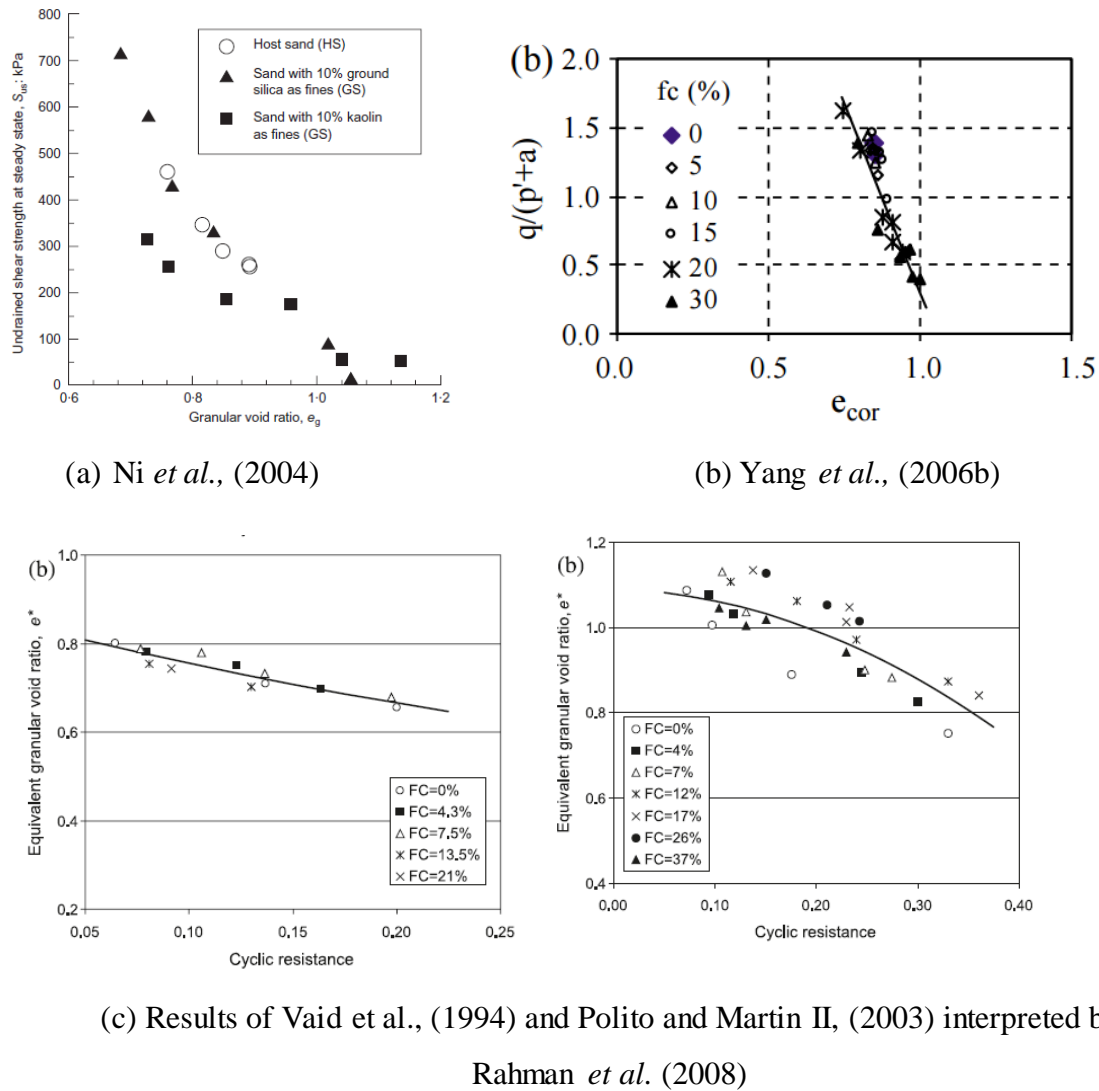


**Figure 1.32 - Analysis of the behavior of silty sands in terms of equivalent granular void ratio**

### 1.5.2.5 Evaluation in terms of state parameter

The state parameter is a physical parameter that combines the influence of void ratio and stress level with reference to an ultimate (steady) state to describe sand behavior. It is defined as the void ratio difference between the initial sand state and the steady state condition at the same mean effective stress (figure 1.33).

In an attempt to interpret the effect of consolidation stress and void ratio with a single parameter, Been and Jefferies (1985) introduced the state parameter  $\psi$  defined as:

$$\Psi = e - e_{cs}$$

where  $\psi$  is the state parameter,  $e$  is the void ratio and  $e_{cs}$  is the void ratio of the critical state,

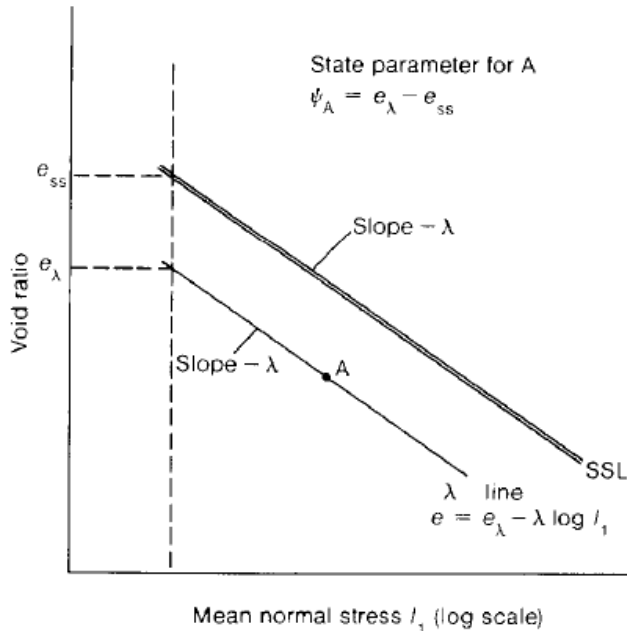


**Figure 1.33 - Definition of state parameter  $\psi$  (Been and Jefferies 1985)**

Chen and Liao (1999) and Stamatopoulos *et al.* (2004) have shown that the relationship between the state parameter and the cyclic strength is approximately linear. Moreover, Stamatopoulos (2010) has also studied the effect of state parameter on the cyclic strength. He has noted that there exists a strong correlation between the cyclic strength and the state parameter. He realized that the cyclic strength decreases as the state parameter increases at a rate that progressively decreases. Also, he indicated that this relationship, for values of fines content less than 25%, is unique and doesn't depend on the fines content (figure 1.34). On the other hand, Sadrekarimi (2013) have studied the effect of fines content on the undrained shear strength in terms of the critical state parameter  $\psi_{cs}$ ; he concluded that the application of the critical state parameter alone for characterizing the influence of FC could be misleading as sand shearing compressibility  $\lambda_{cs}$  also controls  $S_u$  (critical).

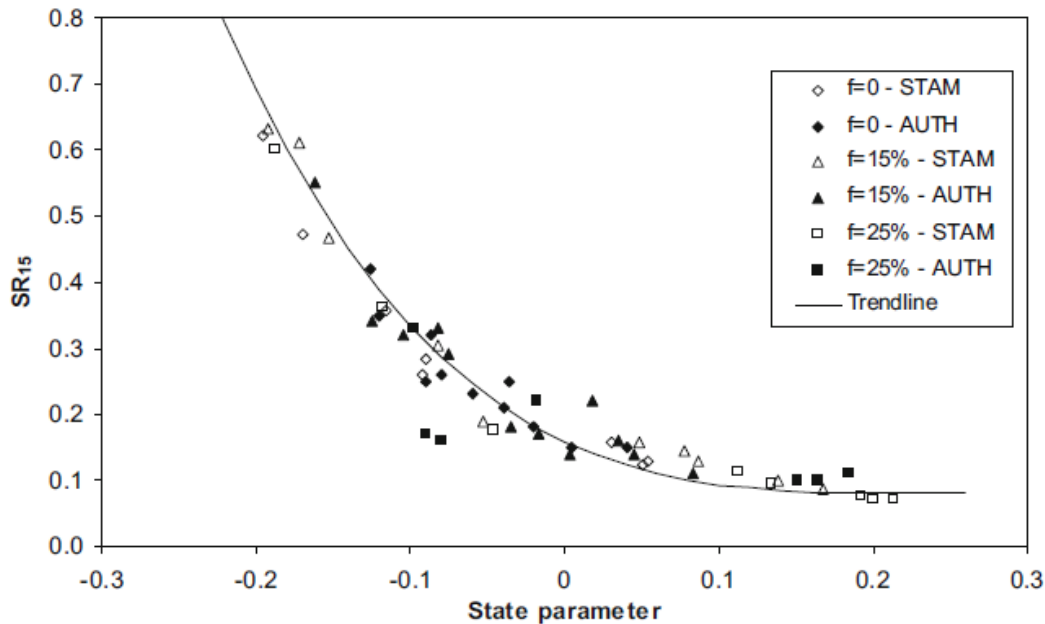


Figure 1.34 - Cyclic strength as a function of state parameter (Stamatopoulos 2010)

Figure 1.35 presents the results of Qadimi and Mohammadi (2014) who studied the capability of six different state indices including  $\psi$ ,  $\psi^*$ ,  $Rs$ ,  $R_s^*$ ,  $\psi_m$ ,  $\psi_m^*$  to predict the cyclic and monotonic strength of various sandy soils over a wide range of fines contents, densities, and stress levels. He defined these parameters as equivalent interparticle parameters to stand for both intergranular and interfines equivalent parameters whether  $fc < fc_{th}$ , or  $fc > fc_{th}$ . He observed that:

- The state indices combine the effect of  $fc$ , density and stress level on the behavior of sands.
- The cyclic and monotonic strengths are strongly correlated with  $\psi$  and  $\psi^*$  through simple exponential functions (see figure 1.35).
- Distribution of the resistance data in terms of  $\psi_m$  and  $\psi_m^*$  are often more scattered than those in terms of other indices.

As a conclusion, he proposed the equivalent interparticle state parameter, that is:

- $\Psi_g^* = e_g^* - e_{gcs}^*$  equivalent intergranular state parameter for  $fc < fc_{th}$
- $\Psi_f^* = e_f^* - e_{fcs}^*$  equivalent interfine state parameter for  $fc > fc_{th}$

as the most preferable state index to predict the cyclic and monotonic strength of sands containing various amounts of fines.

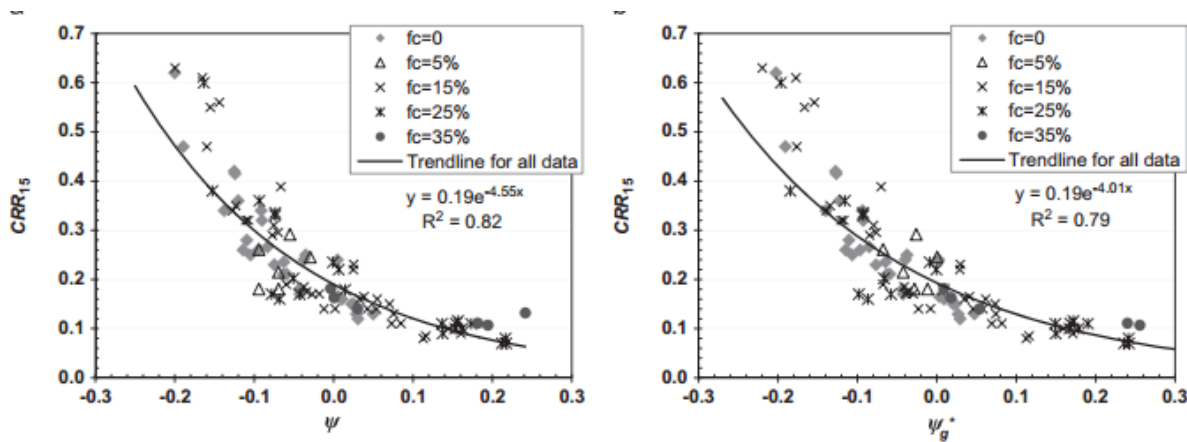


**Figure 1.35 - Cyclic strength of sand with silt for  $fc < f_{th}$  in terms of  $\psi$  and  $\psi g^*$**  (Qadimi & Mohammadi 2014)

### 1.5.2.6 Estimation of liquefaction potential from dry and saturated sandy soils

Since clean sands, silty sands, and clayey sands do not necessarily show identical behavior under seismic loading, Monkul *et al.* (2015) have investigated cyclic simple shear responses of three sandy soils: clean sand (Sile sand), silty sand (Sile sand with 10% IZ silt) and clayey sand (Sile sand with 10% kaolin) to compare the responses of dry and saturated specimens.

Experiments on clean sand specimens demonstrated that liquefaction resistance for both dry and saturated sand specimens can be represented by the same trend curve in a number of cycles versus void ratio diagram (figure 1.36a). This result is compatible with the observation of Finn and Vaid (1977) for Ottawa sand in a constant volume cyclic simple shear condition where they noted that dry and saturated sand specimens showed identical drained constant simple shear behavior.

Similar to the clean sand, Monkul *et al.* (2015) noted that experiments on silty sand specimens demonstrated that liquefaction resistance of both dry and saturated silty sands can be represented by the same trend curve in a number of cycles versus void ratio diagram (see figure 1.36b). Also, it's interesting to mention that for the same amount of decrease in  $e$  (void ratio) the increase in liquefaction resistance for silty sand is smaller than clean sand and this could be interpreted from the figure where the clean sand curve is plotted on the same diagram.

On the other hand, it is very clear from figure 1.36c that unlike the clean sand and sand-silt specimens, the cyclic response of saturated and dry clayey sand specimens are distinctly different. It is observed that saturated clayey sand specimens had considerably greater liquefaction potential compared to the dry ones.

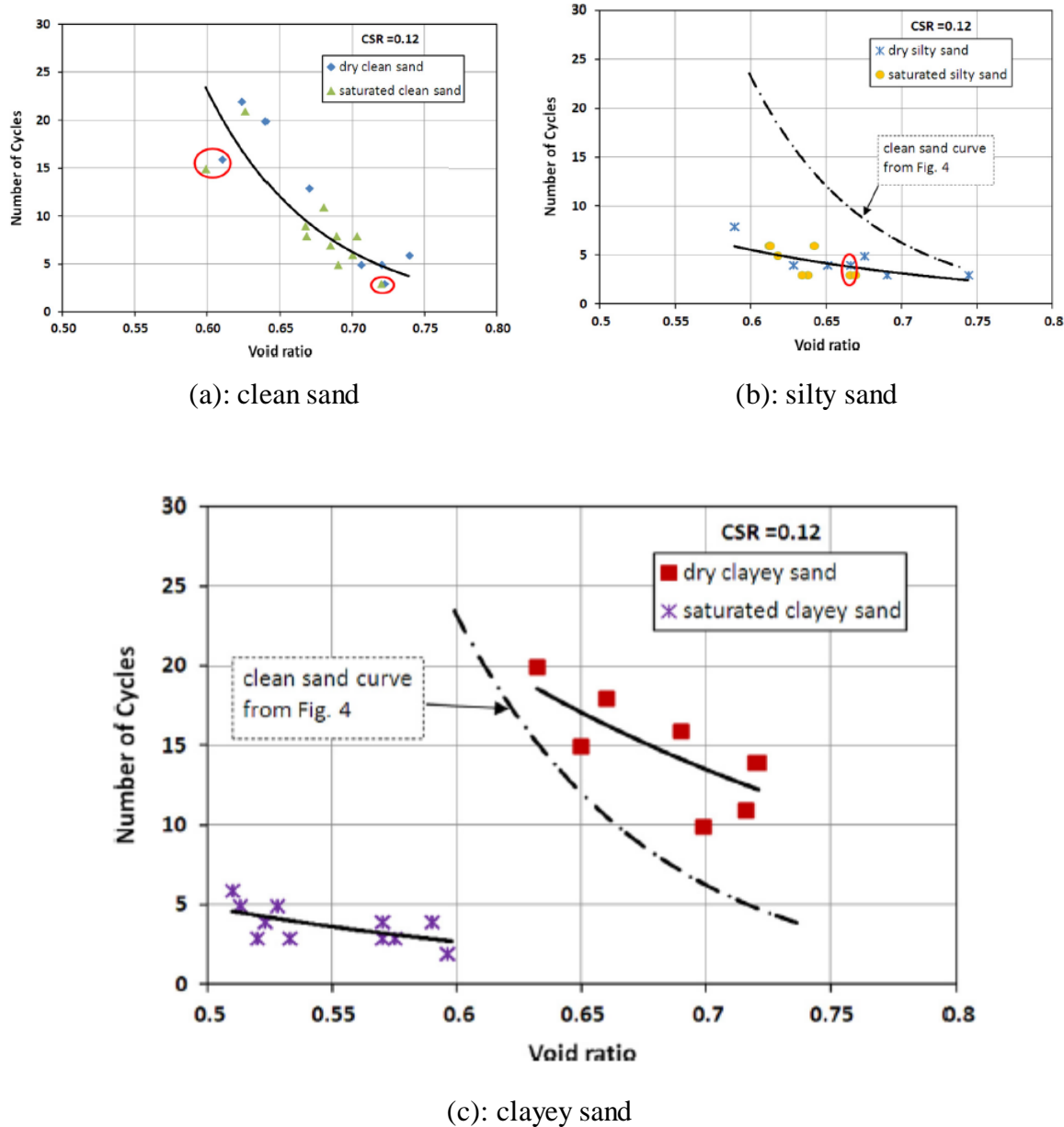


Figure 1.36 - Comparison between dry and saturated sands behavior (Monkul *et al.*, 2015)

### 1.5.3 Influence of the non-plastic fines content on the critical state

#### 1.5.3.1 Definition of the critical state

Critical state soil mechanics (CSSM) is an effective and useful conceptual framework for modelling soil behavior. The main idea of CSSM is that soils upon shearing reach a final state

under a unique combination of effective stresses and void ratio irrespective of the loading history or the stress paths. This state is called the critical state (CS) and it is defined as the state at which the soil continues to deform at constant stress and constant void ratio Roscoe *et al.* (1958).

### **1.5.3.2 Influence of fines content on the friction angle**

Huang *et al.* (2004) have performed a series of undrained tests on reconstituted Mai Liao sand (MLS) with various fine contents ranging between 0 and 50%. They noted that the friction angle is approximately constant with the variation of FC between 0 and 50% (figure 1.37). The same result was reported by Pitman *et al.* (1994) who noticed that the friction angle is equal to  $30^\circ$  for clean sand as well as that for sand with a fines content up to 40%.

Ni *et al.* (2004) did not report any change in friction angle with addition of fines up to 10%. Murthy *et al.* (2007) indicated that the friction angle increases from  $30.2^\circ$  to  $34.4^\circ$  as the fines content increases from 0 to 15% (see figure 1.38). Also, Yang *et al.* (2006c) have noted an increase in friction angle from  $37.3^\circ$  to  $42.2^\circ$  as the fines content varies between 0 and 94%.

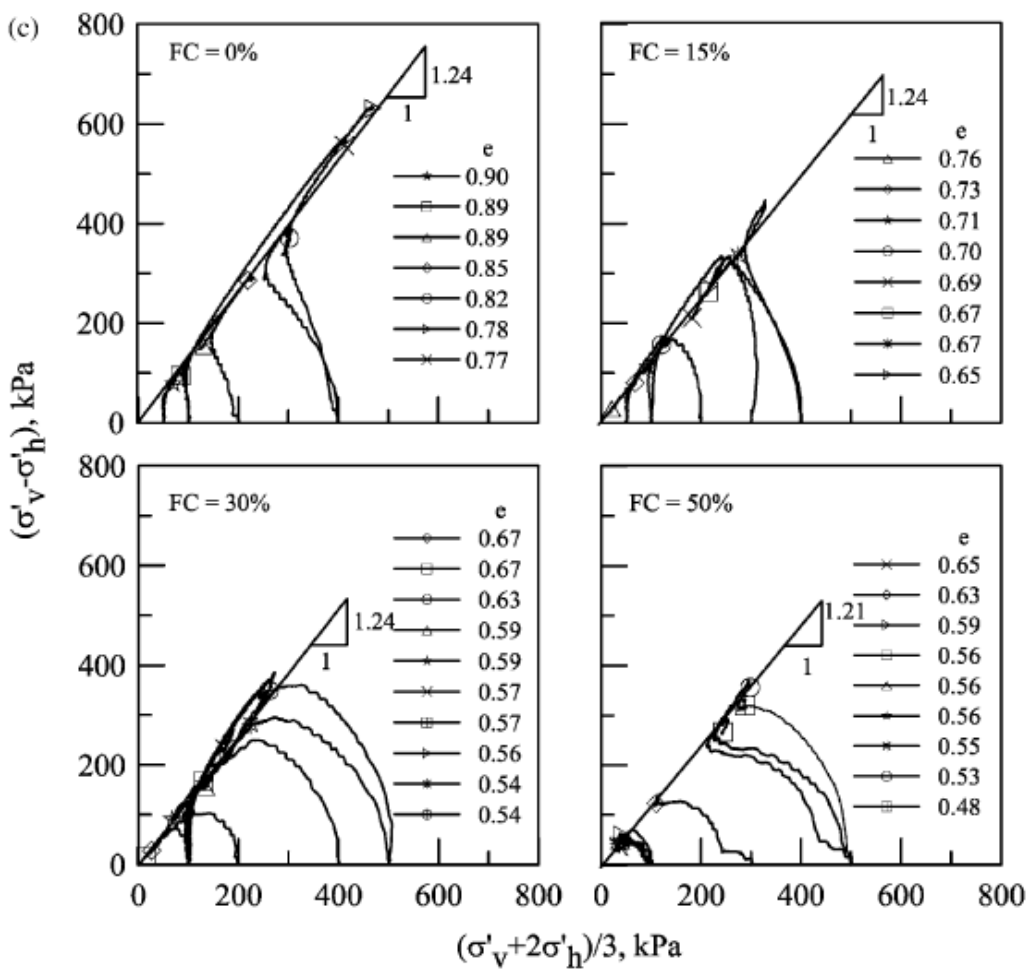
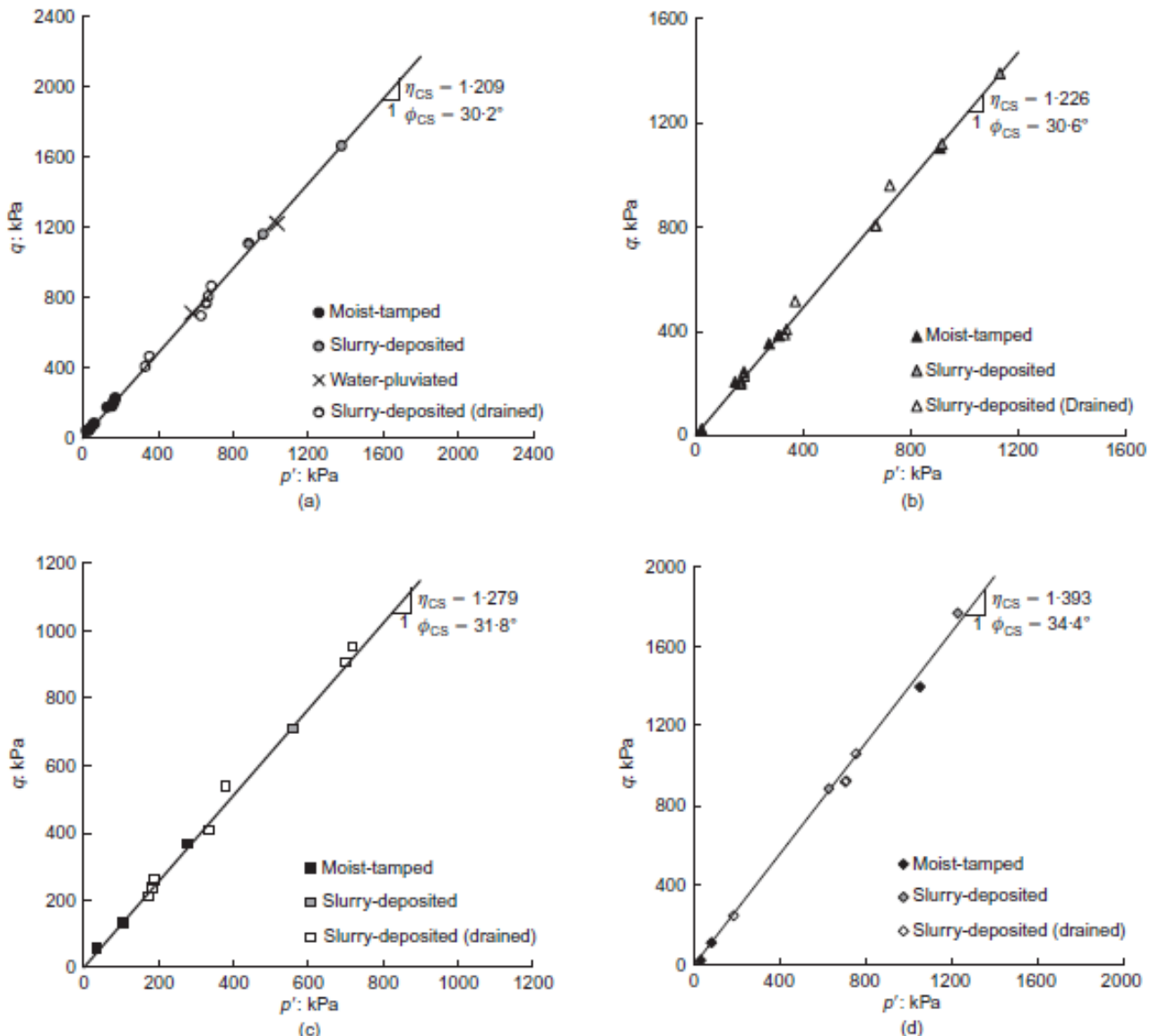


Figure 1.37 - Influence of fines content on the friction angle (Huang *et al.* 2004)

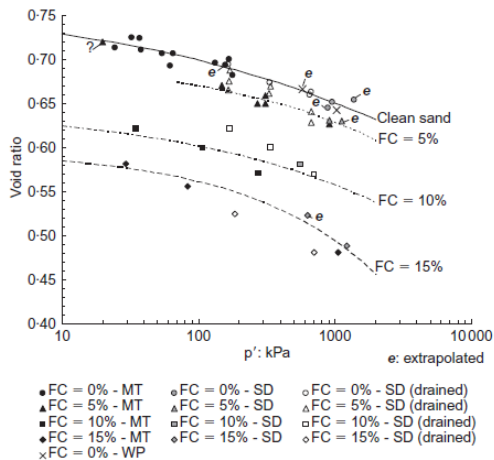


**Figure 1.38 - Influence of fines content on friction angle : (a) 0%, (b) 5%, (c) 10%, (d) 15%** (Murthy *et. al* 2007)

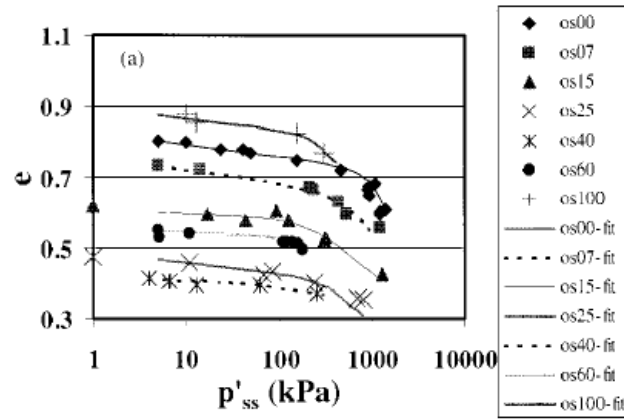
### 1.5.3.3 Influence of the fines content on the critical state line

Murthy *et al.* (2007) performed a series on undrained monotonic triaxial compression tests on Ottawa sand containing 0%, 5%, 10% and 15% of non-plastic silt. It is observed that an increase in the non-plastic fines content leads to a downward shift of the critical state line in the void ratio-mean effective stress space (figure 1.39). Thevanayagam *et al.* 2002; Naeini and Baziar, 2004; Yang *et al.* 2006c; Papadopoulou and Tika, 2008; Rahman *et al.*, 2008 and Stamatopoulos, 2010 observed that the critical state line shifts downwards with the addition of fines content up to the limiting value and then it inveres upwards after the FC exceeds the limiting value (see figure 1.39).

Yin et.al (2014) has also studied the influence of fines on the evolution of the critical state line. Indeed, they have proposed a model that evaluates the evolution of the CSL with the increase in fines content, and simulates the behavior of Foundry sand-silt mixtures for Fc values ranging between 0% -100% and Ottawa sand-silt mixtures with different fine contents (Fc = 0–50%). They have observed a very good comparison between the model predictions with experimental results.



(a) Murthy *et al.*, (2007)



(b) Thevanayagam *et al.*, (2002)

**Figure 1.39 - Influence of fines content on the CSL**

#### 1.5.4 Influence of plastic fines

After the study of the influence of non-plastic fines on the liquefaction phenomenon, it is also interesting to shed the light on the influence of plastic fines.

Ghahremani and Ghalandarzadeh (2006); Ghahremani *et al.* (2006) tested a mixture of Firouzkoooh sand with a variable fraction of bentonite and kaolinite, their results show that the liquefaction resistance decreases for a fraction between 0-30% and then increases for fine content greater than 30%.

Polito (1999) has performed monotonic and cyclic tests on a mixture of Yatesville sand with fines composed of kaolinite and bentonite. He has observed that the static and cyclic liquefaction resistance decreases as the fines content increases from 0 to 20%.

Bouferra and Shahrour (2004) have also noted the same behavior for a mixture of Hostun sand and kaolinite with a variation of fines content between 0 and 15%. They have observed that as the fines content increases the cyclic resistance decreases (see figure 1.40).

As mentioned before, excess pore water pressure (EPWP) generation initiates liquefaction during earthquakes and it affects the shear strength of soils deposits. Therefore, Derakhshandi

*et al.* (2008) studied the effect of plastic fines (kaolinite) on pore pressure generation in saturated sands. He presented results of cyclic tests performed on a mixture of Monterey sand with fines content that ranges between 0-30%, where he observed that for fines content up to 10% the generation of EPWP is very important and then it is almost stable for fc values between 10-20%. Beyond 20% the excess pore pressure decreases significantly (figure 1.41).

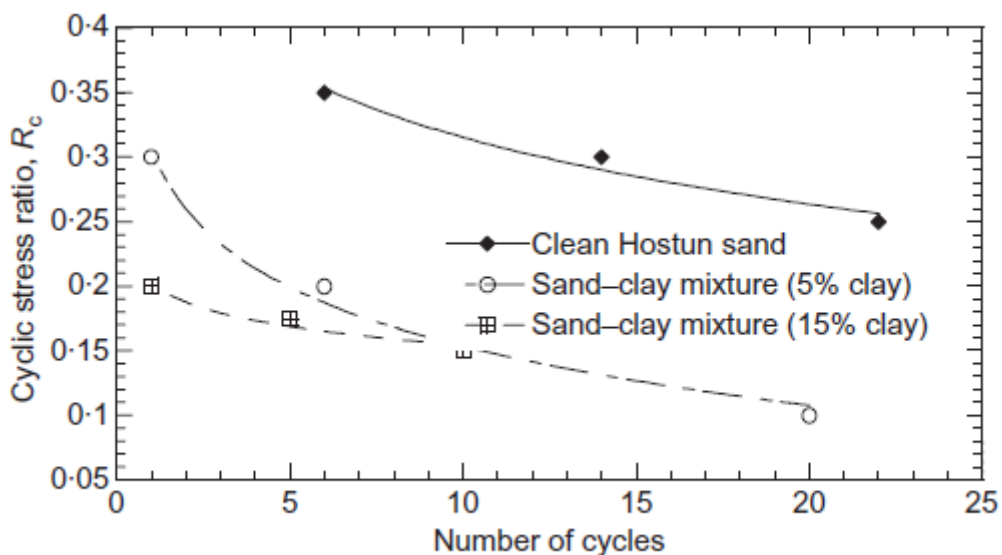


**Figure 1.40 - Influence of fines content on resistance to liquefaction of sand–clay mixture (Bouferra and Shahrour, 2004)**

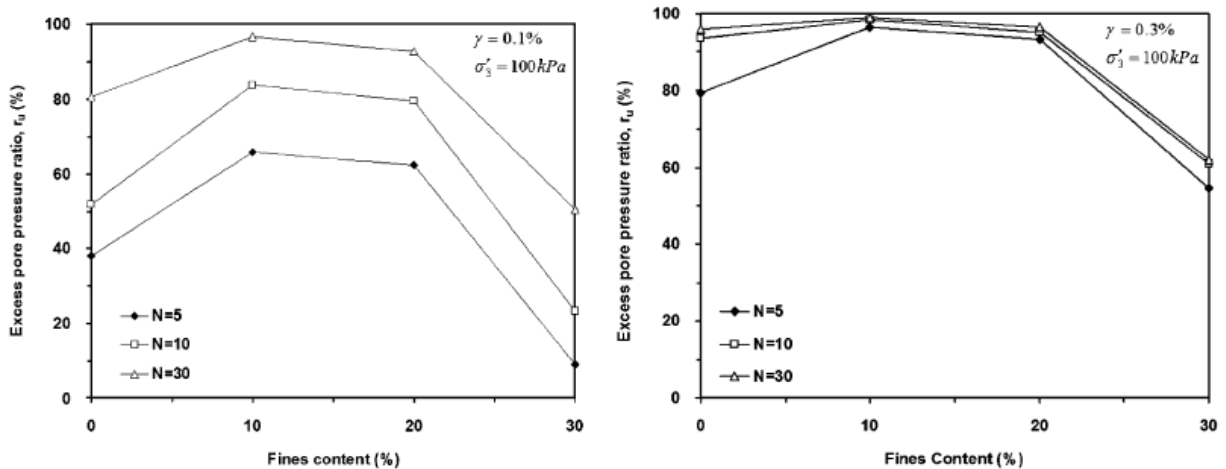


**Figure 1.41 - Influence of plastic fines content on the generation of excess pore water pressure (Derakhshandi 2008)**

Abedi and Yasrobi (2010) tested sand with variation in plastic fines content from 0 to 30%. They have reported that a small increase in amount of fines makes the specimen sustain more instability but with a further increase in the fines content above 10% to 15% the instability decreases.

Concerning the peak strength, it has been noted that the peak strength decreases with all ranges of fines, but its declining rate decreases when  $fc$  exceeds 10% and becomes almost constant after  $fc$  is 20% (figure 1.42). Shelley and Perez also reported the same behavior for samples with small percentages of added kaolin. Abedi et al., (2010) also reported that the instability zone becomes larger with increase in the fines content up to 10%, and after a fines content of 20% it decreases. According to Abedi's results the increase or decrease in the instability zone as a function of fines content is well addressed where the steady state line and the instability line slopes vary with the variation in the fines content.

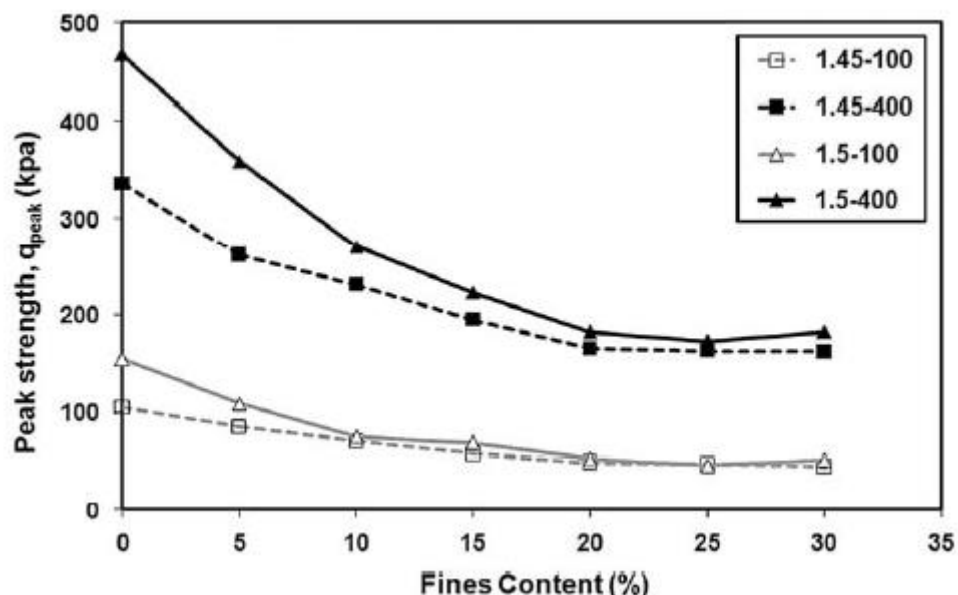


**Figure 1.42 - Variation of peak strength as a function of fines content, (Abedi and Yasrobi 2010)**

## 1.6 Conclusions on literature review

The literature review presented in this chapter has provided a summary of the main studies in the field of sand liquefaction and in particular, the effect of the presence of fine particles on the behavior of these sands with emphasis on the most recent development.

Early studies has focused on the liquefaction of clean sands, however, as sand exists in nature under the form of a mixture of sand and fines and due to recorded case histories of actual soils

(containing fines) behavior during earthquakes, it was realized that the presence of silt and clay particles will in some manner affect the resistance of a sand to liquefaction.

When reviewing the studies published in the literature, no definite and clear conclusion can be drawn as to in which manner altering the fines content affects the liquefaction resistance of a sand under either monotonic or cyclic loading, particularly for the case of soils containing non-plastic fines (silts). This could be explained due to the fact that the mechanical response of silty sands depends on several parameters which aren't often taken into consideration in the analysis of the experiments such as: the type of sand, the grains shape, the range of fines content and their plasticity.... The review of the literature shows that there are several approaches for the analysis of the behavior of silty sands, for example, the global void ratio, inter-granular void ratio, equivalent inter-granular void ratio...

In fact, the literature review has allowed us to orient and delimit the research work developed in this thesis. In particular, we have focused on two important points which are, on one hand, the effect of the presence of low percentages of fines content (less than 5%) on the initiation of the phenomenon of liquefaction under both monotonic and cyclic loading and on the other hand the effect of the plasticity of fines on this behavior (plastic/ non-plastic fines) also for both monotonic and cyclic shear while trying to push further the analogies existing between these two types of loadings.

## 2 Chapter II: Materials, experimental protocols and testing setup

### 2.1 Characterization of the materials studied

The sand used in our study is a reference sand used in different French and European laboratories, which is Fontainebleau sand (NE34). Whereas for the selected fines, we have chosen two types, a non-plastic fine called silica C500 and a plastic one known as kaolinite Speswhite.

### 2.2 Fontainebleau sand

Fontainebleau sand is a fine silica sand ( $\text{SiO}_2 > 98\%$ ) of a light beige color. It is characterized by sub-rounded grains. The shape of its grains is important to mention since it has been shown in the literature that the grains shape presents a very important effect on the susceptibility of the material to liquefaction.

Table 2.1 presents the main characteristics of Fontainebleau sand as given by the supplier. The gradation curve of Fontainebleau sand is presented in figure 2.1. According to this curve Fontainebleau sand can be classified as a uniform fine sand.

Sand	$D_{50}$ ( $\mu\text{m}$ )	$C_U$	$e_{\min}$	$e_{\max}$	$\rho_s$ ( $\text{t/m}^3$ )	$\rho_{d\min}$ ( $\text{t/m}^3$ )	$\rho_{d\max}$ ( $\text{t/m}^3$ )
Fontainebleau	210	1.52	0.54	0.94	2.65	1.37	1.72

Table 2.1 - Characteristics of Fontainebleau sand (Seif El Dine *et al.*, 2010)

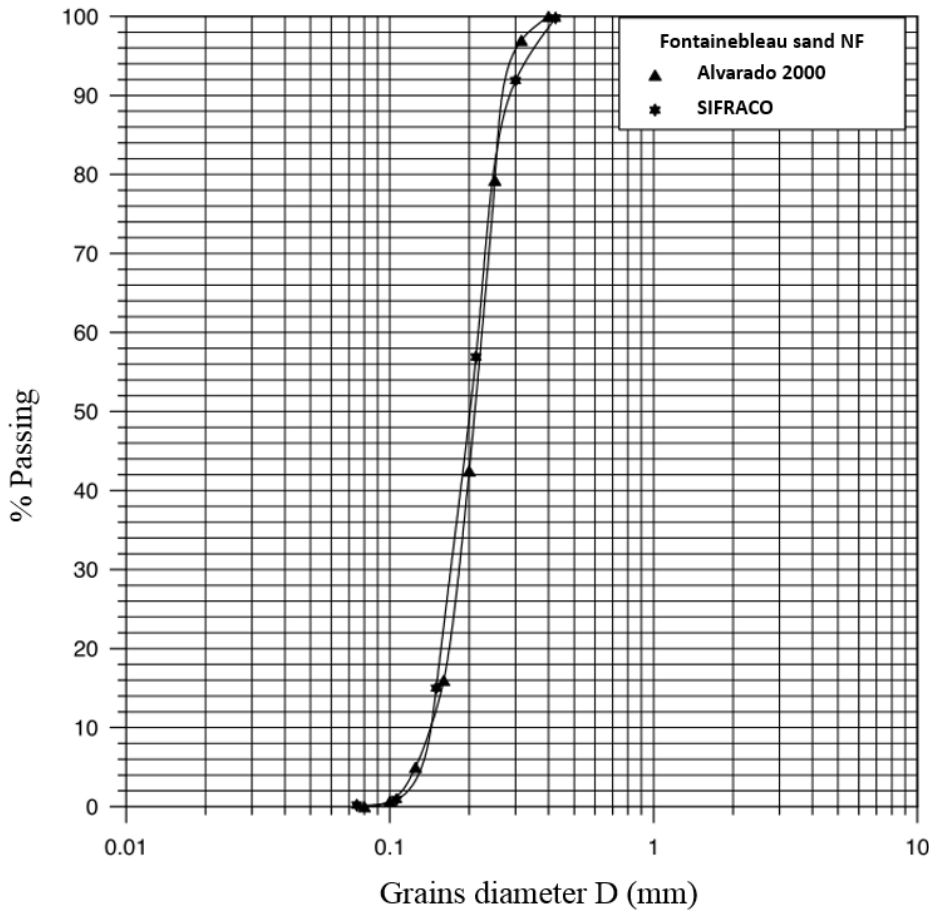


**Figure 2.1 - Gradation curve of Fontainebleau sand, (Benahmed, 2001)**

### 2.2.1 Silica C500

Silica C500 is a fine silica flour ( $\text{SiO}_2 > 99\%$ ) and it has a white color. It is characterized by a sub-angular grain shape. Its density as given by the supplier is equal to  $2.65 \text{ t/m}^3$ . Therefore, this material is very similar in physical properties to that of the Fontainebleau sand. The gradation curve of silica flour C500, given by the supplier, is presented in figure 2.2.

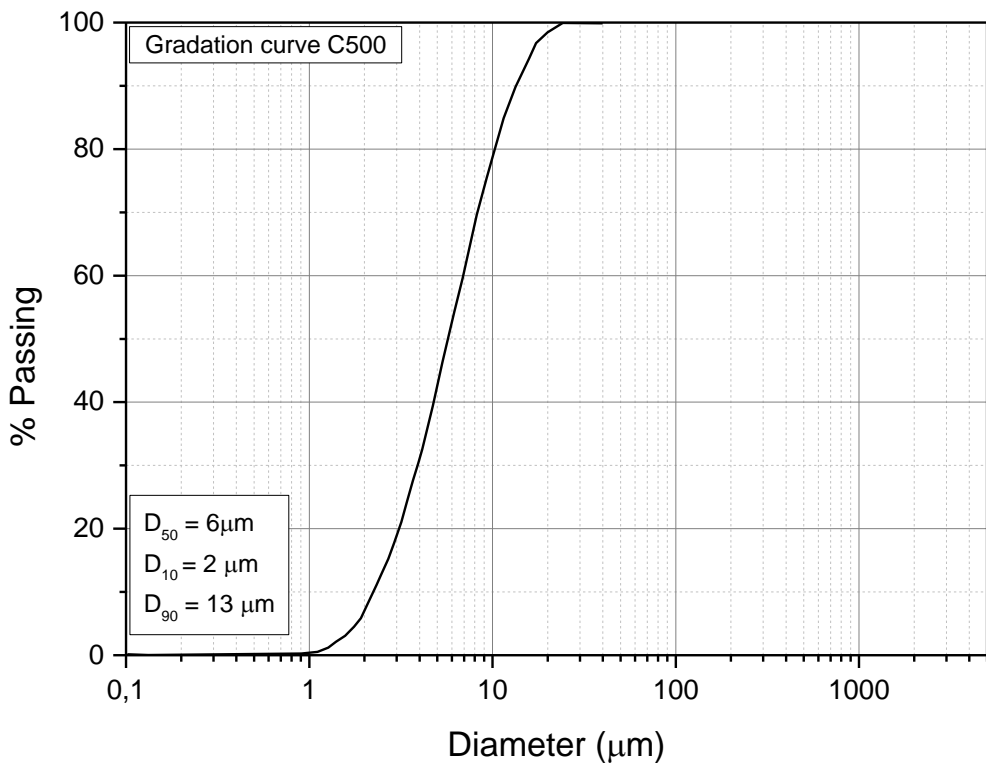


Figure 2.2 - Gradation curve of Silica flour C500

### 2.2.2 Kaolinite Speswhite

Speswhite is a low plastic clay of the kaolinite type that is frequently used in the geotechnical field and in laboratory tests as a reference clay. It is generally considered as a reference material in laboratories in France and all over the world.

Kaolinite is composed of hydrated aluminum silicates ( $\text{Si}_4\text{O}_{10}\text{Al}_4(\text{OH})_2$ ). Its microstructure consists of sheet of silica and sheet of alumina. The kaolinite particles are particularly stable and kaolinite is frequently used because its permeability is quite high compared to other types of clay. The consolidation phase is therefore quite fast. In addition, kaolinite does not swell in the presence of water (inactive clay).

The gradation curve of Speswhite is presented in figure 2.3. It may be observed that 98% of particles are smaller than 10 μm in size, and besides 76 to 83% of particles have a size less than 2 μm.

The physical characteristics of Speswhite are also presented in table 2.2. It is observed that the liquidity limit is of the order of 58% and the plasticity limit is equal to 28% which results in a plasticity index of 30%.

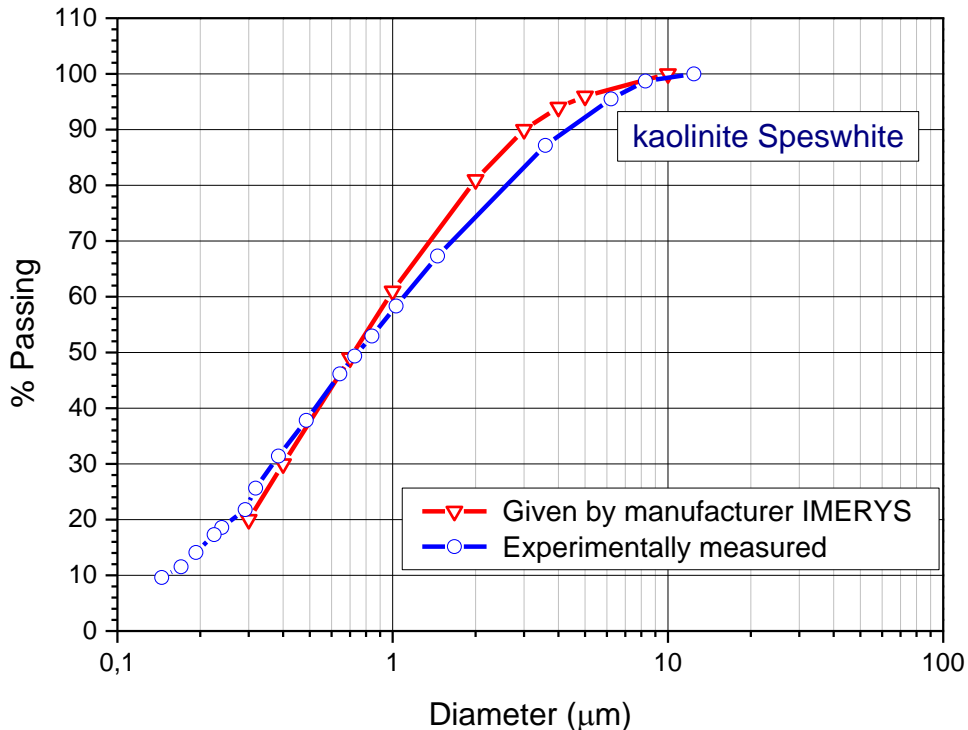


Figure 2.3 - Gradation curve of kaolinite Speswhite (Muhammed, 2015)

Material	Liquid limit $w_L$ (%)	Plastic limit $w_p$ (%)	Plasticity index $I_p$ (%)	Density $\rho_s$ (t/m <sup>3</sup> )	Percentage less than 80 $\mu\text{m}$
Kaolinite	58	28	30	2.64	98

Table 2.2 - Characteristics of kaolinite Speswhite (Muhammed 2015)

### 2.3 Triaxial testing

The triaxial test is one of the most performed tests in the geotechnical field where this device allows the characterization of soil or rock by determining their shear strength and stiffness. The advantage of the triaxial testing is found in its ability to control the specimen drainage and the measurement of pore water pressure. The mechanical characteristics that can be computed using the triaxial test include the Mohr Coulomb friction angle  $\phi'$ , the apparent

cohesion  $c'$ , undrained shear strength  $c_u$  and other parameters such as Young modulus  $E$  (or shear stiffness  $G$ ).

### 2.3.1 Triaxial device $\Phi 100$ mm

A new triaxial device has been developed by the geotechnical team of NAVIER laboratory in order to study the mechanical behavior of soils. This triaxial apparatus involves placing a cylindrical specimen of soil of 100 mm in diameter and 200 mm in height into a cell that allows the consolidation and the shear of the specimen. This device allows to run both monotonic and cyclic loading by controlling either the displacement or the force using a 25 kN hydraulic actuator. A schematic diagram of this device is shown below in figure 2.4.

This device consists of the following elements

- a triaxial cell that rests on a slab (83 cm x 55 cm) fitted with a two column loading frame (figure 2.5a);
- a rigid cylindrical metal base pierced with different pipes to ensure the passage of fluids between the inside and the outside of the cell (figure 2.5b);
- an upper metal base, of the same diameter as the specimen and comprising also drainage circuits (figure 2.5b);
- a confinement enclosure composed of several pieces (figure 2.5c);
- a metallic cover having a central passage for the piston (figure 2.5d);
- a piston sliding through the cover with low friction (figure 2.5d);
- Porous stones that ensure drainage of the specimen, they serve as a filter to prevent the intrusion of particles into the drainage circuits of the apparatus.

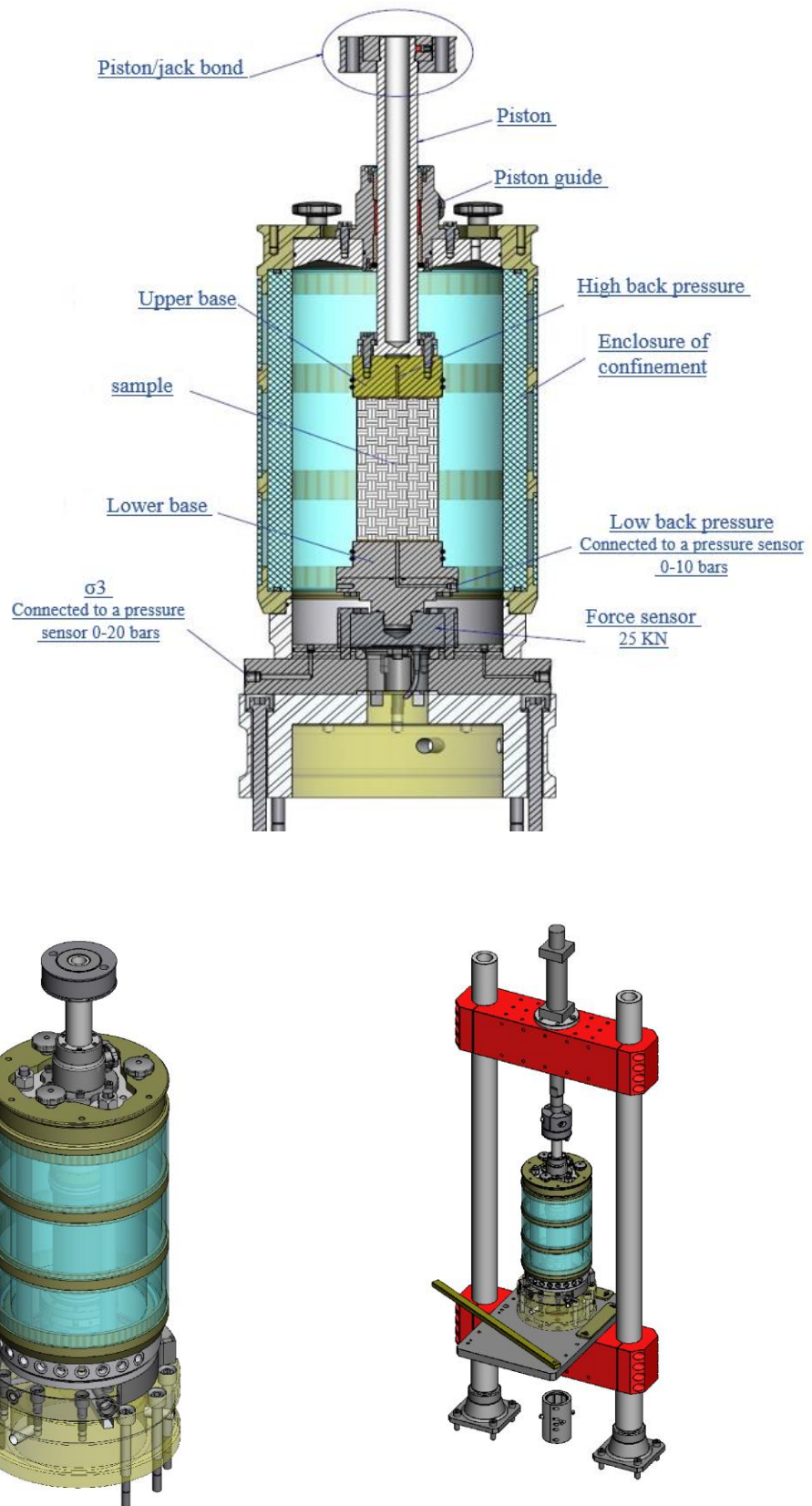
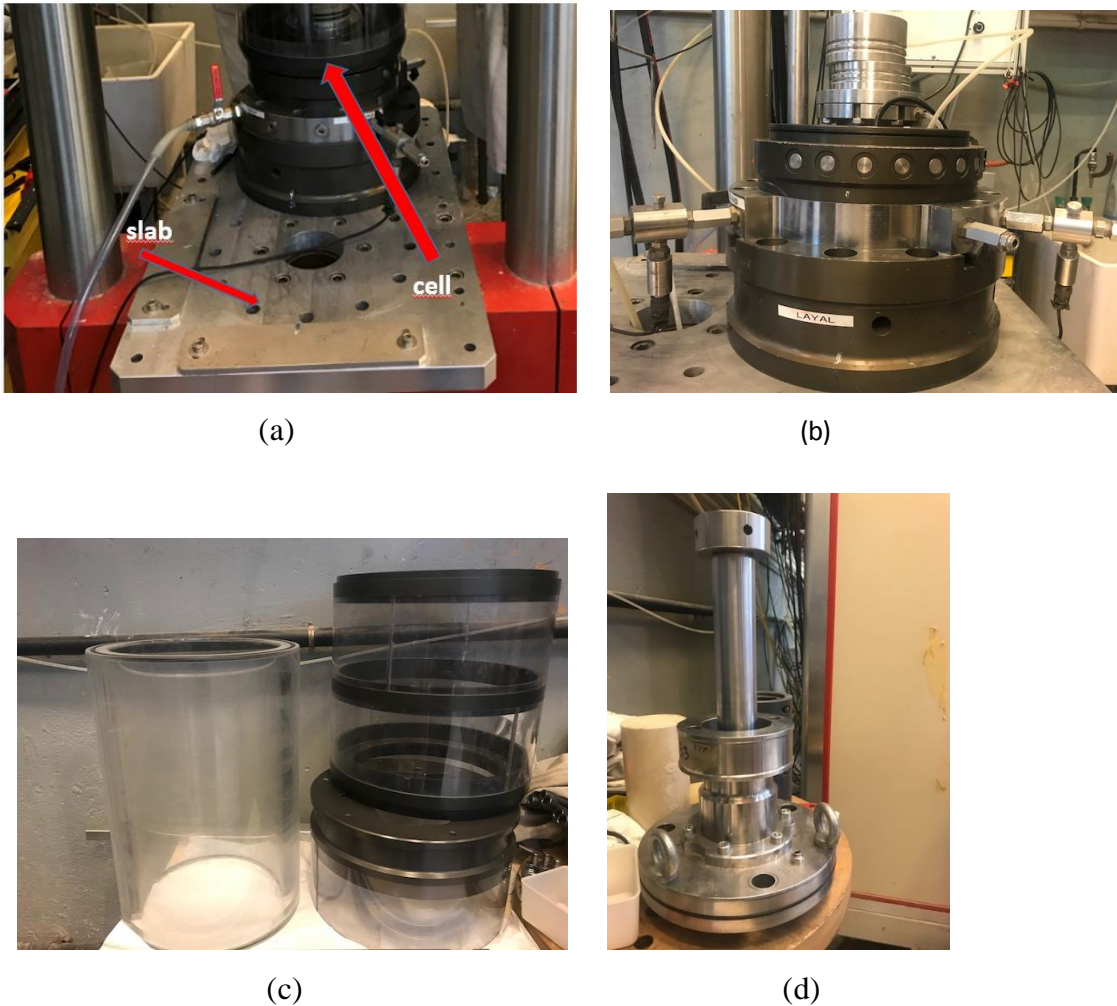


Figure2.4 - Schematic diagram of the triaxial testing device



**Figure 2.5 - Different parts of the triaxial device:** (a) triaxial cell and slab; (b) cylindrical support metal; (c) confinement enclosure; (d) piston

### 2.3.1.1 Axial loading system

The axial loading is applied through a digital MTS system that gives orders to the servo controlled actuator of capacity 25kN. This actuator can be controlled either by displacement or by force under both monotonic and cyclic loading.

The axial force is measured using a force transducer that is placed under the lower base of the specimen to overcome the effects of parasite friction between the piston and the top cover. The accuracy on the measurement of the vertical force is greater than 0.2% kN.

### 2.3.1.2 Measuring devices of the deformation of the specimen

#### a) Axial deformation

The axial deformation of the tested specimen is evaluated from the measurement of the piston displacement as soon as it is in contact with the specimen, using an LVDT sensor incorporated within the servo-actuator. The accuracy of the measurement is greater than 300 µm and the measuring range is 150 mm.

#### b) Confining pressure

There are two ways to apply the confining pressure

- using a pressure circuit which is composed of two air-water cells;
- using a dynamic pressure control device (System MTS,). This device is controlled by a control software (Flextest).

The confining pressure is measured using a pressure transducer (2 MPa range). The measurement accuracy is greater than 1 kPa.

### 2.3.2 Calibration of the cell

The application of a confining pressure inside the cell induces directly a force that can be measured and read by the force transducer. In order to determine the efficiency and accuracy of the cell, it is essential to first calibrate the cell and to validate the workability and the experimental procedure of the apparatus.

A typical monotonic test has been done on a loose specimen of Fontainebleau sand ( $I_D = 0.10$ ). The results of this test are shown in figure 2.6. The shear curve (figure 2.6a) shows an increase in the deviator stress until reaching a peak of resistance that is followed by a sharp decrease in resistance which stabilizes at a value of 33 kPa. This stabilization at this value is not acceptable as we witness the total collapse of the sample which indicates the occurrence of total liquefaction phenomenon (see figure 2.7) and hence this value must go back to zero as the sample loses totally its resistance.

Another look at the curves of the variation of the excess pore water pressure (EPWP) as a function of the axial strain shows that the pore pressure increases gradually until reaching 100 kPa which is equal to the initial consolidation stress of the sample. As for the case of deviatoric stress, the effective stress path (figure 2.6c) shows a migration of this path towards

the origin of axes but again it stops at 33 kPa of deviatoric stress at a mean effective stress  $p'$  equal to 10 kPa. This is also not acceptable as this curve should go back to the point (0, 0) accounting for total liquefaction of the specimen.

For this reason, it was essential to verify the testing procedure in order to detect the problem causing this shift.

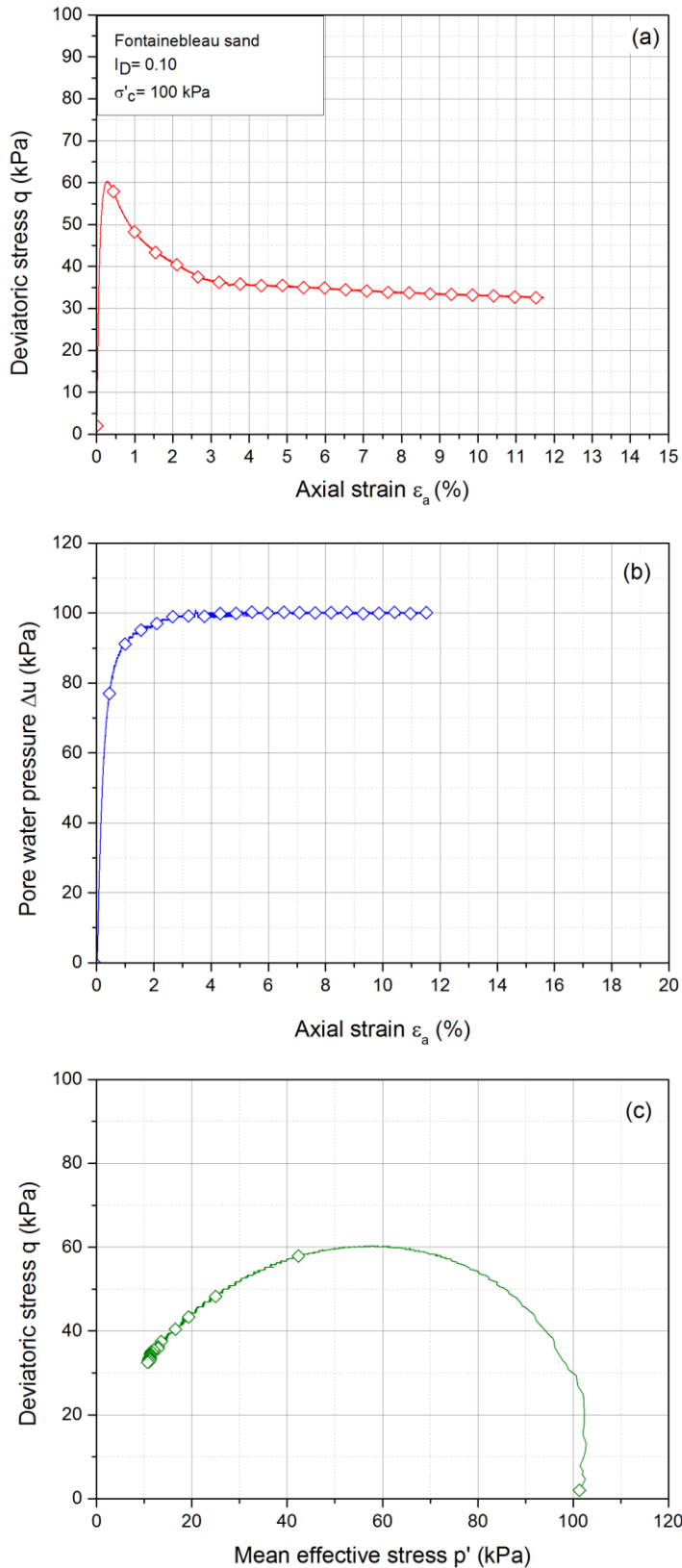


**Figure 2.6 - Typical monotonic test of clean Fontainebleau sand: (a) ( $q$ - $\varepsilon_a$ ) curve; (b) ( $\Delta u$ - $\varepsilon_a$ ) curve; (c) ( $q$ - $p'$ ) curve**



**Figure 2.7 - Total collapse of a loose specimen of Fontainebleau sand**

The calibration test has been done with the aid of a fake specimen of 100 mm diameter and 200 mm height identical to that of the sand specimen.

Due to the fact that the piston can either be blocked or free during the preparation procedure and during the application of the confining pressure, three tests were performed by varying the state of the piston:

- the first test was performed without placing a specimen;
- the second one consists of blocking the piston without having contact between the piston and the specimen;
- the third one consists of solidarizing the piston and the upper part of the specimen while unblocking the piston.

The first test was carried out to obtain the right and appropriate calibration curve in order to detect the right method to use since the force sensor will read the corresponding force upon increasing the consolidation stress.

The second test is explained as follows. Once the specimen is built and unmolded, the piston is decreased and positioned above the upper base of the sample leaving a gap of several centimeters between them, and we introduce two screws to hold the sample from falling down upon the occurrence of the total liquefaction phenomenon (see figure 2.8a). In this case we block the piston and therefore it is prevented from moving during the consolidation phase

(figure 2.8b). It is important to note here, that during the consolidation phase the system is not yet placed under the hydraulic jack. Before launching the test and after the execution of all the phases (consolidation, saturation ...) the cell is placed under the jack where the jack is decreased until it touches the piston. At this point, the piston is unblocked and it is noticed that the force doesn't record any variation since the jack blocks the piston and prevents it from moving. Then the force value is set to zero and the jack is lowered using the displacement control option until we achieve a slight contact between the piston and the sample ( $F = 0.005 \text{ kN}$ ). Finally, the test can be launched after achieving this contact.

The third test differs from the second one where after placing the two screws between the piston and the upper base of the sample, the piston is kept unblocked.

For the three tests mentioned above, the applied pressures were increased from 0 kPa to 400kPa corresponding to the values used during the shear test. Besides, the consolidation stresses were also decreased reversibly from 400 kPa to 0 kPa

The results of these three tests are presented in figure 2.9. It is observed that the red curve corresponding to the case where no sample was placed shows a linear progression of the force with the increase in consolidation stress. The discharging phase also seems good as it goes back on the same line linearly. The black curve which corresponds to the second test seems very close to that of the first one which indicates that upon blocking the piston, the system functions well in terms of the increase of force with the increase in consolidation stress. However, the third test which corresponds to the adopted procedure for the loose sample of Fontainebleau sand, is located below the other curves and also it presents two remarkable drops in the force at 240 kPa and 360 kPa respectively. These two drops in the force value could be explained due to the fact that as the piston is set free during the consolidation phase, and as its two section areas (top S1 and bottom S) aren't similar, hence the exerted force on section S1 is not identical to that exerted on section S (see figure 2.10). Besides, the piston itself has a friction force due to the inner joint placed in it. Therefore, as the lifting force F is bigger than F1, the piston will shift upwards upon increasing the cell pressure at a certain point where this force F exceeds the friction force combined with F1 (as it is remarked at 240 kPa). As the piston is attached to the sample with the screws it will automatically shift the sample upwards and the force will drop as it would be read by the sensor as a traction force.

For this reason, the second procedure was adopted for the monotonic test. The same monotonic test has been repeated while using this procedure. The results of this test are shown in figure 2.11. It is observed that the results of this procedure are logical and reliable since it

is clear that after a peak resistance in the deviatoric stress, the latter increases sharply until reaching a zero value indicating the total collapse of the sample.

Concerning the effective stress paths, it is remarked that this path migrates towards the origin of the axes until reaching the point (0, 0) as expected to have for a total liquefaction phenomenon. The procedure chosen for the realization of the cyclic tests will be explained later in this chapter.



(a)



(b)

**Figure 2.8 - Piston position during a monotonic test**

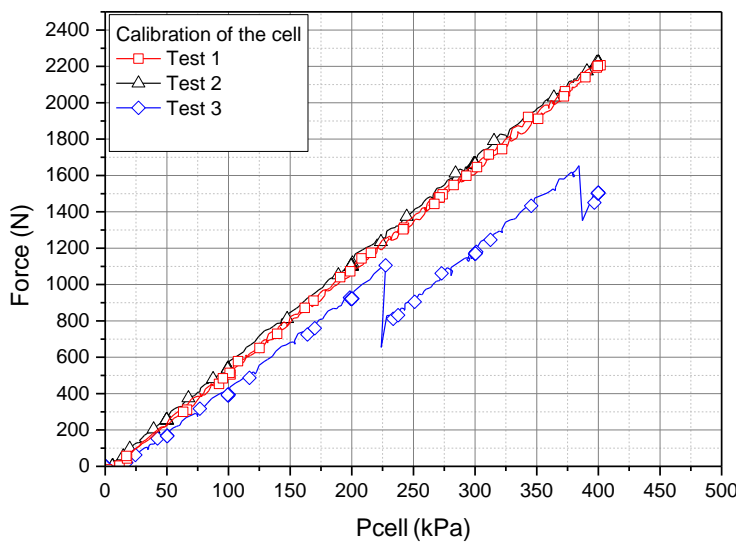


**Figure 2.9 - Results of calibration of the cell**

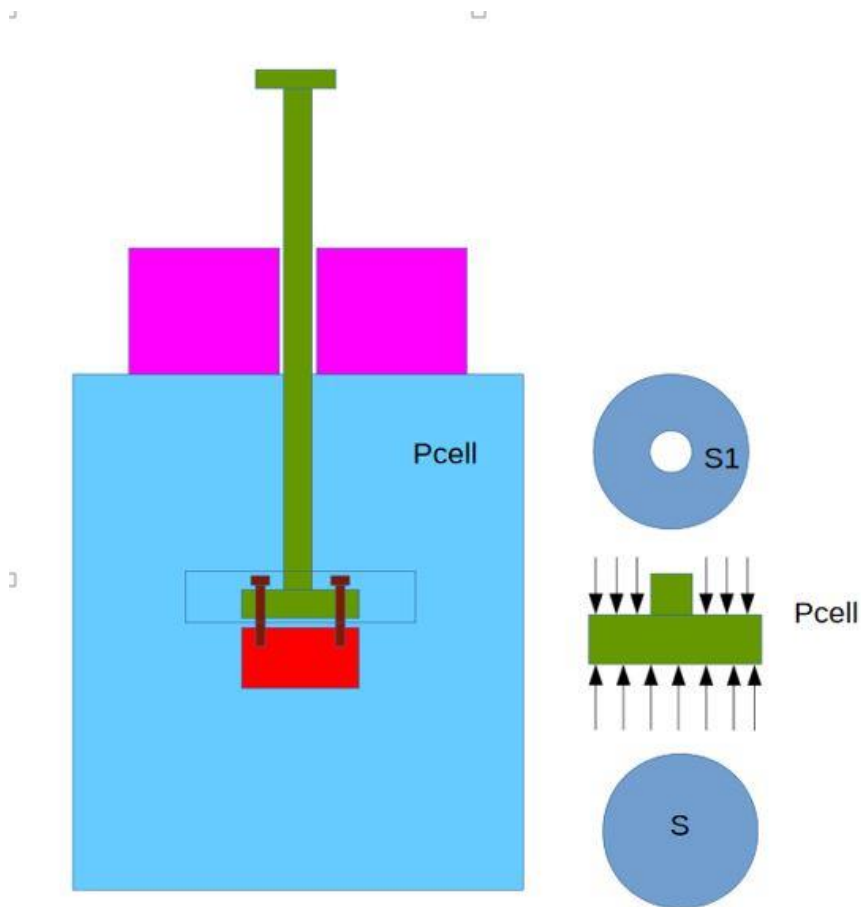


**Figure 2.10 - Schematic diagram of the piston effect**

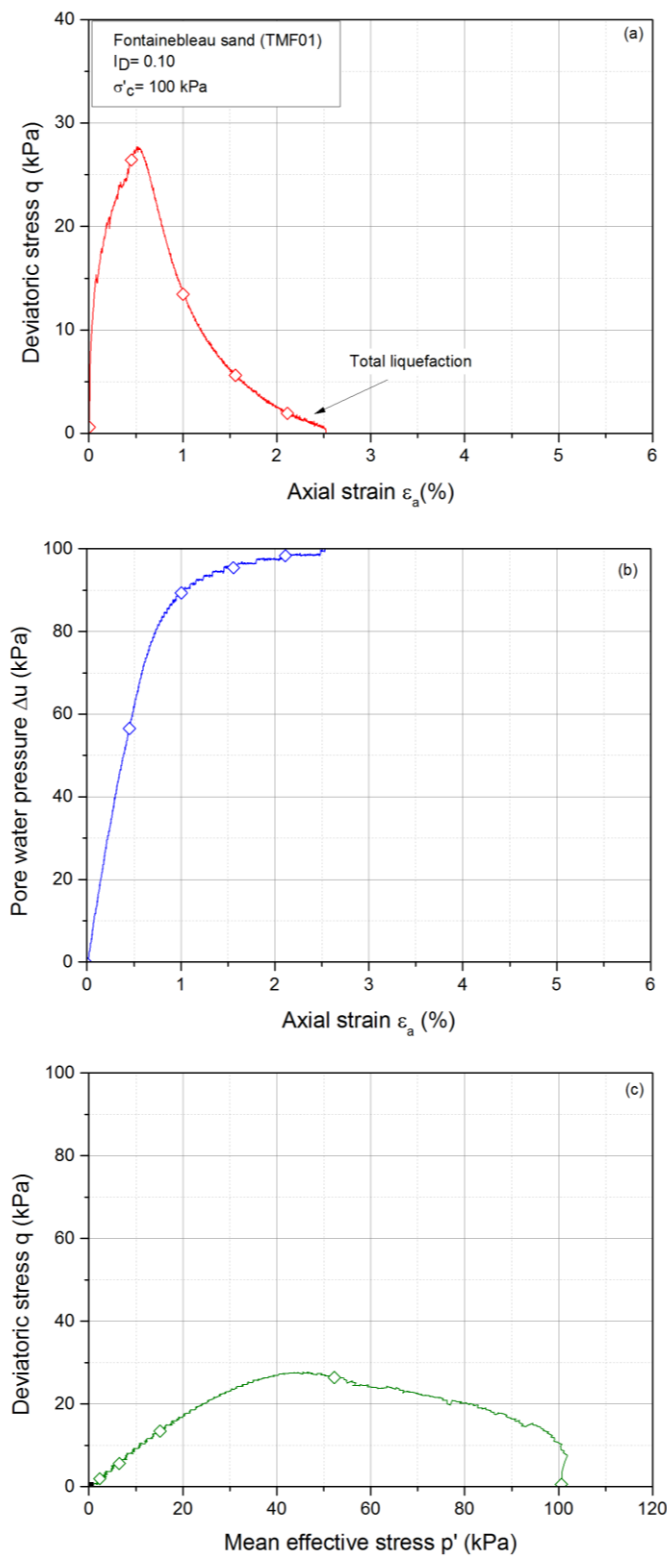


**Figure 2.11- Results of repeated monotonic test with the adopted method: (a) ( $q$ - $\varepsilon_a$ ) curve; (b) ( $\Delta u$ - $\varepsilon_a$ ) curve; (c) ( $q$ - $p'$ ) curve**

## 2.4 Homogeneity of mixtures

The fact that the studied specimen consist of a mixture of sand and various amounts of fines requires to test the efficiency of the reconstitution method in terms of the homogeneity of these mixtures in order to insure obtaining good results. For this reason, two groups of mixtures of sand and fines were prepared at different fines content (1%, 3% and 5%) where for each case three samples were extracted and subjected to laser granulometry. The reconstitution methods chosen for the preparation of these two mixtures will be explained later on in this chapter.

### 2.4.1 Laser granulometry

The laser granulometry is done with the aid of the laser diffraction analyzer apparatus that allows to study the distribution of the size of particles present within samples. This technique can be very precise, and offers advantages of speed and cost over many other methods when used to analyze mixtures of sand, silt and clay. The principle of this apparatus is based on using the diffraction patterns and scattering of a laser beam passing through any object ranging from nanometers to millimeters in size and therefore it quickly measures the geometrical dimensions of a particle.

Light from a laser is shone on a cloud of particles, which are suspended in a dispersant. The particles scatter the light, the larger the particles the smaller the scattering angles. The scattered light is measured by a series of photodetectors placed at different angles. This is known as the diffraction pattern for the sample. The diffraction pattern can be used to measure the size of the particles.

Results obtained allow to draw a curve, called particle size distribution (volumetric distribution). A view of this apparatus is shown in figure 2.12 below.



**Figure 2.12 - View of the laser diffraction analyzer apparatus**

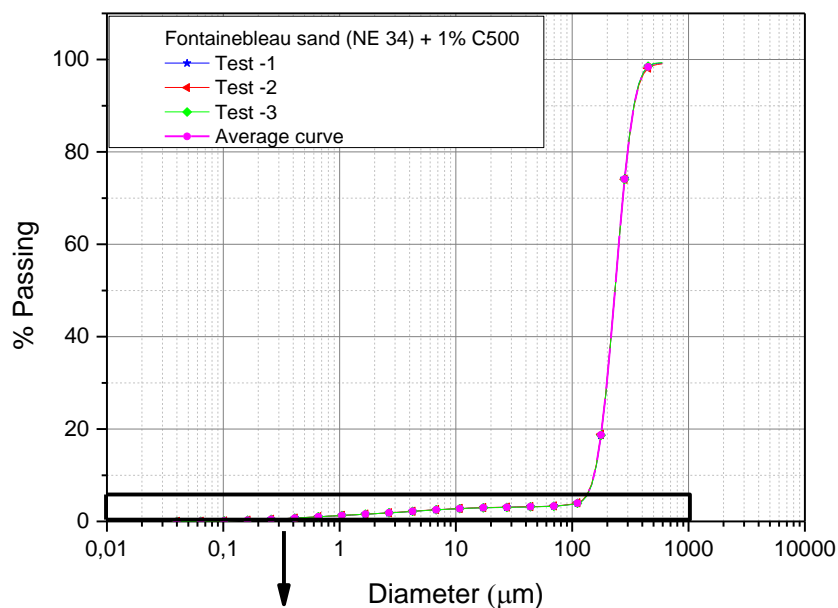
#### 2.4.2 Particle size distribution of mixtures

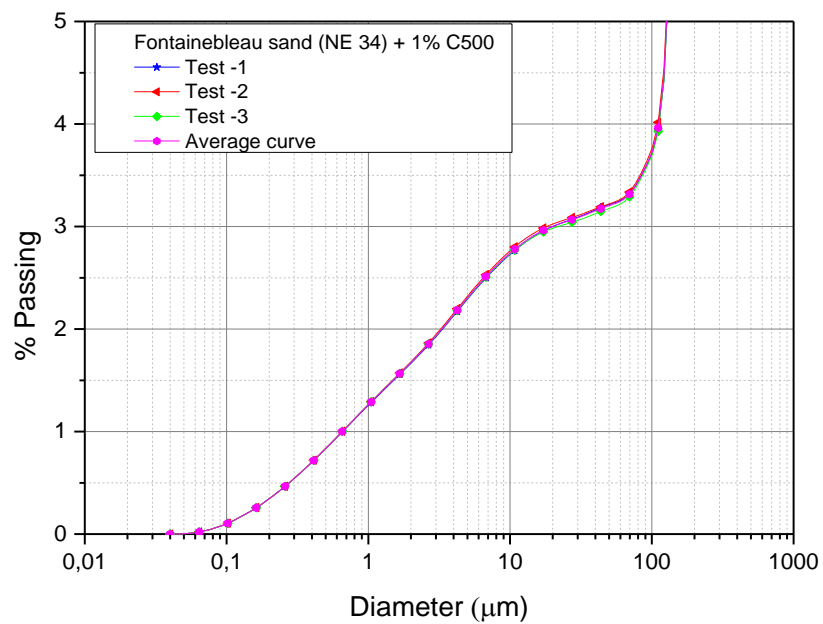
The first group consists of mixtures of sand and C500 prepared using the wet tamping method (WT) explained before since for loose density indices it is very difficult to prepare these mixtures in dry conditions. Whereas the second group consists of mixtures of sand and Speswhite where these specimens were prepared in dry conditions due to the fact that upon adding water the kaolinite Speswhite has formed like a paste structure which prevented us from obtaining a homogeneous mixture.

The gradation curve for each case is plotted and presented below in order to check the homogeneity of the mixture in terms of the fine particles distribution inside each sample. Note that the three sample were extracted from top, middle and bottom of the specimen. For the case where fines content is equal to 5%, five samples were extracted instead of three in order to obtain more specific results.

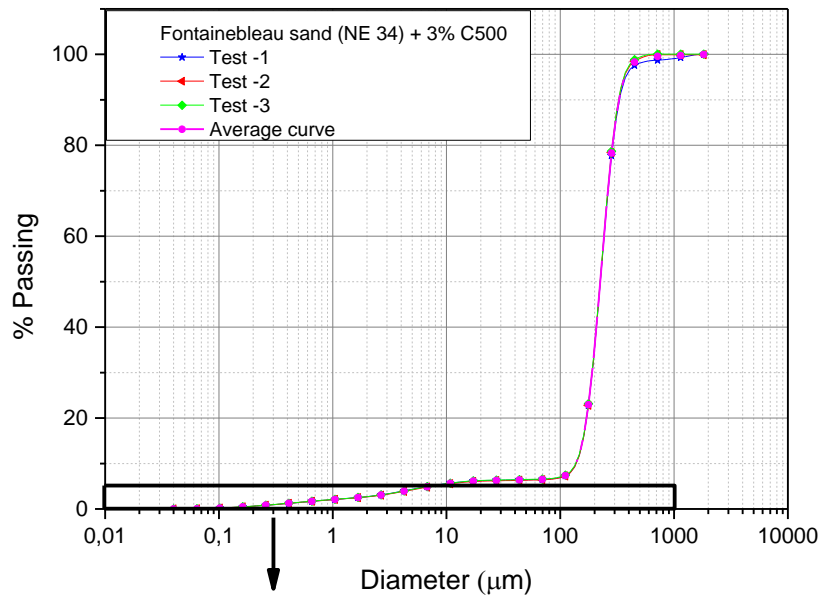
Based on the results of the granulometry, it is obvious that the mixtures are homogeneous where the three samples present almost three confounded granulometric curves. A closer view on the distribution of the particles is also presented in order to verify the distribution of the fine particles. For the case of sand-C500 mixtures, the mixtures of 1% and 3% fines content present very close curves which proves the efficiency of the reconstitution method. The differences between the 3 curves of the mixture with  $F_c = 1\%$  are in the range of 0.03% which

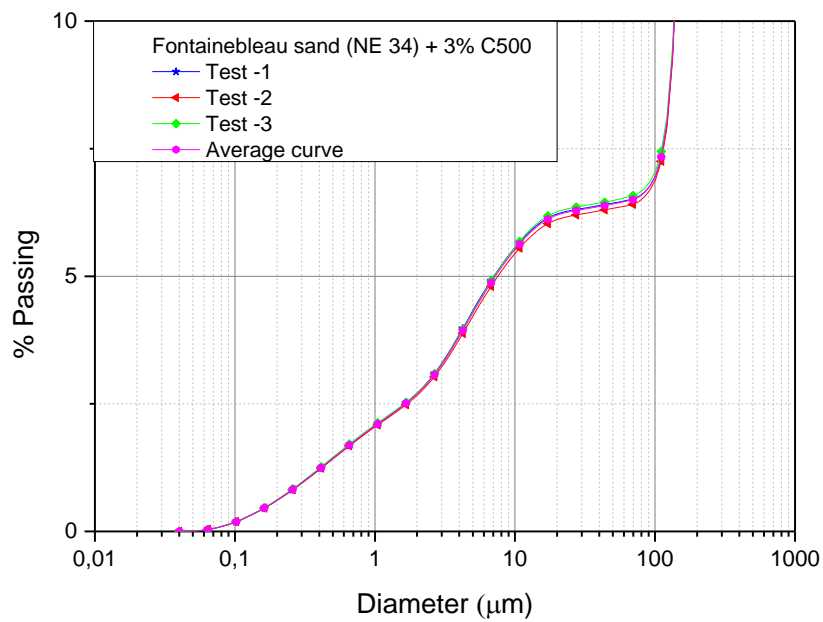
is almost negligible (figure 2.13). Whereas for the case of the mixtures of Fontainebleau sand and 3% of fines the maximum difference between the three curves is in the range of 1.2% corresponding to a diameter of 13  $\mu\text{m}$  that is equivalent to the  $D_{90}$  of the silica C500 (figure 2.14). This difference continues to increase with the increase in fines content as it complicates more the mixture. For  $F_c = 5\%$ , the differences between the curves increase to approximately 5% (figure 2.15). For this reason, for the three different fines content values, an average curve was traced for which the characteristics of each mixture were studied later.



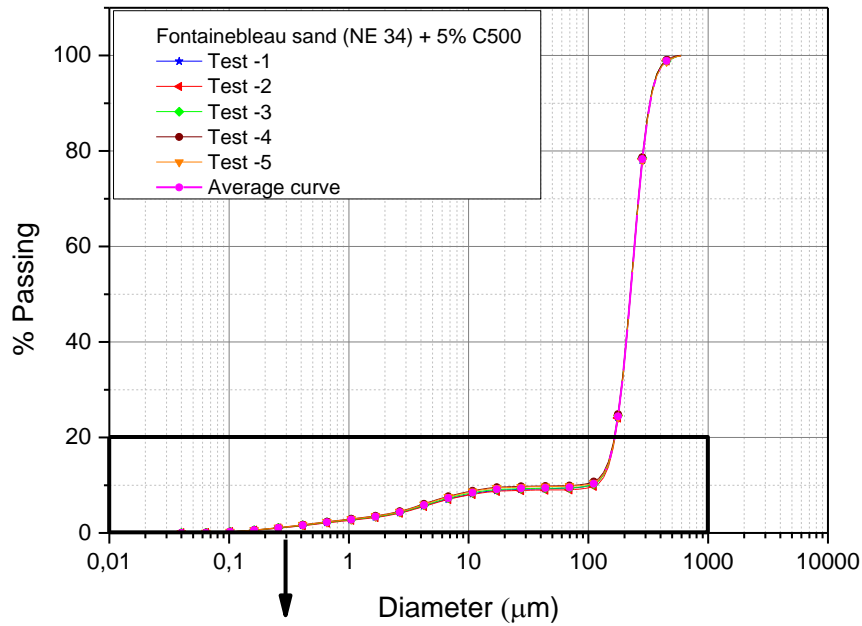


**Figure 2.13 - Gradation curve of mixture of Fontainebleau sand and C500 for  $F_c = 1\%$**





**Figure 2.14 - Gradation curve of mixture of Fontainebleau sand and C500 for  $F_c = 3\%$**



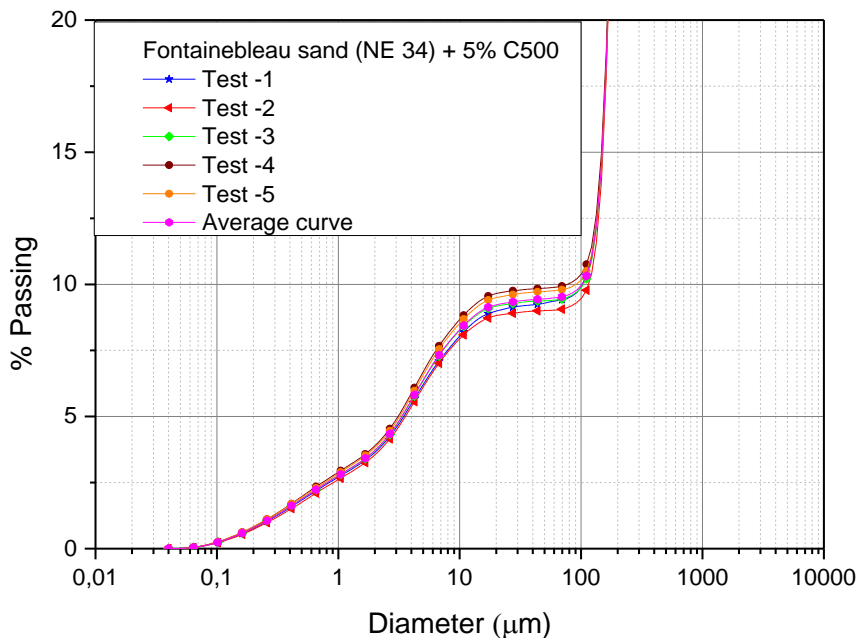


**Figure 2.15 - Gradation curve of mixture of Fontainebleau sand and C500 for  $F_c = 5\%$**

On the other hand, the sand-Speswhite mixtures of fines content ranging between 1% and 5% present larger differences compared to those of C500. For the case of  $F_c = 1\%$ , it is noted that the three curves are very similar for diameter less than 10 $\mu\text{m}$ . Beyond this value, the differences are more pronounced but still reasonable in the range of 3% (figure 2.16). These differences also increase for  $f_c = 3\%$  and 5% (figures 2.17 and 2.18 respectively).

An average curve was plotted for each case as for the case of C500, characteristics of the samples were computed based on the values obtained from this average curve.

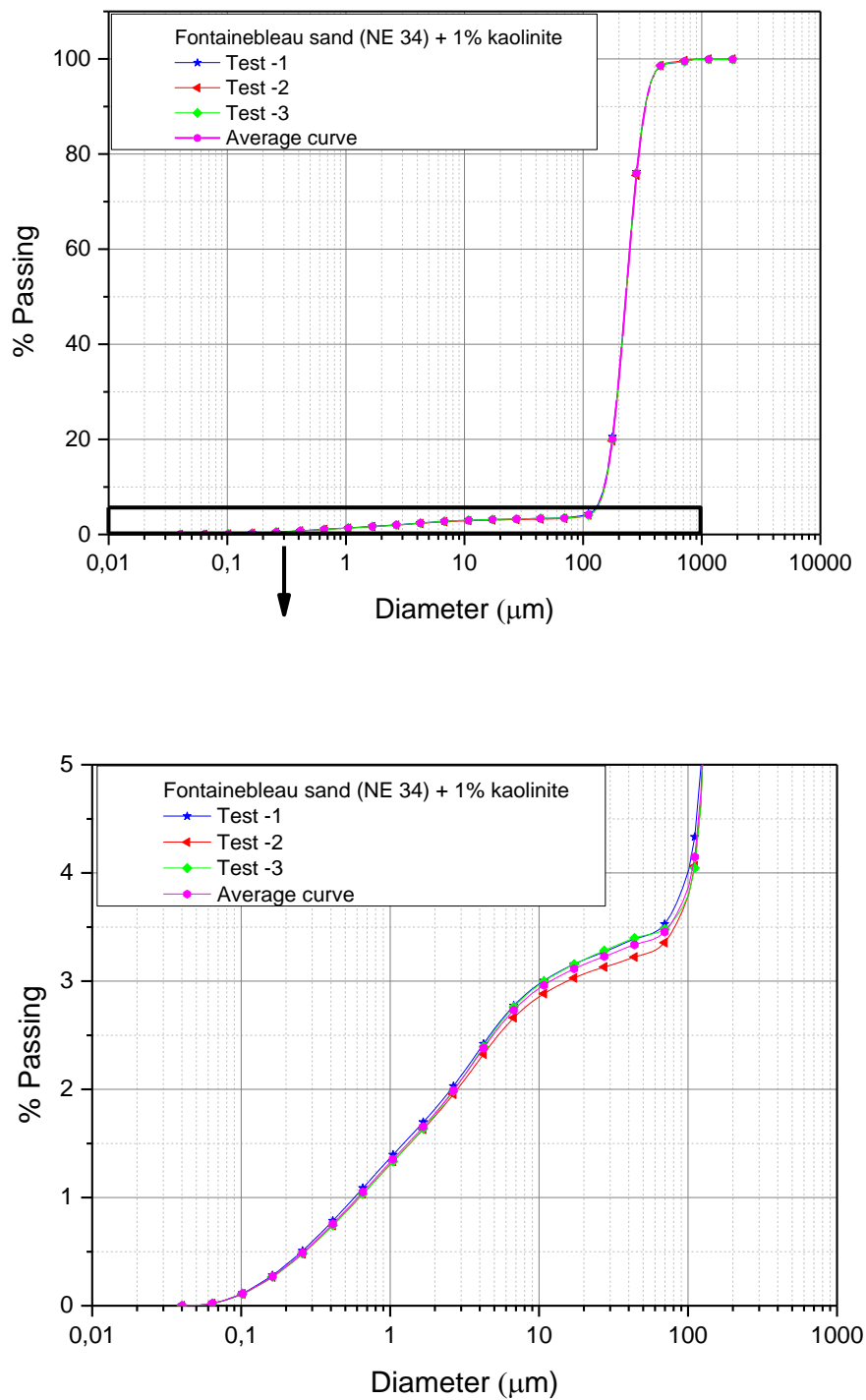


**Figure 2.16 - Gradation curve of mixture of Fontainebleau sand and Speswhite for  $F_c = 1\%$**

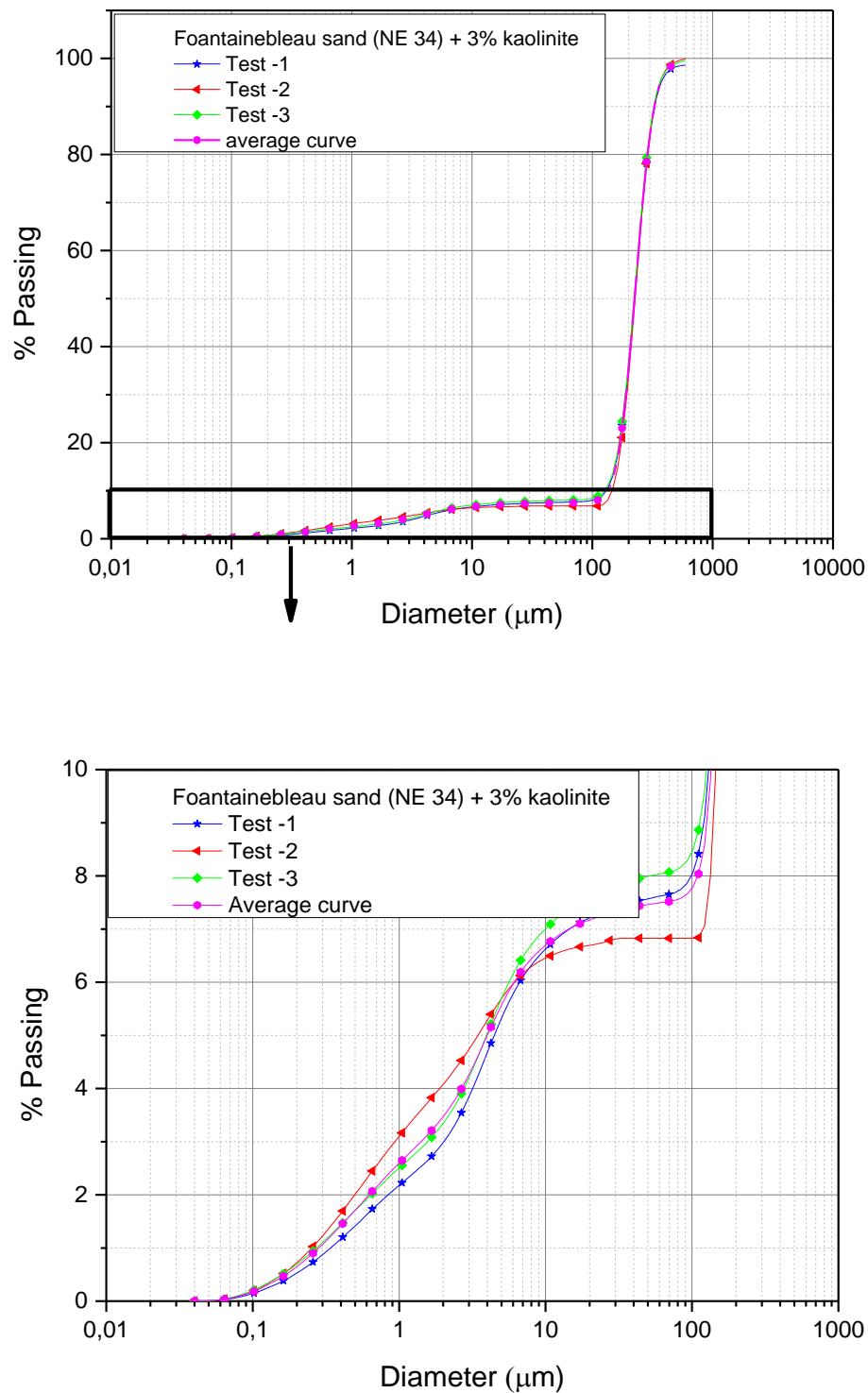


**Figure 2.17 - Gradation curve of mixture of Fontainebleau sand and Speswhite for  $F_c = 3\%$**

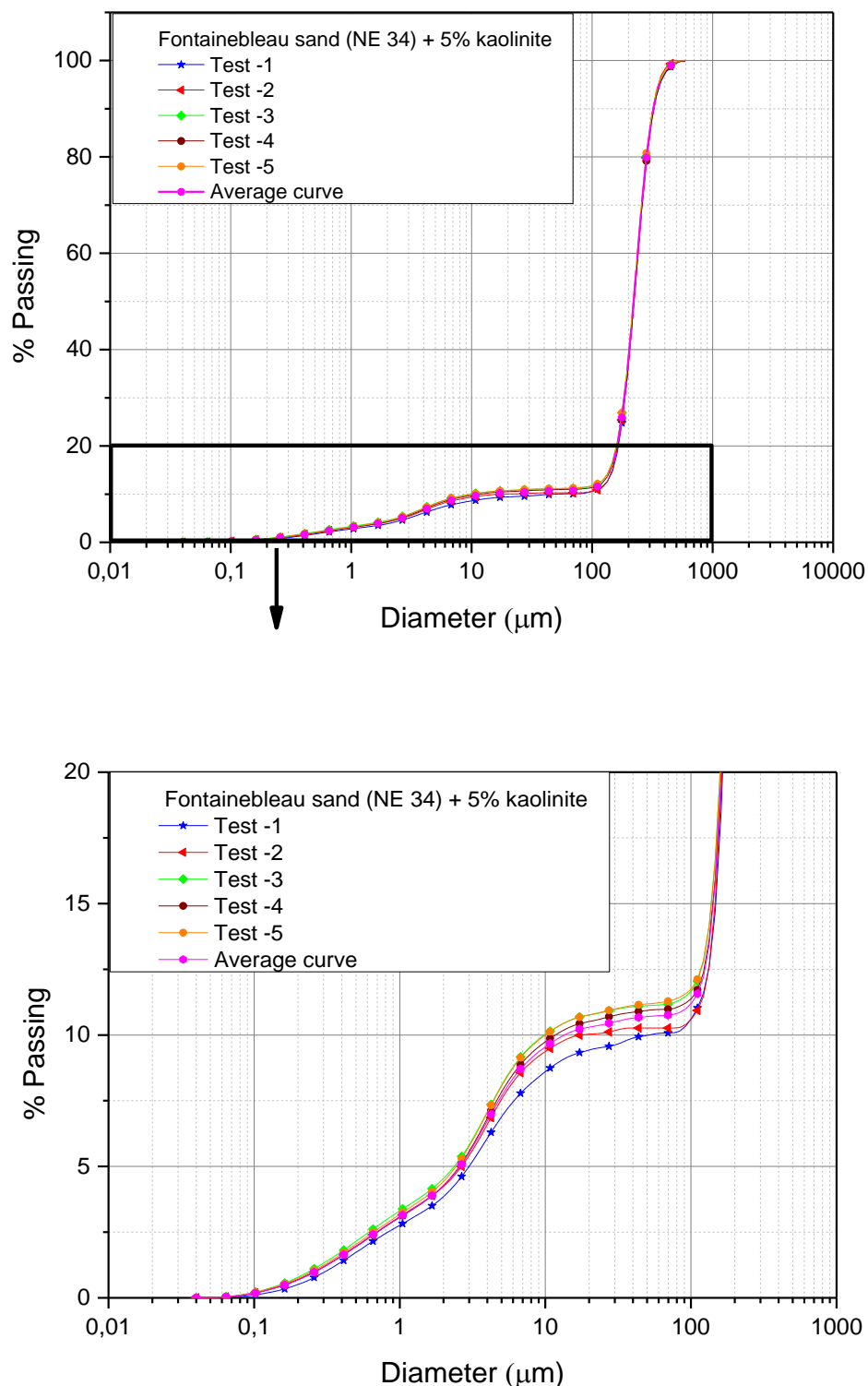


**Figure 2.18 - Gradation curve of mixture of Fontainebleau sand and Speswhite for  $F_c = 5\%$**

The effect of the fines content on the gradation curve of Fontainebleau sand is also presented below for the three cases ( $F_c = 1\%, 3\%$  and  $5\%$ ). It is obvious that the curve is shifted upwards demonstrating the increase in percentage of fines content for each case. This shift becomes more pronounced with the increase in fines content from  $1\%$  to  $5\%$ .

It is interesting to note that the gradation curves of sand-Speswhite are always above those of sand-C500 mixtures due to the fact that the Speswhite particles are finer than those of C500. Figure 2.19 presents the plot of these curves, note here that we have plotted the average curves corresponding to each case.

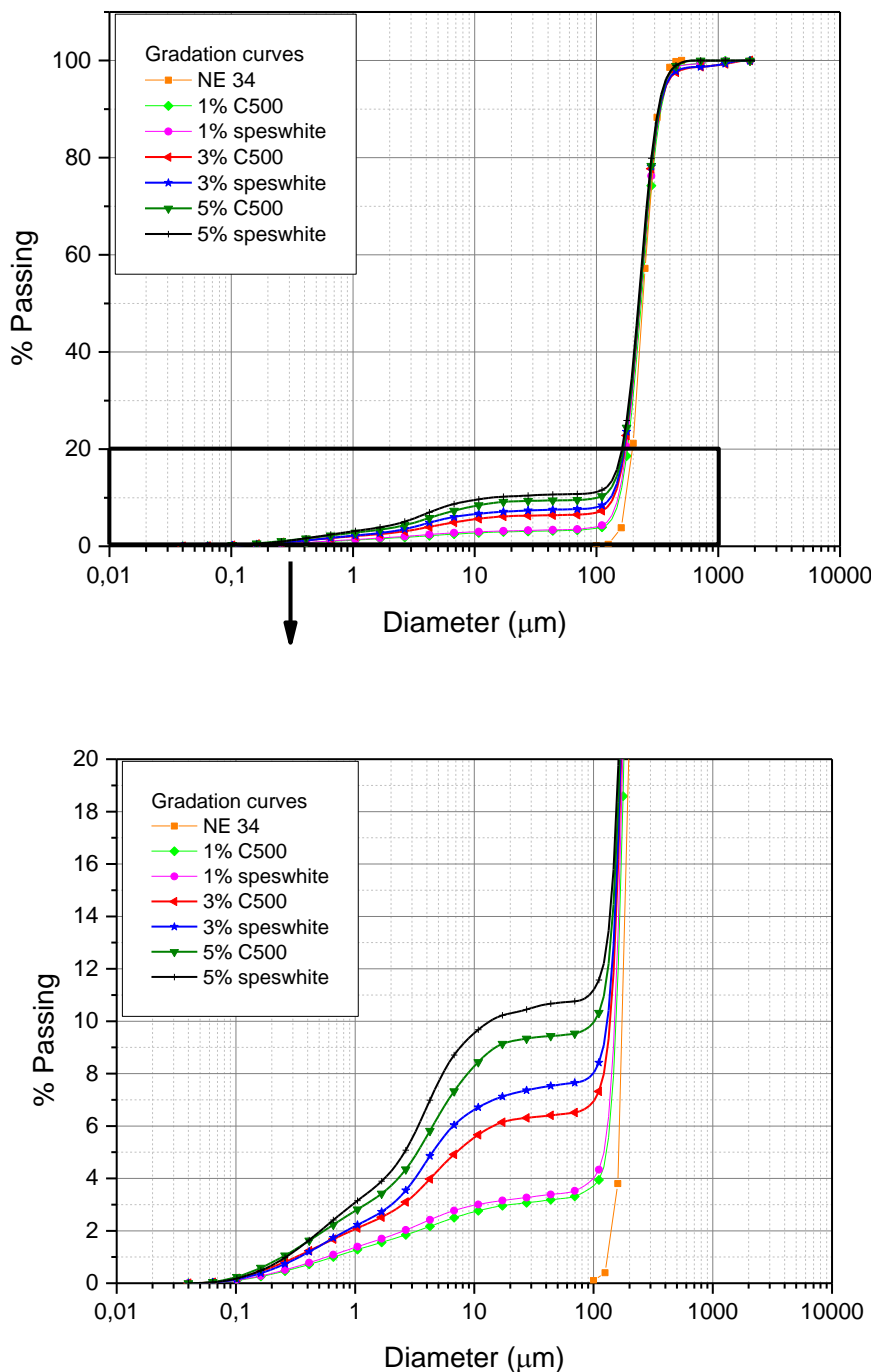


**Figure 2.19 - Gradation curves of sand-fines mixture**

The analysis of the gradation curves obtained allow to determine the coefficient of uniformity and coefficient of curvature for these mixtures and hence verify the effect of the addition of fines on the gradation curve of sand. The results of these tests are shown in table 2.3 It is noted that the coefficient of uniformity  $C_u$  increases from 1.67 to 3.57 with the increase in

fines content from  $F_c = 1\%$  to  $F_c = 5\%$ . It is interesting to note that Fontainebleau sand has a  $C_u$  value equal to 1.52 which is lower than the value obtained for all the mixtures.

On the other hand, the mixtures of sand and Speswhite also shows an increase in the  $C_u$  value from 1.76 to 19.17 as the fines content is increased from 1% to 5%.

<b>Material</b>	<b>Percentage (%)</b>	<b>D<sub>10</sub> (μm)</b>	<b>D<sub>50</sub> (μm)</b>	<b>D<sub>90</sub> (μm)</b>	<b>D<sub>60</sub> (μm)</b>	<b>C<sub>u</sub> (μm)</b>
<b>C500</b>	1	155.5	240	357	260	1.67
	3	137.5	220	333	240	1.74
	5	70	225	333	250	3.57
<b>Kaolinite</b>	1	158.8	220	333	280	1.76
	3	137	230	333	258	1.88
	5	13.3	223	325	255	19.17

**Table 2.3 - Characteristics of mixtures**

## 2.5 Experimental procedure

The triaxial test as described by geotechnical test standards typically consists of 4 main stages: specimen and system preparation, saturation, consolidation and shearing (note saturation and consolidation are not required for UU test). General outlines of each stage are discussed in the following part:

### 2.5.1 Preparation of specimens

The preparation techniques of specimens in the laboratory differ according to the nature and the materials composing the specimen, the targeted compactness and they must meet certain requirements in order to obtain a good homogeneity of the samples in order to approach the natural deposition mode and to ensure a wide range of density indexes.

For the case of loose to very loose states, the reconstitution of the specimen is very delicate and requires some precautions. The reconstitution process chosen for the fabrication of samples of clean sand and mixtures of sand and C500 fines is the wet tamping method which has been already described and used first by Castro (1969) and then adopted by several researchers (Sladen et al., 1985, Been and Jefferies, 1985, Been et al., 1992, Kramer and Seed,

1988; Canou, 1987; 1989, Canou et al., 1990, 1994; Konrad, 1990; Konrad et al., 1991; Zlatović et Ishihara, 1997; Vaid et al., 1999). This method consists of moistening the sand with a water content of approximately 1 to 5% before placing it and then inserting it by layers into the mold with compaction of each layer in order to achieve a target density.

The humidification process allows the creation of capillary cohesion between the sand grains and allows us to obtain very loose structures with very low or even negative density indexes below the ASTM standards. Canou (1989) has succeeded to obtain using this method, the phenomenon of liquefaction with total collapse of the specimen.

On the other hand, mixtures of sand and speswhite which is a plastic fine were prepared in dry conditions in order to avoid segregation of particles.

### 2.5.2 System preparation

A porous stone is placed on the lower base of the cell in order to facilitate the drainage of water (figure 2.20a), then the latex membrane of 0.3mm thickness is placed and fixed on this base with an O'ring (figure 2.20b). After that, the forming mold of diameter 100 mm and 200 mm height is adjusted on the bottom end plate (figure 2.20c). Vacuum is then applied between the wall of the mold and the membrane to press the latter against the mold. Once this step has been achieved, the sand is poured into the mold in order to reconstitute the specimen respecting the chosen reconstitution method.

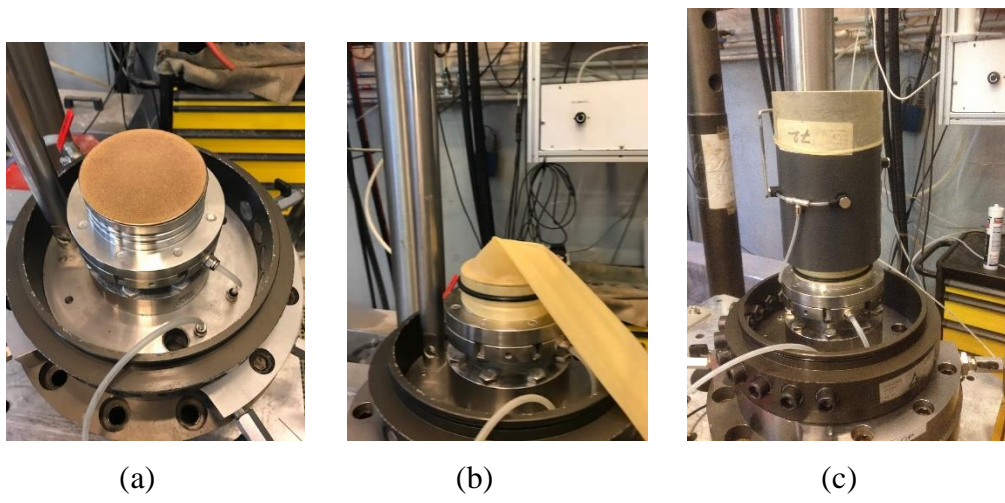


**Figure 2.20 - Preparation of the sample- placing (a) the porous stone, (b) the membrane, (c) the mold**

The test specimen itself must be firstly prepared from a sample of soil before placing into the triaxial test. In our case, the specimen consists of a mixture of Fontainebleau sand (NE34) and a given amount of fines ranging between 0% and 5%.

In order to preserve the dominancy of the sand matrix, the fines content values chosen were small ( $F_c = 1\%, 3\%$  and  $5\%$ ). As we have seen in the literature review, there are several approaches to the evaluation of the liquefaction phenomenon, in our case we have chosen to evaluate this phenomenon according to the relative density of the sand matrix. Therefore, the reconstitution process of the sample consists of adding fines by mass to a given amount of sand, where this quantity of sand is calculated according to a predetermined density of the matrix. In our case we have chosen two density indices ( $I_{Dmat} = 0.10$  for loose samples and  $I_{Dmat} = 0.50$  for medium dense samples).

The relative density as defined previously is presented in the formula below

$$I_D = \frac{e_{\max(sand)} - e_{(sand)}}{e_{\max(sand)} - e_{\min(sand)}} \quad (2.1)$$

As the maximum and minimum void ratios of the Fontainebleau sand are known, it is possible to compute the void ratio of the desired sample corresponding to a definite density index.

Consequently, as the volume of our specimen is known we can compute the volume of the sand using the following relationship between the void ratio, total volume of the sample and the sand volume

$$e_{sand} = \frac{V_T - V_s}{V_s} \quad (2.2)$$

where  $V_T$  is the total volume of the sample,  $V_s$  is the volume of the sand particles

Then the required mass of Fontainebleau sand can be determined as its volume is computed and as the density is known

$$\rho_s = \frac{M_s}{V_s} \quad (2.3)$$

where  $M_s$  is the mass of the Fontainebleau sand

Upon calculating the mass of sand, the fines particles quantity is determined by mass percentage and then added to the sand particles.

The reconstitution method chosen is the wet tamping method for sand-C500 mixtures that consists of adding 5% by mass of water to the dry mixture to facilitate the capillarity and

mixing it using the blender for 5min. Meanwhile, the required amount of fines is weighed and added to the wet sand. The mixture is blended again for 5 minutes with stirring of the mixture during the mixing procedure (figure 2.21). Note that the percentages of added fines were computed by mass according to the sand matrix. On the other hand, the same reconstitution method was applied for the preparation of the sand-Speswhite mixtures but in dry conditions to avoid particles segregation due to the plasticity of the fines.



**Figure 2.21 - Mixture preparation, (a) sand, (b) addition of water, (c) addition of fines, (d) mixing**

The mixture is then divided into 10 layers each 20 mm thick (figure 2.22a). Particular care was taken to avoid any particle segregation, subsequently the wet mixture was placed in the split mold and then compacted carefully at a predetermined height to achieve the target density.

Compaction was performed by a hand tamper with a graduated vertical rod and a small removable horizontal tab to control the desired height by abutting against the edges of the mold (figure 2.22b).



**Figure 2.22 - Preparation of the specimen by layers, (a) division into 10 layers, (b) compaction**

Once the mold has been filled by one of these two methods, the second porous stone is placed and so is the upper base on which the membrane is flipped and fixed with a joint. Unmolding process is carried out by applying a slight vacuum ( $\approx -20$  kPa) in the sample which will then be increased to -100 kPa in the case of consolidation equal to or greater than this value. If the chosen consolidation stress is smaller, the vacuum to be applied must be smaller, otherwise the sample will be over-consolidated (figure 2.23).

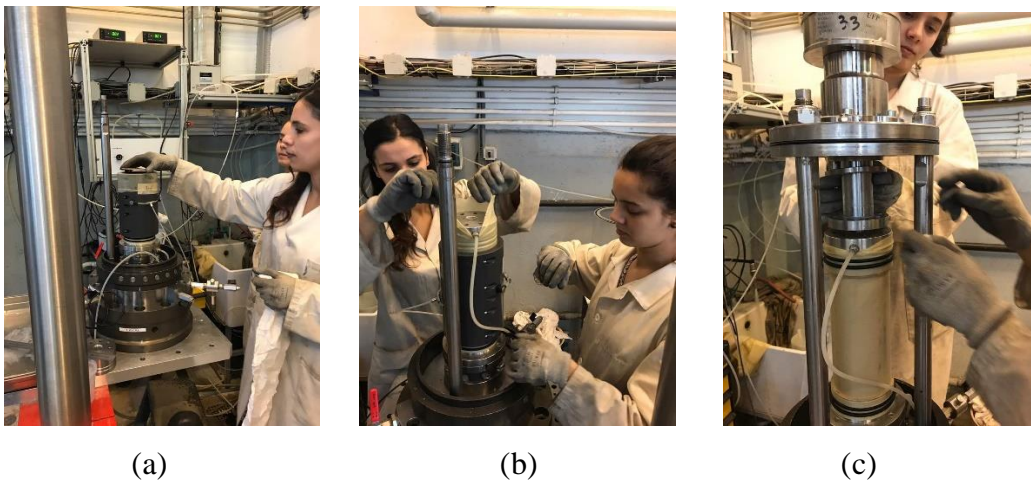


**Figure 2.23 - Sample preparation, (a) placing the second porous stone, (b) the upper base, (c) demolding the sample**

At this point, it is essential to verify that the system doesn't show any leakage. The dimensions are measured, the height at three diametrically opposite points, and the circumference at three places (top, middle and bottom of the specimen). At this stage of the operation, the triaxial cell is assembled, filled up with water to the upper base, and then the specimen maintain pressure is transferred from vacuum to cell pressure (figure 2.24). This is achieved by progressive application of the confining pressure and by decreasing in parallel the vacuum which is inside the specimen until we reach a value of  $\sigma'c$  equal to 100 kPa with total cancellation of the vacuum. At this stage, a normally consolidated specimen is obtained under a confining pressure of 100 kPa and it is ready to be saturated.



**Figure 2.24 - Assemblage of the triaxial cell**

Here it is important to clarify that the procedure of the assembling of the setup in the monotonic test differs than that for the case of cyclic test.

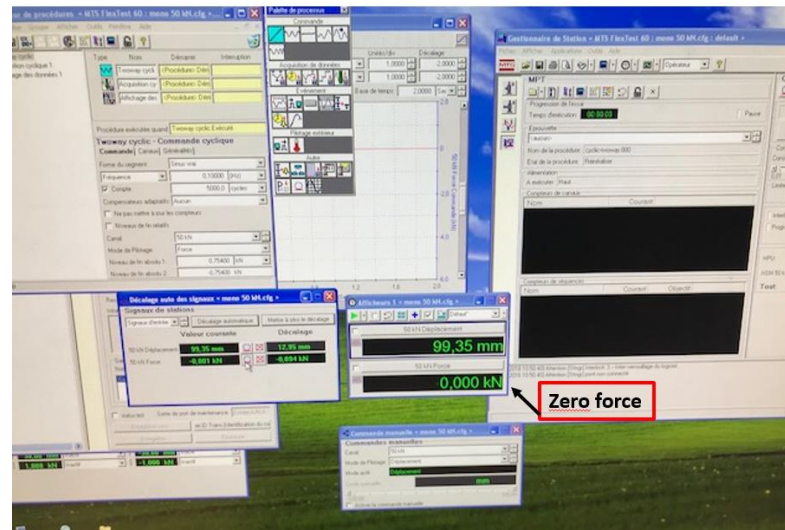
Concerning the monotonic test, upon building the specimen and unmolding it the pistons' position is adjusted in a way that we ensure there is no contact between the sample and the piston with the emplacement of two screws that prevent the specimen from falling down in the case of total collapse (liquefaction) as explained before in the beginning of this chapter (see figure 2.25). At this stage, the piston is blocked in order to prevent its movement upon consolidating the specimen as we have explained before.

The piston is kept blocked during all the stages of saturation and consolidation. However, after placing the setup under the actuator, the actuator ram is lowered until reaching contact with the piston (at this stage there is no real contact between the piston and the sample). The ram is set in contact with the piston in order to prevent the latter from moving upwards upon freeing it. At this point, the piston is set free and the force is reset back to zero in order to detect the contact point.



**Figure 2.25 - Piston position during a monotonic test**

On the other hand, the cyclic test procedure differs than that of the monotonic part concerning the position of the piston where after the specimen has been built, the force value is set to zero (figure 2.26a) and then the piston is lowered until it slightly gets in contact with the specimen. At this point, we can see that the force value increases slightly (several newtons). After that the piston is blocked, and the screws are inserted and tightened in order to solidarize the two pieces (the blockage of the piston at this point is very important in order to avoid the torsion of the sample as shown in figures 2.26 b and 2.26c). After the two pieces are well solidarized, the piston is unblocked again, here it is important to note that upon screwing the screws the sample is lifted a little bit upwards causing the force value to decrease until small negative values. Therefore, the piston is pressed slightly by hands to get back the force to zero value and consequently the sample to its initial position. For this test, the piston is left free during the consolidation phase.



(a)



(b)



(c)

**Figure 2.26 - Particular steps for a cyclic test, (a) setting the force to zero, (b) piston-sample contact, (c) unblocking the piston**

### 2.5.3 Saturation

It has been shown that the degree of saturation is an important parameter that interferes in the estimation of the resistance characteristics of the soil. In fact, a bad saturation degree could have a considerable influence on the drained and undrained response where it induces an under estimation of pore pressure and volumetric deformations. Therefore, it is essential to obtain a good degree of saturation of the specimen before shearing in order to have a good quality test and good results.

The saturation process is performed in order to ensure all voids within the test specimen are filled with water, and that the pore pressure transducer and drainage lines are properly de-aired. This procedure consists of three main steps. First, carbon dioxide CO<sub>2</sub> is flushed throughout the specimen at 15 kPa for approximately 15 min. The aim of this operation is to remove the air contained in voids and replace it with CO<sub>2</sub> which is very soluble in water.

The second step consists of circulating de-aired water through the specimen until reaching a relatively high value of saturation. Once this step is over, we pass to the final phase that consists of applying a back pressure of minimum 200 kPa in order to improve the degree of saturation of the specimen by dissolution of the remained gas bubbles. This step is achieved by applying, at the same time, two pressures in the interior and exterior of the specimen followed by the verification of the value of Skempton coefficient.

To check the degree of specimen saturation before moving to the consolidation stage, a short test is performed to determine Skempton's B-value. This is called a B-check, and requires specimen drainage to be closed whilst the cell pressure is raised by approximately 50kPa. The B- value is computed as the ratio of the difference in pore pressure to the difference in cell pressure that is equal to 50 kPa in our case.

$$B = \frac{\Delta u}{\Delta P_{cell}} \quad (2.4)$$

The final value of the applied back pressure depends on the degree of saturation obtained. If the obtained value is not suitable to perform the test, the back pressure is increased again. Generally, the specimen is considered saturated when the Skempton coefficient B is superior to 0.96. In our case, the B value was equal or greater than 0.98 in all of our tests.

#### 2.5.4 Consolidation

The consolidation stage allows to bring the specimen to the effective stress state required before shearing. It is typically conducted by increasing the cell pressure whilst maintaining a constant back pressure (often equal to the pore pressure reached during the final saturation B-check). If the consolidation stress required for realizing the test is equal to 100 kPa, the specimen is already consolidated and hence it is ready for shearing. However, if the desired value of consolidation stress is superior to 100 kPa, then it is necessary to progressively increase it until we reach the desired value.

### 2.5.5 Shearing

Shearing of the specimen is carried out after the contact between the piston and the head of the specimen is achieved. This operation is easy to carry out when the loading device is operating in displacement mode. On the other hand, when the latter is subjected to stress as is the case for cyclic tests, the operation becomes rather delicate and requires a great deal of care and precaution for its realization. In fact, the decrease of the piston must be kept sufficiently low to make a soft contact and do not crush the sample. Ensure that drainage tap is closed for undrained testing prior to testing.

The monotonic tests were carried out at an axial rate equal to 0.5% per minute equivalent to a displacement of 1 mm/min. Whereas for the cyclic tests, they were carried out with force control with a loading frequency equal to 0.1 Hz however for some cyclic tests that required a large number of cycles or that showed an accommodation in the pore water pressure the frequency was increased to 0.2 Hz in order to reach higher number of cycles.

### 2.5.6 Measurements and acquisition of data

The triaxial test is equipped with several sensors that allow the measurement of the force applied by the actuator (capacity  $\pm 50$  kN), the vertical displacement ( $\pm 150$  mm), confining pressure of capacity (0-2 MPa) and pore water pressure. These transducers are connected to the computer. A data acquisition and processing software makes it possible to visualize in during the test the evolution of the various parameters of the test.

The values of force during the tests permits the calculation of the deviator stress  $q$  as the dimensions of the sample are known. The confining pressure and the pore water pressure as well permit the calculation of the effective stresses in an undrained test. The axial strain can be computed by using the values of the recorded displacement during the test.

## 2.6 Conclusion

In this chapter, we have presented the new prototype triaxial device  $\Phi 100$  mm developed in the geotechnical team of Navier laboratory that permits to perform both monotonic and cyclic loading for a sample of 200 mm height and 100 mm diameter. Based on the use of this

device, a study of the influence of several parameters (density index, consolidation stress, fines content and nature of fines) on the initiation of the liquefaction phenomenon has been achieved.

Also, we have presented the materials used in our study (Fontainebleau sand, Silica C500 and kaolinite Speswhite) besides we have explained the adopted reconstitution method for the reconstitution of our samples as well as the validation of the workability of this method in terms of the homogeneity of the mixtures.

## **Chapter III: Undrained behavior of sand containing fines under monotonic shear**

This chapter examines the behavior of clean sand, sand and fines mixtures (plastic/non-plastic) under undrained monotonic shear. This study will allow to focus and shed the light on the influence of the initial parameters (density index, consolidation stress, fines content, type of fines ...) on the mechanical behavior and initiation of the phenomenon of liquefaction in terms of shear resistance and excess pore water pressure (EPWP) under monotonic loading. Based on the results of our tests, attention was paid to the notion of the initiation of instability and evaluation of the instability line defined by Lade (1993).

### **3.1 Experimental program**

An experimental program was defined for a series of monotonic tests on clean sand, sand-C500 mixtures and sand-Speswhite mixtures in order to study the influence of several parameters on the mechanical behavior and on the initiation of the phenomenon of liquefaction.

Two density indexes were chosen (0.10 and 0.50) to evaluate the behavior of loose and medium specimens. Concerning the consolidation stress  $\sigma'_c$ , tests were done for two values of  $\sigma'_c$  (100 kPa and 400 kPa) in which these results permit to study the effect of this parameter. As for fines content, three different percentages were chosen (1%, 3% and 5%) to study their effect on the behavior of the mixtures. It is interesting to note that the values of fines content were selected at low percentages in order to preserve the dominancy of the sand matrix and to highlight the influence of low fine contents on the initiation of liquefaction phenomenon as it has been shown in the literature that actual soils that have liquefied through history contained less than 5% of fines.

The two different types of fines chosen C500 (non-plastic) and Speswhite (plastic) allow to study the effect of fines type on the behavior of the mixture.

The experimental program corresponding to monotonic shear tests for clean sand and sand-fines mixtures is presented in tables 3.1 and 3.2 respectively.

<b>Test reference</b>	<i>I<sub>Dmat</sub></i>	$\sigma'c$ (kPa)
TMF01	0.1	100
TMF02	0.1	400
TMF03	0.5	100
TMF04	0.5	400

**Table 3.1- Testing program for clean Fontainebleau sand**

<b>Test reference</b>	<b>Type of fines</b>	<b>F<sub>c</sub> (%)</b>	<i>I<sub>Dmat</sub></i>	$\sigma'c$ (kPa)
TMC01	C500	1	0.10	100
TMC02	C500	1	0.10	100
TMC03	C500	3	0.10	100
TMC04	C500	5	0.10	100
TMC05	C500	1	0.50	100
TMC06	C500	3	0.50	100
TMC07	C500	5	0.50	100
TMC08	C500	1	0.10	400
TMC09	C500	3	0.10	400
TMC10	C500	5	0.10	400
TMC11	C500	1	0.50	400
TMC12	C500	3	0.50	400
TMC13	C500	5	0.50	400
TMS14	Speswhite	1	0.10	100
TMS15	Speswhite	3	0.10	100
TMS16	Speswhite	5	0.10	100
TMS17	Speswhite	1	0.50	100
TMS18	Speswhite	3	0.50	100
TMS19	Speswhite	5	0.50	100
TMS20	Speswhite	1	0.10	400
TMS21	Speswhite	3	0.10	400
TMS22	Speswhite	5	0.10	400
TMS23	Speswhite	1	0.50	400
TMS24	Speswhite	3	0.50	400
TMS25	Speswhite	5	0.50	400

**Table 3.2 - Testing program for sand-fines mixtures**

### 3.2 Typical results

It is interesting to note that the review of the literature presents different types of behaviors for sand containing fines due to the difference in the type of fines (plastic / non-plastic). Therefore, it is essential to highlight the influence of the type of fines on the mechanical response of the material.

#### 3.2.1 Clean sand

Figure 3.1 shows the result of a typical static liquefaction test performed on a very loose specimen of Fontainebleau sand ( $I_{Dmat} = 0.10$ ) consolidated under 100 kPa. The shape of the shear curve presented in figure 3.1a is characterized by a very marked low level peak of resistance reached for a relatively small axial deformation (of the order of 0.5%), followed by a sharp drop in the deviatoric stress to a zero value in this case, corresponding to a total collapse (total liquefaction) of the specimen.

The evolution of the EPWP  $\Delta u$  (figure 3.1b) presents a very high generation rate which reaches a maximum value of 100 kPa thus equalizing the value of the consolidation stress and causing at the same time a collapse of the specimen.

Figure 3.1c presents the corresponding effective stress path. It is noted that after reaching the peak resistance, this path migrates progressively towards the origin of the axes until reaching zero value of deviatoric stress  $q$  for a zero value of the mean effective stress  $p'$  indicating again the collapse and total liquefaction of the sample.

#### 3.2.2 Sand-C500 mixture

Figure 3.2 presents the results of monotonic test carried out on a mixture of sand-C500 at a fines content  $F_c = 1\%$  characterized by an initial density index  $I_{Dmat} = 0.10$ . It is noted that the behavior of the mixture resembles that of the clean sand which is essentially contracting. This behavior is characterized by a marked peak resistance followed by a sharp decrease of the deviator stress until reaching a null value and hence causing the total collapse of the sample.

The evolution of the EPWP is presented in figure 3.2b where it is noted that the latter increases sharply until reaching 100 kPa that is equal to the initial consolidation stress of the sample.

Concerning the effective stress paths, figure 3.2c reveals a migration of the deviator stress towards the left until reaching a null value for a mean effective stress  $p'$  equal to zero as for the case of clean sand.

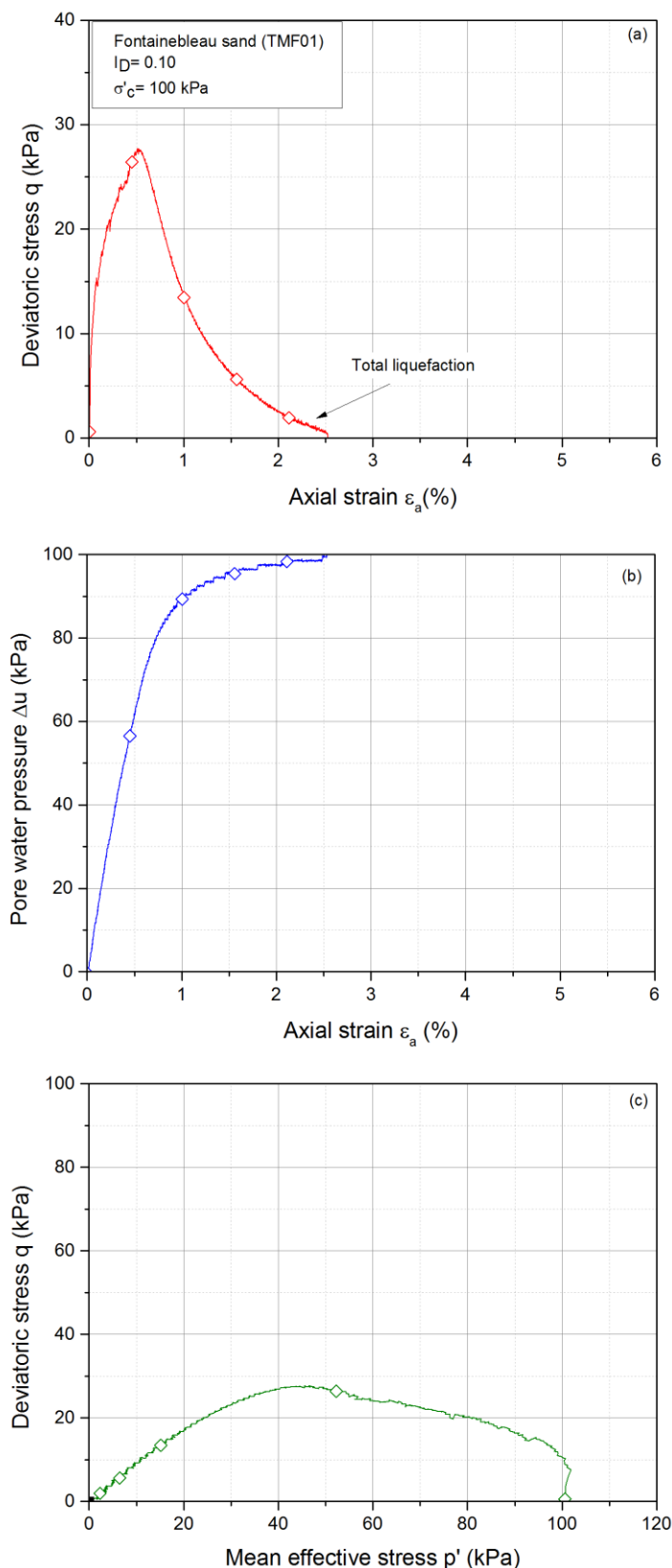


**Figure 3.1 - Undrained behavior of clean Fontainebleau sand**

**(a)  $(q-\varepsilon_a)$  curve ; (b)  $(\Delta u-\varepsilon_a)$  curve ; (c)  $(q-p')$  curve**

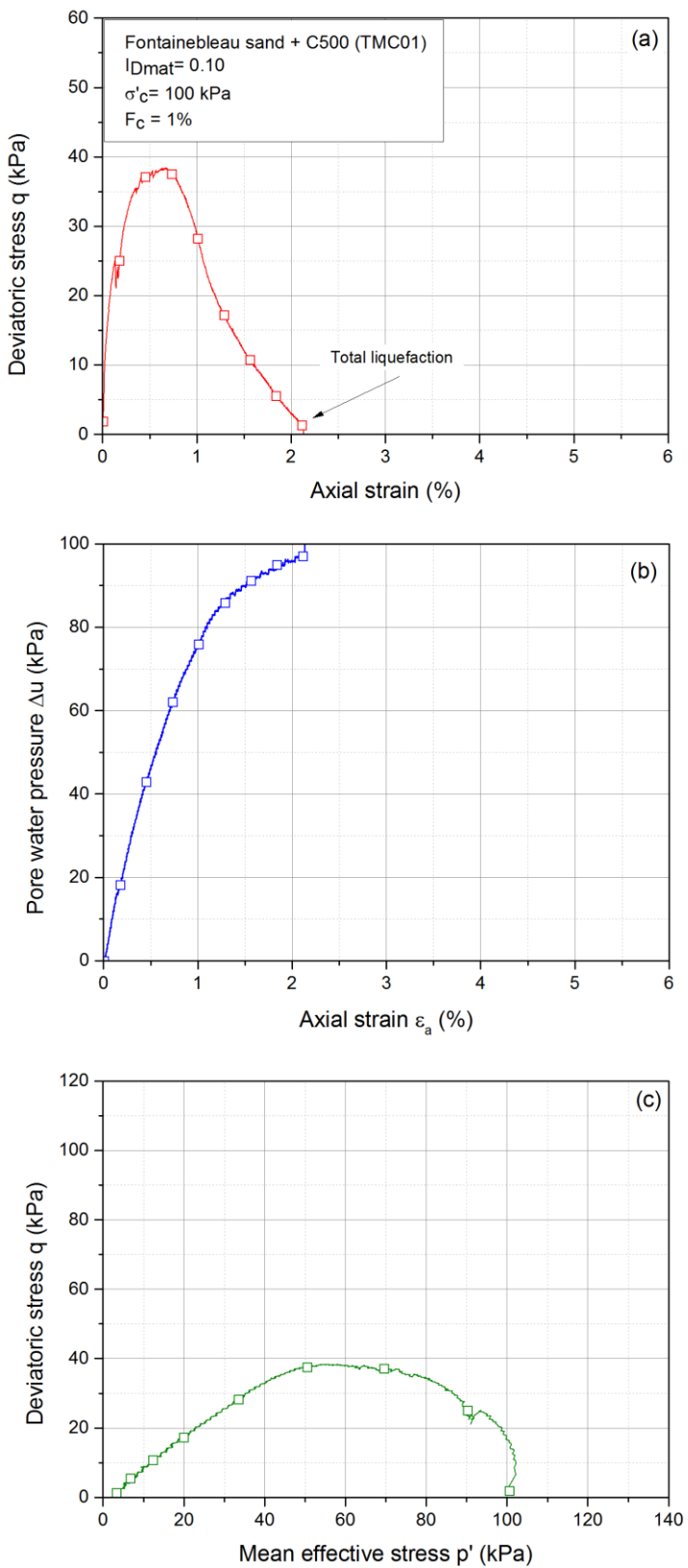


**Figure 3.2 - Undrained behavior of Fontainebleau sand-C500 mixture (loose state)**

**(a) ( $q$ - $\varepsilon_a$ ) curve ; (b) ( $\Delta u$ -  $\varepsilon_a$ ) curve ; (c) ( $q$ - $p'$ ) curve**

### 3.2.3 Sand-Speswhite mixture

Unlike the clean sand and sand-C500 mixtures, the mixture with Speswhite (plastic fines) exhibits a totally different behavior. For the same initial conditions, ( $I_{Dmat} = 0.10$ ,  $\sigma'_c = 100$  kPa), we observe a peak resistance without significant softening followed by a very rapid re-increase in the deviatoric stress and hence leading to stability in the structure where no liquefaction phenomenon is observed despite its low density (figure 3.3a).

The evolution of the pore water pressure presents a high generation rate at the beginning that reaches a value of 86 kPa that stabilizes for a short period and then follows by a decrease in the EPWP which reaches negative values in the order of -250 kPa. This tendency is consistent with that of the shear curve indicating stability of the structure (figure 3.3b).

Figure 3.3c shows the evolution of the stress paths which, after reaching the peak resistance, migrates towards to origin of the axes before it goes back and presents a dilatant behavior due to the re-increase in shear resistance. A closer view on the response of sand-Speswhite mixture is also shown in figure 3.3 next to each curve respectively.

According to these results, it is interesting to note that sand-C500 mixture favors a very contractant and unstable behavior (strain softening) with a liquefaction type response whereas sand-Speswhite mixture favors a slightly dilatant and more stable response (strain hardening).

## 3.3 Repeatability

Evaluation of testing repeatability is a very important point, in particular to check the repeatability of the reconstitution method and to validate the experimental procedure as well as to test the efficiency of the testing setup. For this reason, two monotonic undrained tests were performed for identical initial conditions: initial density index  $I_{Dmat} = 0.10$ , confining pressure of 100 kPa and fines content  $F_c = 1\%$ .

The comparison of the results of these tests is presented in figure 3.4. Very good repeatability was observed in terms of shear strength where the test values show nearly a zero deviation of the order of 2 kPa.

Concerning the EPWP and the stress paths, the plots show almost two confounded curves confirming the good level of repeatability of the reconstitution method and the validation of the testing setup and protocol.

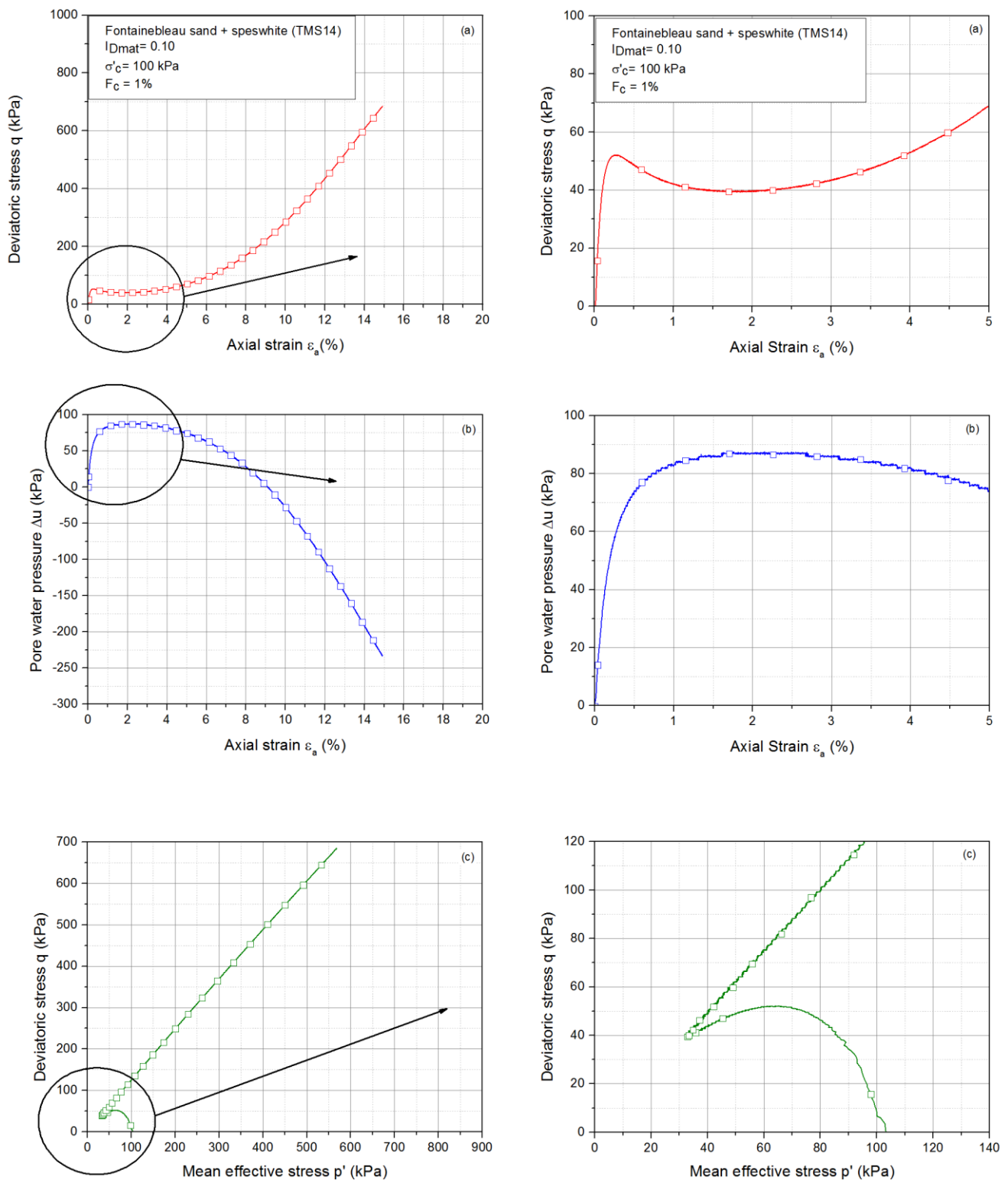


**Figure 3.3 - Undrained behavior of Fontainebleau sand-speswhite mixture (loose state)**

**(a) ( $q$ - $\epsilon_a$ ) curve ; (b) ( $\Delta u$ - $\epsilon_a$ ) curve ; (c) ( $q$ - $p'$ ) curve**

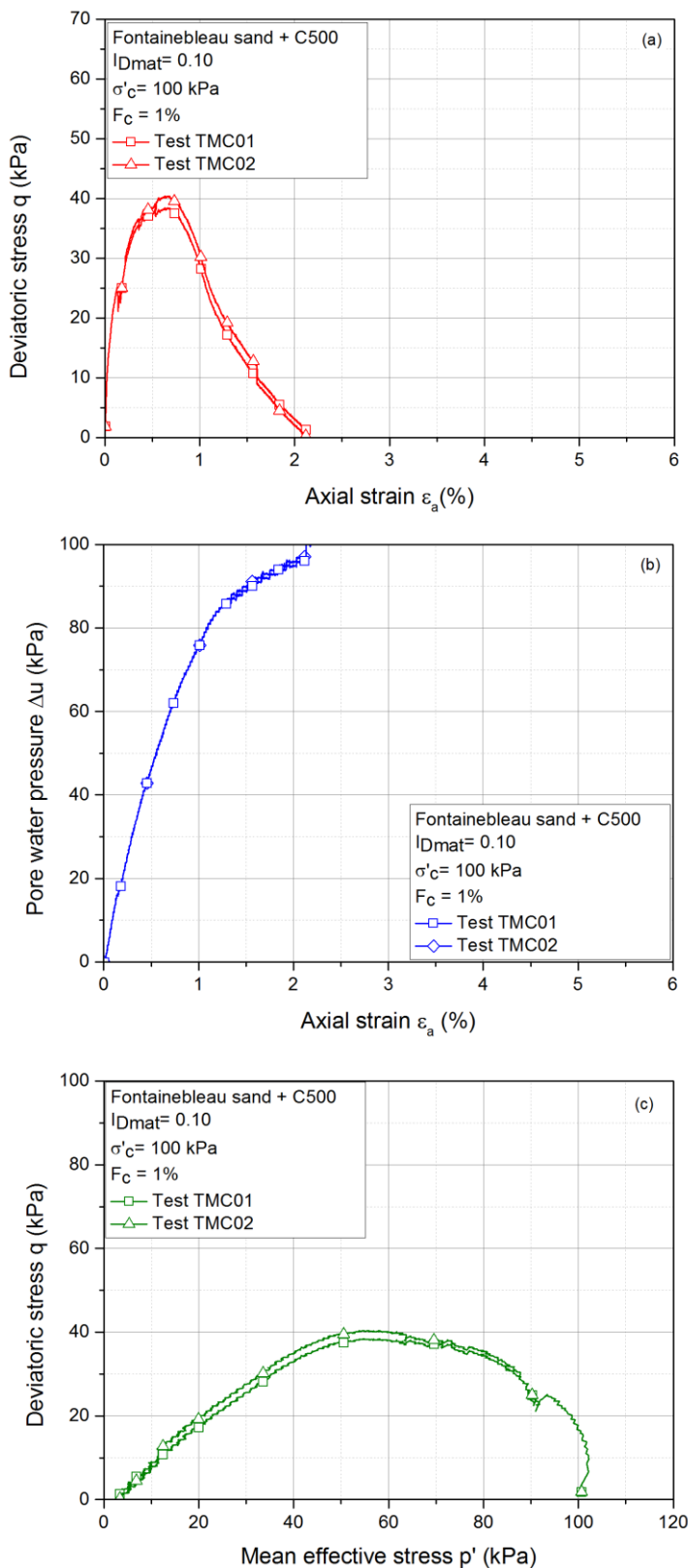


**Figure 3.4 - Repeatability test of Fontainebleau sand-C500 mixtures (loose state)**

**(a) ( $q$ - $\varepsilon_a$ ) curve ; (b) ( $\Delta u$ - $\varepsilon_a$ ) curve ; (c) ( $q$ - $p'$ ) curve**

### 3.4 Influence of the density index of sand matrix $I_{Dmat}$

In order to highlight the influence of the density index on the mechanical behavior of both clean sand and sand-fines mixtures in undrained conditions, a series of monotonic tests for specimens having different initial density indexes and consolidated under two confining pressure 100 kPa and 400 kPa has been carried out.

#### 3.4.1 Sand and non- plastic fines

Based on the shear curves presented in figure 3.5, it is clear that the density index has a very significant effect on the undrained response of sand and sand-fines mixtures. The shear curves reveal the passage from a softening behavior (liquefaction) for very loose mixtures to a hardening behavior for denser mixtures.

For a consolidation stress  $\sigma'_c$  at 100 kPa and a low density index ( $I_{Dmat} = 0.10$ ), the mixture exhibits a very marked level of peak resistance for an axial deformation of about 0.5% followed by a sharp decrease in resistance until reaching a zero value and thus revealing a contracting behavior and total liquefaction of the specimen. On the other hand, the case of high density index ( $I_{Dmat} = 0.50$ ), the shear curve shows a continuous increase in the deviator stress which indicates a hardening behavior of the mixture.

Concerning the pore water pressure values, the latter decreases with the increase in the density index. The generated EPWP increases to very high values that reach the value of the consolidation stress and hence lead to total liquefaction and collapse of the material, this phenomenon is observed for the case of loose material ( $I_{Dmat} = 0.10$ ). On the other hand, for dense material ( $I_{Dmat} = 0.50$ ) the pore water pressure records a small increase at the very beginning stage followed by a sharp decrease that reaches negative values (- 300 kPa) indicating a dilatant and stable behavior of the mixture.

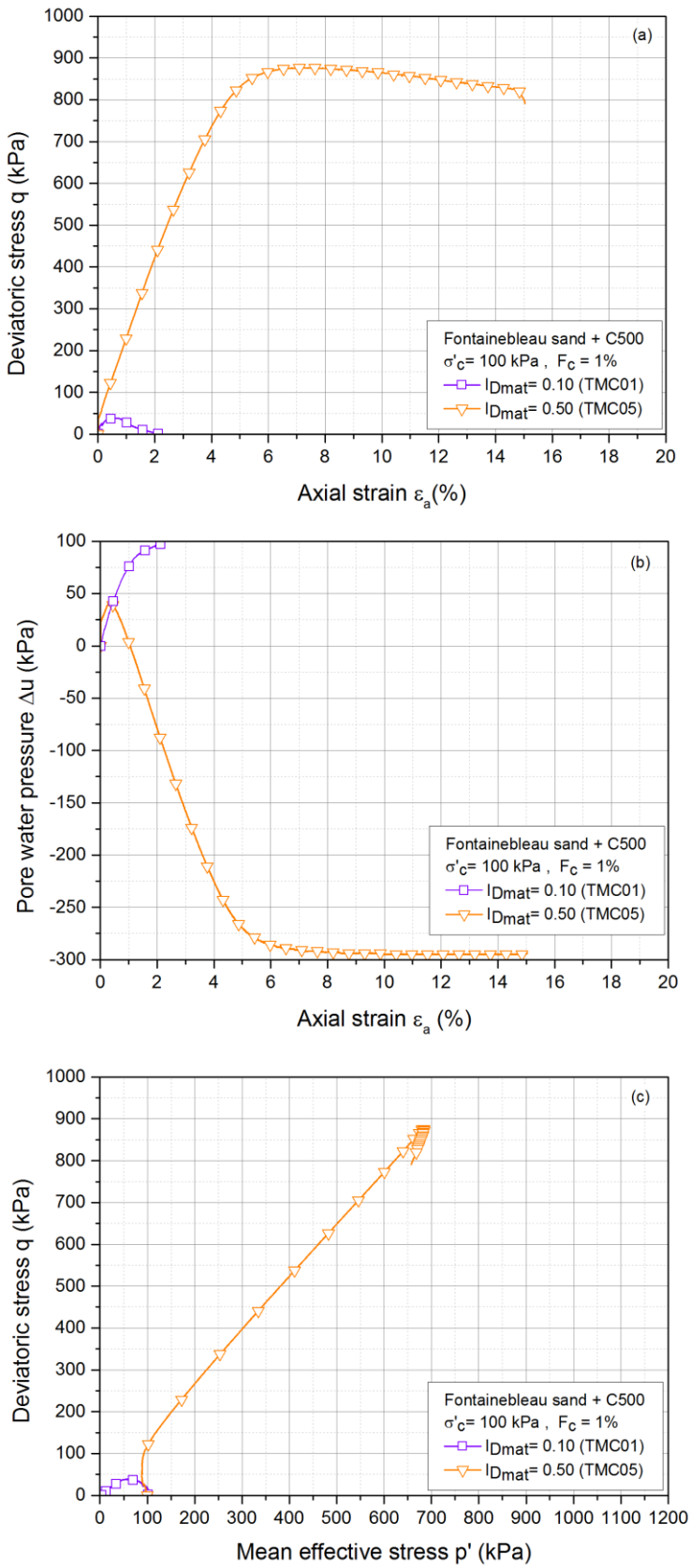


Figure 3.5 - Influence of density index on the behavior of Fontainebleau sand-C500 mixtures

### 3.4.2 Sand and plastic fines

Another series of monotonic tests was carried out on mixtures of sand-Speswhite under the same initial conditions of those performed on sand-C500 with the variation in density index between  $I_{Dmat} = 0.10$  corresponding to very loose material and  $I_{Dmat} = 0.50$  for dense material. Unlike the silty mixture (sand-C500), the mixtures of Speswhite at low density indexes ( $I_{Dmat} = 0.10$ ) present a different behavior where no liquefaction phenomenon takes place. Indeed, the specimen shows at first a tendency to liquefy translated by a peak resistance followed by a decrease in the deviatoric stress that approaches zero before it shows regrowth in the shear curve and exhibits a dilatant behavior. On the other hand, the dense material ( $I_{Dmat} = 0.50$ ) presents a much more stable structure showing a contracting behavior at first for small values of axial strain before it dilates and records a continuous and important increase in the shear resistance that stabilizes with the evolution of the phenomenon of cavitation (figure 3.6).

As for the EPWP, the results are consistent with those of the shear resistance where for loose material the EPWP records a high generation rate that reaches 95 kPa before it starts to decrease. However, the dense mixture presents an increase at the beginning in pore pressure followed by a huge decrease that reaches negative values.

The influence of the density index on the evolution of the undrained shear resistance of the peak is presented in Fig 3.7 for the three values of fines content (1%, 3% and 5%) for the case of sand and C500 mixtures. Indeed, the undrained shear resistance increases with the increase in density index. It is also noted that this increase is more important and more pronounced as the consolidation stress is increased from 100 kPa to 400 kPa.

In conclusion, the liquefaction initiation potential decreases with the increase in density index, and depending on the latter value we could pass from a perfectly unstable state for a low value of the density index to a very stable state for a high density. These results confirm those already found by Canou (1989), Ishihara (1993), Benahmed (2001) and Nguyen (2014).

The same analysis was done on sand-speswhite mixtures. The results for the three fine contents (1%, 3% and 5%) are presented in figure 3.8. It is clear that the density index has a very marked influence on the mechanical response of the material, this influence is more pronounced with the increase in consolidation stress similar to the case of sand-C500 mixtures.

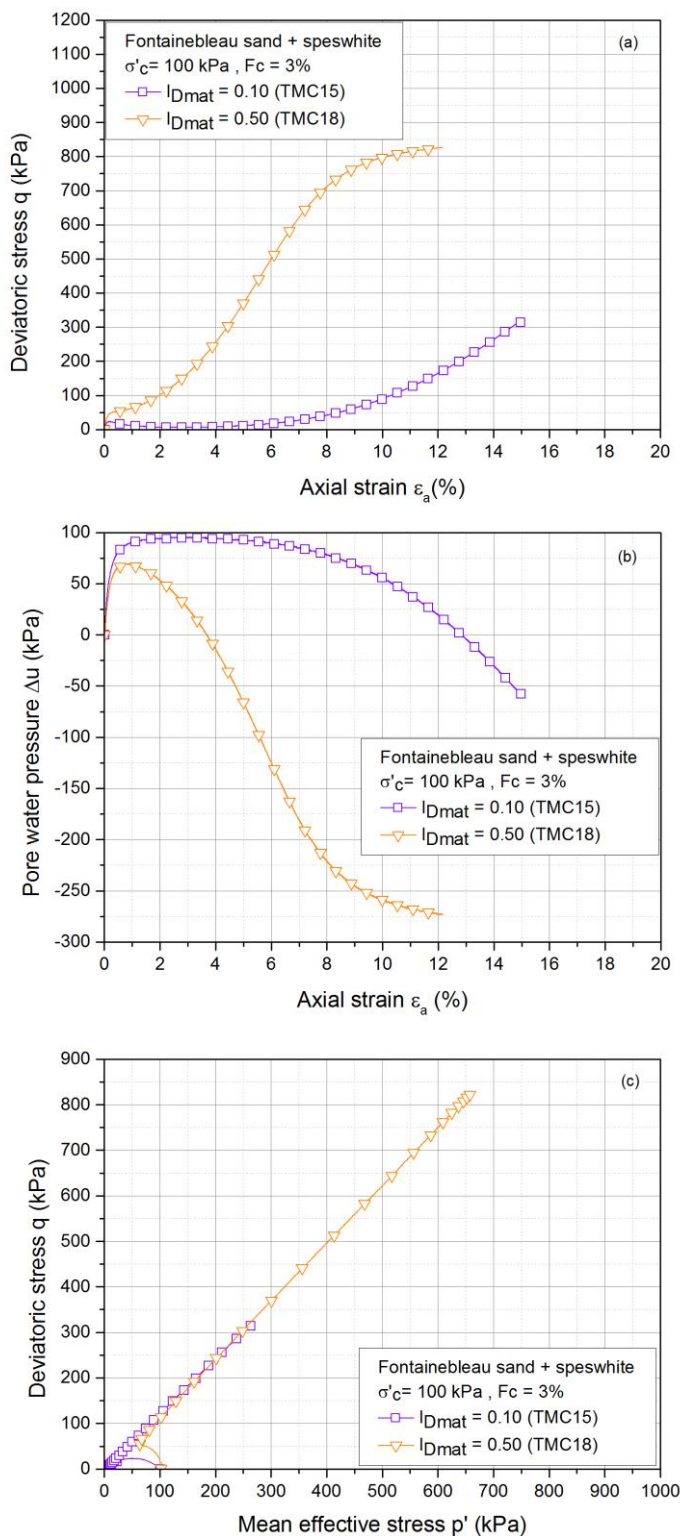


**Figure 3.6 - Influence of density index on the behavior of Fontainebleau sand-Speswhite mixtures**

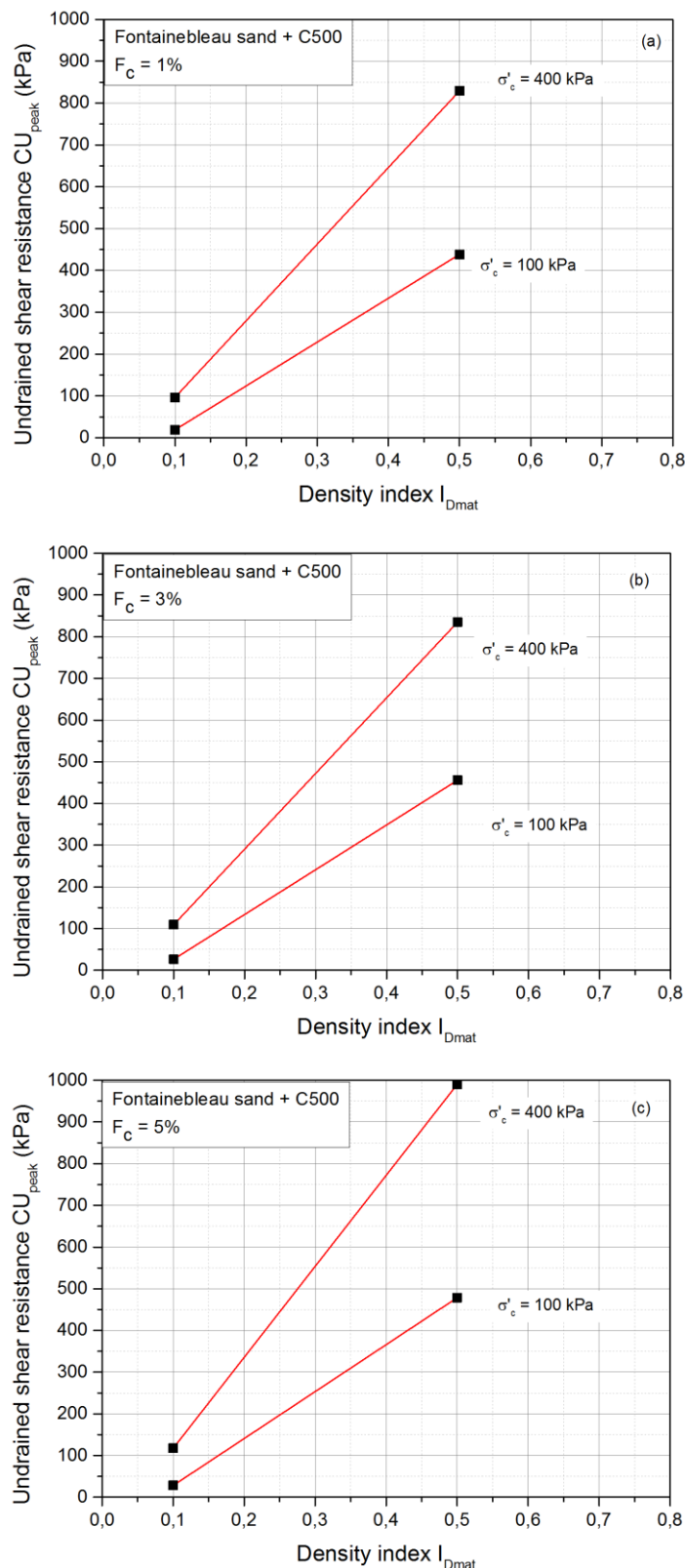


**Figure 3.7 - Influence of the density index on the evolution of the peak shear resistance of Fontainebleau sand-C500 mixtures (a) F<sub>c</sub> = 1% ; (b) F<sub>c</sub> = 3% ; (c) F<sub>c</sub> = 5%**

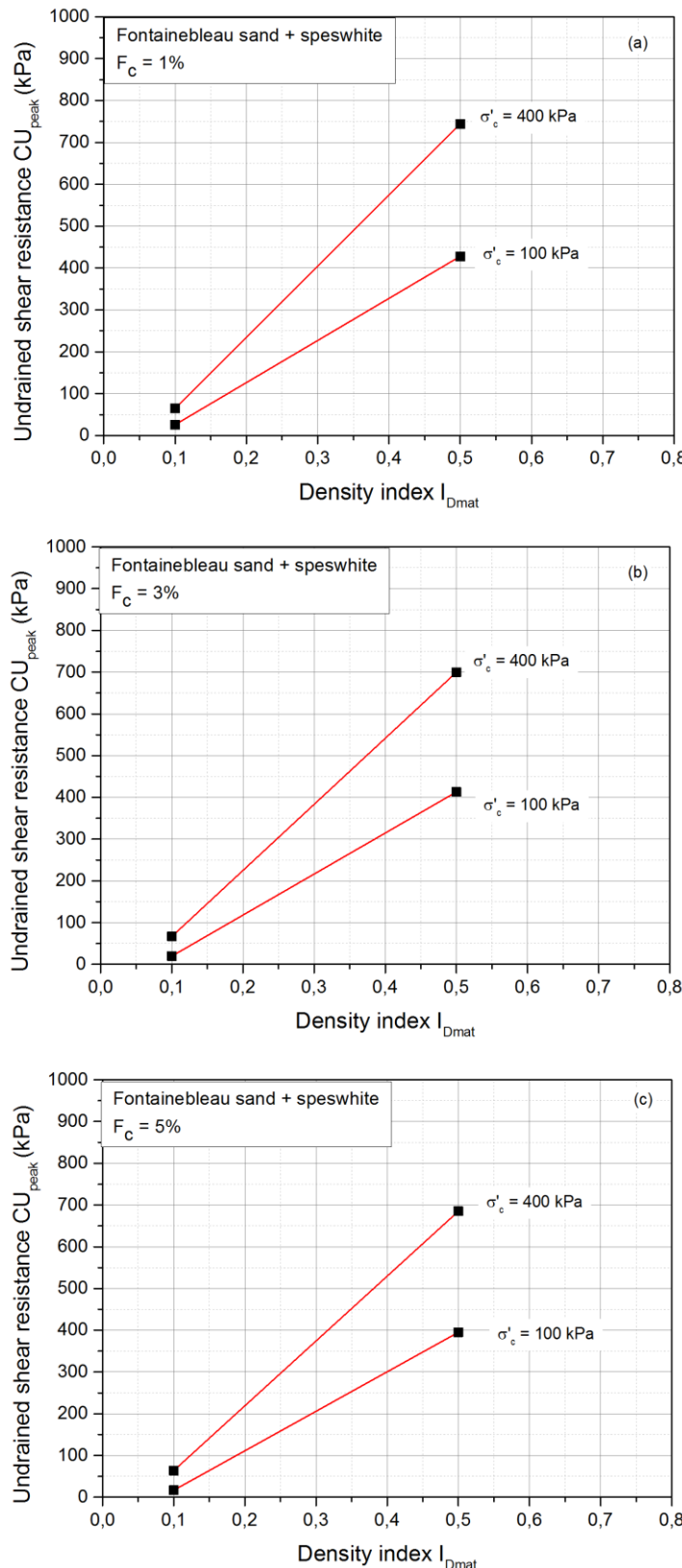


**Figure 3.8 - Influence of the density index on the evolution of the peak shear resistance of Fontainebleau sand-speswhite mixtures (a)  $F_c = 1\%$ ; (b)  $F_c = 3\%$ ; (c)  $F_c = 5\%$**

### 3.5 Influence of the consolidation stress

The isotropic consolidation stress  $\sigma'_c$  is one of the fundamental parameters controlling the mechanical behavior of soils. For this reason, a series of monotonic tests was carried out on specimens having the same initial conditions (density index, fines content ...) consolidated at different values of  $\sigma'_c$  (100 kPa and 400 kPa). Several series were also carried out by varying the initial density index in order to describe different isotropic compressibility curves. In addition, tests were carried out at different fines content (1%, 3% and 5%).

#### 3.5.1 Sand and non-plastic fines

Figure 3.9 presents the results of sand-C500 mixtures. It is clear that the consolidation stress has a significant influence on the response of the material. It is noted that the peak resistance increases with the increase in consolidation stress from 100 kPa to 400 kPa in a practically proportional way. Thus, the value of the peak of resistance where the liquefaction phenomenon is initiated increases with the increase in consolidation stress and its value is practically proportional to the latter. The axial deformation for which the peak appears also increases with the increase of  $\sigma'_c$ . For example, for a density index  $I_{Dmat} = 0.10$  and  $F_c = 1\%$  the peak resistance reaches a value of 38 kPa at an axial deformation of 0.5% under 100 kPa of consolidation. Whereas at 400 kPa consolidation the peak resistance increases to 193 kPa for an axial deformation of 0.76%. The same progression in peak resistance and its associated axial strain is observed for the other series of tests which present a contracting behavior. It is interesting to note that only loose mixtures present a total contracting behavior with an ultimate peak resistance. However, for higher density index the mixture present either contracting-dilating or dilating behavior.

Concerning the pore water pressure curves, the results show a similar general appearance for both loose and dense material. It is noted that the generation rate of the evolution of pore water pressure increases at higher consolidation stresses.

The stress paths in the  $(q, p')$  plane are presented for both loose and dense material. It is noted that for the case of loose material, the stress paths migrate towards the origin of the axes until reaching a null value of deviatoric stress for a zero mean effective stress  $p'$  indicating the collapse and total liquefaction of the material. However, the dense material stress path turns to the right and exhibits a dilatant behavior.

### 3.5.2 Sand and plastic fines

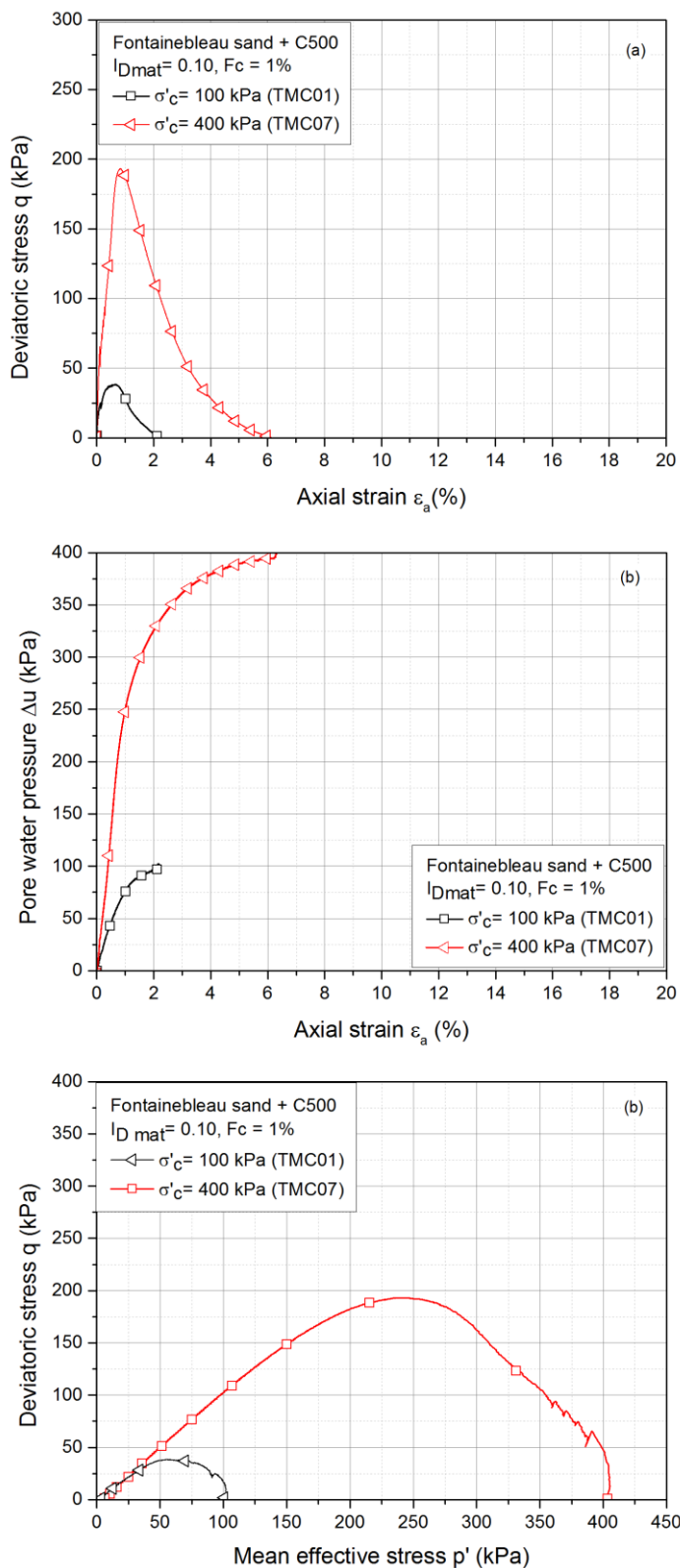
The same series of tests was also performed on sand-Speswhite mixtures to detect the influence of the consolidation stress on this type of mixture.

Figure 3.10 presents the results of two series of tests done on sand-Speswhite mixtures for loose mixture ( $I_{Dmat} = 0.10$ ) at two consolidation stresses 100 kPa and 400 kPa at a fines content  $F_c = 3\%$ .

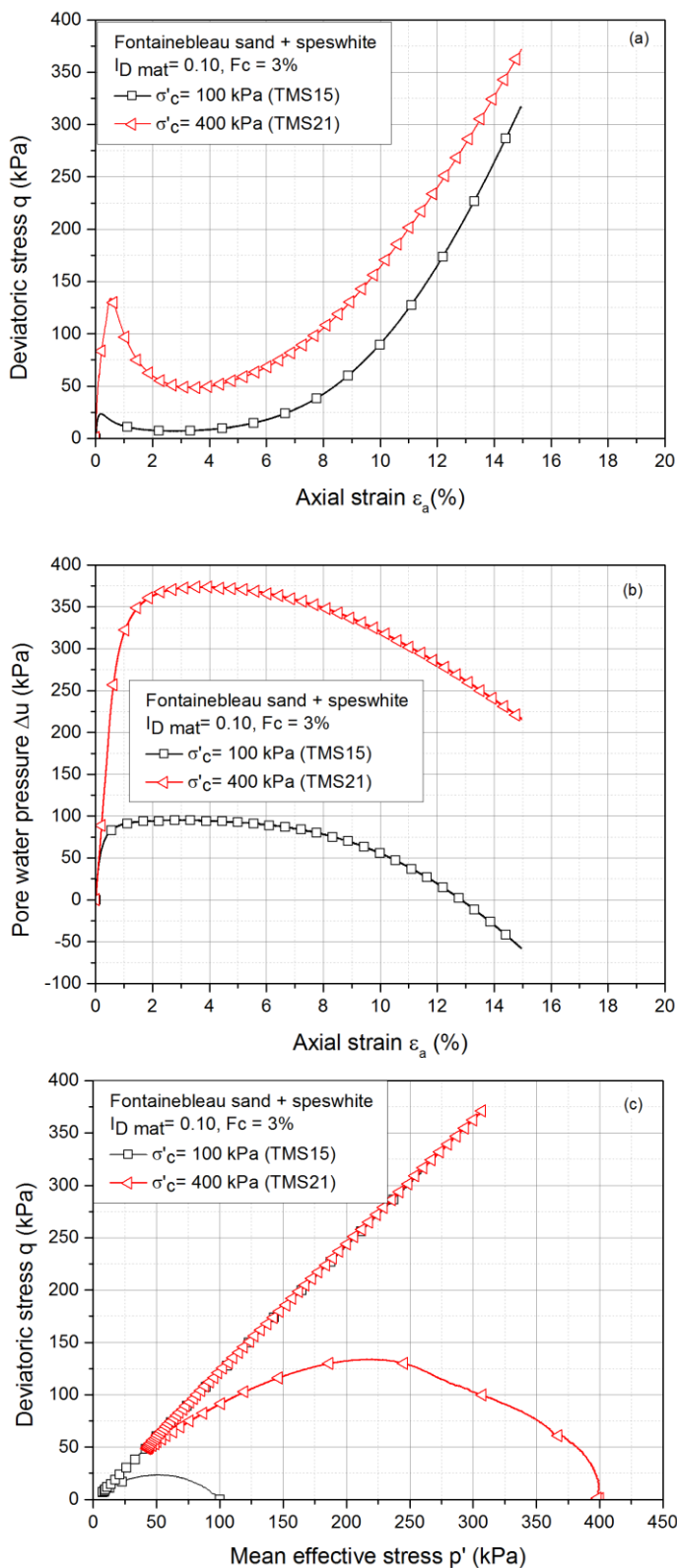
The influence of the consolidation stress is clear for both cases in terms of shear strength where the peak resistance increases with the increase in consolidation stress. However, it is important to note that for the case of loose material, mixtures with Speswhite do not liquefy unlike those of C500. In fact, the loose material presents a contracting-dilating behavior where after it reaches a peak resistance for a small value of the axial strain of the order 0.5% the shear resistance decreases sharply before it goes back and increases showing the dilation of the material. The same results can be interpreted concerning the pore pressure and stress paths as those noted by mixtures with C500.

Figure 3.11 presents in a synthesized manner the evolution of the undrained shear resistance at peak  $c_{u,peak}$  as a function of the isotropic consolidation stress for both mixtures of sand-C500 and sand-Speswhite. For the sand-C500 mixture, it is observed that the undrained shear resistance is proportional to the isotropic consolidation stress and hence it is possible to define a coefficient of proportionality  $\lambda_{cu}$ . It is reported that this coefficient increases with the increase in fines content (it varies from 0.16 for clean sand to 0.29 for the case of  $F_c = 5\%$ ).

The same analysis has been done for mixtures of sand and Speswhite. The corresponding results are presented in figure 3.12. It is noted here that the undrained shear resistance is also proportional to the isotropic consolidation stress, however, the coefficient of proportionality reports first an increase from 0.16 for the case of clean sand to 0.21 for sand-speswhite mixture at  $F_c = 1\%$  followed by a decrease upon increasing the fines content beyond 1% to 5% that reaches the value 0.17.



**Figure 3.9 - Influence of the consolidation stress on the undrained behavior of loose and medium dense Fontainebleau sand-C500 mixtures:** (a) ( $q$ - $\varepsilon_a$ ) curve; (b) ( $\Delta u$ - $\varepsilon_a$ ) curve; (c) ( $q$ - $p'$ ) curve



**Figure 3.10 - Influence of the consolidation stress on the undrained behavior of loose and medium dense Fontainebleau sand-Speswhite mixtures: (a) ( $q$ - $\varepsilon_a$ ) curve; (b) ( $\Delta u$ -  $\varepsilon_a$ ) curve; (c) ( $q$ - $p'$ ) curve**

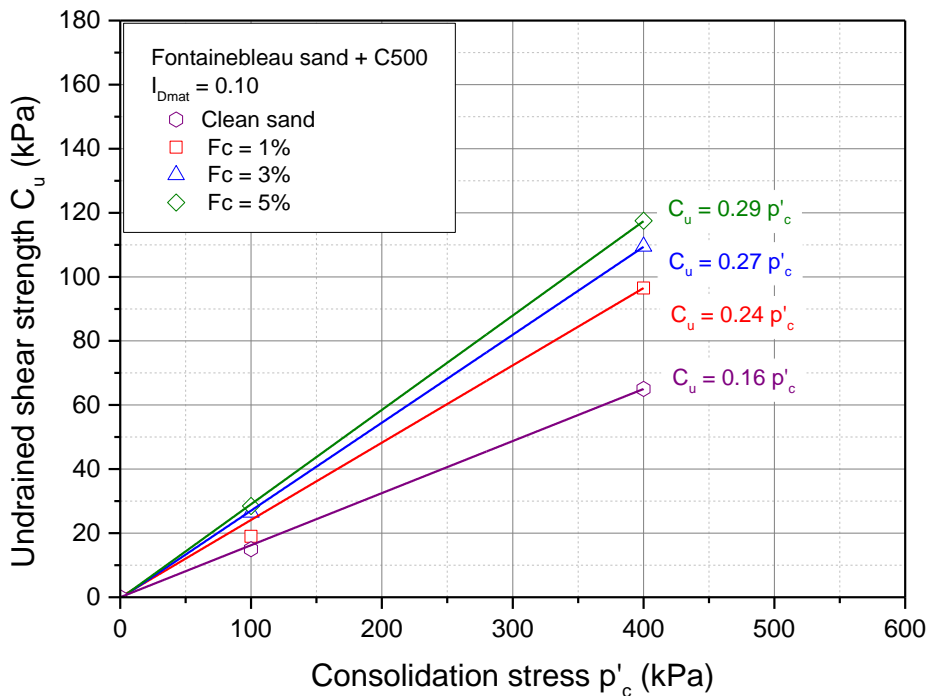


**Figure 3.11 - Influence of the consolidation stress on the undrained peak resistance of loose Fontainebleau sand-C500 mixtures**

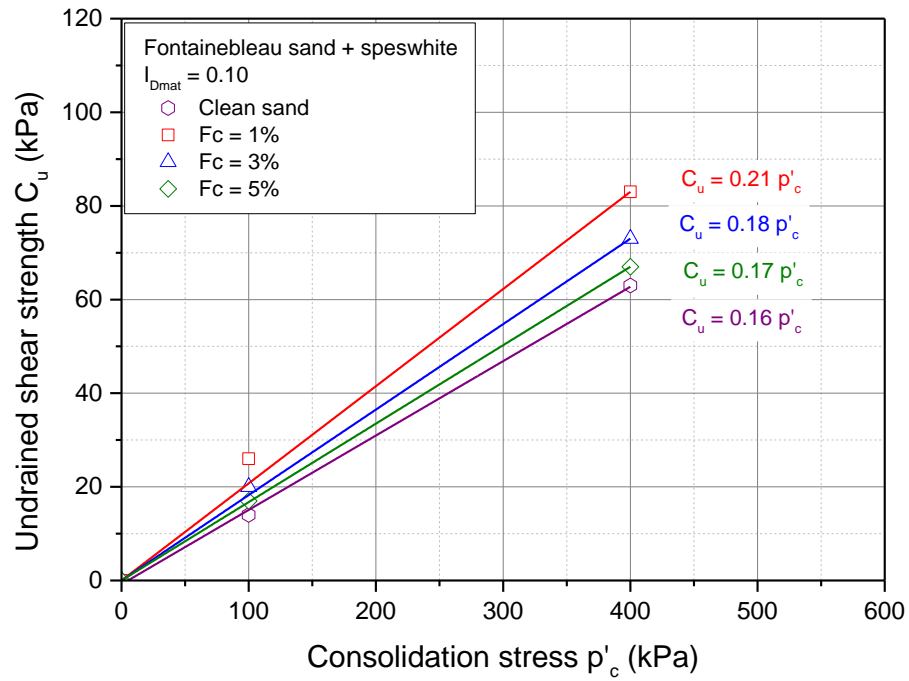


**Figure 3.12 - Influence of the consolidation stress on the undrained peak resistance of loose sand-C500 mixtures**

### 3.6 Influence of fines content

In order to study the effect of fines content on the behavior of silty sands, it is interesting to reconstitute different specimens at various fines contents. The common method used in the literature consists of preparing samples with the same initial density index. Therefore, we have adopted this method to prepare two groups of specimens having two different density index of the sand matrix,  $I_{Dmat} = 0.10$  for the first group and  $I_{Dmat} = 0.50$  for the second one. Two values of consolidation stress were chosen (100 kPa and 400 kPa). The values chosen for the fines content are 1%, 3% and 5%. These values were chosen below 5% in order to keep the predominance of the sand matrix.

#### 3.6.1 Sand and non-plastic fines

Figure 3.13 presents the shear curves, the EPWP curves and the effective stress paths for the case of sand-C500 mixtures at a density index  $I_{Dmat} = 0.10$  and consolidated at 100 kPa. We note that the mechanical response of the samples is similar with the increase in the values of fines content. All the specimens present a contracting behavior. It is noted that the shear resistance increases with the increase in fines content, from 27 kPa for clean sand to 57 for the case of silty sand at  $F_c = 5\%$ . These results confirm those already found by Dezfulian 1984, Pitman 1994 and Amini and Qi 2000 who reported an increase in the shear resistance of sands with the increase in fines content. The observed behavior is characterized by an increase in the deviatoric stress until it reaches a peak value at a small value of the axial strain. This increase is followed by a sharp decrease of strength until reaching a null value and thus leading to a total liquefaction of the sample.

Concerning the EPWP, all curves exhibit the same behavior, finally reaching 100 kPa which is equal to the value of the initial consolidation stress and thus lead to the collapse of the material. It is interesting to note that the EPWP generation rate decreases with the increase in fines content.

The stress paths in the  $(q, p')$  plane after reaching a peak resistance migrate towards the origin of the axes until reaching a null value of resistance and hence indicating the total liquefaction of the specimens.

Figure 3.13 also shows the results of the same group of tests consolidated at 400 kPa. As for the case of 100 kPa, total liquefaction is observed for the different specimens but with an increase in the values of the shear resistance and the corresponding axial strains where the phenomenon of liquefaction was initiated.

Another series of tests were performed on specimens at different fines content ( $F_c = 1\%, 3\%$  and  $5\%$ ) with an initial density index  $I_{Dmat} = 0.50$  consolidated at  $100 \text{ kPa}$ . The results of silty sands are presented in figure 3.15. All the curves exhibit a dilatant behavior resulting in a continuous increase in the shear resistance along the line of rupture.

After a slight increase in the EPWP at the very beginning of the test, the latter decreases sharply after that to become negative and reaches a value of approximately  $-300 \text{ kPa}$ . At this stage of the test, the cavitation phenomenon develops and stops the evolution of EPWP within the specimen, besides to the stabilization of the deviatoric stress, which then passes through a maximum followed by a slight softening.

The stress paths in the  $(q, p')$  plane exhibits a dilatant behavior of the material which is translated by a continuous increase in the deviatoric stress.

Therefore, it is noted that upon adding the non-plastic fines (C500) to sand, these particles participate in the shear resistance of the mixture and hence they decrease the liquefaction potential of the material. In fact, the addition of these particles will lead to a global increase in the density index of the total specimen and consequently will lead to a higher peak resistance. Also, it is interesting to note that upon adding  $5\%$  of fines, the sand skeleton structure will remain unchanged and the fine particles will be placed between the sand grains where these particles will increase the friction between the grains and therefore they will favor dilatancy. As the sand structure remains unchanged, the modification of the soil resistance could be attributed to the fine particles. Indeed, the fine particles contribute to the overall chain forces and therefore they increase the resistance against liquefaction.

### **3.6.2 Sand and plastic fines**

In addition to the silty sands (sand-C500 mixtures), a similar series of tests were carried out sand-Speswhite mixtures. The results for loose material ( $I_{Dmat} = 0.10$ ) are presented in figure 3.14 in terms of shear resistance, EPWP and stress paths. Unlike the silty sands, sand-Speswhite mixtures present no liquefaction phenomenon. In fact, the shear resistance increases to a peak value at a small axial strain followed by a decrease in the resistance that approaches zero before observing re-increase in the deviatoric stress and increases along the line of rupture. However, it is interesting to note that the trend is reversed for this case, where the shear resistance decreases with the increase in fines content unlike the case of silty sands where an increase in the deviatoric stress was observed. These results confirm those found in the literature concerning the effect of the addition of plastic fines. Indeed, several

authors as Polito 1999, Bouferra and Shahrour 2004, Ghahremani and Ghalandarzadeh (2006), and Derakhshandi *et al.* (2008) have reported a decrease in the shear resistance of sands upon adding plastic fines until a certain limiting value usually greater than 15% followed by a re increase in the latter. For our case, as we didn't exceed 5% fines content, it is supposed that we are below the threshold value and therefore the behavior is characterized by a decrease in shear resistance.

The results of the evolution of the EPWP show an increase at the beginning of the test that approaches the value of 100 kPa for the specimens consolidated at 100 kPa at a fines content  $F_c = 1\%$ . This approach increases with the increase in fines content to 5%. This trend can be explained by the exhibited behavior of the shear resistance where the latter decreases for higher values of fines content.

Concerning the stress paths, the curves present a migration of the paths towards the origin of the axes before this migration is reversed to the right indicating a dilating behavior of the material.

It is important to recall here that the clean sand specimens have been prepared in wet conditions due to the fact that such loose states are impossible to reach in dry condition as already explained in chapter II. Therefore, the effect of the reconstitution method must be taken into consideration as it has been shown in the literature that the latter can affect the behavior of sand. Actually we can pass from a totally contracting behavior (wet specimen) to a totally dilating behavior (dry specimen). In addition, beyond 1%, the increase in plastic fines leads to a decrease in the peak resistance of the specimens. Since density index increases with the addition of fines, one might expect that the peak shear resistance must increase and this is contrary what we have encountered. Actually, this decrease in shear resistance upon adding fines could be attributed to the nature of these fines (plasticity), leading to the sliding between the sand grains and therefore favoring the contractancy of the whole specimen.

The effect of fines content on the behavior of sand-Speswhite mixtures for dense samples was also studied. Figure 3.16 present the results of tests carried out on samples of sand-Speswhite at various fines content consolidated at 100 kPa for an initial density index  $I_{Dmat} = 0.50$ . All the specimens present a contracting-dilating behavior where after a small peak resistance the deviatoric stress presents a small decrease in its value before it is followed by a re increase indicating the dilation of the material. However, it is important to note that unlike the silty sands the increase in fines content for mixtures of sand and speswhite lead to a decrease in the shear resistance of the material.

Concerning EPWP and stress paths curves, the same results could be interpreted but with a reversible effect of the increase in fines content.

### 3.6.3 Synthesis of results

The analysis of the influence of fines content on the behavior of loose sands is presented in a synthetic manner in figure 3.17 that presents the plot of the peak resistance as a function of fines content. It is noted that the mixtures of sand and non-plastic fines (C500) present an increase in resistance upon increasing the fines content. However, the trace of the latter with the increase in plastic fines (Speswhite) reveals a reversed behavior translated by a decrease in the peak resistance. Note here that for the case of sand-Speswhite (blue curve) the first part is plotted as dotted line since it corresponds to the peak resistance reached for clean sand that has been prepared in wet conditions unlike the sand-plastic fines mixtures as it has been already clarified in the previous chapter and therefore, it must be taken into consideration the influence of the reconstitution method.

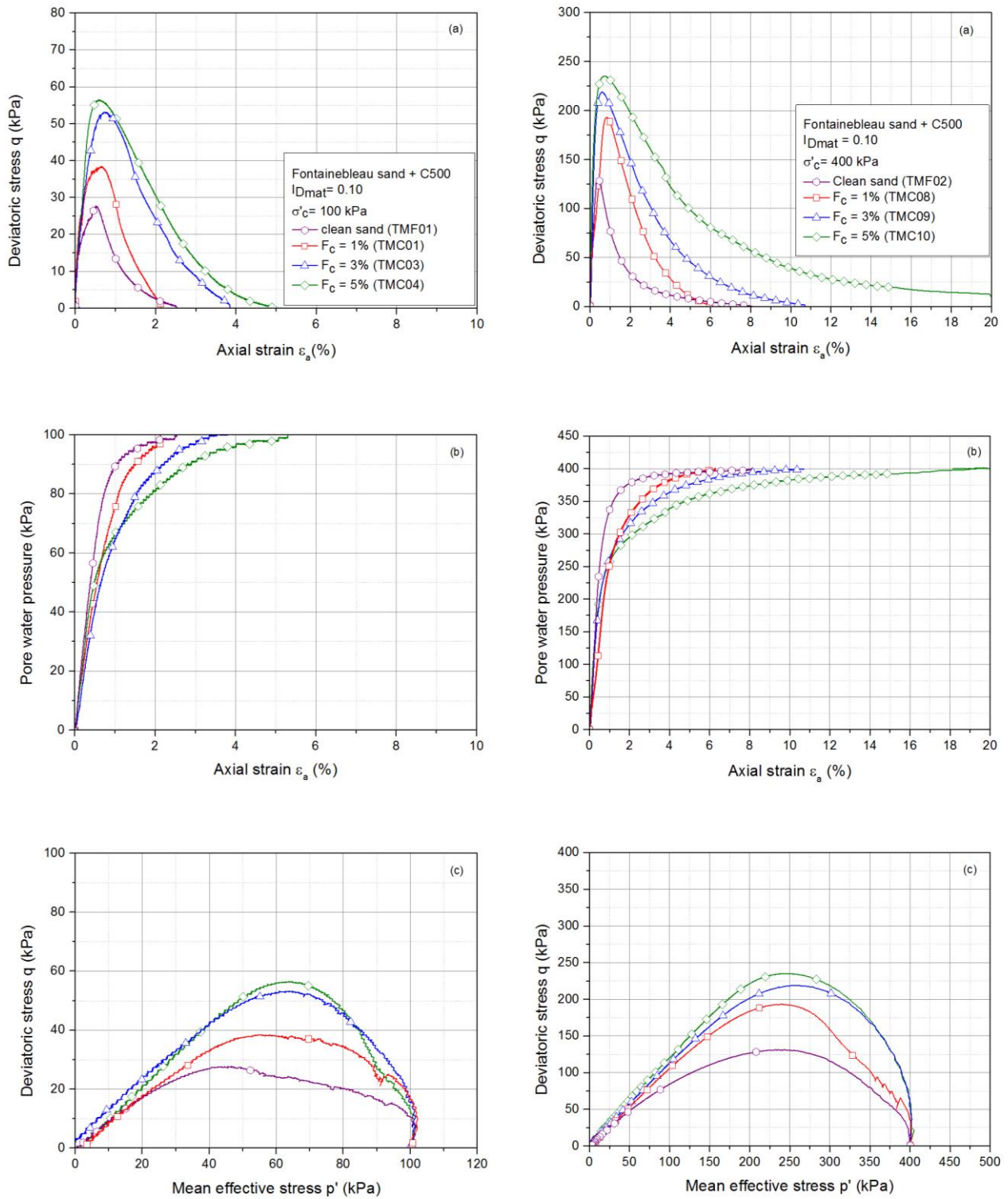


**Figure 3.13 - Influence of non-plastic fines (C500) on the mechanical behavior of loose Fontainebleau sand**

**(a) ( $q$ - $\varepsilon_a$ ) curve ; (b) ( $\Delta u$ - $\varepsilon_a$ ) curve ; (c) ( $q$ - $p'$ ) curve**

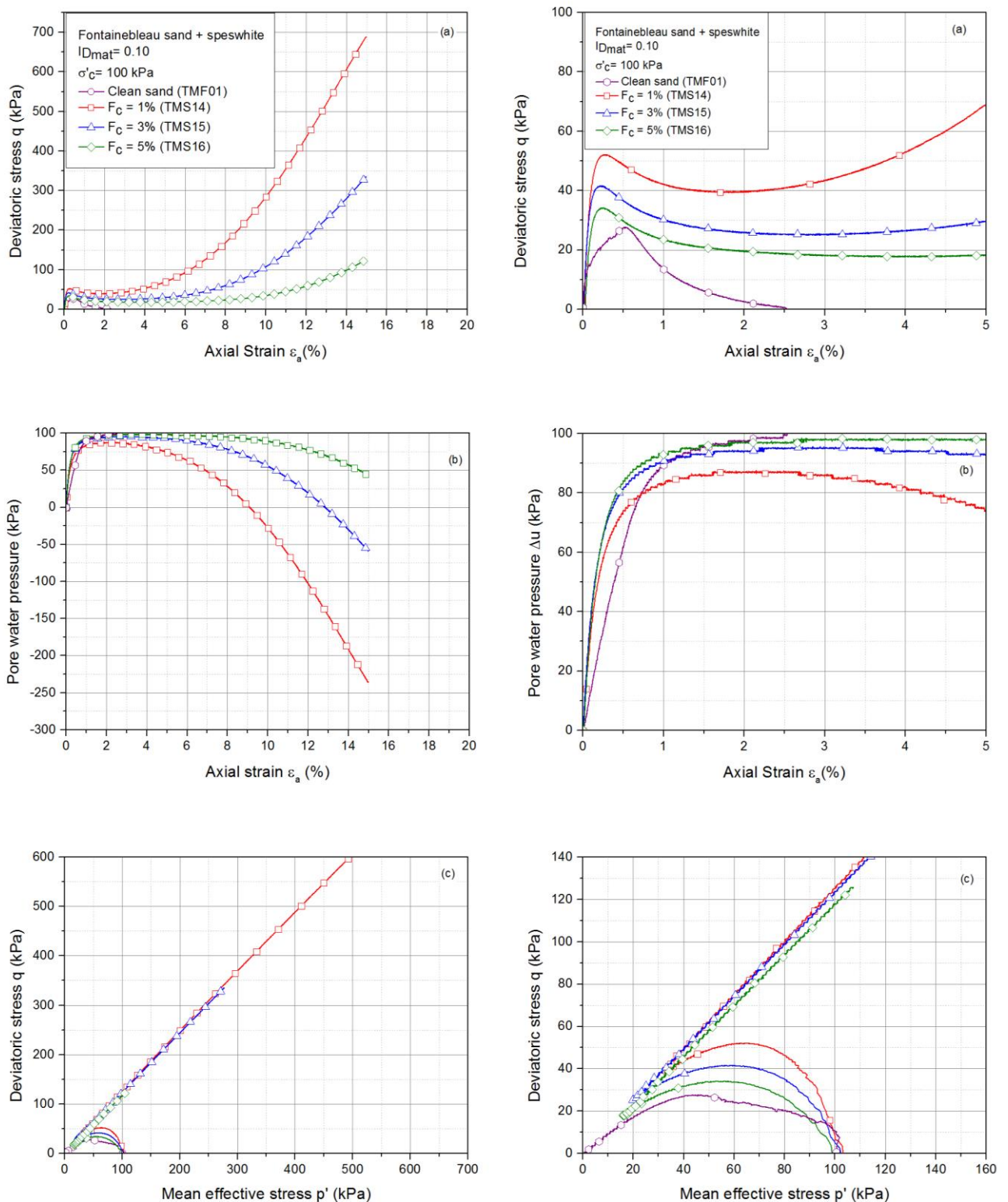


**Figure 3.14 - Influence of plastic fines (Speswhite) on the mechanical behavior of loose Fontainebleau sand**

(a) ( $q-\varepsilon_a$ ) curve ; (b) ( $\Delta u-\varepsilon_a$ ) curve ; (c) ( $q-p'$ ) curve

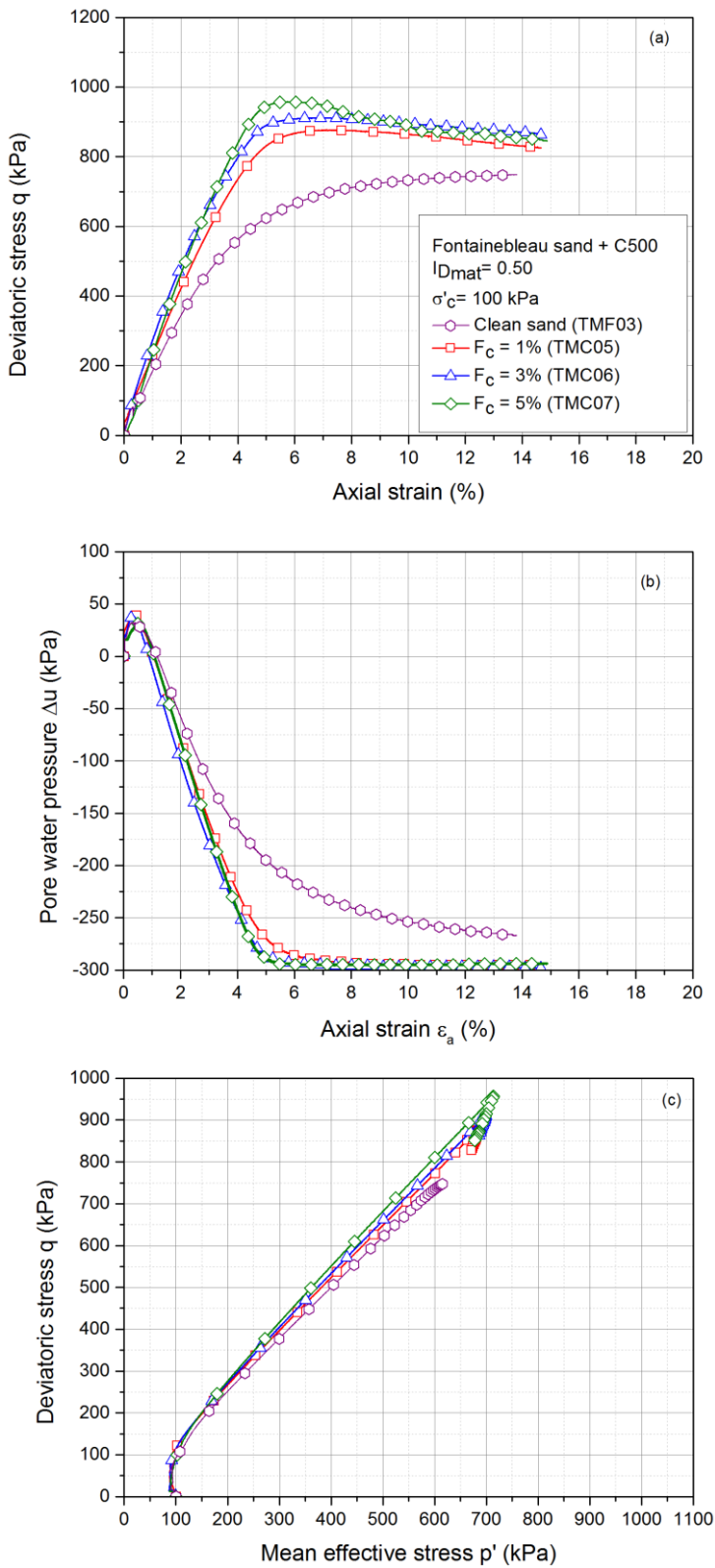


**Figure 3.15 - Influence of non-plastic fines (C500) on the mechanical behavior of medium dense Fontainebleau sand**

: (a) ( $q$ - $\varepsilon_a$ ) curve ; (b) ( $\Delta u$ -  $\varepsilon_a$ ) curve ; (c) ( $q$ - $p'$ ) curve

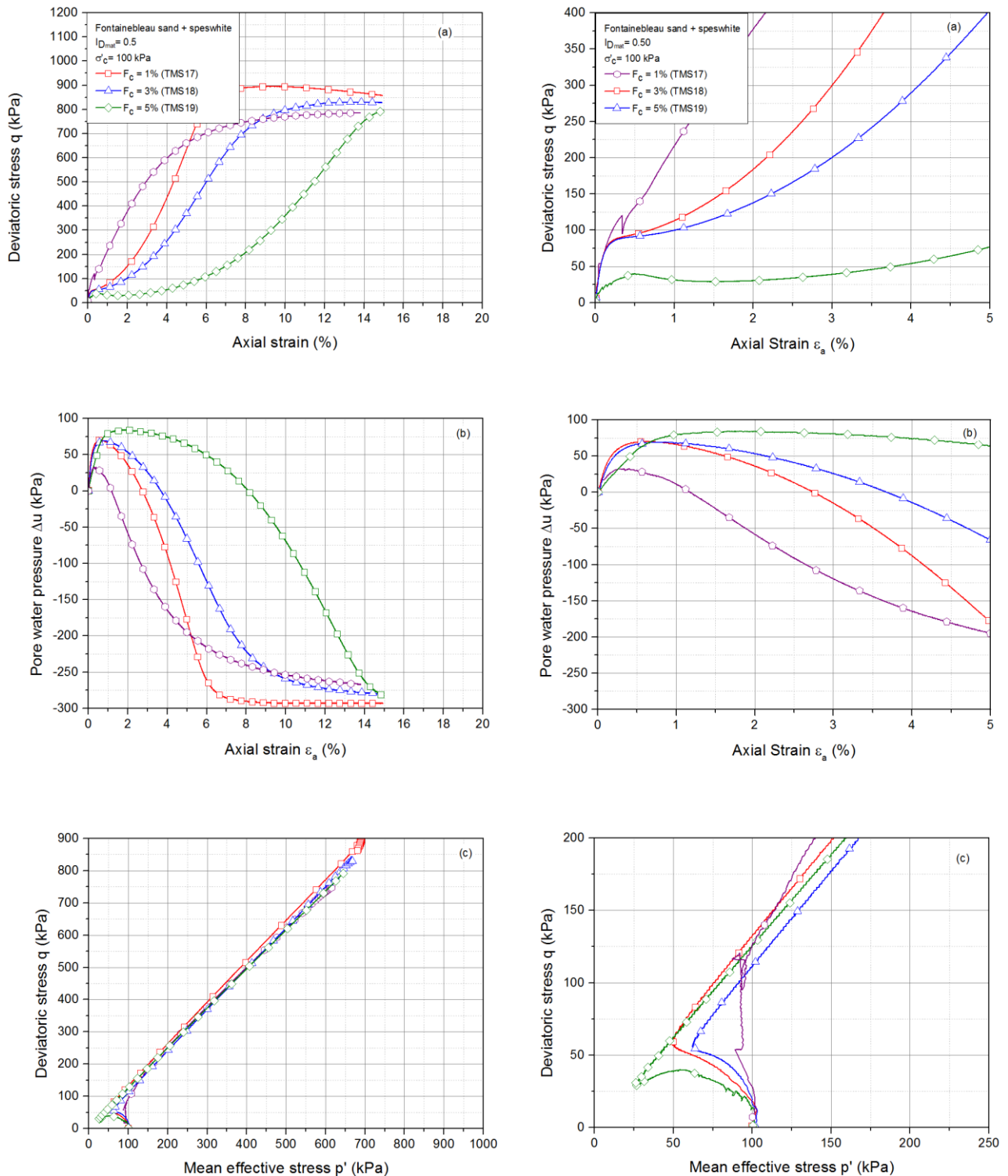


**Figure 3.16 - Influence of plastic fines (Speswhite) on the mechanical behavior of loose Fontainebleau sand:** (a) ( $q$ - $\varepsilon_a$ ) curve; (b) ( $\Delta u$ - $\varepsilon_a$ ) curve; (c) ( $q$ - $p'$ ) curve

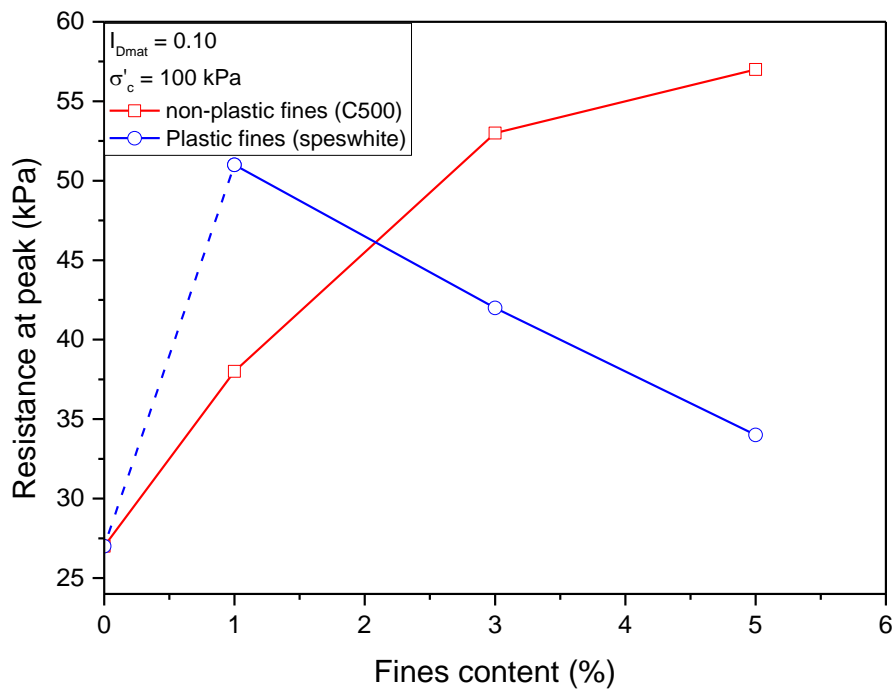


**Figure 3.17 - Influence of fines content on peak shear resistance**

### 3.7 Influence of type of fines

In order to study the effect of the type of fines on the mechanical behavior of sands, two types of fines were chosen C500 (non-plastic) and Speswhite (plastic) for this study. A series of monotonic tests was carried out on two groups of sand-fines mixtures at various fines content  $F_c = 1\%$ ,  $3\%$  and  $5\%$  and for two density indexes ( $I_{Dmat} = 0.10$  and  $0.50$ ) consolidated either at  $100 \text{ kPa}$  or  $400 \text{ kPa}$ .

Figure 3.18 presents a comparison between the behavior of sand-C500 and sand-Speswhite mixtures consolidated at  $100 \text{ kPa}$  and having an initial density index  $I_{Dmat} = 0.10$  for a fines content  $F_c = 3\%$ . It is observed that the mixture of sand-C500 present a typical behavior of liquefaction characterized by a small peak resistance at an axial strain of  $0.5\%$  followed by a sharp decrease in the resistance that reaches zero indicating the total liquefaction and collapse of the sample. On the other hand, the sand-speswhite mixture and after a slight softening exhibits a significant hardening phase characterized by a re increase in the shear resistance along the line of rupture indicating the dilatancy of the material.

Concerning the EPWP, the sand-C500 mixture shows a high generation rate that increases and reaches 100 kPa which is equal to the initial consolidation stress and thus indicates a total liquefaction of the sample. Whereas, the speswhite mixture presents an increase in the pore pressure at the beginning followed by a continuous decrease that reaches negative values.

The stress paths corresponding to the C500 mixture migrate towards the origin of the axes until reaching a null value of deviatoric stress however, the speswhite mixture migrates at first towards the origin before it goes back to the right and records an increase in the deviatoric stress indicating a dilating behavior. Figure 3.18 also presents the results of tests consolidated at 400 kPa for a fines content  $F_c = 3\%$ . The same results could be interpreted as those for the case of consolidation at 400 kPa but with higher values of shear resistance due to the effect of the increase in consolidation stress.

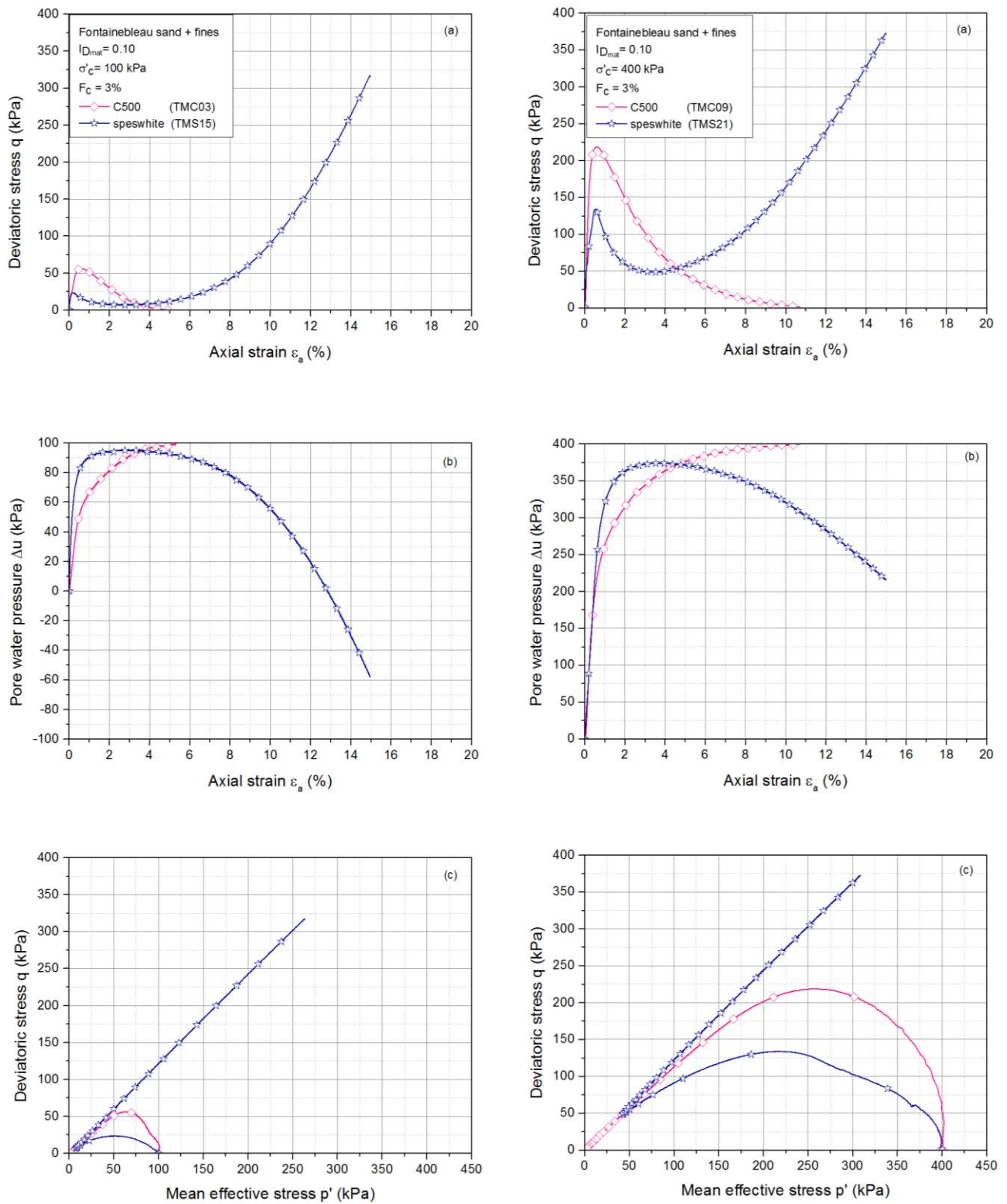


**Figure 3.18 - Influence of type of fine (plastic/non-plastic) on the mechanical response of Fontainebleau sand**

### 3.8 Evaluation of different mechanical parameters

This part presents a summary of all the results obtained from the tests carried out. We are mainly interested in the evaluation of the mechanical properties of the materials such as maximum friction angle, characteristic angle, instability friction angle ... The different parameters calculated are presented in a synthetic manner as a function of the characteristics of the material such as density index, consolidation stress and fines content.

#### 3.8.1 Maximum friction angle $\Phi'_{\max}$

The analysis of the results concerning the effect of consolidation stresses at two different values of confining pressure (100 kPa and 400 kPa) for the case of medium dense samples allows us to detect the ultimate states of our samples.

Figure 3.19 presents the evolution of the maximum friction angle with the increase in fines content for the mixtures of sand and fines for the two different values of consolidation stresses (100 kPa and 400 kPa). It is realized that for sand-C500 mixtures the maximum friction angle increases from  $32.9^\circ$  to  $36.1^\circ$  as the fines content increases from  $F_c=0\%$  to  $F_c = 5\%$  (figure 3.19a). These results confirm those found by Yang *et al.* (2006) who indicated an increase in the friction angle from  $37.3^\circ$  to  $42.2^\circ$  with the increase in fines from 0% to 94%, as well as those found by Murthy *et al.* (2007) who has also reported an increase in friction angle from  $30.2^\circ$  to  $34.4^\circ$  with an increase in fines content from 0% to 15%. However, it is interesting to note here that these values are recorded for the case where the samples are consolidated at 100 kPa, whereas for those where the initial confining pressure is equal to 400 kPa the values are reduced by about  $2^\circ$ . These results confirm those already found by Benahmed (2001) concerning the effect of the consolidation stress on the evaluation of the maximum friction angle of clean sand. Hence, it can be noted here that this influence of the consolidation stress on the evaluation of the maximum friction angle is also applicable for the case of mixtures of sand and fines in the same manner.

The same interpretation has been done for the mixtures of sand and Speswhite. However, in this case this trend is reversed with a decrease of the maximum friction angle with an increase in fines content (figure 3.19b).

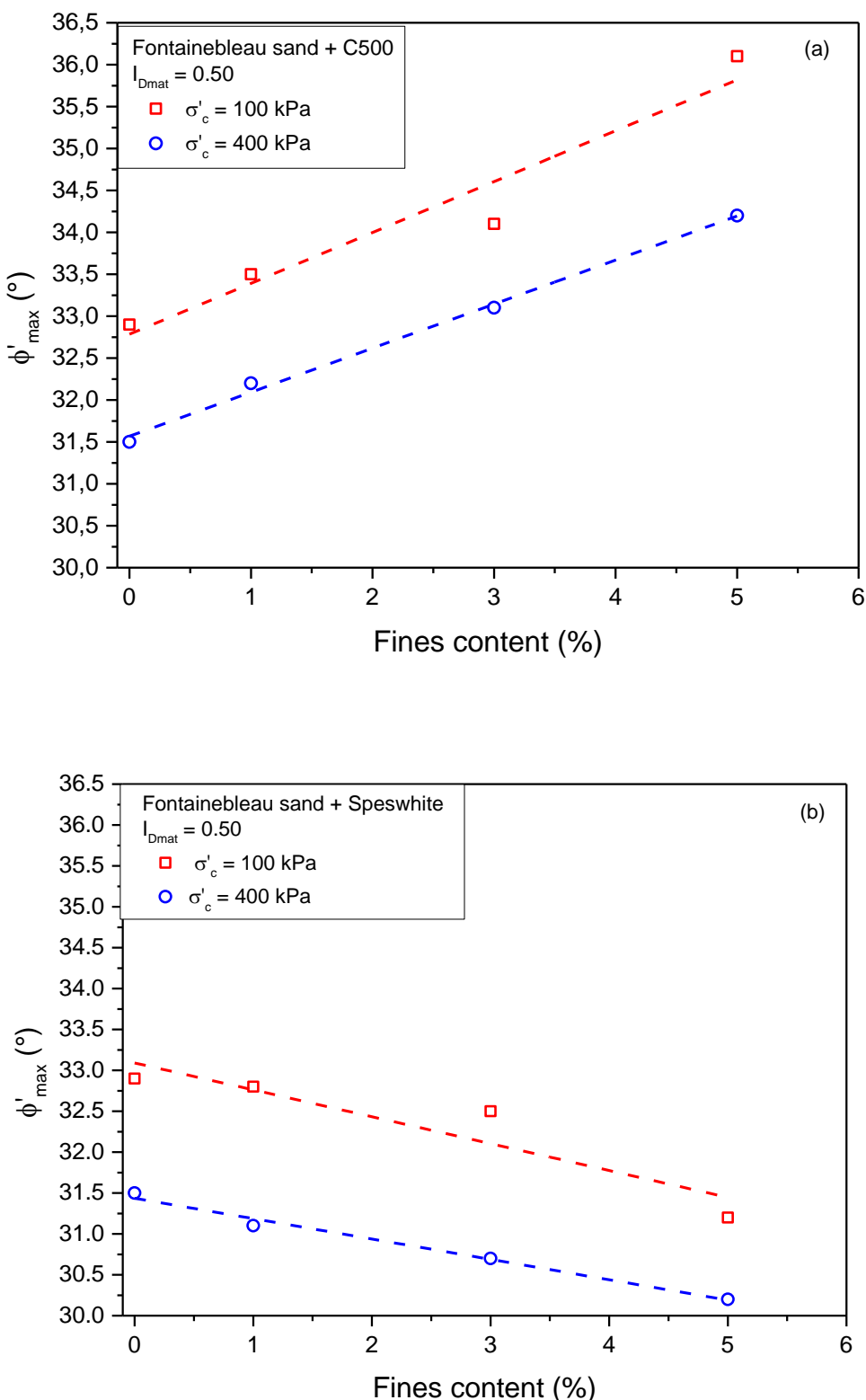


**Figure 3.19 - Evolution of maximum friction angle as a function of fines content**

**(a) Non-plastic fines; (b) plastic fines**

The plot of the average values of the maximum friction angle  $\Phi'_{\max}$  for both mixtures of sand-non-plastic fines and sand-plastic fines is presented in figure 3.20. It is noted that the evolution of the maximum friction angle with the increase in fines content can be represented by a straight line of increasing positive slope for the mixtures with non-plastic fines, however, for the case of plastic fines the slope is negative as the maximum friction angle decreases with the increase in fines content. It is also interesting to note that the slopes are quasi identical in absolute value, which indicates the same evolution of the maximum friction angle of these soils but in opposite senses.

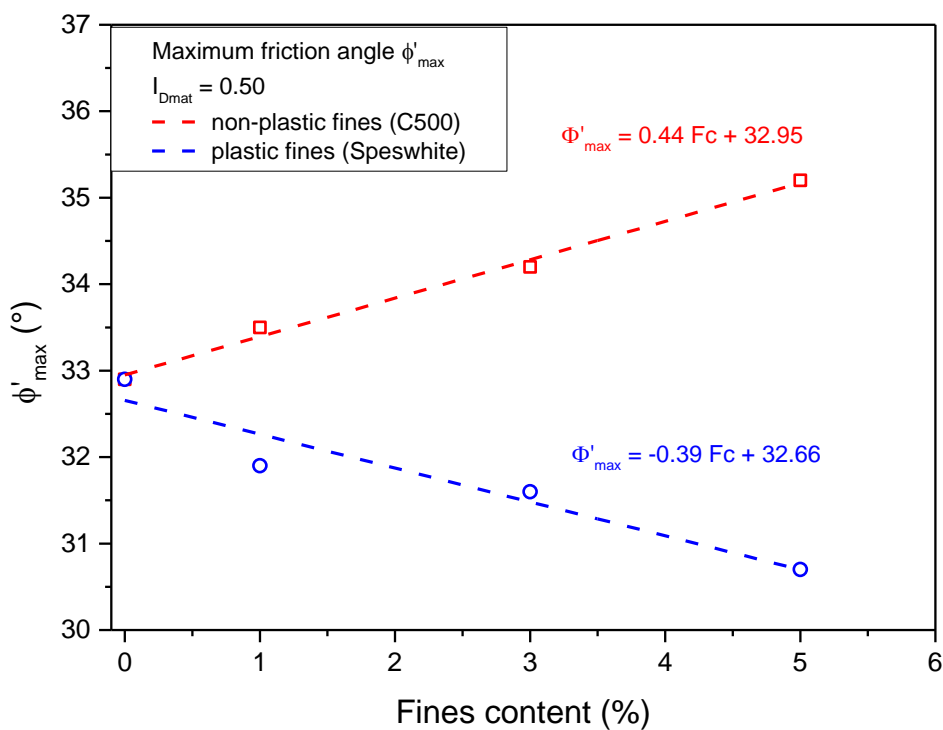


**Figure 3.20 - Linear correlation of the evolution of maximum friction angle with fines content**

### 3.8.2 Characteristic angle $\Phi'_{car}$

The characteristic state corresponds to the transition point between the contracting and the dilating behavior of the soil. This state can be clearly identified from the effective stress paths, where the samples show a sudden change in behavior as mentioned before, the slope of the line passing through this point and the origin defines the characteristic state.

Figure 3.21 presents a summary of the characteristic angle values obtained for the different tests performed at different fines contents for two values of consolidation stresses. Note that

the characteristic angle remains almost constant or varies very little according to the consolidation stress, which confirms the reasonably unique character of the characteristic threshold. This has been also reported by Benahmed (2001) for clean sands.

For the case of mixtures with silica C500, the characteristic angle decreases with the increase in fines content, however for sand and speswhite the latter increases with the increase in Fc. Note that this evolution is relatively small especially for the case of sand-C500 mixtures and could be considered negligible where the characteristic friction angle increases very slightly with the increase in fines content and it could even be considered constant.

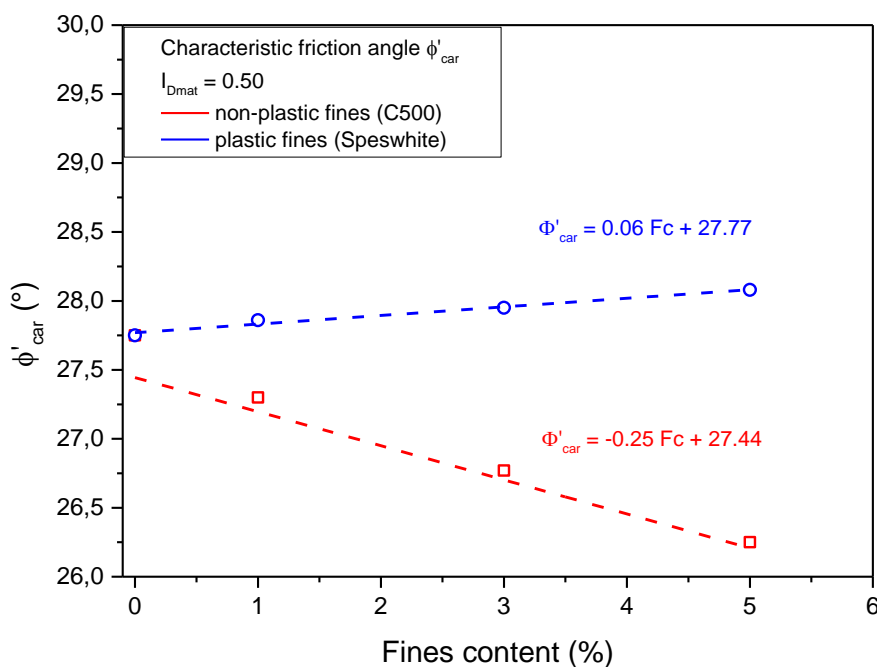


**Figure 3.21 - Evolution of characteristic friction angle as a function of fines content**

### 3.9 Analysis of the conditions of initiation of instability

The instability of loose sands under monotonic loading is initiated at the peak resistance. Beyond this peak, the material softens and develops large deformations. In other words, this phenomenon takes place when the effective stress state crosses the instability zone.

The initiation of the instability is characterized by two parameters that are the deviator stress at the initiation of the instability  $q_{inst}$  and the mobilized friction angle at the initiation of the instability  $\Phi_{inst}$  and is defined by the following equation:

$$\eta_{inst} = \frac{q_{inst}}{p'_{inst}} = \frac{6 \sin \varphi'_{inst}}{3 - \sin \varphi'_{inst}} \text{ (in compression)} \quad (3.1)$$

$$\eta_{inst} = \frac{q_{inst}}{p'_{inst}} = \frac{6 \sin \varphi'_{inst}}{3 + \sin \varphi'_{inst}} \text{ (in extension)} \quad (3.2)$$

$$\varphi'_{inst} = \arcsin\left(\frac{3 \eta_{inst}}{6 + \eta_{inst}}\right) \quad (3.3)$$

Figure 3.22 presents the stress paths corresponding to different series of tests carried out on loose sand and sand-fines mixtures. It may be observed that for each series of tests, the points corresponding to the initiation of liquefaction are aligned and joined by a line that passes through the origin axis. This instability line has been already defined by Lade (1993) and it is interesting here to note that this definition of the instability that joins the peak resistance at different consolidation stresses with the origin of axes is also applicable for the sand-fines mixtures. Besides, it is clear that this line is affected by the fines content added to the sand. In fact, the stress ratio at the instability initiation  $\eta_{inst}$  varies from 0.58 for the case of pure sand to 0.98 for the case of mixture with non-plastic fines (C500) at  $F_c = 5\%$ .

The evolution of the instability line with the fines content is also presented in figure 3.23 to clarify this effect. We can remark that we have a set of instability lines passing through the origin, whose evolution is a function of the fines content value  $F_c$ . As the fines content increases the slope of the instability line increases in the  $(q, p')$  plane.

The same analysis has been done to the mixtures of sand and Speswhite at different fines content  $F_c = 1\%, 3\% \text{ and } 5\%$  in order to see the effect of the addition of these fines on the instability of the mixtures. Although these specimens haven't shown total liquefaction, it is possible to define the instability line in the  $(q, p')$  planes as shown in figure 3.24. The graph of the evolution of the instability line as a function of fines content is also presented in figure 3.25. It is noted that first upon adding 1% of fines the instability slope increases and then this increase is followed by a decrease as we add more fines.

Figure 3.26 presents the evolution of the instability friction angle  $\Phi'_{inst}$  with the increase in fines content. It is noted that this evolution can be translated by a straight line with increasing slope for non-plastic fines. Whereas for the plastic fines, the first part of the line is dotted since the first point corresponds to the loose clean sand specimen that is prepared in wet

conditions as already mentioned before unlike the mixtures with plastic fines which were prepared in dry conditions. The second part of this line presents the evolution of the instability angle upon increasing fines, and it shows a decrease in the latter (negative slope).

The values of the different mechanical parameters that have been computed based on the results of the undrained monotonic shearing for clean sand and sand-fines mixtures are presented in table 3.3.

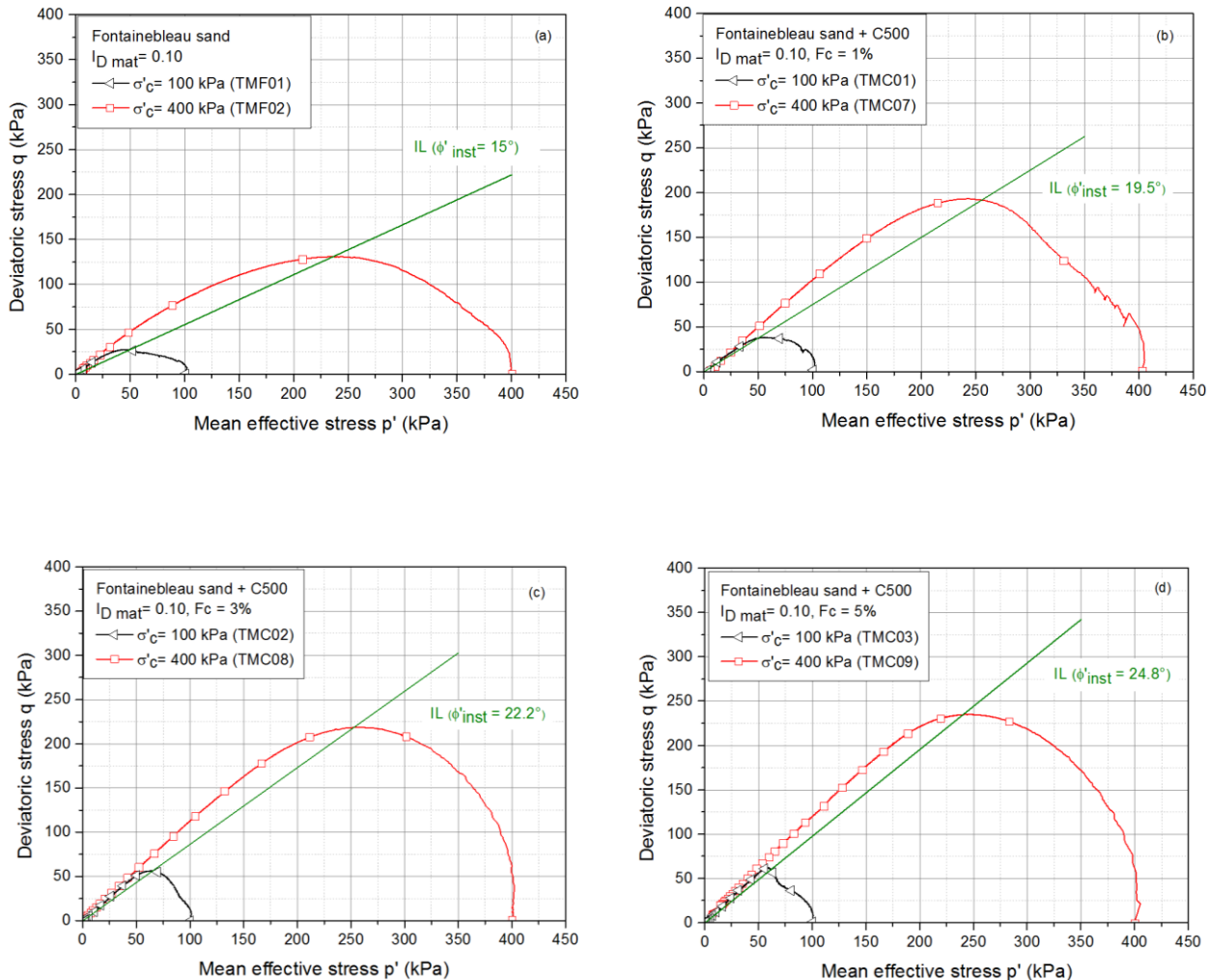


**Figure 3.22 - Plot of the instability line in the  $(p',q)$  plane for Fontainebleau sand-C500 mixtures**

**(a) Clean sand; (b)  $F_c = 1\%$ ; (c)  $F_c = 3\%$ ; (d)  $F_c = 5\%$**

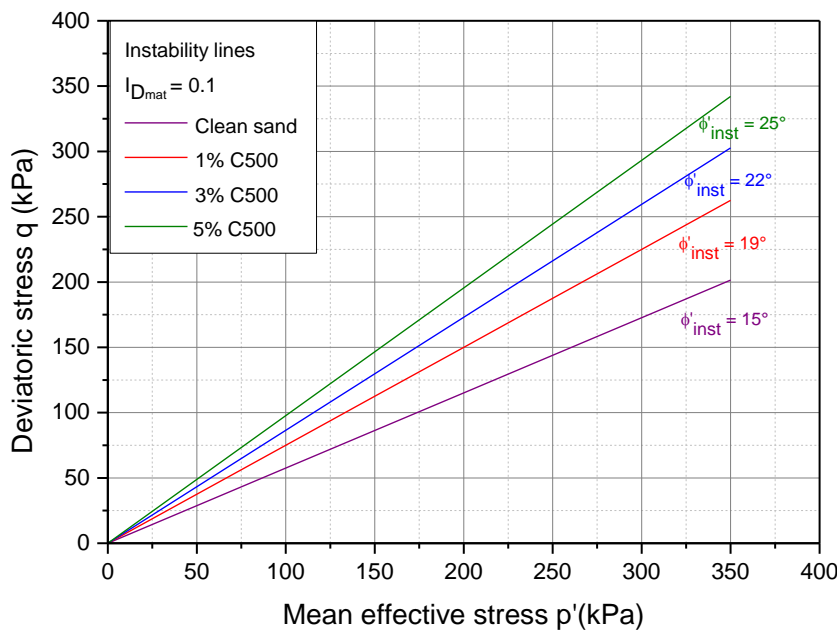


**Figure 3.23 - Evolution of the instability line for Fontainebleau sand-C500 mixtures**

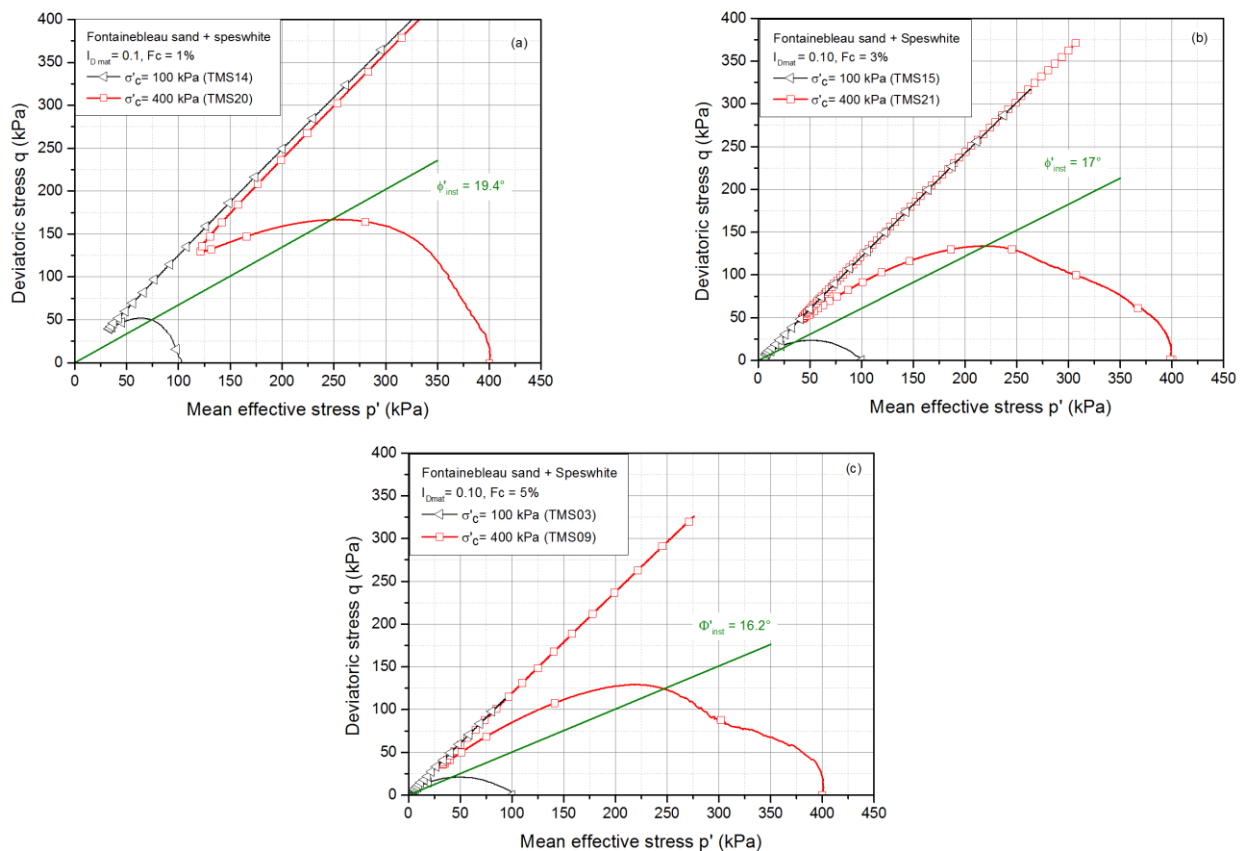


**Figure 3.24 - Plot of the instability line in the  $(p',q)$  plane for Fontainebleau sand-Speswhite mixtures**

**(a)  $F_c = 1\%$ ; (b)  $F_c = 3\%$ ; (c)  $F_c = 5\%$**

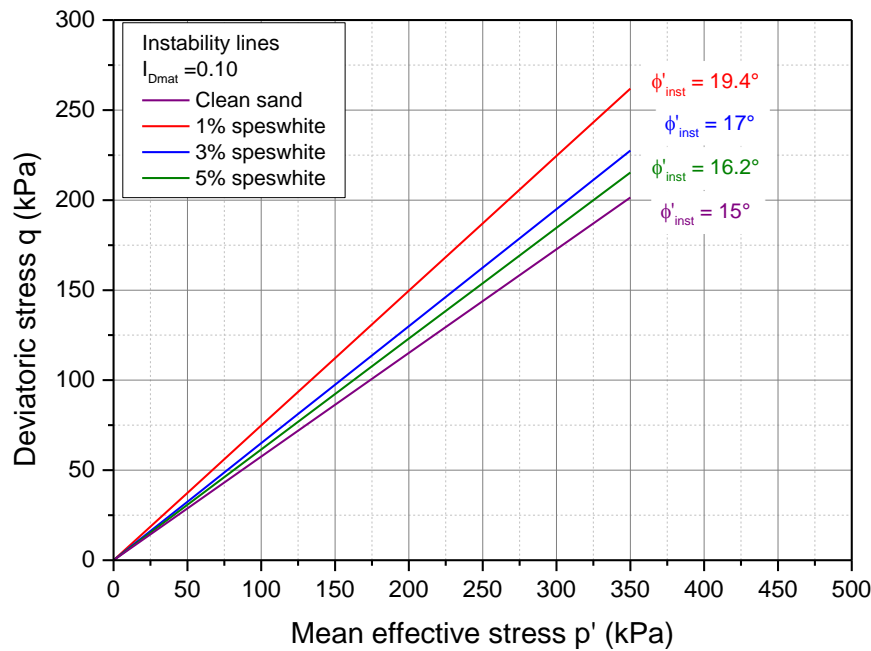


Figure 3.25 - Evolution of the instability line Fontainebleau sand-Speswhite mixtures

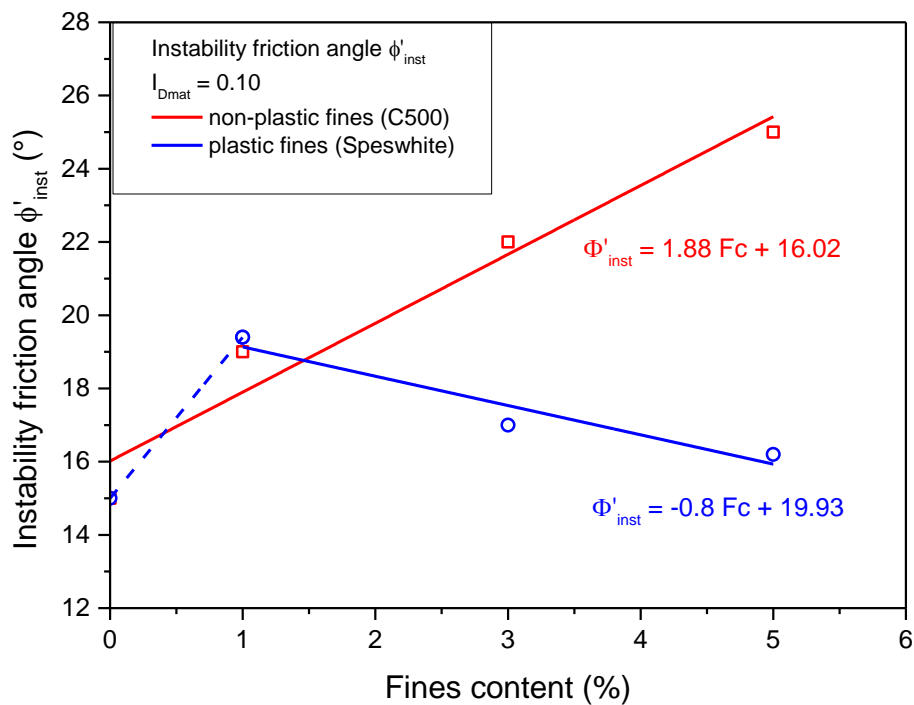


Figure 3.26 - Evolution of instability friction angle with fines content

<b>Test reference</b>	$\sigma'c$	$I_{Dmat}$	$e_{mat}$	$F_c$	Type of fines	$\Phi'_{inst}$	$\Phi'_{max}$	$\Phi'_{car}$
TMC01	100	0.10	0.9	1	C500	20.6	-	-
TMC02	100	0.10	0.9	1	C500	20.6	-	-
TMC03	100	0.10	0.9	3	C500	22.6	-	-
TMC04	100	0.10	0.9	5	C500	26.7	-	-
TMC05	100	0.50	0.74	1	C500	-	33.5	27.4
TMC06	100	0.50	0.74	3	C500	-	34.2	26.7
TMC07	100	0.50	0.74	5	C500	-	36.1	26.3
TMC08	400	0.10	0.9	1	C500	18.3	-	-
TMC09	400	0.10	0.9	3	C500	21.8	-	-
TMC10	400	0.10	0.9	5	C500	22.9	-	-
TMC11	400	0.50	0.74	1	C500	-	32.2	27.2
TMC12	400	0.50	0.74	3	C500	-	33.1	26.7
TMC13	400	0.50	0.74	5	C500	-	34.2	26.2
TMS14	100	0.10	0.9	1	Speswhite	20.6	31	28.2
TMS15	100	0.10	0.9	3	Speswhite	18	30.4	28.7
TMS16	100	0.10	0.9	5	Speswhite	16.8	30	29
TMS17	100	0.50	0.74	1	Speswhite	-	32.8	27.9
TMS18	100	0.50	0.74	3	Speswhite	-	32.5	27.9
TMS19	100	0.50	0.74	5	Speswhite	-	31	28.08
TMS20	400	0.10	0.9	1	Speswhite	18.2	31	28
TMS21	400	0.10	0.9	3	Speswhite	16	30	28.3
TMS22	400	0.10	0.9	5	Speswhite	15.6	29.5	28.7
TMS23	400	0.50	0.74	1	Speswhite	-	31.1	27.8
TMS24	400	0.50	0.74	3	Speswhite	-	30.7	27.9
TMS25	400	0.50	0.74	5	Speswhite	-	30.2	28

Table 3.3 - Characteristics of the undrained monotonic tests of Fontainebleau sand and fines

### 3.10 Interpretation and discussion of results

According to the series of undrained monotonic tests carried out on both sand-silica (non-plastic fines) and sand-kaolinite (plastic fines) mixtures, we have noted two totally different behaviors in terms of the influence of fine particles on the mechanical behavior of sands, in particular, in terms of the initiation of liquefaction phenomenon. Results have shown that the increase in non-plastic fines (silica) tends to increase the resistance of sands to liquefaction that is translated by favoring the dilatancy of these mixtures. However, adding plastic fines (kaolinite) has shown a totally reversed behavior translated in the decrease of the sand shear resistance and therefore favoring the contracting of these specimens.

In fact, Yang and Wei (2012) have presented a study that investigates the role of the particle shape in the shear behavior of mixtures of sand and fine particles through macroscale and laboratory experiments. He has presented four models to explain the different patterns of overall response associated with particle shape (see figure 3.27).

In each conceptual model, the two equal sides of the triangle simulate the path of the fine particle moving along the surface features of the coarse particle: as the base angle of the triangle becomes larger, the coarse particle becomes more angular, and thereby more work is required for the fine particle to move along the path to yield particle rearrangement. Compared with the Type I model, the coarse particle in the Type III model shares a similar, rounded shape but the fine particle is more angular. This means that, upon loading, the fine particle needs more effort to move along the path, because its angular shape does not favour rolling but rather favours sliding. Among the four models, Type IV represents the case in which particles are the most difficult to move and rearrange (i.e. the case of the most stable structure), whereas Type I represents the case in which particle movement and fabric change are the easiest to trigger (i.e. the most unstable structure).

Yang & Wei (2012) tested two types of sand (Fujian and Toyoura) and two non-plastic fines (crushed silica and glass beads). Crushed silica is characterized by angular shape whereas glass beads have rounded shape. He noted that, for a clean sand without fines, the critical state friction angle tends to decrease with increasing roundness of sand particles. When fines of rounded shape, such as glass beads, are added to the clean sand, the critical state friction angle of the mixture tends to decrease with an increase in fines content. However, when fines of angular shape, such as crushed silica, are present, the critical state friction angle tends to

increase with fines content. This result explains the increase in shear resistance for our mixtures of Fontainebleau sand (rounded shape) with non-plastic silica (angular shape). In fact, the addition of these fine particles tend to increase the density index of the mixture and they fill the voids between then sand grains and consequently decrease the pores and increase the resistance of the material.

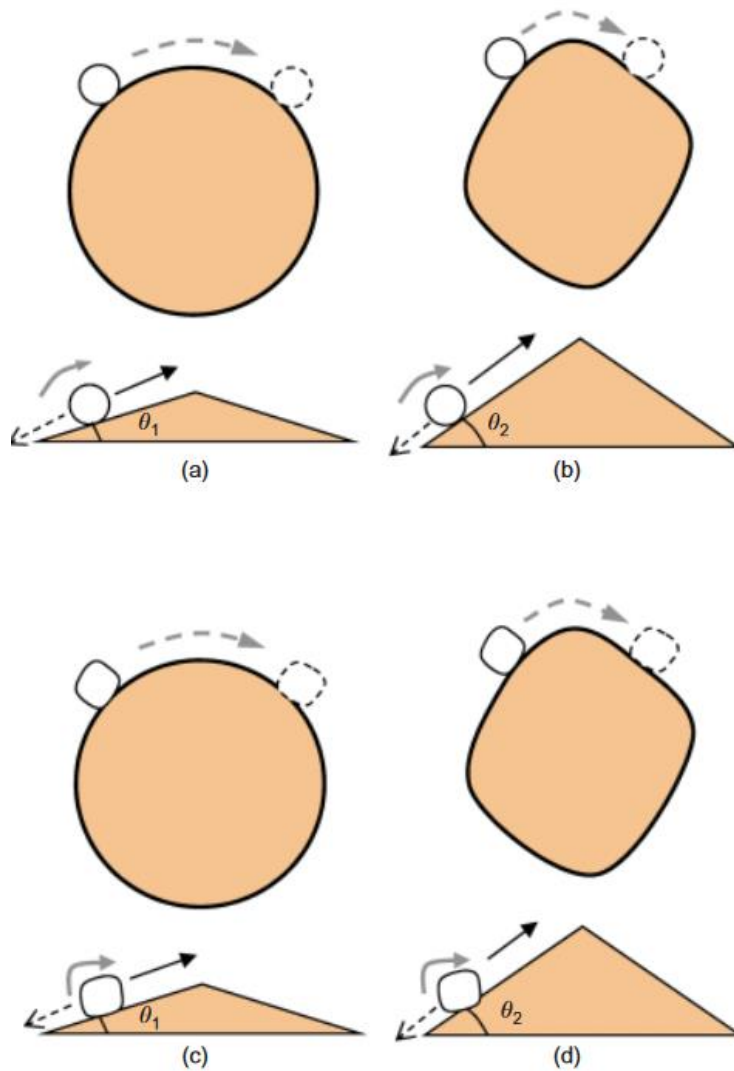


**Figure 3.27: Conceptual models explaining particle shape effects in mixed soils**  
 (a) Type I, round-to-round; (b) Type II, round-to-angular; (c) Type III, angular-to-round; (d) Type IV, angular-to-angular (Yang and Wei, 2012)

### 3.11 Evaluation of the liquefaction resistance in terms of other parameters

According to the literature, the liquefaction of sands containing fines has been a controversial subject. Therefore, there have been several approaches for the evaluation of this effect depending on different parameters (global void ratio, relative density index, intergranular void ratio, equivalent intergranular void ratio).

#### 3.11.1 Evaluation in terms of intergranular void ratio

Many authors have evaluated the effect of fine particles on the initiation of liquefaction phenomenon using the concept of the intergranular void ratio and interfine void ratio. The intergranular void ratio proposed by Kuerbis et Vaid (1988) considers the volume of fine particles as void as long as these particles don't exceed the limiting value (LFC). Beyond this value, the fine particles become active and they participate in the shear resistance of the material and therefore they control the behavior. In this case, the interfine void ratio must be taken into consideration. For our case study, as the maximum value of fines content is equal to 5% and eventually its less than the limiting content that is usually found for higher values ( $\geq 15\%$ ) as reported in the literature, we are going to evaluate the intergranular void ratio defined by the following equation as mentioned before in chapter I.

$$e_s = \frac{e + f_c}{1 - f_c} \quad (3.4)$$

It is obvious that the intergranular void ratio increases with the increase in fines content very slightly due to the fact that we have chosen to reconstitute the mixtures with a relatively small amount of fines. In fact, the intergranular void ratio varies from 0.9 for a loose clean sand to 1 for sand fines mixture having  $F_c = 5\%$ . As we have chosen the density index of the sand matrix as a constant parameter, we can note that the increase in fines content leads to an increase in intergranular void ratio accompanied with an increase in the shear resistance of the mixtures of sand with non-plastic fines (figure 3.28). These results have been reported by Kuerbis et Vaid (1988), Xenaki *et al.* (2003) and Stamatopoulos (2010). In fact, this increase in the resistance can be explained, as mentioned before, that the increase in fines content will in fact increase the density index of the total mixture.

On the other hand, concerning the behavior of sand and plastic fines, the increase in the intergranular void ratio for mixtures prepared at the same density index of the matrix is accompanied by a decrease in the resistance upon adding fines. Nguyen (2014) has reported the same behavior upon testing a group of specimens prepared at the same void ratio. Indeed, he has noted that as the intergranular void ratio increases, the resistance decreases for a fines content equal to 5%. In fact, several authors have reported that the intergranular void ratio isn't a reliable parameter for the evaluation of the influence of fines on the phenomenon of liquefaction of sands since this parameter doesn't take into consideration the influence of fines on the overall behavior of the mixture and it considers these fines inactive as long as they don't exceed the limiting value. In fact, this concept doesn't agree with the results found in the present study where it is obvious that the fine particles affect the resistance of sands to liquefaction and they participate in the shear resistance of the material.

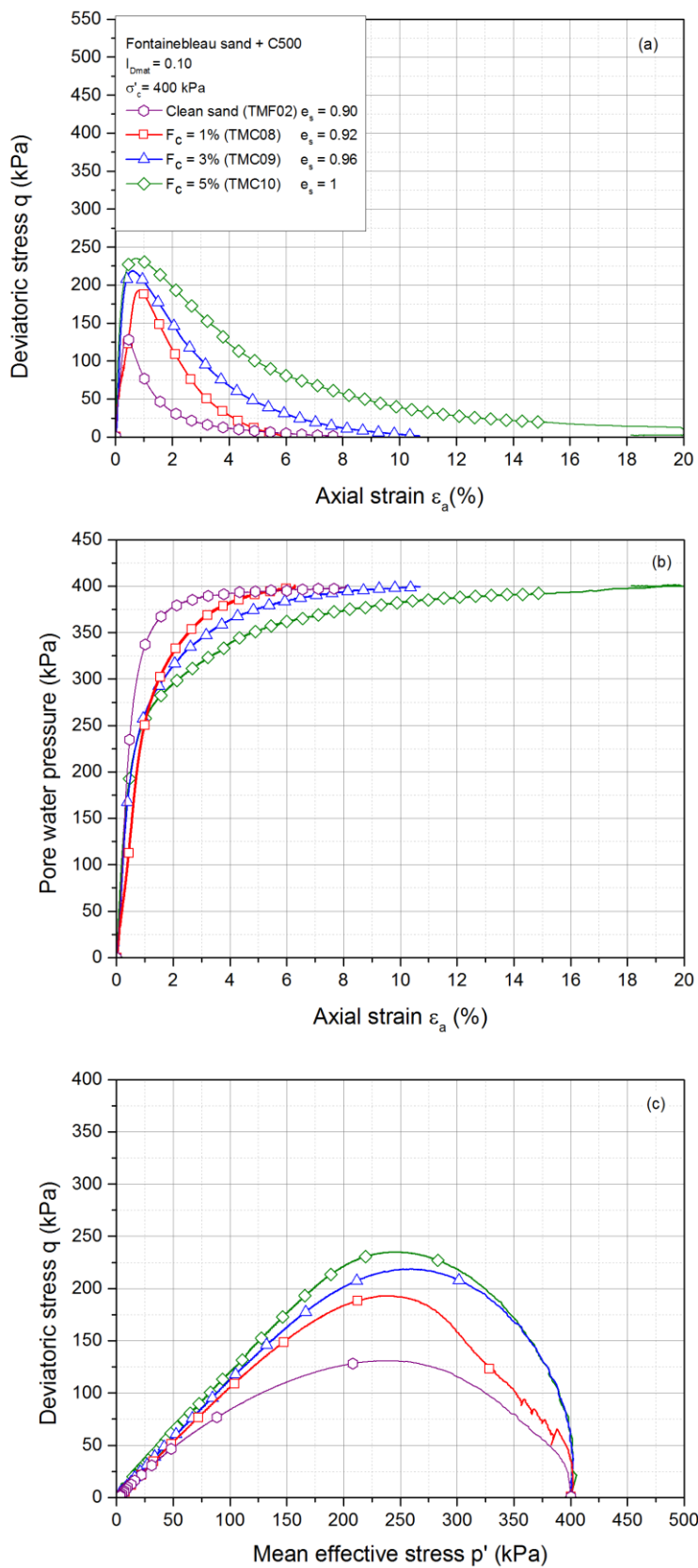


**Figure 3.28- Influence of fines content in terms of intergranular void ratio**

### 3.11.2 Evaluation in terms of equivalent void ratio

Thevanayagam and Martin (2002) have improved the concept of intergranular and interfine void ratio and introduced the equivalent void ratio. In fact, they have decomposed the sand-fines mixtures into several categories. For our case, we are concerned in the category that falls below the limiting fines content where the fine particles are decomposed into two different parts, one of them is found inside the grains matrix that is the inactive part, whereas the second part starts to touch the sand grains and hence becomes active. Therefore, Thevanayagam and Martin (2002) has proposed the concept of the equivalent intergranular void ratio according to the following formula:

$$e^{eq} = \frac{e + (1 - b)f_c}{1 - (1 - b)f_c} \quad (3.5)$$

where  $b$  corresponds to the fraction of fines that is active and participates in the force structure.

Later on, Rahman *et al.* (2008) has examined the factors affecting the  $b$  value based on published work in which that led him to a semi-empirical equation for predicting the  $b$  value based on fines size and fines content.

$$b = [1 - \exp(-0.3 \frac{f_c/f_{thre}}{k})] (r \frac{f_c}{f_{thre}})^r \quad (3.6)$$

Where  $k = (1 - r^{0.25})$  and  $r = d_{50}/D_{10}$  where  $d_{50}$  is the fines particles diameter at 50% finer and  $D_{10}$  is the sand particle diameter at 10% finer and  $f_{thre}$ , is the threshold fines content or limiting fines content defined previously. Hence, in order to determine the  $b$  value and eventually the equivalent intergranular void ratio, we must first determine the limiting fines content.

### 3.11.3 Estimation of the critical fines content based on Westman and Hugill diagram

Westman and Hugill (1930) have studied the packing of mixtures containing particles of different sizes where they have developed a diagram that can predict theoretically the volume occupied by a mixture of two particles having different dimensions as a function of the volumetric fraction rate.

The horizontal axis presents the volumetric fraction of the fine particles in a coarse grain, it varies from 0 value that corresponds to the case of a material that contains only coarse particles ( $F_c = 0\%$ ) to 1 corresponding to the case of material containing only fines ( $F_c = 100\%$ ). Hence, point C on the diagram corresponds to  $F_c = 0\%$ , as the fines content increases slightly these fine particles are confined in the voids formed between the sand grains and they don't contribute to the volume of the material that is composed of the sand grains volume and the void volume. Consequently, the value of the materials volume will be situated on the line joining the point C and the right lower corner of the diagram. On the other hand, upon adding coarse particles to a large quantity of fines the solid particles will be immersed in the fines and the volume curve will be the straight line joining F to the point 1.00 at the left side of the diagram (see figure 3.29). These two straight lines cross at r and thus CRF represents the transition phase from a coarse particle dominant structure to a fine particle dominant one.

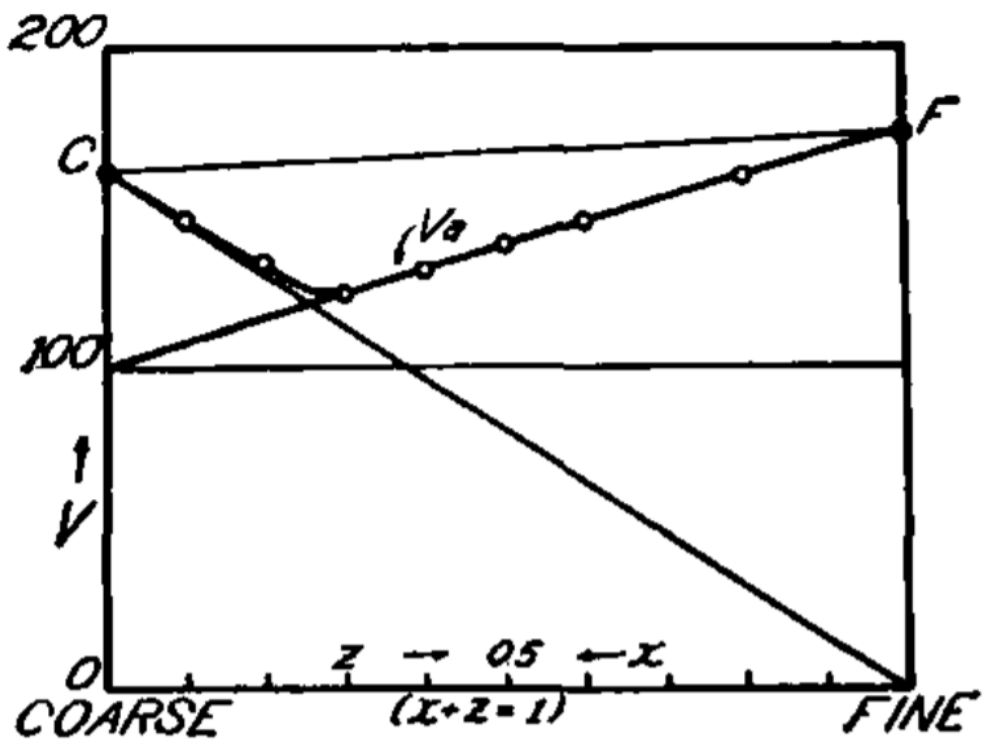


Figure 3.29 - Westman and Hugill diagram (1930)

A very important observation has been also reported by Westman and Hugill (1930) concerning the peak of this curve that notes that the latter is not affected by the diameter ratio of the two components. This observation permits us to determine the critical fines content based on the critical curve of the minimal volume.

Figure 3.31 presents the evolution of the minimal volume on the Westman diagram using the following formula :

$$V_{\min} = e_{\min} + 1 \quad (3.7)$$

In order to trace the theoretical curve of the minimal volume of the material, we only need the minimum void ratios corresponding to the two cases where  $F_c = 0\%$  and  $F_c = 100\%$ . Figure 3.30 presents the application of the Westman and Hugill diagram for the mixtures of sand and kaolinite speswhite in order to estimate the critical fines content value. It is noted that the critical fines content is found at  $F_c = 24\%$ . Nguyen (2014) has shown that the estimated critical fines content value of Camargue sand and silt using the Westman and Hugill diagram is very close to the value obtained experimentally from the evolution curve of the maximum and minimum void ratios.

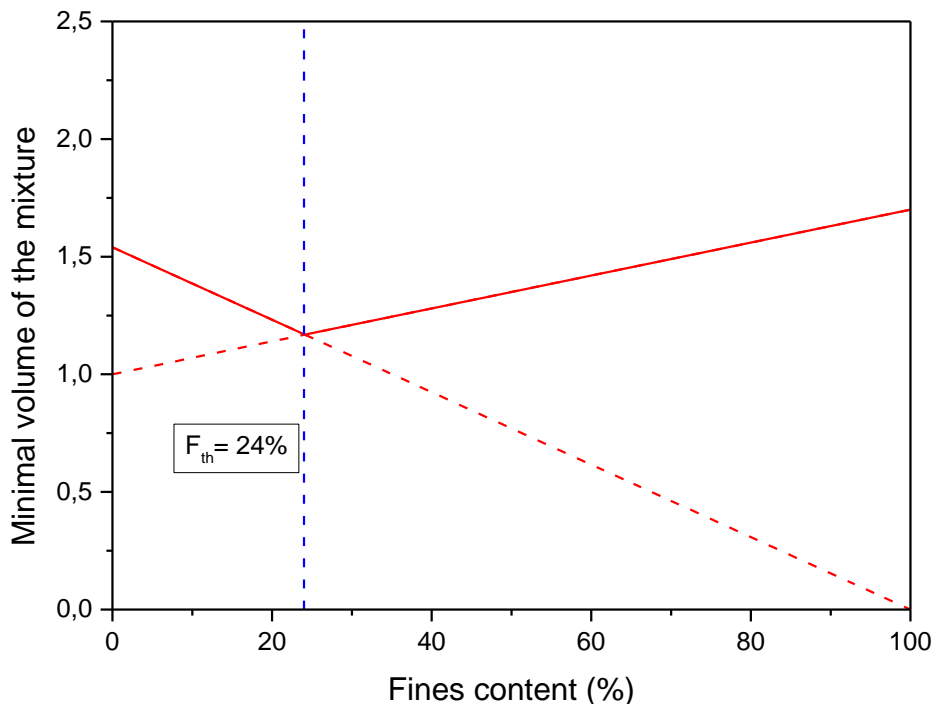


**Figure 3.30 - Estimation of the critical fines content using the Westman diagram**

As we determined the limiting fines content, it is possible now to compute the  $b$  value according to the equation proposed by Rahman *et al.* (2010) in order to evaluate the equivalent intergranular void ratio. Table 3.4 presents the values of the different parameters. It is interesting to note that the evolution of the equivalent intergranular void ratio with the increase in fines content up to 5% is almost negligible and therefore the density index of the

sand matrix that we have chosen as a constant parameter for our study and for the fabrication of the specimens is a reliable parameter for such low values of fines content. Note that this negligible effect of fines content on the evolution of the equivalent intergranular void ratio is due to the low percentages of fines ( $\leq 5\%$ ). Therefore, in this case, the evaluation of the liquefaction phenomenon of sand containing fines in terms of the relative density of the sand matrix is reliable as the other initial parameters remain constant and therefore the comparison between these specimens can be established in terms of the effect of addition of fine particles.

<b>Test reference</b>	$\sigma'c$	$I_{Dmat}$	$e_{mat}$	$Fc$	$es$	<b>Type of fines</b>	$b$	$e^{eq}$
TMC01	100	0.10	0,9	1	0,92	C500	0,336	0,9067
TMC02	100	0.10	0,9	1	0,92	C500	0,336	0,907
TMC03	100	0.10	0,9	3	0,96	C500	0,322	0,921
TMC04	100	0.10	0,9	5	1	C500	0,334	0,934
TMC05	100	0.50	0,74	1	0,76	C500	0,336	0,747
TMC06	100	0.50	0,74	3	0,79	C500	0,322	0,761
TMC07	100	0.50	0,74	5	0,83	C500	0,334	0,774
TMC08	400	0.10	0,9	1	0,92	C500	0,336	0,907
TMC09	400	0.10	0,9	3	0,96	C500	0,322	0,921
TMC10	400	0.10	0,9	5	1	C500	0,334	0,934
TMC11	400	0.50	0,74	1	0,76	C500	0,336	0,747
TMC12	400	0.50	0,74	3	0,79	C500	0,322	0,761
TMC13	400	0.50	0,74	5	0,83	C500	0,334	0,774
TMS14	100	0.10	0,9	1	0,92	Speswhite	0,336	0,907
TMS15	100	0.10	0,9	3	0,96	Speswhite	0,322	0,921
TMS16	100	0.10	0,9	5	1	Speswhite	0,334	0,934
TMS17	100	0.50	0,74	1	0,76	Speswhite	0,336	0,747
TMS18	100	0.50	0,74	3	0,79	Speswhite	0,322	0,761
TMS19	100	0.50	0,74	5	0,83	Speswhite	0,334	0,774

TMS20	400	0,10	0,9	1	0,92	Speswhite	0,336	0,907
TMS21	400	0,10	0,9	3	0,96	Speswhite	0,322	0,921
TMS22	400	0,10	0,9	5	1	Speswhite	0,334	0,934
TMS23	400	0,50	0,74	1	0,76	Speswhite	0,336	0,747
TMS24	400	0,50	0,74	3	0,79	Speswhite	0,322	0,761
TMS25	400	0,50	0,74	5	0,83	Speswhite	0,334	0,774

Table 3.4 : Characteristics of the undrained monotonic tests of Fontainebleau sand and fines

## **Chapter IV: Undrained behavior of sand containing fines under cyclic shear**

This chapter presents a study of the behavior of Fontainebleau sand containing fines under cyclic loading. The approach developed is similar to the one used for studying behavior under monotonic shear in order to highlight the influence of various fundamental parameters on the behavior of these mixtures, in addition to the cyclic stress ratio. In order to establish a parallel between monotonic and cyclic behaviors, we have worked with initial states as close as possible to those used for the monotonic tests with the aim of developing analogies between the two types of loadings. After describing the experimental program and giving typical results corresponding to dense behavior (cyclic mobility phenomenon) and loose behavior (total liquefaction), we have studied the influence of significant parameters on the observed behaviors, consequently, we present the extension of the notion of cyclic shear resistance curves (CSR) that sum up all the achieved work. Finally, a comparison is established between the monotonic and cyclic test results.

### **4.1 Experimental program**

The experimental program was defined in order to meet the main objectives aiming at highlighting the influence of the fines particle on the initiation of liquefaction phenomenon and studying the influence of different parameters on the resistance of sand to liquefaction, such as density index, cyclic stress ratio, fines content, and nature of fines ....

The corresponding experimental program is presented in tables 4.1 and 4.2 for clean sand and for sand-fines mixtures respectively. The tests were carried out force-controlled, as explained before in chapter II. The loading frequency selected was set to 0.1 (1 cycle/10 seconds). However, for some tests requiring a very large number of cycles, we have increased the latter to 0.2. We recall that the specimens of sand-C500 have been prepared by wet tamping method. However those of sand-Speswhite were prepared in dry conditions. Different density indexes as well as different cyclic stress ratio values were chosen in order to establish the cyclic shear resistance curves. In addition, the initial conditions set for the cyclic tests were derived directly from those used under monotonic conditions. Indeed, the results obtained from the monotonic triaxial tests served as a guideline for the definition of cyclic tests. In particular,

this allowed us to establish the analogies between the monotonic and the cyclic behavior for clean Fontainebleau sand, sand-C500 and sand-Speswhite.

<i>Test reference</i>	$I_{Dmat}$	$\sigma'_c \text{ (kPa)}$	$T_{cc}$	$\Delta q_{cyc} \text{ (kPa)}$
TCF01	0.10	400	0.036	28,8
TCF02	0.10	400	0.06	48
TCF03	0.10	400	0.1	80
TCF04	0.50	400	0.18	144
TCF05	0.50	400	0.14	112
TCF06	0.50	400	0.13	104

Table 4.1 - Clean sand cyclic testing program

<i>Test reference</i>	<i>Type of fines</i>	$F_c \text{ (%)}$	$I_{Dmat}$	$\sigma'_c \text{ (kPa)}$	$T_{cc}$	$\Delta q_{cyc} \text{ (kPa)}$
TCC01	C500	1	0.10	400	0.04	32
TCC02	C500	1	0.10	400	0.06	48
TCC03	C500	1	0.10	400	0.1	80
TCC04	C500	1	0.10	400	0.1	80
TCC05	C500	3	0.10	400	0.04	32
TCC06	C500	3	0.10	400	0.06	48
TCC07	C500	3	0.10	400	0.1	80
TCC08	C500	3	0.10	400	0.12	96
TCC09	C500	5	0.10	400	0.06	48
TCC10	C500	5	0.10	400	0.1	80
TCC11	C500	5	0.10	400	0.12	96
TCC12	C500	1	0.50	400	0.18	144
TCC13	C500	1	0.50	400	0.15	120
TCC14	C500	1	0.50	400	0.2	160
TCC15	C500	3	0.50	400	0.18	144
TCC16	C500	3	0.50	400	0.2	160
TCC17	C500	3	0.50	400	0.15	120
TCC18	C500	3	0.50	400	0.22	176
TCC19	C500	5	0.50	400	0.22	176
TCC20	C500	5	0.50	400	0.2	160

TCC21	C500	5	0.50	400	0.18	144
TCC22	Speswhite	1	0.10	400	0.1	80
TCC23	Speswhite	1	0.10	400	0.06	48
TCC24	Speswhite	1	0.10	400	0.04	32
TCC25	Speswhite	3	0.10	400	0.1	80
TCC26	Speswhite	3	0.10	400	0.06	48
TCC27	Speswhite	3	0.10	400	0.12	96
TCC28	Speswhite	3	0.10	400	0.08	64
TCC29	Speswhite	5	0.10	400	0.1	80
TCC30	Speswhite	5	0.10	400	0.06	48
TCC31	Speswhite	5	0.10	400	0.04	32
TCC32	Speswhite	1	0.50	400	0.2	160
TCC33	Speswhite	1	0.50	400	0.18	144
TCC34	Speswhite	1	0.50	400	0.12	96
TCC35	Speswhite	3	0.50	400	0.12	96
TCC36	Speswhite	3	0.50	400	0.1	80
TCC37	Speswhite	3	0.50	400	0.18	144
TCC38	Speswhite	3	0.50	400	0.08	64
TCC39	Speswhite	5	0.50	400	0.1	80
TCC40	Speswhite	5	0.50	400	0.14	112
TCC41	Speswhite	5	0.50	400	0.16	128

Table 4.2 - Sand-fines mixtures cyclic testing program

## 4.2 Typical results

### 4.2.1 Clean sand

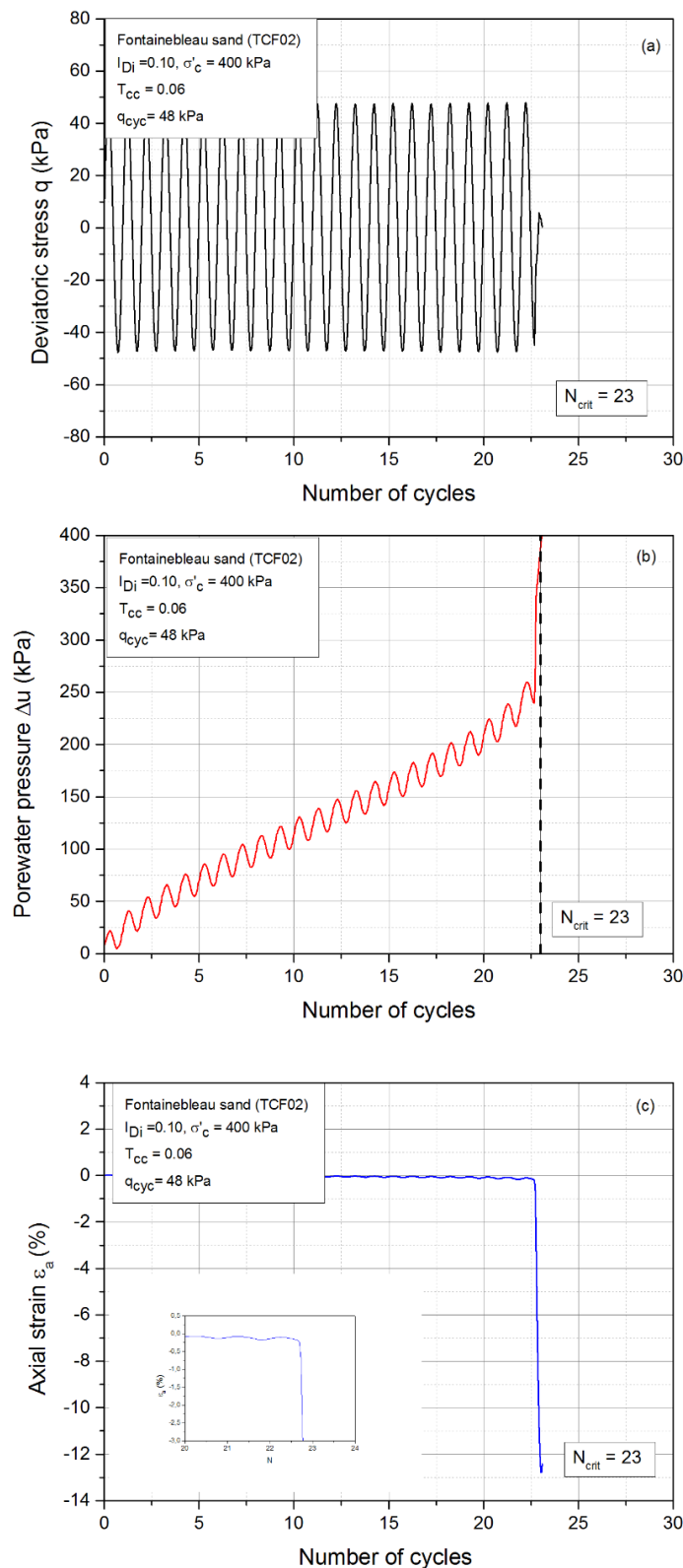
#### 4.2.1.1 Phenomenon of total liquefaction (loose state)

Figure 4.1 presents a typical result corresponding to the phenomenon of total liquefaction obtained for a loose specimen of Fontainebleau sand characterized by a density index of 0.10, an isotropic consolidation stress of 400 kPa and subjected to an alternating cyclic loading having an amplitude  $\Delta q_{cyc} = 48$  kPa. The cyclic stress ratio defined by  $T_{cc} = \tau_{cyc}/\sigma'_c = \Delta q_{cyc}/2\sigma'_c$  is equal to 0.06.

The evolution of the excess pore water pressure (EPWP) as a function of the number of cycles is presented in figure 4.1b where it can be noted that the EPWP increases steadily and continuously at the beginning of the test before it passes an accumulation phase that can be considered relatively linear at the middle of the test and finally it passes through the last phase which records a significant and sharp rise in the EPWP that reaches the value of the initial consolidation stress  $\sigma'_c$ . In fact, the mechanism of the generation of the EPWP corresponds to an increase in the pressure in the loading phase and decrease in the unloading phase with an accumulation for each cycle. According to Eurocode 8, the moment at which the sudden increase in the EPWP occurs and reaches the value of the consolidation stress ( $\Delta u = \sigma'_c$ ) or when the axial deformation reaches 5% (crest to crest) corresponds to a particular cycle called “critical cycle”. For the present study, the chosen criterion for the definition of the critical cycle corresponds to the moment where the axial deformation reaches 5% from crest to crest, although for the loose specimens where total liquefaction occurs these two criteria occur at the same time for the same cycle, that is in this case the twenty third cycle ( $N_{crit} = 23$ ). The axial deformations that remained limited and very small throughout the test (of the order 0.3%) rapidly pass into large deformations ( $\epsilon_a = 13\%$ ) during and beyond this critical cycle (Figure 4.1c).

Figure 4.1d clearly shows the increase in the EPWP that is accompanied by the large deformations. Also, the evolution of the deviatoric stress as a function of the axial strain shows, after an almost stable oscillation inside a very tight zone reflecting the weakness of the deformations, a sudden drop in the shear strength which reaches a marked minimum for an axial deformation of the order of -5% in correspondence with the development of high EPWP and large deformations (Figure 4.1e).

The effective stress paths in the  $(q, p')$  plane shows a progressive migration of the cycles to the left until reaching the critical cycle at which the phenomenon of liquefaction is initiated in the extension phase (figure 4.1f). The migration of the stress paths towards the origin of the axes accounts for the contracting character of the sample that is in agreement with its density state (loose sample).



**Figure 4.1 - Phenomenon of cyclic liquefaction of Fontainebleau sand (loose specimen)**

**(a) Curves  $q$ - $N$ ; (b)  $\Delta u$ - $N$ ; (c)  $\varepsilon_a$ - $N$**

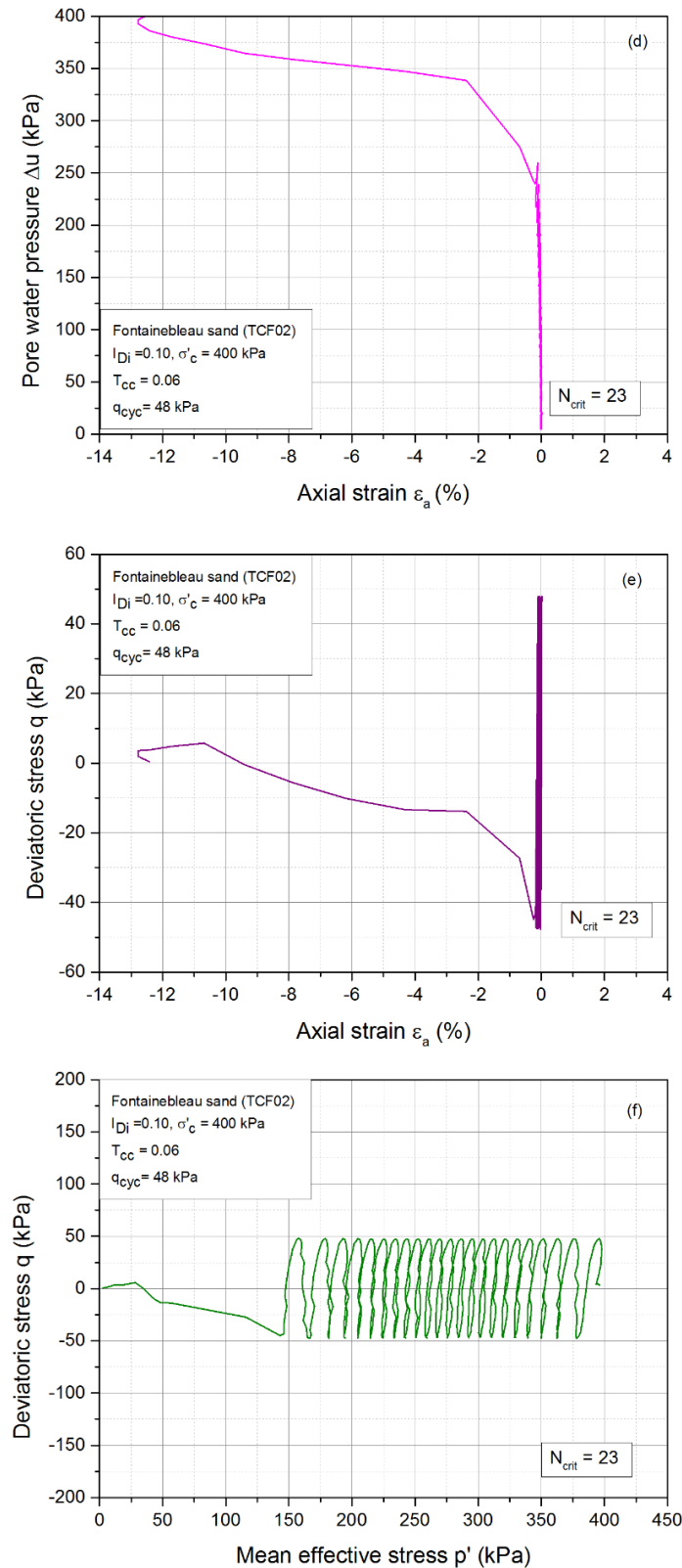


**Figure 4.1- Phenomenon of cyclic liquefaction of Fontainebleau sand (loose specimen)**

Curves  $\Delta u - \varepsilon_a$ ; (e)  $q - \varepsilon_a$ ; (f)  $p' - q$

#### 4.2.1.2 Phenomenon of cyclic mobility (medium dense state)

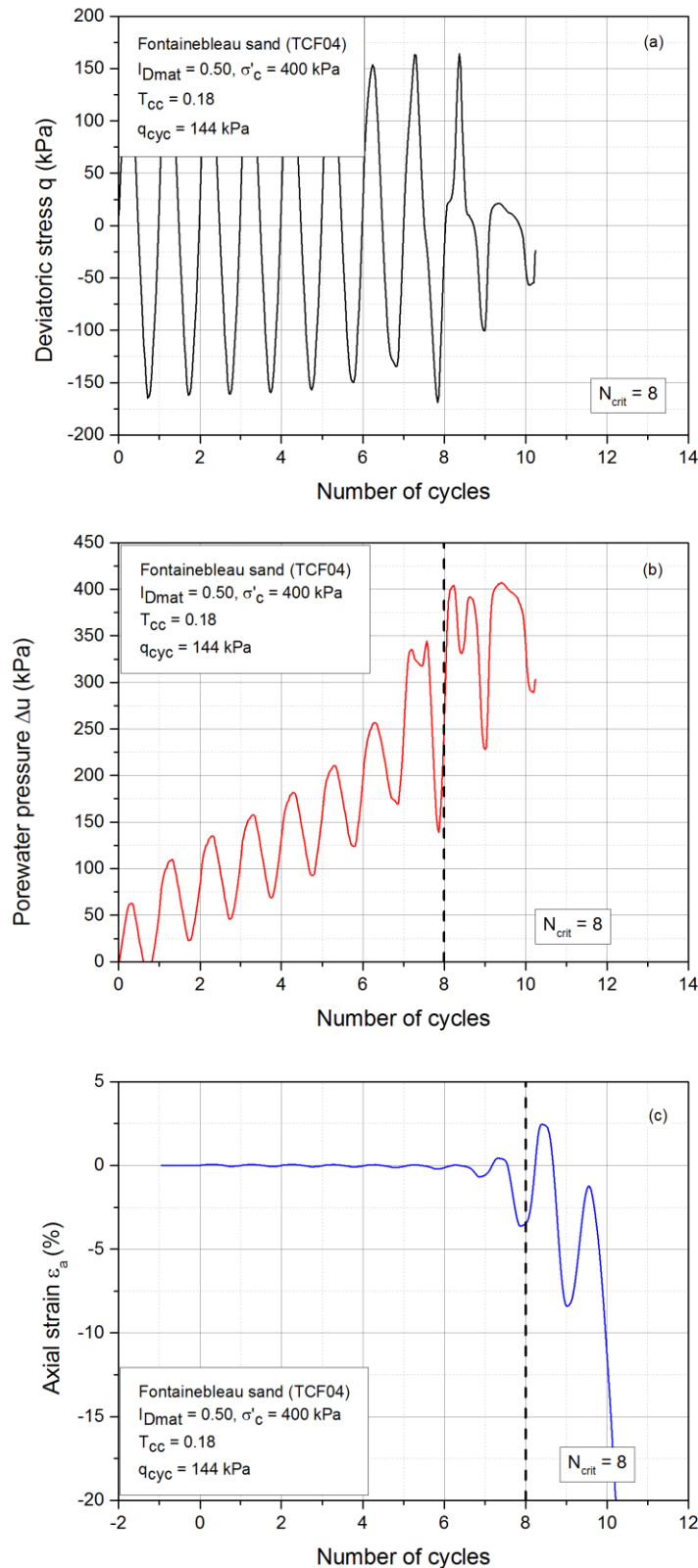
Figure 4.2 shows the results of an undrained cyclic shear test performed on a medium dense specimen of clean Fontainebleau sand having a density index of 0.50, consolidated at an isotropic consolidation stress of 400 kPa and subjected to a symmetrical alternating cyclic loading of amplitude  $\Delta q_{cyc}$  equal to 144 kPa corresponding to a cyclic stress ratio  $T_{cc} = 0.18$ . The EPWP evolution curve during the test presents two distinct zones. The first one is characterized by a progressive generation of the EPWP having a mechanism of one peak per cycle and is accompanied by very small deformations qualitatively similar to those of loose sands. The second one is characterized by the rapid establishment of a two-peak mechanism of the EPWP generation curve during which it reaches the value of the consolidation stress (400 kPa) twice per cycle and it is accompanied by a high increase in axial strain.

Figure 4.2b shows the phase of initiation of the mechanism of cyclic mobility where it is noted that the first appearance of the double peak occurred at the 7<sup>th</sup> cycle causing deformations that become more pronounced later on. It is also noted that the deformations developed are non-symmetrical and present higher values in the extension phase.

Figure 4.2e presents the evolution of the deviatoric stress as a function of the axial strain, showing very tight and concentrated loops at almost zero axial deformation up to the 8<sup>th</sup> cycle at which the cyclic mobility mechanism is initiated and then amplified with accumulation of large deformations in the neighborhood of zero deviator and thus causing the widening of these loops.

The effective stress paths are represented in the  $(q, p')$  plane where it is noted that the stress paths first migrate gradually towards the origin of the axes with a reduction in the effective mean stress  $p'$  at each cycle. After that, and during the period of cycling loading the material becomes strongly contracting during the unloading phases in both compression and extension with generation of high EPWP and a rapid migration of the effective stress paths towards the origin. During the reloading phases, however, the material becomes dilatant and regains strength, which allows this mechanism to be maintained for a number of cycles. This repeated mechanism of charge - discharge and thus of contractancy - dilatancy gives rise to hysteresis loops called dilatancy loops, one for the compression phase and the other one for the extension phase. These loops form on the abscissa axis a mechanism that is called “butterfly wing” and it is characterized by a twice passage per cycle by a zero effective stress one corresponding to the end of unloading during compression and the other one corresponds to

the end of unloading during extension phase. During the passage by these two points, the sample deforms without showing any resistance and it undergoes large axial deformations. The examination of the compression and extension loops reveals that these loops are not symmetrical in the  $(p',q)$  plane. In fact, it is noted that the extension loops are more inclined towards the horizontal which indicates that the characteristic state was first reached on an extension phase.



**Figure 4.2 - Phenomenon of cyclic mobility of Fontainebleau sand (medium dense specimen)**

**Curves  $q$ - $N$  (a); (b)  $\Delta u$ - $N$ ; (c)  $\varepsilon_a$ - $N$**

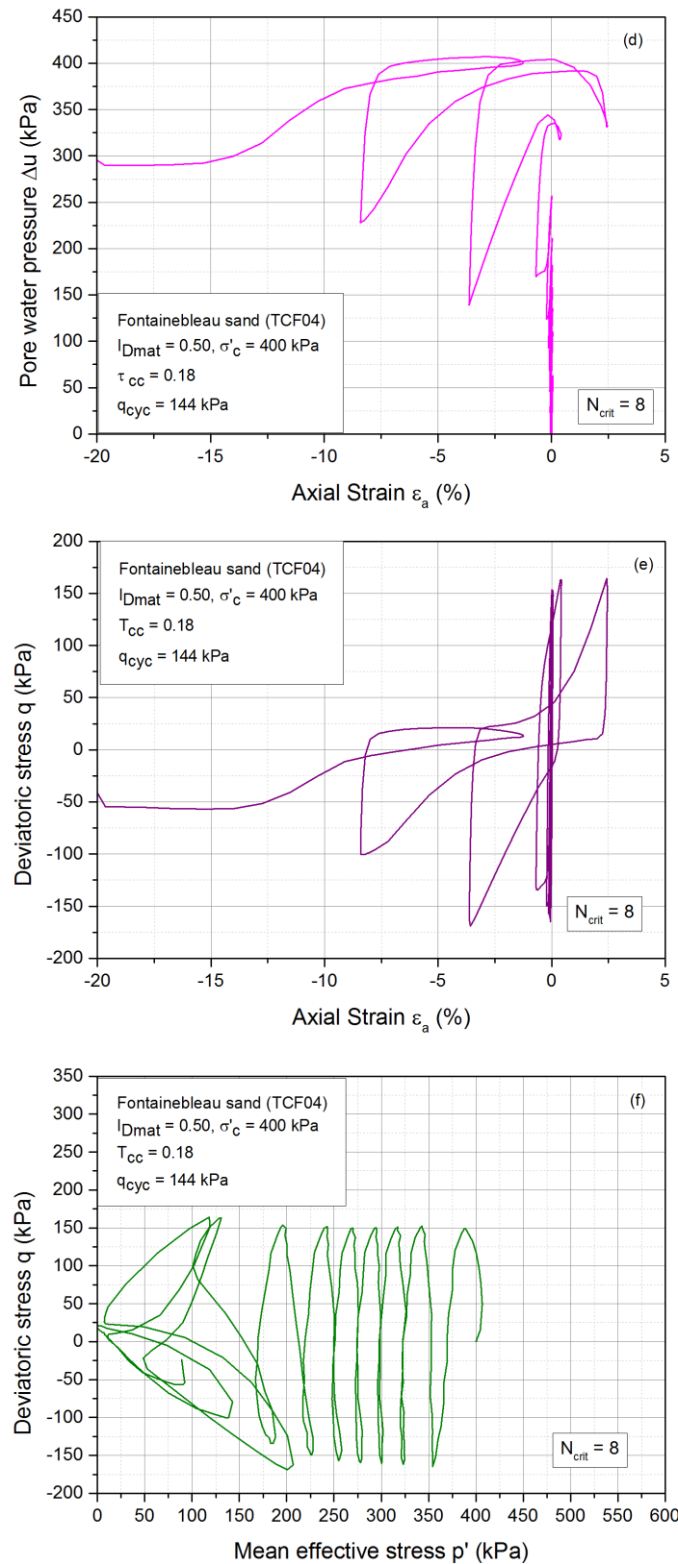


**Figure 4.2 - Phenomenon of cyclic liquefaction of Fontainebleau sand (medium dense specimen)**

**Curves  $\Delta u$ -  $\varepsilon_a$ ; (e)  $q$ - $\varepsilon_a$ ; (f)  $p'$ - $q$**

## 4.2.2 Sand-fines mixtures

### 4.2.2.1 Phenomenon of total liquefaction (loose state)

Figure 4.3 presents the results of a cyclic test carried out on a specimen of sand-C500 mixture having a density index  $I_{Dmat} = 0.10$ , consolidated at 400 kPa and subjected to a symmetrical cyclic loading having an amplitude  $\Delta q_{cyc} = 32$  kPa. The results are similar to the case of clean sand where it is noted that the phenomenon of total liquefaction has taken place.

The evolution curve of the EPWP pressure shows a significant increase in the generation of EPWP at the very beginning of the test followed by an accumulation phase during the middle of the test that rests almost linear before it goes back and witness a sudden and very sharp increase that reaches the value of the initial consolidation stress and thus leads to the total collapse of the sample.

In fact, the loose specimen of sand and fines mixture exhibits the same behavior of that of clean sand but, of course, with some differences regarding the resistance of the sample and the required number of cycles to reach liquefaction.

A brief discussion about the effect of the addition of fines contents to the clean sand will be presented in the following paragraphs shedding the light on the effect of the fines content and the type of fines on the cyclic behavior of Fontainebleau sand.

### 4.2.2.2 Phenomenon of cyclic mobility (medium dense state)

Similar to the case of clean sand, the results of a cyclic test realized on a mixture of Fontainebleau sand and C500 are presented in figure 4.4. The test was conducted at an isotropic consolidation stress equal to 400 kPa, with a fines content  $F_c = 5\%$  and subjected to an alternating loading of amplitude  $\Delta q_{cyc} = 144$  kPa. The obtained results also reveal the appearance of the phenomenon of cyclic mobility.

For this case of the matrix density, and similar to the case of clean sand, the notion of the initial liquefaction is introduced characterized by the double peak per cycle in terms of the pore water pressure curve where the latter approaches the initial value of the consolidation stress twice accompanied with large deformations at this stage.

Figure 4.5, which presents a zoom on the phase of the initiation of the mechanism of cyclic mobility, shows that the first appearance of the double peak occurred during the 115th cycle and gave rise to an increase in deformations, which then increased and amplified rapidly

during the succession of subsequent cycles. We can notice the non-symmetry of the deformations developed with much larger values during the extension phases.

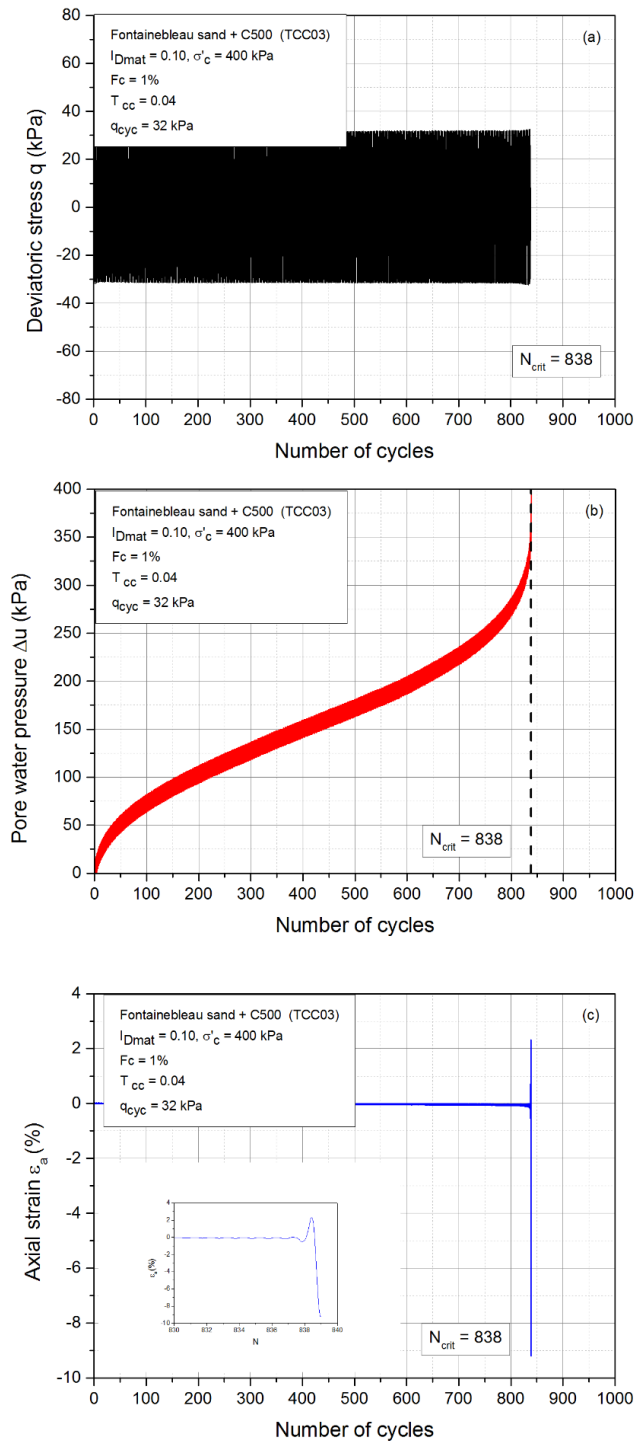


**Figure 4.3 - Phenomenon of liquefaction for Fontainebleau sand and non-plastic fine mixture (loose specimen)**

**Curves  $q$ - $N$  (a); (b)  $\Delta u$ - $N$ ; (c)  $\varepsilon a$ - $N$**

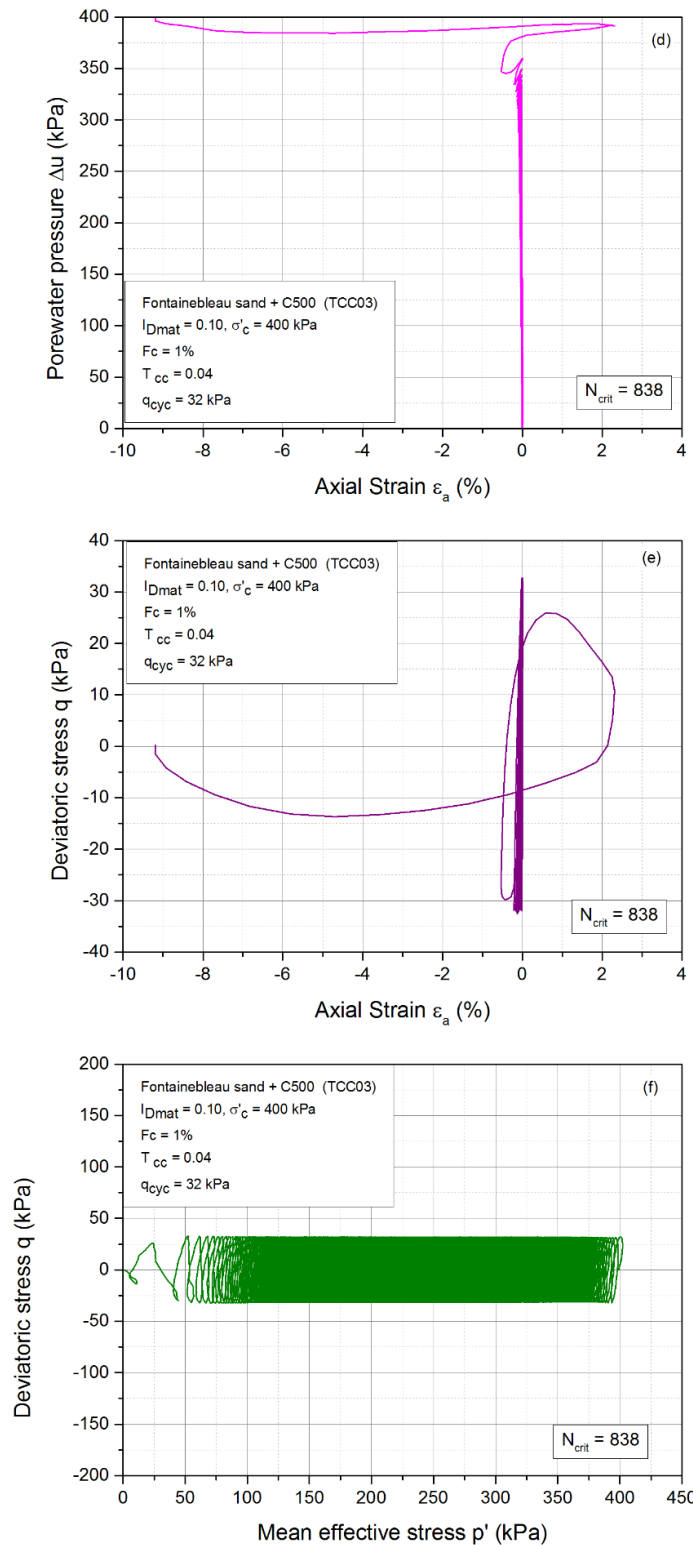


**Figure 4.3 - Phenomenon of liquefaction for Fontainebleau sand and non-plastic fine mixture (loose specimen)**

Curves  $\Delta u - \varepsilon_a$ ; (e)  $q - \varepsilon_a$ ; (f)  $p' - q$

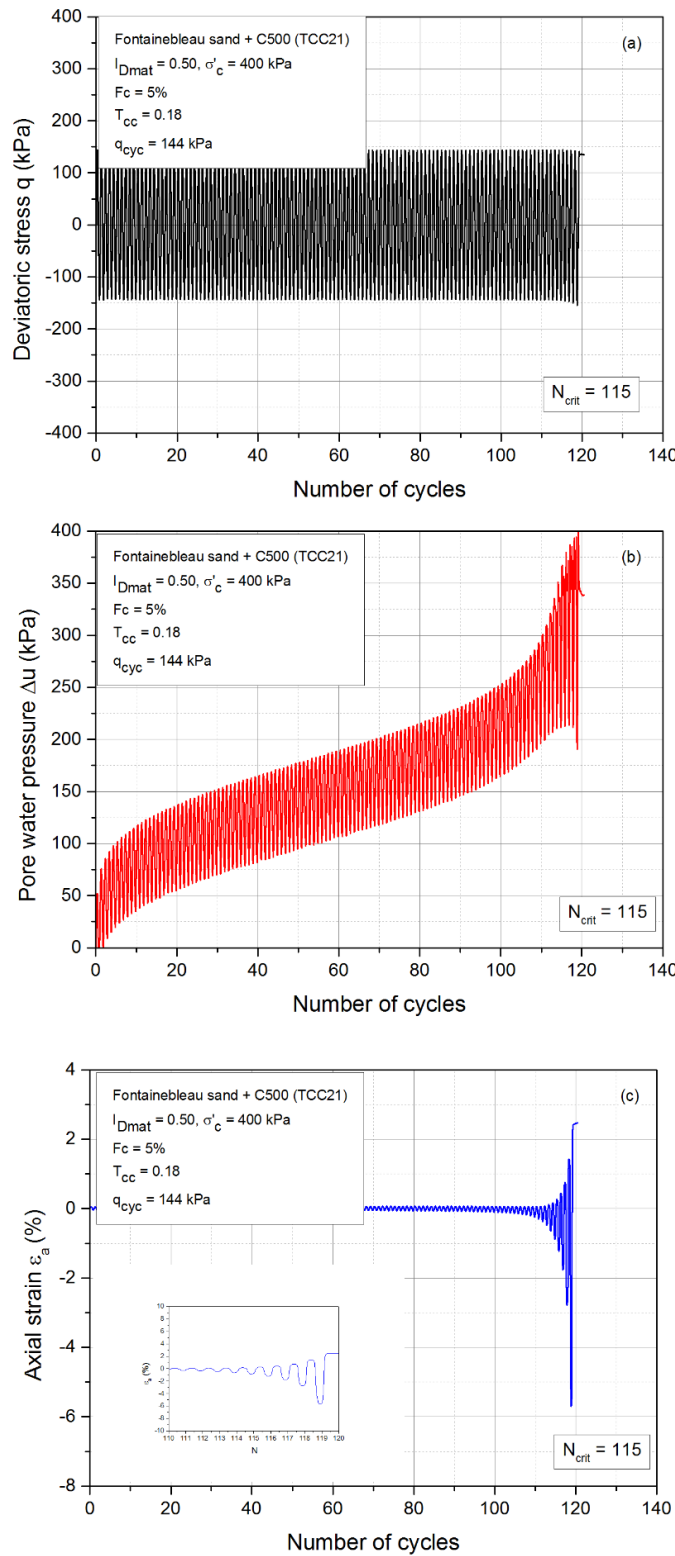


**Figure 4.4 -Phenomenon of cyclic mobility for Fontainebleau sand and non-plastic fine mixture (medium dense specimen)**

**Curves  $q-N$  (a); (b)  $\Delta u-N$ ; (c)  $\varepsilon a-N$**

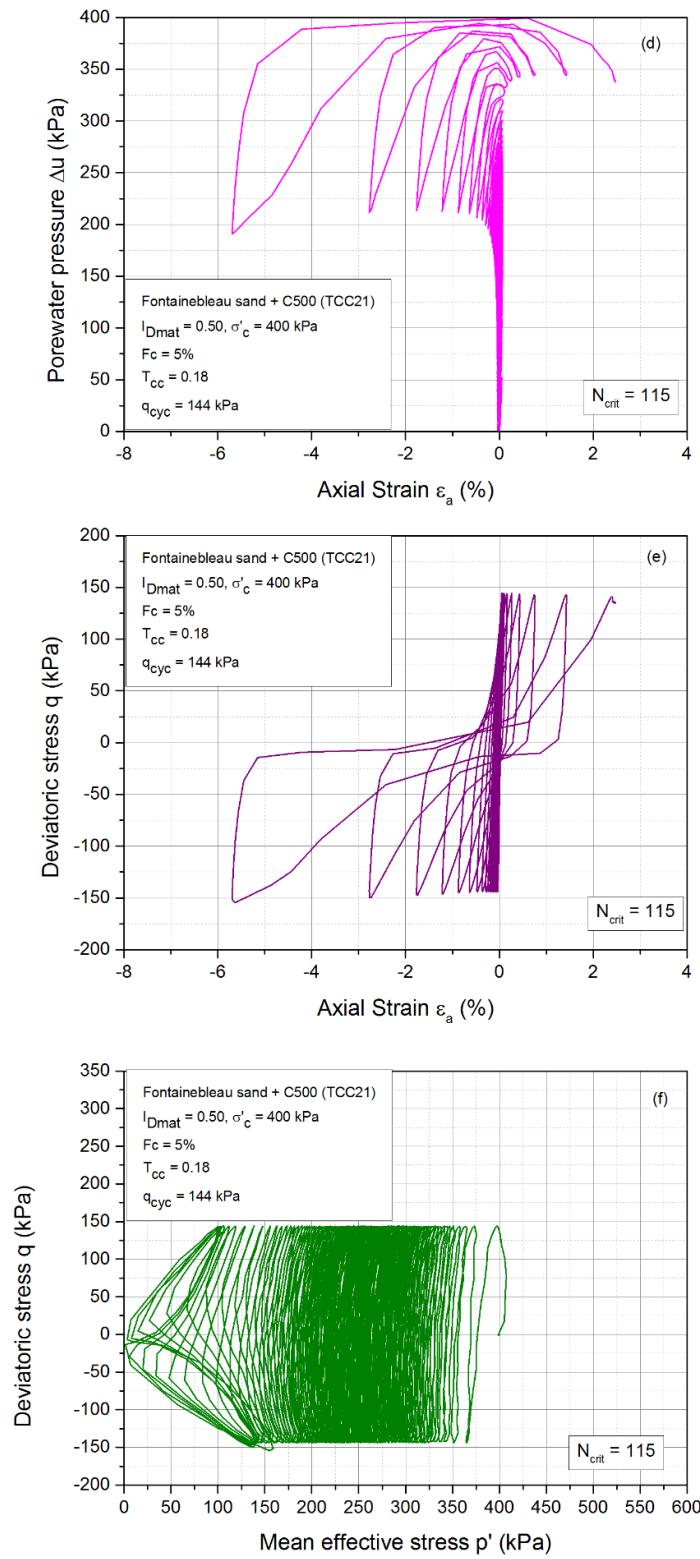


**Figure 4.4: Phenomenon of cyclic mobility for Fontainebleau sand and non-plastic fine mixture (medium dense specimen)**

Curves  $\Delta u - \varepsilon_a$ ; (e)  $q - \varepsilon_a$ ; (f)  $p' - q$

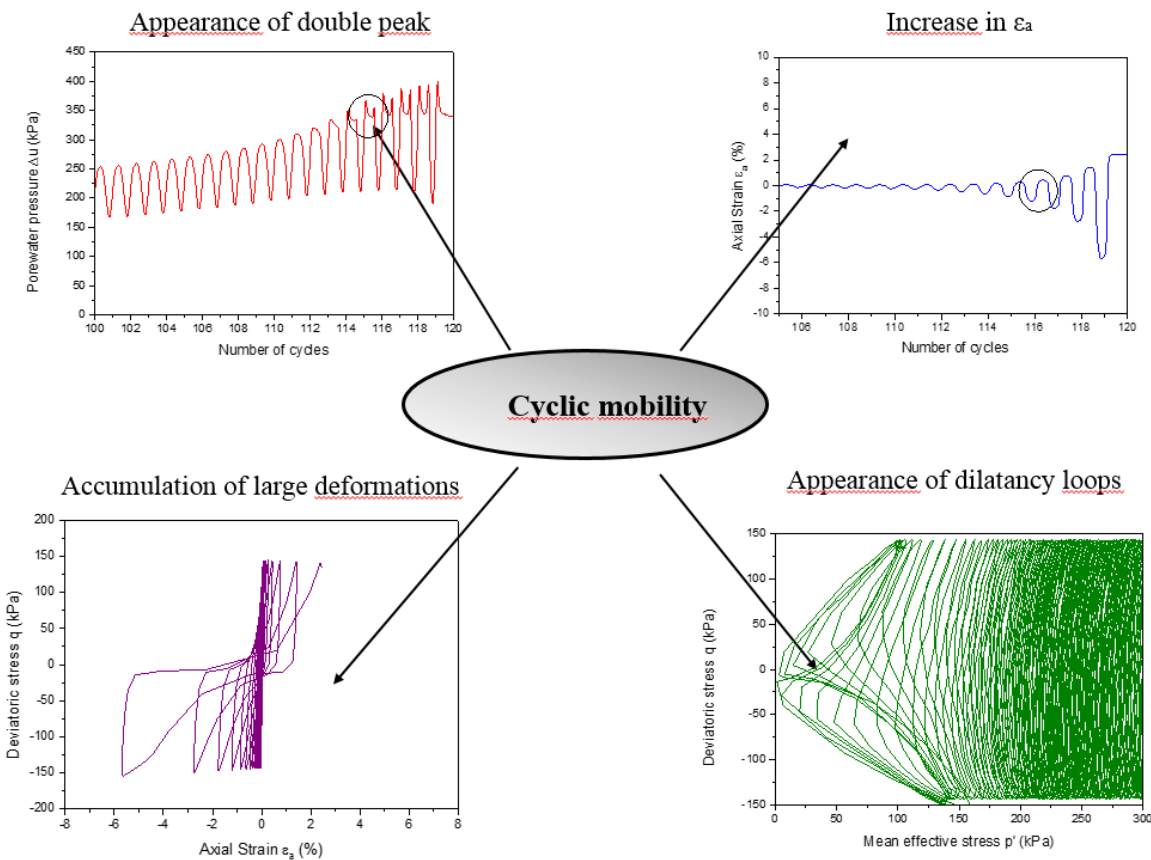


**Figure 4.5 - Initiation of the cyclic mobility phenomenon for sand and non-plastic fines (medium-dense specimen)**

It is interesting to note that for the case of loose specimens, during the critical cycle, the behavior observed is very similar to the phenomenon of static liquefaction that was reported under undrained monotonic shear in chapter III. An enlargement of this critical cycle showing more clearly the phase of the initiation of liquefaction is presented in figure 4.6.

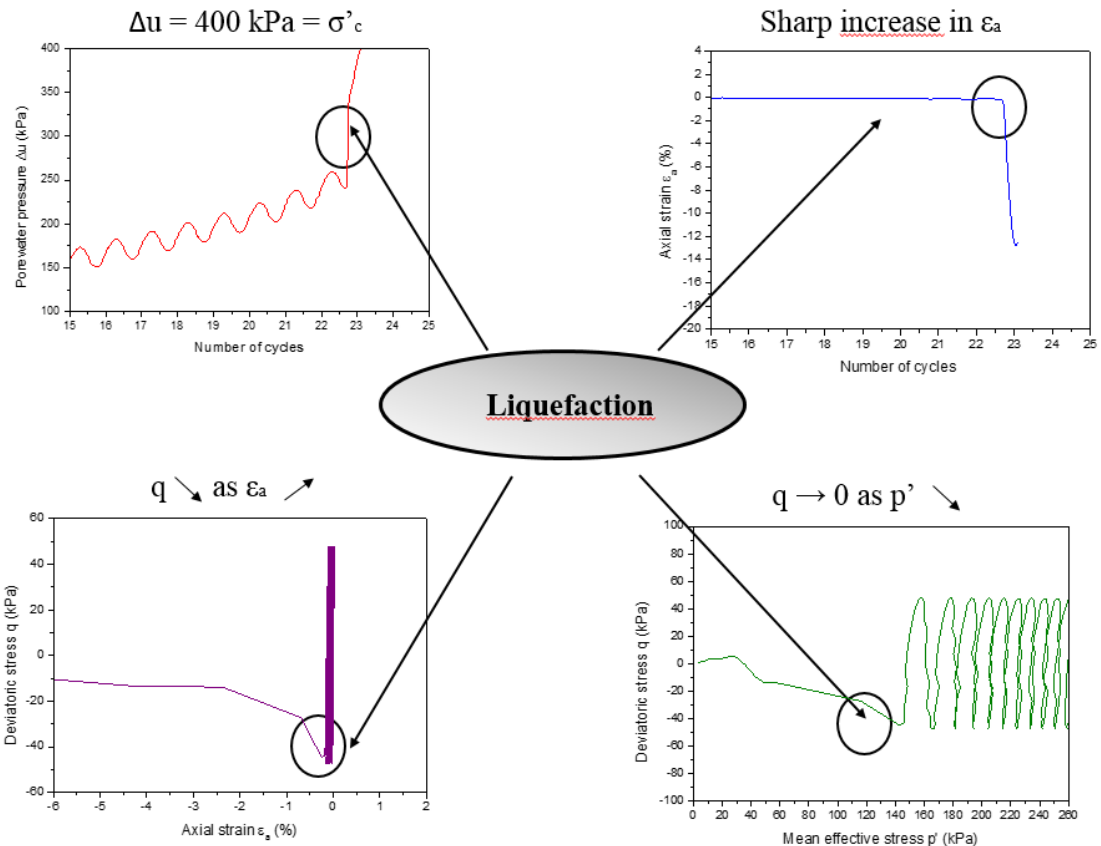


**Figure 4.6 - Initiation of total liquefaction phenomenon at a critical cycle (loose specimen)**

### 4.3 Repeatability test

Figure 4.7 presents the results of two repeatability tests. The two tests were performed on a loose specimen of a mixture of Fontainbleau sand and C500 having a fines content  $F_c = 1\%$  a,d characterized by a density index  $I_{Dmat} = 0.10$  consolidated at 400 kPa and subjected to an alternating cyclic loading having an amplitude  $\Delta q_{cyc} = 80$  kPa corresponding to a cyclic stress ratio  $T_{cc} = 0.1$ . The results show good repeatability in terms of the initiation of pore water pressure. In fact, it is noted that the liquefaction phenomenon is initiated at the 24<sup>th</sup> cycle for the first test and at the 26<sup>th</sup> cycle for the repeated one at two close values of pore water pressure 265 kPa and 275 kPa respectively.

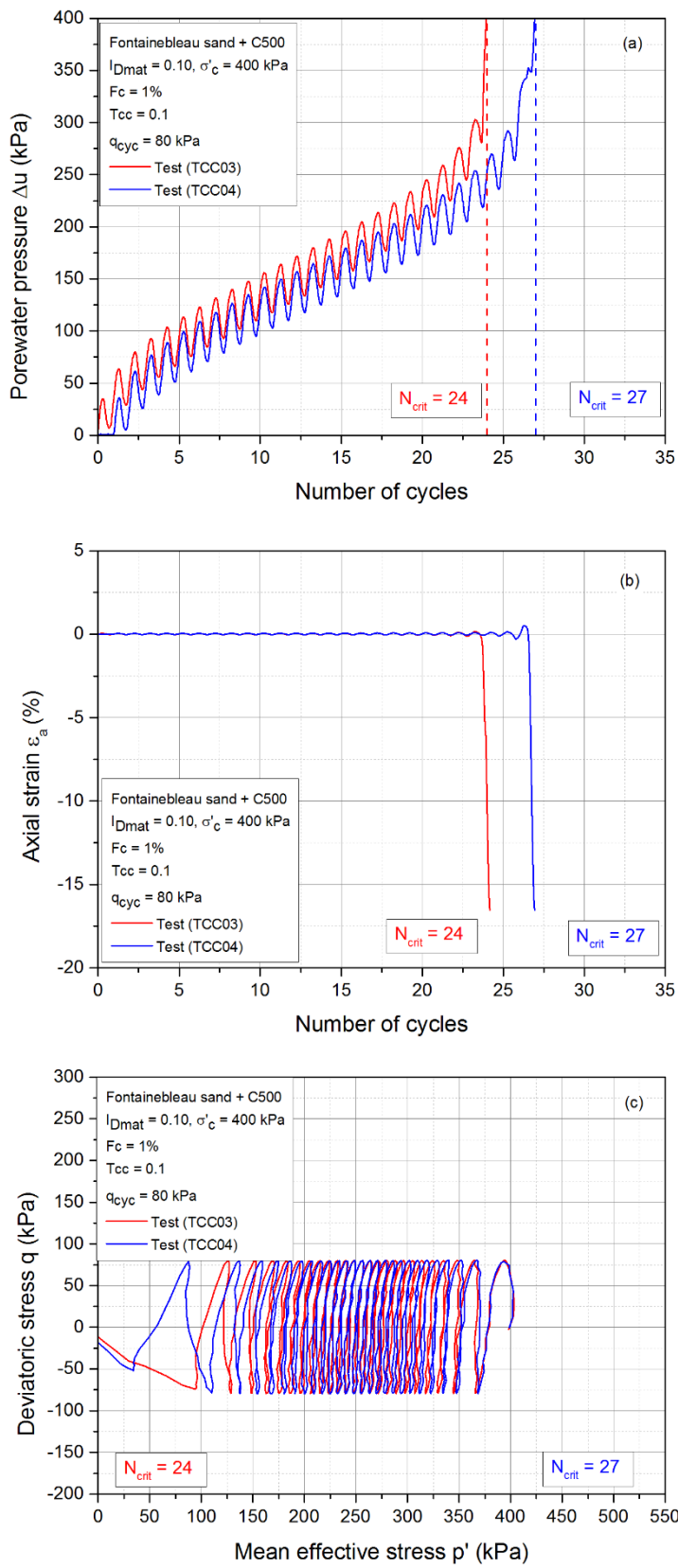
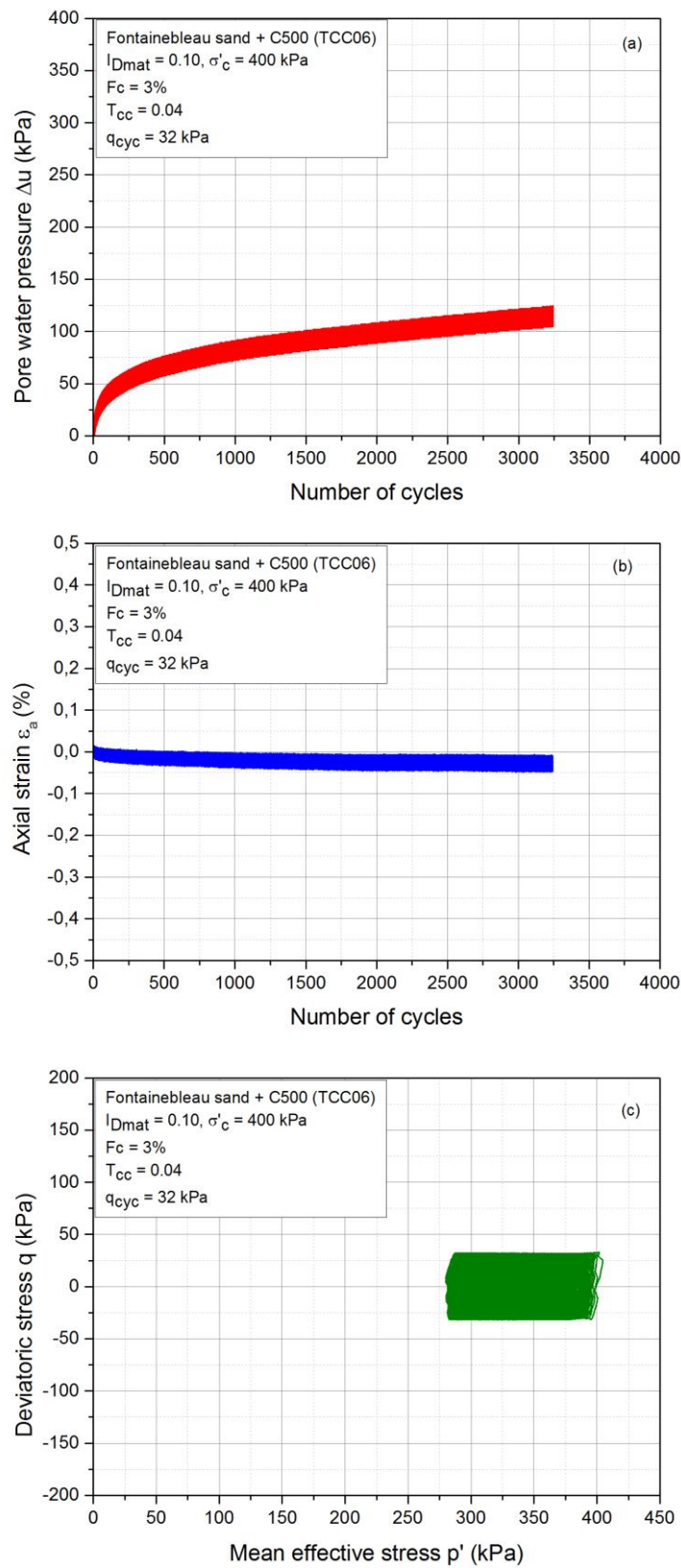


Figure 4.7: Repeatability test of a cyclic total liquefaction phenomenon

It is interesting to note that for some tests where the cyclic stress ratio is very low, the material might exhibit a stabilizing behavior (accommodation behavior) or require a very large number of cycles in order to reach failure.

Figure 4.8 presents the results of an alternating cyclic test realized with a loading amplitude  $\Delta q_{cyc} = 32 \text{ kPa}$  on a loose mixture of sand and C500 with a fines content  $F_c = 3\%$  and a density index  $I_{Dmat} = 0.10$  consolidated at 400 kPa. It can be noted that the axial deformation presents a very low evolution. After a gradual increase in the pore water pressure during the first cycles, it is observed that the generation rate of the pore pressure decreases to become less and less significant beyond the 1000<sup>th</sup> cycle. The effective stress path shows a slight decrease in  $p'$  and a short migration towards the origin of stresses and then it stabilizes on a loop at a value of  $p'$  of approximately 280 kPa. This behavior corresponds to the accommodation of the material.



**Figure 4.8: Stabilization of the behavior of the specimen at a small loading amplitude**

## 4.4 Influence of significant parameters on the behavior of sand-fines mixtures under cyclic loading

### 4.4.1 Matrix density index

As in the case of monotonic loading where the density index governs the mechanical response of sands, the density index has also a significant influence on the cyclic behavior regarding the liquefaction and cyclic mobility phenomena. In fact, when the loading amplitude is sufficient, loose material will tend to exhibit total liquefaction whereas dense material exhibits cyclic mobility.

In order to highlight the influence of this parameter, we have carried out undrained cyclic tests on a mixture of sand and Speswhite by varying the initial density index of the sand matrix while keeping the other parameters fixed (consolidation stress, loading amplitude and fines content).

Figure 4.9 presents the results of two tests performed at two different density indexes ( $I_{D\text{mat}} = 0.10$  and  $I_{D\text{mat}} = 0.50$ ). It is observed that for the same loading amplitude 80 kPa in this case, the critical number of cycles to liquefaction  $N_{\text{crit}}$  increases from 9 cycles for the case of loose material ( $I_{D\text{mat}} = 0.10$ ) to  $N_{\text{crit}}$  equal to 49 cycles for a density index  $I_{D\text{mat}} = 0.50$ . It is also interesting to note that not only the number of cycles has increased but also we have witnessed a passage of the observed behavior from a total liquefaction phenomenon for the case of loose soils to a phenomenon of cyclic mobility as we increase the density index to 0.50. Similar results have been reported by Benahmed (2001) for Hostun sand.

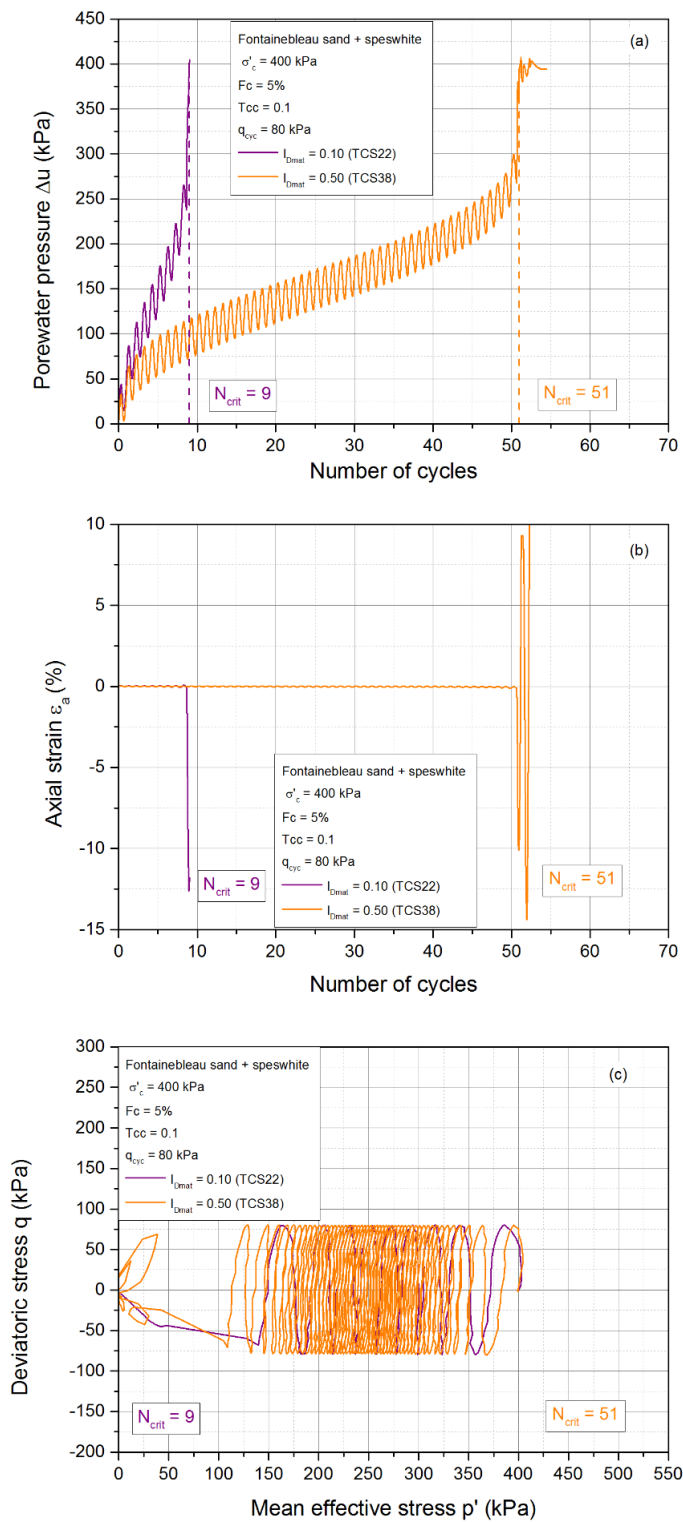


**Figure 4.9: Influence of the density index on the cyclic behavior of Fontainebleau sand-Speswhite mixtures**  
**Curves  $\Delta u$ - $N$  (a); (b)  $\varepsilon a$ - $N$ ; (c)  $p'$ - $q$**

#### 4.4.2 Influence of cyclic stress ratio

It is commonly known that the cyclic stress ratio has a very significant influence on the undrained cyclic shear strength of sands and it plays an important role in the risk of failure by liquefaction.

##### 4.4.2.1 Case of loose material

Figures 4.10a, 4.10b and 4.10c present the results of a series of tests carried out on loose specimens of Fontainebleau sand-C500 mixtures with fines content  $F_c = 3\%$  and initial density index  $I_{Dmat} = 0.10$ , consolidated at the same stress of 400 kPa and then sheared at three different cyclic stress ratios  $T_{cc}$  (0.06, 0.10 and 0.12).

The examination of the EPWP evolution curves as a function of the number of cycles shows that the generation rate decreases with the decrease in the charging amplitude ( $T_{cc} = 0.06$ ). Besides, it may be noted that the EPWP generation is increased and more pronounced as we increase the loading amplitude ( $T_{cc} = 0.12$ ) where it is noted that the pore water pressure exhibits large cycles and the phenomenon of liquefaction is reached and attained in few cycles. Concerning the axial deformation evolution, it may be noted that they all exhibit the same trend, remaining very small until a critical cycle is reached where they develop suddenly and quickly a large and very important deformation. However, this occurs at different critical cycles each time depending on the value of the corresponding shear amplitude. Therefore, it can be conducted that as the applied loading amplitude increases from 0.06 to 0.12 the critical number of cycles to liquefaction decreases from 293 cycles to 10 cycles respectively.

The effective stress paths corresponding to the three tests are presented in figure 4.10c. These curves follow a similar trend with cycles that are more numerous and narrower as the cyclic stress ratio is lower. However, it is interesting to note that for the three cases, the liquefaction phenomenon is initiated in the extension phase.

As a result, the number of cycles required to induce the liquefaction informs us about the effect of the cyclic stress ratio on the undrained behavior of material under cyclic loading.

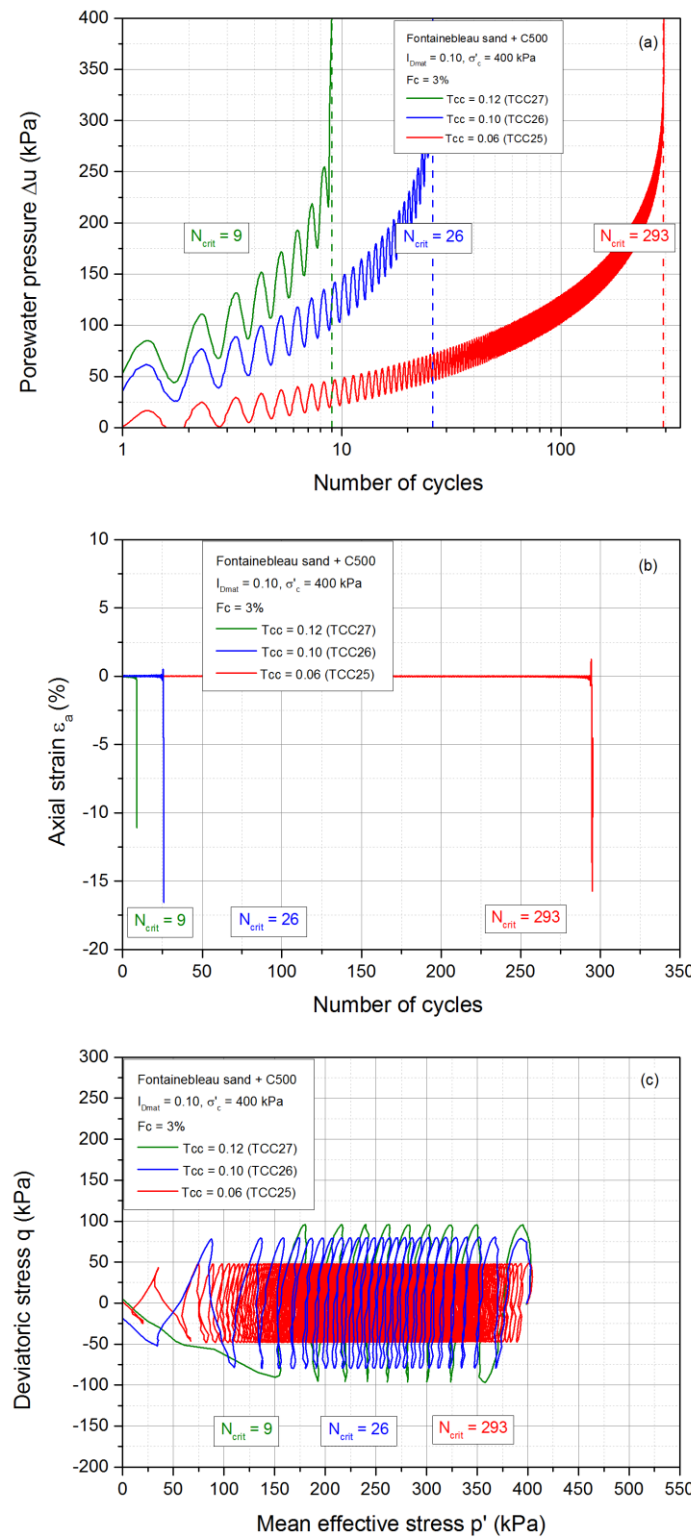


**Figure 4.10: Influence of loading amplitude on the cyclic shear resistance of loose Fontainebleau sand-C500 mixtures**

**C500 mixtures**

**Curves  $\Delta u$ - $N$ ; (b)  $\epsilon a$ - $N$ ; (c)  $p'$ - $q$**

#### 4.4.2.2 Case of dense material

The influence of the cyclic shear ratio is also found in the cyclic mobility behavior of dense material. Indeed, when the magnitude of the cyclic shear ratio is very important and approaches the characteristics of rupture of the soil, the dense soils can manifest a failure behavior which would result from the accumulation of very important deformations following the generation of very high EPWP. On the other hand, if the cyclic shear ratio is low the sample will present a stabilization behavior which is characterized by accommodation of pore pressure that is usually noticed after a very large number of cycles.

In order to highlight the effect of the cyclic stress ratio on the behavior of dense material, and also to have the required data base to trace the shear stress curves of dense samples, we have performed a series of tests on clean sand, sand-C500 mixtures and sand kaolinite mixtures at different cyclic shear ratios. All the tests were carried out at a frequency  $f=0.1$ , consolidated at 400 kPa for a chosen value of density index  $I_{Dmat} = 0.50$ . Figures 4.11a, 4.11b and 4.11c present the results of silty sands at  $F_c = 3\%$  in terms of EPWP, axial deformation and stress paths.

The curves showing the evolution of the EPWP presents two phases, the first one is characterized by a progressive generation of the pore pressure having a mechanism of one peak per cycle and is accompanied by very small deformations. The second one is characterized by development of a two-peak mechanism of the pore water pressure generation curve during which it reaches the value of the consolidation stress (400 kPa) twice per cycle and it is accompanied by a high increase in the axial strain. As the loading amplitude is more important, the less number of cycles are required to reach the initial liquefaction state. For example, it took 76 cycles to initiate the phenomenon of cyclic mobility for a loading amplitude of 144 kPa whereas for an amplitude of 176 kPa the cyclic mobility is initiated at the 24<sup>th</sup> cycle.

The evolution of the axial deformations also presents the same trend. High amplitudes cause the initiation of large deformations much earlier. It is also interesting to note here the dissymmetry between the phases of extension and compression.

The effective stress paths present always a migration towards the origin of the axes during a few or several cycles according to the level of the imposed shear. Indeed, when the amplitude of the applied loading is weak, the cycles are very tight and very numerous before arriving at the origin whereas when the amplitude is important, these are ample and reach quickly the origin after a rapid reduction in the average effective stress  $p'$ .

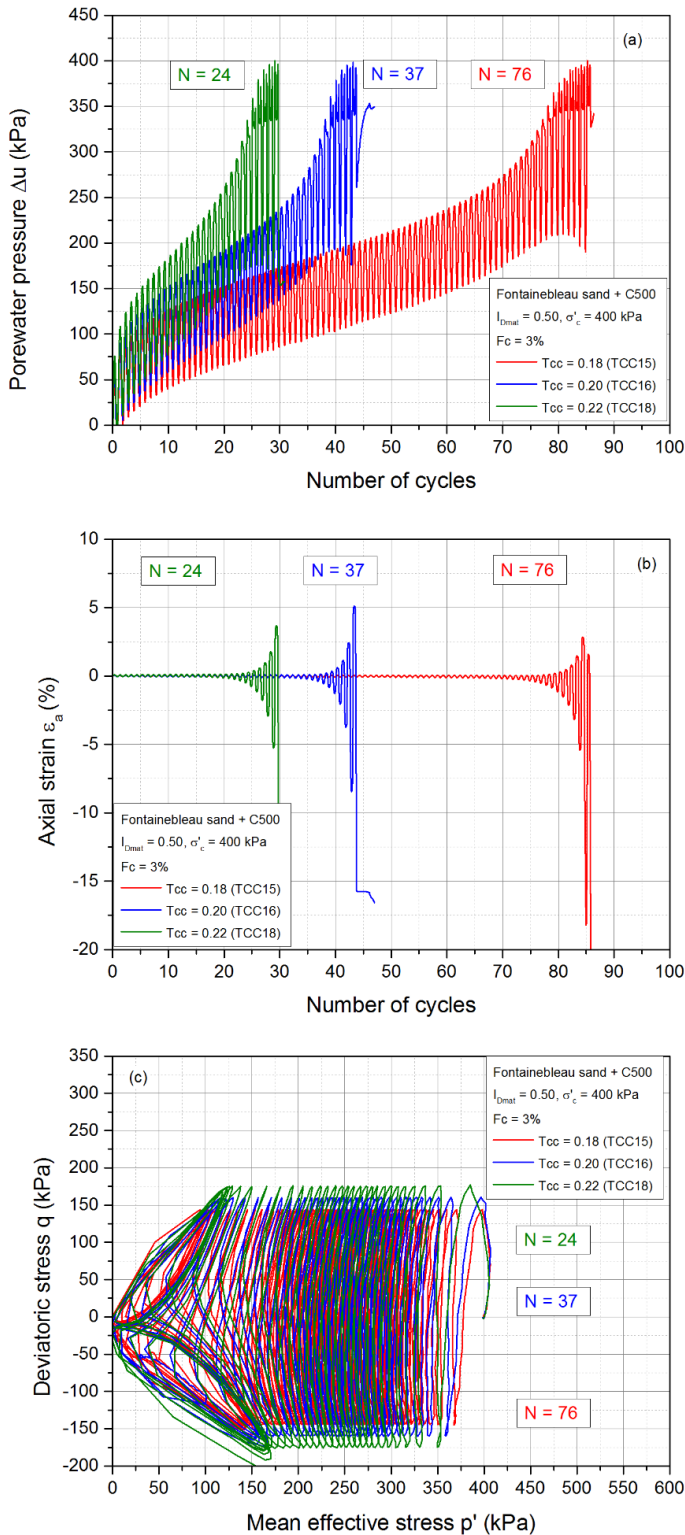


**Figure 4.11: Influence of loading amplitude on the cyclic shear resistance of dense Fontainebleau sand-C500 mixtures**

**C500 mixtures**

**Curves  $\Delta u$ -N (a); (b)  $\varepsilon a$ -N; (c)  $p'$ -q**

#### 4.4.3 Influence of fines content

As for the case of monotonic testing, the effect of adding fines to the sand matrix is also studied under the cyclic loading. For this reason, several series of cyclic tests were executed on two types of mixtures, sand-c500 mixtures and sand-speswhite mixtures.

The first group of tests were done on sand-C500 mixtures at different fines content ( $F_c = 0\%, 1\%, 3\% \text{ and } 5\%$ ). Figure 4.12 presents the results for a group of tests for loose material having an initial density index  $I_{Dmat} = 0.10$ , consolidated at 400 kPa and subjected to a loading amplitude of 48 kPa corresponding to  $T_{cc} = 0.06$ . It is noted that the four specimens exhibit the same behavior. Concerning the pore water pressure, it can be noted that the latter increases steadily and continuously at the beginning of the test before it passes an accumulation phase that can be considered relatively linear at the middle of the test and finally it passes through the last phase which records a significant and sharp rise in the pressure that reaches the value of the initial consolidation stress. However, it can be noted that this generation rate decreases with the increase in fines content. In fact, it is interesting to note that the moment at which the sudden increase in the pore water pressure occurs which corresponds to the critical cycle increases with the increase in fines content from 0% to 5%. For example, the required number of cycles to liquefaction for clean sand at the level of loading is equal to 25 cycles, this  $N_{crit}$  increases to 161 cycles as we increase the fines content to 1% and keeps increasing to 293 cycles and 400 cycles for the cases where  $F_c = 3\%$  and  $5\%$  respectively.

The effective stress paths corresponding to the different tests are presented in figure 4.12c. These curves follow a similar trend with cycles that are more numerous and narrower as the fines content value increases.

Concerning the axial deformations, it is remarked that they all exhibit the same trend, that they remain practically insignificant until they reach a critical cycle where they develop suddenly and quickly a large and very important deformation. However, this occurs at different critical cycle each time depending on the value of the corresponding fines content.

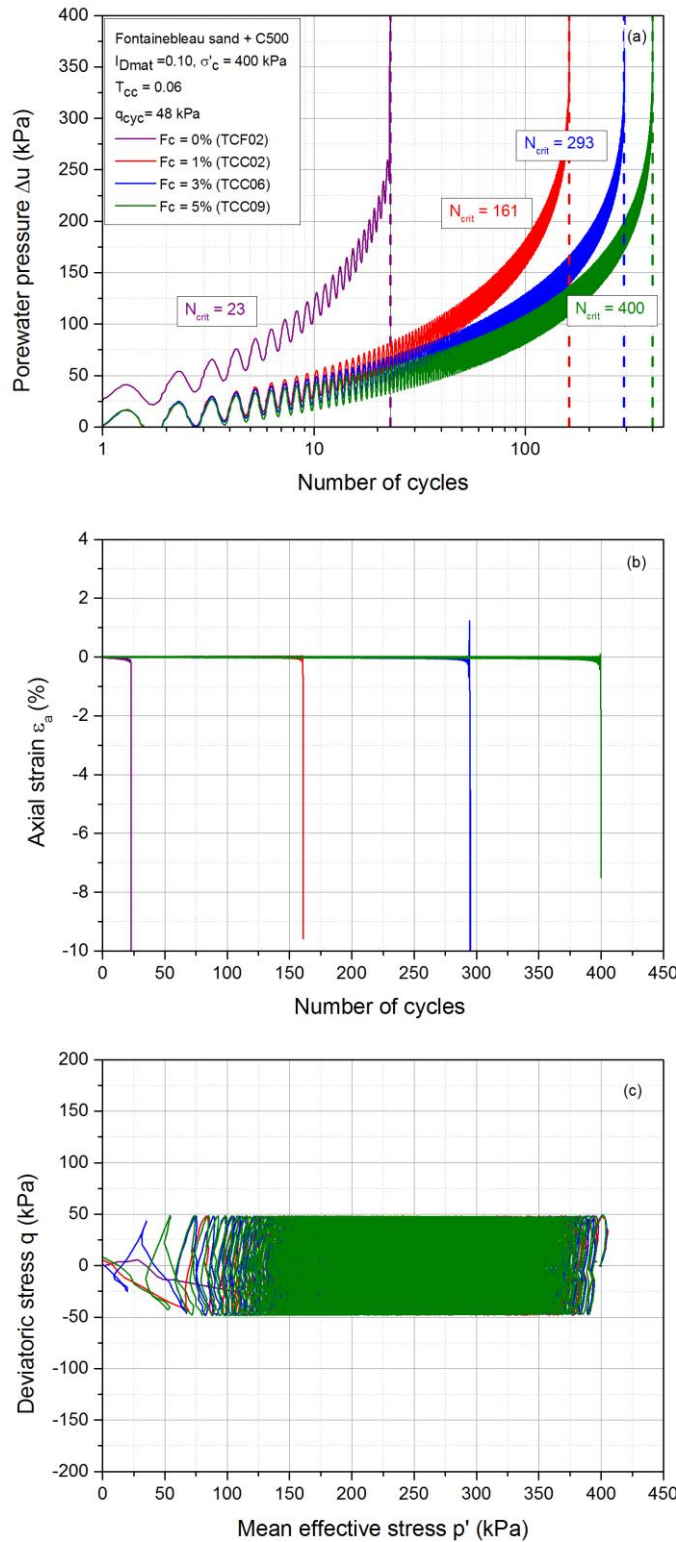


**Figure 4.12: Influence of fines content on the cyclic shear resistance of loose Fontainebleau sand-C500 mixtures**

Curves  $\Delta u$ - $N$  (a); (b)  $\varepsilon_a$ - $N$ ; (c)  $p'$ - $q$

The second group of tests was done on sand-speswhite mixtures for various values of fines content. These results will be presented later in the cyclic shear stress curves.

#### 4.5 Cyclic shear resistance curves

The cyclic shear resistance curves CSR corresponds to the representation of the total number of cycles required to reach failure (liquefaction in our case) as a function of the cyclic shear rate. This type of representation in the  $(\tau_{cyc} / 2\sigma'_c, \log N)$  plane is usually parametrized by the density index or the relative density index. In fact, with the aid of these curves it is possible to evaluate the greater or lesser the susceptibility of a soil to generate EPWP under cyclic loading and to develop axial deformations of liquefaction type or cyclic mobility type.

These curves can be established for loose to very loose soils whose behavior corresponds to the phenomenon of total liquefaction where the failure criterion is very easy to define and corresponds to the critical cycle  $N_{crit}$  during which the phenomenon of liquefaction is initiated. Besides, these curves have been generally established for dense soils which present the cyclic mobility behavior in which the rupture criterion is given in terms of the maximum admissible deformation threshold.

The cyclic shear resistance curve obtained for loose Fontainebleau sand having a density index  $I_D = 0.10$  is plotted in the  $(\tau_{cyc} / 2\sigma'_c, \log N)$  plane with the plot of the corresponding curve obtained by Benahmed (2001) for Fontainebleau sand under same conditions (figure 4.13). It is noted that the two curves show very good results in terms of repeatability.

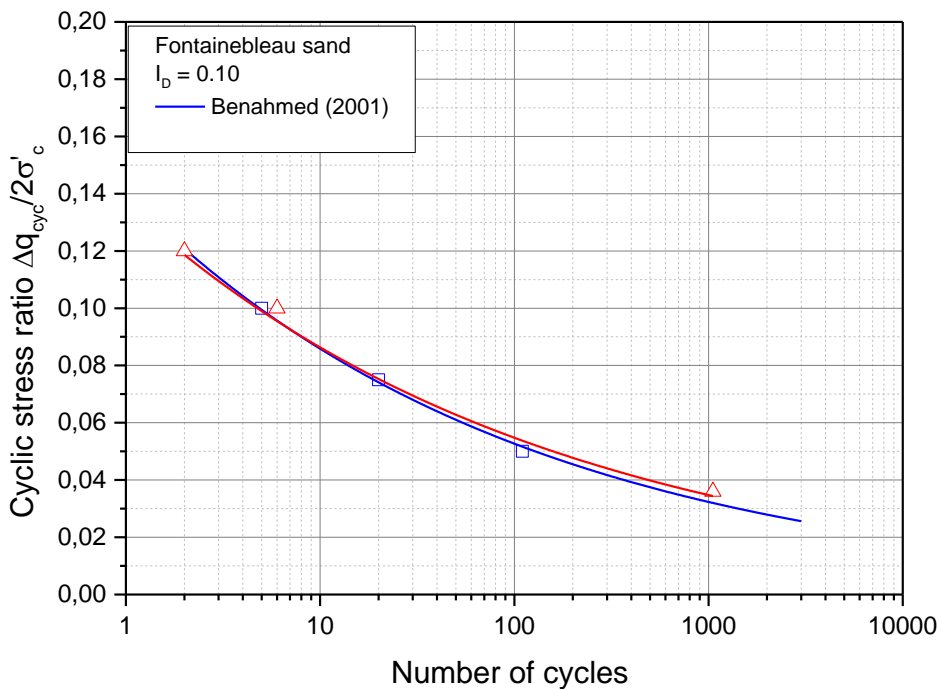


**Figure 4.13: Cyclic shear resistance curve for Fontainebleau sand**

#### 4.5.1 Case of loose states

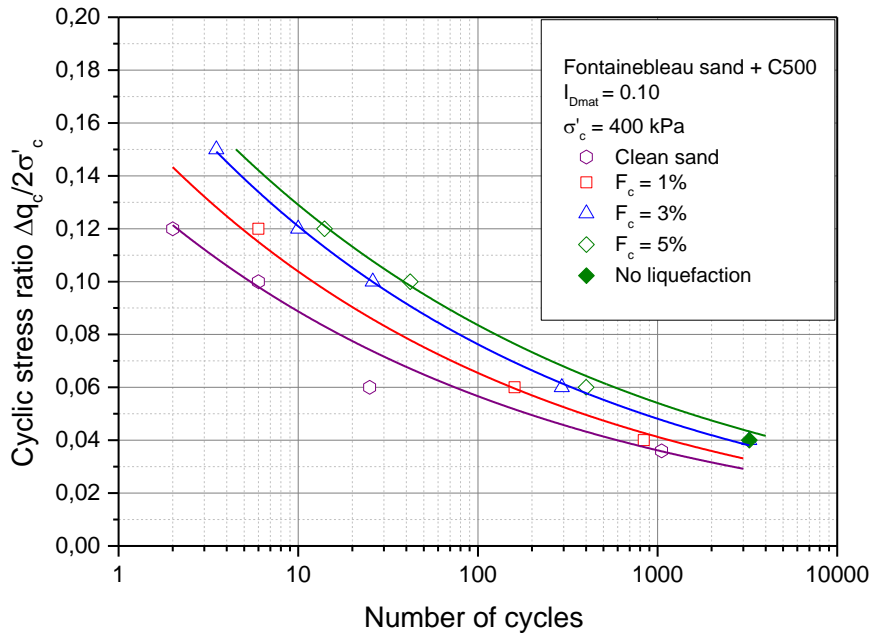
##### 4.5.1.1 Sand-C500 mixtures

Figure 4.14 shows the CSR curves for clean Fontainebleau sand in addition to mixtures with C500 at various fines content  $F_c = 1\%, 3\%$  and  $5\%$ . All the specimens were consolidated at 400 kPa since generally these curves are established for a given value of the isotropic consolidation stress. The initial density index for all the mixtures is fixed at  $I_{D\text{mat}} = 0.10$ .

The rupture criterion for these loose soils corresponds to the critical cycle defined before at which the liquefaction phenomenon is initiated and translated with the sudden development of large deformations at this critical cycle.

It is noted that the cyclic shear resistance curve of the clean sand is situated below the curves of sand-fines mixtures. In addition, it's recorded that these curves shift upwards each time we increase the fines content from 0% to 5%. In other words, we can conclude that the addition of fine particles to the sand matrix has increased its resistance against liquefaction, which also confirms the results found in our monotonic testing. These results are coherent with those

found in the literature by Chang *et al.* (1982); Dezfulian (1984) and Amini & Qi (2000). Note that the points with a solid interior correspond to specimens that didn't liquefy after large number of cycles and therefore these points define the asymptotes of our curves.



**Figure 4.14: Influence of the non-plastic fines content (C500) on the cyclic shear resistance curves (loose state)**

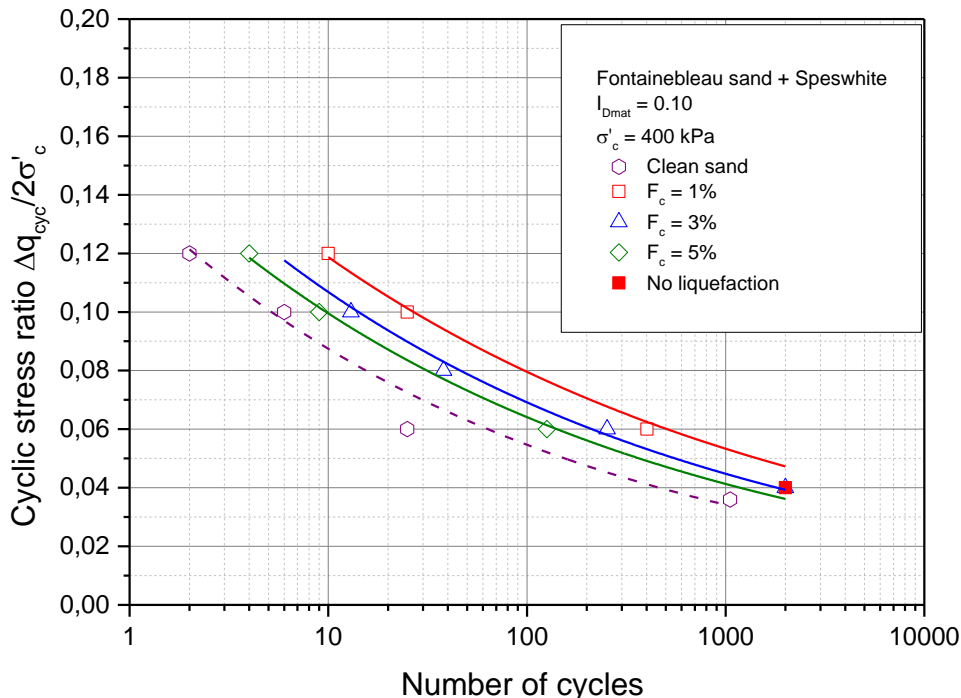
#### 4.5.1.2 Sand-speswhite mixtures

Figure 4.15 presents the cyclic shear resistance (CSR) curves obtained for the loose mixtures of sand and kaolinite speswhite fines at various fines content  $F_c = 0\%, 1\%, 3\% \text{ and } 5\%$ . All the specimens were prepared at an initial density index  $I_{Dmat}= 0.10$  and consolidated at 400 kPa.

The CSR curves reveal that upon adding 1% of fines to clean sand the curve corresponding to this mixture shift upwards and is above that of clean sand. However, upon increasing again the fines content to 3% and 5% these curves shift downwards indicating a decrease in the CSR. It is important here to recall that the specimens of clean sand were prepared using wet tamping method due to the difficulties of reconstituting them for a low density index  $I_D = 0.10$  in dry conditions. However, the mixtures of sand-Speswhite were prepared in dry conditions and therefore we should take into consideration the effect of the reconstitution method on the

behavior of these soils. For this reason, the curve corresponding to the clean sand has been plotted as a dashed line. These results confirm those found under monotonic loading where it is found that the addition of plastic fines (Speswhite) has a reversible effect on clean sand with respect to that of non-plastic fines. The decrease in CSR with the increase in fines content from 1% to 5% is consistent with the results reported by Polito (1999), Bouferra et Shahrour (2004), Ghahremani & Ghalandarzadeh (2006), and Derakhshandi *et al.* (2008). However, it is important to mention here that unlike the monotonic testing where the loose specimens of sand and speswhite exhibited no liquefaction and were characterized by a contracting-dilating behavior, these specimens have liquefied under cyclic loading.

As for the case of the loose sand-C500 mixtures, the failure criterion is easily defined and corresponds to the critical cycle  $N_{crit}$  at which the phenomenon of liquefaction is initiated.



**Figure 4.15: Influence of the plastic fines content (Speswhite) on the Evolution of cyclic shear resistance curves (loose state)**

#### 4.5.2 Case of dense states

The characterization of the cyclic shear resistance curves for medium dense to dense material, which generally exhibit a dilatant behavior differs from that for loose soils where the

predominant behavior is the total liquefaction with appearance of large deformations during a particular critical cycle as previously seen.

On the other hand, for the case of the development of cyclic mobility, the reference element characterizing the failure is defined as being either the appearance of the initial liquefaction or a deformation criterion defining the maximum peak-to-peak amplitude that can be attained.

#### **4.5.2.1 Sand-C500 mixtures**

The cyclic shear resistance curves for clean Fontainebleau sand in addition to mixtures of sand and C500 at various fines content  $F_c = 0\%, 1\%, 3\%$  and  $5\%$  are presented in figure 4.16. All the specimens were prepared at a given initial density index  $I_{D_{mat}} = 0.50$  and consolidated at the same isotropic consolidation stress 400 kPa.

In order to make it possible to make comparisons, we have subjected them to the same loading amplitude under the same initial conditions.

For example, if we take the CSR value of 0.18, we note that, although the samples behaviors are qualitatively identical, the required numbers of cycles to collapse differs in each case. For this CSR, the clean sand collapse at the 7<sup>th</sup> cycle whereas upon adding 1% of fines the number of cycles increases up to 29 and keeps increasing with increasing in fines content.

Indeed, despite identical initial conditions, the difference in terms of number of cycles necessary to initiate liquefaction is very significant. It is noted that the CSR curves shifts upwards each time the fines content is increased. We thus find under cyclic loading the similar results as the ones found under monotonic loading.

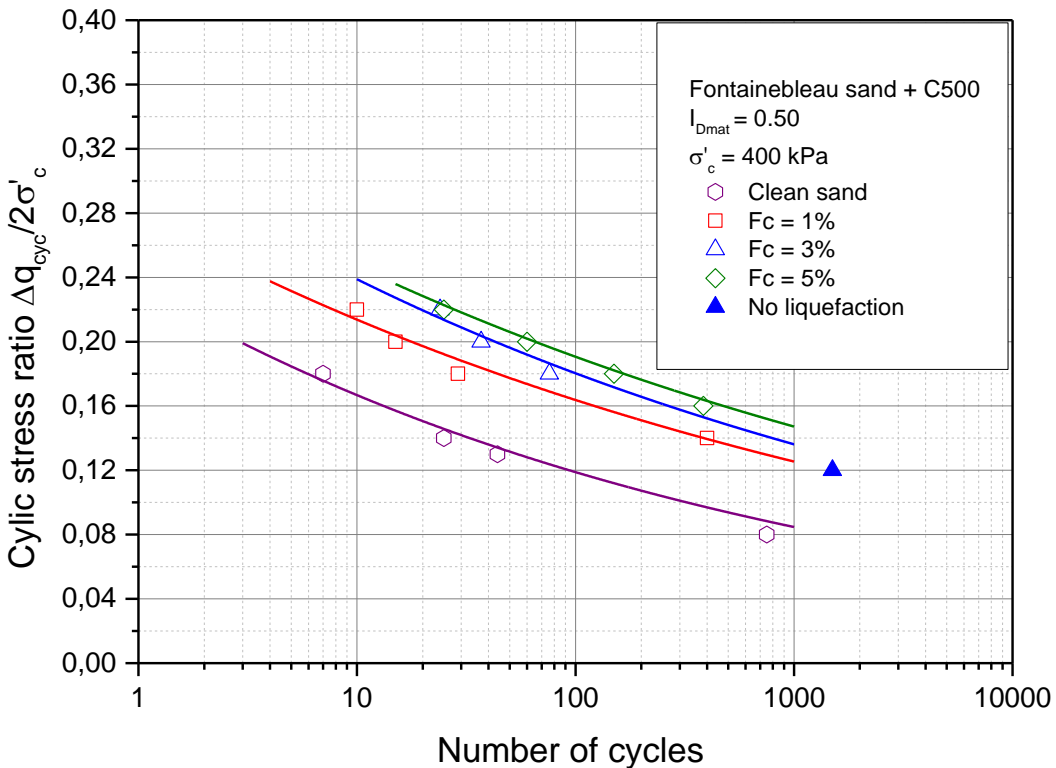


**Figure 4.16: Influence of the non-plastic fines (C500) content on the evolution of cyclic shear resistance curves (dense state)**

#### 4.5.2.2 Sand-Speswhite mixtures

Figure 4.17 presents the CSR curves for the medium dense mixtures of sand and kaolinite Speswhite at various fines content  $F_c = 0\%, 1\%, 3\% \text{ and } 5\%$ . As for the sand and C500 mixtures, all the specimens were prepared at an initial density index  $I_{D\text{mat}}$  of 0.50 and consolidated at 400 kPa.

It may be noted that upon increasing the fines content, the cyclic resistance of the mixtures decreases. For example, for a cyclic stress ratio of 0.14 the required numbers for the initiation of cyclic mobility for a clean sand is equal to 25 cycles, whereas this number decreases gradually as we increase the fines content up to 5% where this phenomenon occurs at the 6<sup>th</sup> cycle. Bouferra et Shahrour (2004) performed a series of cyclic tests on mixtures of Hostun sand and kaolinite, he has reported a decrease in the CSR upon adding fines up to 15%. Figure

4.18 presents the plot of results found by Bouferra et Shahrou (2004) for a specimen of Hostun sand and kaolinite ( $F_c = 5\%$ ) prepared at a density index  $I_D = 0.52$  which is very similar to our case. It is noted that for a specimen of Hostun sand and 5% kaolinite at a cyclic stress ratio equal to 0.20, the number of cycles to reach liquefaction is equal to 6 whereas for our case (Fontainebleau and 5% kaolinite) the latter is equal to 1 cycle. This increase in the CSR is due to the difference in the type of sand matrix, in fact, Hostun sand is more resistant to liquefaction than Fontainebleau sand, consequently the specimen of Hostun sand and kaolinite will require a higher number of cycles to attain liquefaction. It is also noted that the specimen of clean Hostun sand is situated above the curve of Fontainebleau since the latter is more resistant to liquefaction. This result has also been reported by Benahmed (2001) who has presented a comparison between the cyclic behavior of Hostun and Fontainebleau sand and indicated that Fontainebleau sand is more susceptible to liquefaction.

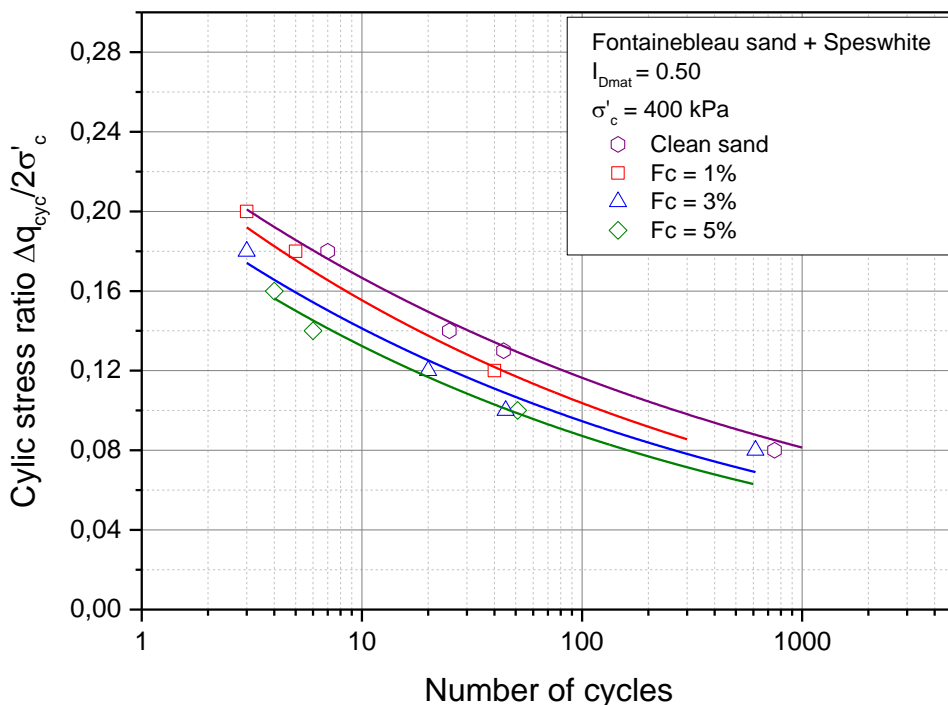


**Figure 4.17: Influence of the plastic fines (Speswhite) content on the evolution of cyclic shear resistance curves (dense state)**

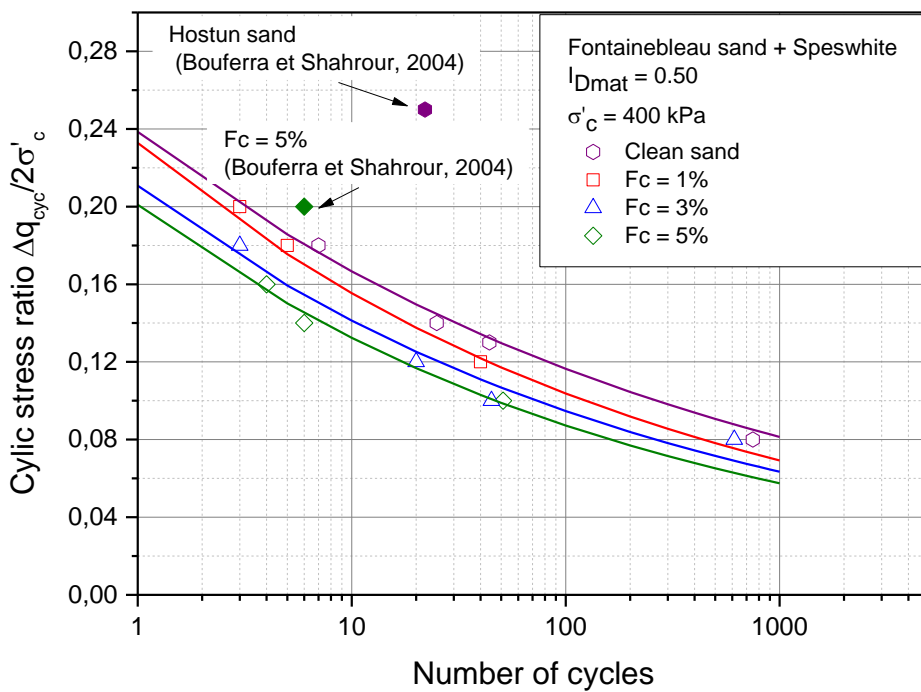


**Figure 4.18: Comparison of the cyclic shear resistance curves of Fontainebleau sand and plastic fines (Speswhite) with literature results**

The analysis of the CSR curves obtained for Fontainebleau sand and mixtures of sand and fines allow to plot the influence of fines content on the initiation of instability in terms of required numbers of cycles to liquefaction. Figure 4.19 shows the plot of the initiation of liquefaction as a function of fines content for mixtures of sand-C500 and sand-speswhite for a density index  $I_{Dmat} = 0.10$ , consolidated at 400 kPa and sheared under an alternating loading amplitude equal to 0.10.

It may be noted that the addition of non-plastic fines (C500) increases the resistance of sand to liquefaction where it is noted that the corresponding red curve has an increasing slope upon adding fines. However, the blue curve that corresponds to the mixture of sand and Speswhite (plastic fines) present a reversed behavior characterized by a negative slope. The first part of the blue curve is traced in plotted line since it corresponds to the loose clean sand ( $I_D = 0.10$ ) that as mentioned before has been prepared in wet conditions.

The same analysis has been done for medium dense specimens of clean sand, sand-C500 and sand-Speswhite mixtures prepared at an initial density index  $I_{Dmat} = 0.50$ , consolidated at 400 kPa and subjected to an alternating loading equal to 0.16. The same trend is observed, with an

increase of the resistance to liquefaction upon adding non-plastic fines whereas the latter decreases with the increase in plastic fines content (figure 4.20).

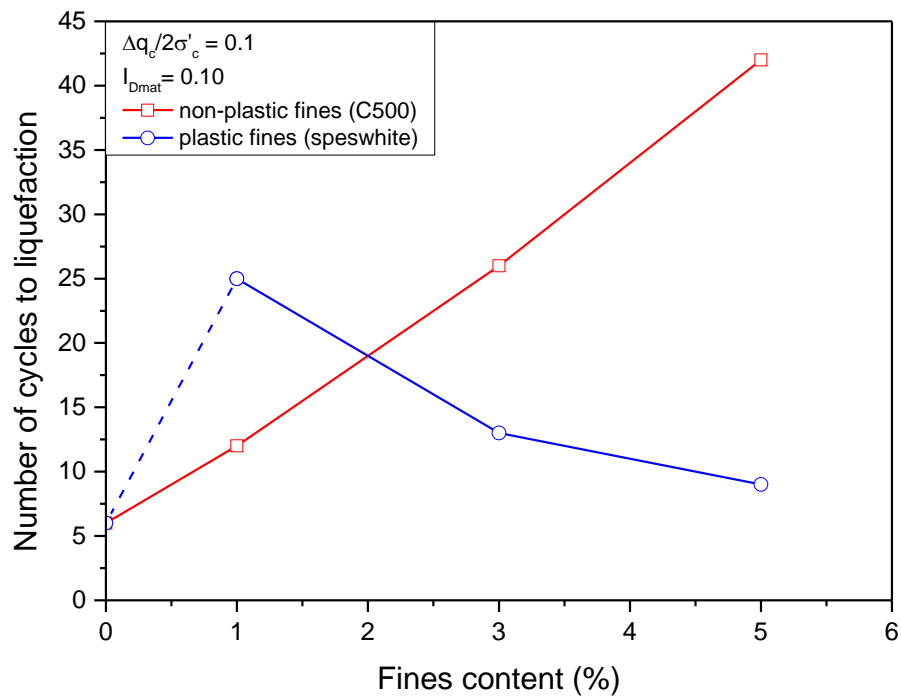


Figure 4.19: Influence of fines content on the number of cycles to liquefaction of loose specimens

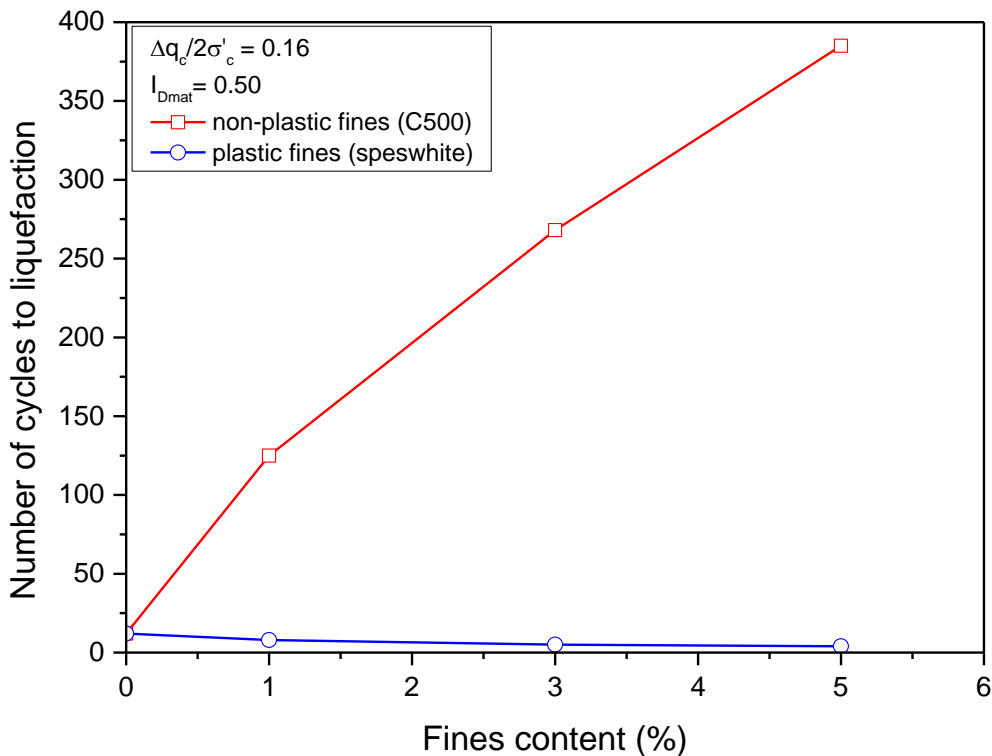


Figure 4.20: Influence of fines content on the number of cycles to liquefaction of dense specimens

## 4.6 Proposition of a model for predicting the cyclic shear resistance

### curve based on the fines content

The analysis of the cyclic shear resistance curves obtained from the series of undrained cyclic shearing on clean sand, sand-C500 and sand-speswhite shows that these curves present a non-linear evolution of the form :  $y = a \cdot x^b$

It has been shown in the previous part that the increase in the non-plastic fines content lead to an upward shift or translation of the CSR curves with a relatively parallel evolution. However, the curve corresponding to sand-Speswhite specimens show a reversed trend with a downward translation upon increasing the fines content.

The analysis of the corresponding equations reveals that the translation of these curves is a function of the parameter  $a$  where parameter  $b$  remains relatively constant. The values for these parameters as a function of the fines content are presented below in tables 4.3 and 4.4 for sand-C500 and sand-Speswhite respectively at two different density indexes.

<b>Fc (I<sub>Dmat</sub> = 0.10)</b>	<b>a</b>	<b>b</b>	<b>Fc (I<sub>Dmat</sub> = 0.50)</b>	<b>a</b>	<b>b</b>
0	0,139	-0,195	0	0,234	-0,147
1	0,165	-0,2	1	0,279	-0,146
3	0,197	-0,2	3	0,316	-0,142
5	0,208	-0,203	5	0,32	-0,135

**Table 4.3 - Values of a and b for sand-C500 mixtures**

<b>Fc (I<sub>Dmat</sub> = 0.10)</b>	<b>a</b>	<b>b</b>	<b>Fc (I<sub>Dmat</sub> = 0.50)</b>	<b>a</b>	<b>b</b>
0			0	0,238	-0,176
1	0,177	-0,174	1	0,233	-0,175
3	0,165	-0,188	3	0,211	-0,174
5	0,154	-0,191	5	0,2	-0,18

**Table 4.4 - Values of a and b for Fontainebleau sand-Speswhite mixtures**

The evolution of the parameter “a” with the increase in fines content for both sand-C500 and sand-Speswhite is presented in figures 4.21a and 4.21b respectively. According to the plot of the parameter a as a function of fines content, we have established a linear relationship that correlates these two parameters. In order to validate this result, we have applied this method on results from literature. For example, Chang *et al.* (1982) has performed a series of cyclic testing on sand containing non-plastic fines. For a density index of 0.50 he has noted that the increase in fines content increases the resistance to liquefaction. Based on our evolution line of the parameter “a”, we can predict this value for a fines content = 20% as for the case of Chang *et al.* (1982). Then the cyclic shear resistance curve for a mixture of sand and 20% fines has been plotted (see figure 4.22a). Two points corresponding the cyclic testing done by Chang *et al.* (1982) are also plotted on the CSR curve, it is noted that these points are very close to the predicted CSR curve. For example, for a loading amplitude  $T_{cc} = 0.30$ , the required number of cycles to liquefaction reported by Chang is 9 cycles, and the critical cycle

predicted by our curve is equal to 12. Also for a cyclic stress ratio of 0.25, Chang et al. (1982) has reported a critical number of cycles that is equal to 90. However, according to the predicted curve, this number of cycles is reduced to 60 but still acceptable. Here it is important to note that the nature of the sand matrix and of the fine used also play an important role in the behavior of these soils and affects this parameter “a”. Also, it is interesting to note that the evolution of this parameter presents the same trend with the variation in density index, actually we can note that the slope at  $I_{Dmat} = 0.10$  and  $0.50$  is constant, but with a different intercept that corresponds to  $Fc = 0\%$  (clean sand). Therefore, it is sufficient to realize one cyclic test for a clean sand to determine the intercept of this line, and then according to this equation, we can compute the parameter “a” for any value of  $Fc$ .

The same comparison has been done for the case of sand-Speswhite mixtures. Figure 4.22b shows the curve corresponding to  $Fc = 15\%$  based on the proposed model for the prediction of the CSR curve. Then we compared this curve with the results found by Bouferra et Sharour (2004) who tested a specimen of Hostun sand and kaolinite for  $Fc = 15\%$  at a density index of 0.52. It is noted that the total number of cycles to liquefaction at a cyclic stress ratio equal to 0.10 is equal to 10 according to the predicted curve, whereas for Shahrou test, this number exceeds the latter where he recorded 20 cycles. This result is logical and can be explained due to the difference of sand matrix. As indicated before, Hostun sand is more resistant to liquefaction than Fontainebleau sand. Consequently, a mixture of Hostun sand and kaolinite is more resistant than a mixture of Fontainebleau sand and kaolinite for the same initial conditions.

Although this method presents some differences in terms of the critical number of cycles due to the differences in the sand and fines types, it still gives an idea and an approximation of the liquefaction of sand containing fines.

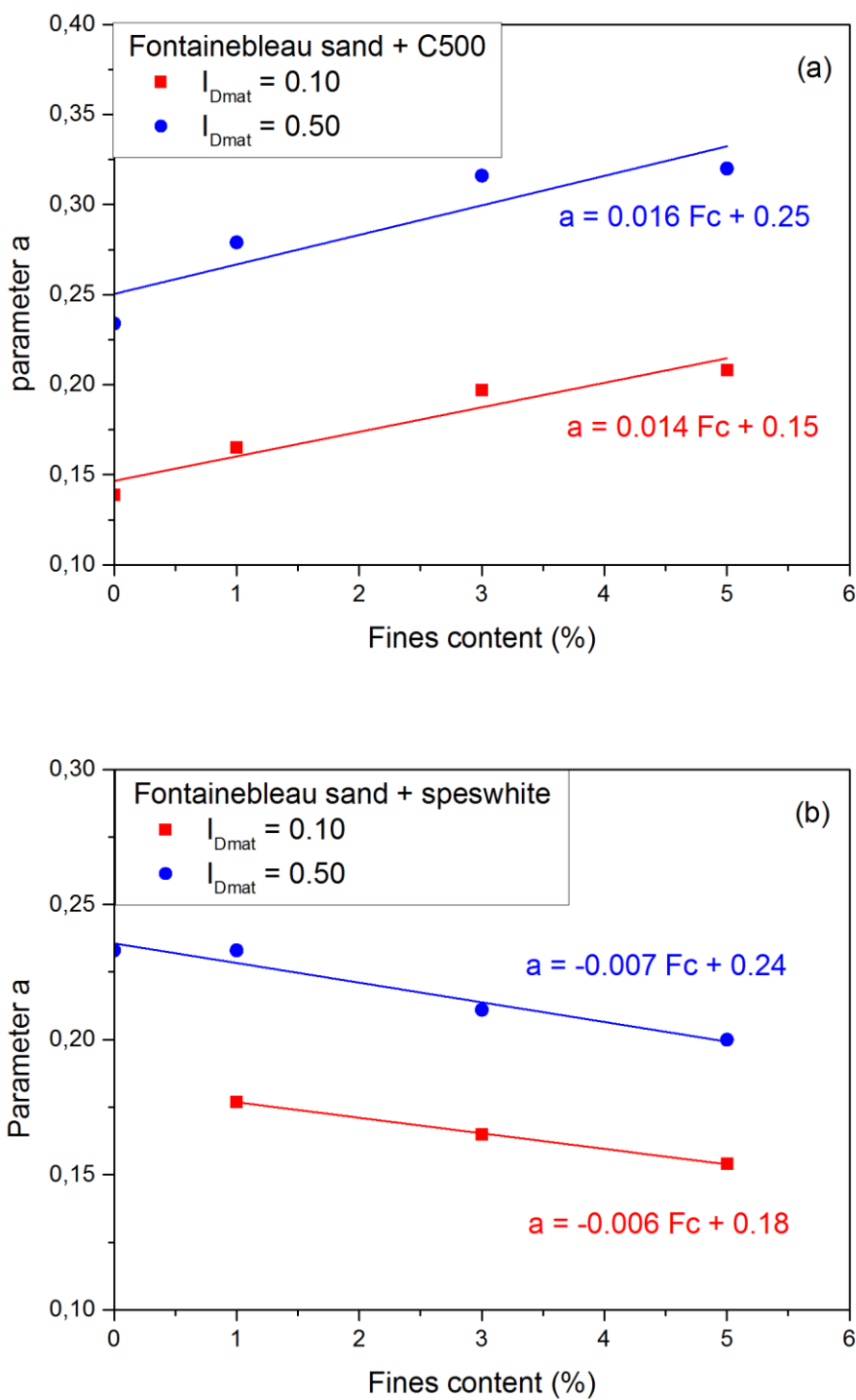


Figure 4.21 : Evolution of the parameter « a » with the increase in fines content

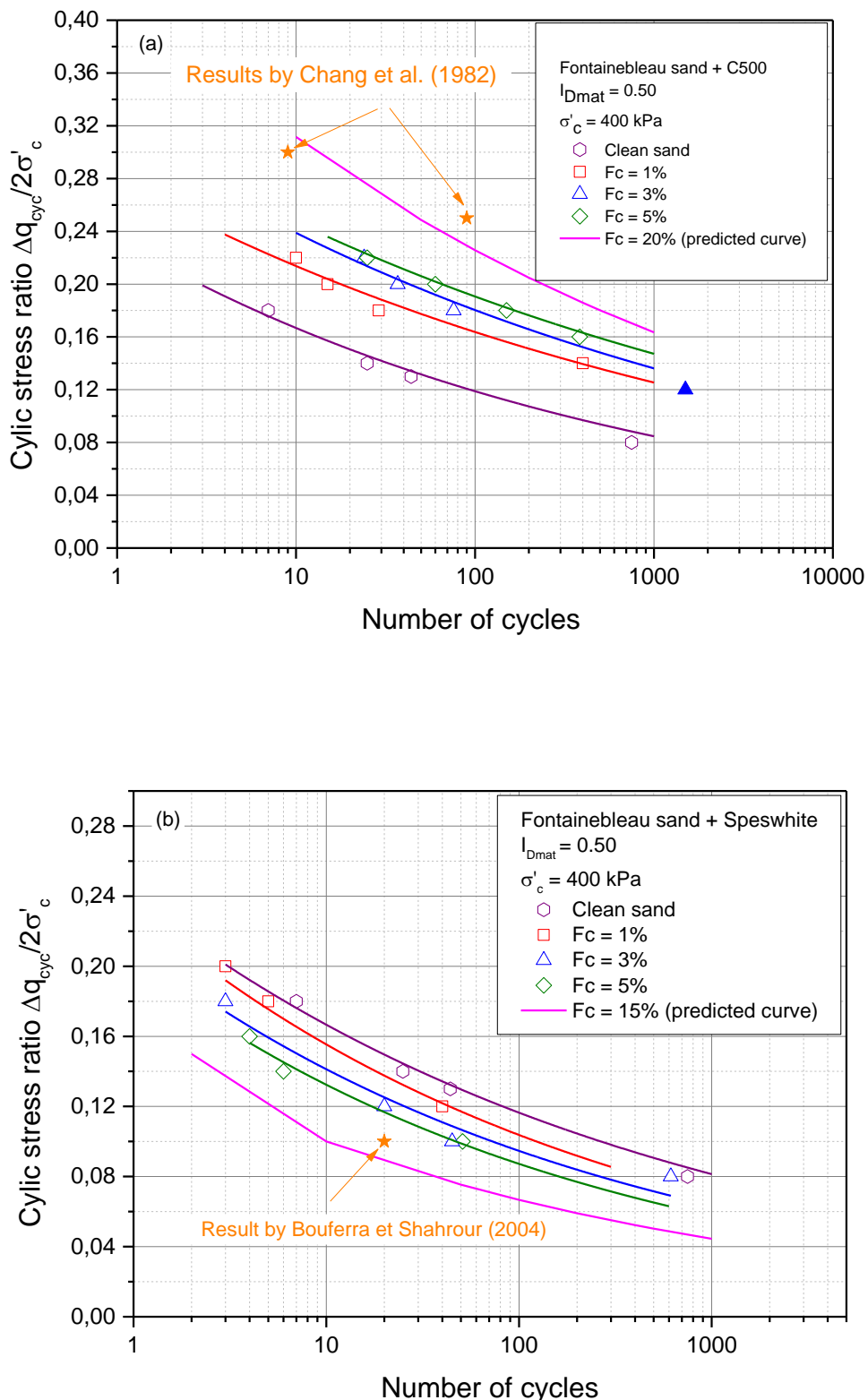


Figure 4.22: Evaluation of the proposed method

(a) non-plastic fines; (b) plastic fines

## **4.7 Synthesis of behaviors observed under undrained monotonic and cyclic loading (Comparison between monotonic and cyclic behaviors of mixtures)**

### **4.7.1 Total liquefaction phenomena (case of loose materials)**

In this part, we are concerned by the case of contracting samples that have presented the initiation of instability phenomenon under both monotonic and cyclic loading. A comparison has been made on the responses obtained under monotonic and cyclic loading in terms of global behavior observed, on one hand and, on the development and evolution of the instability line on the other hand.

Figures 4.23a, 4.23b and 4.23c present a comparison of the behaviors observed under monotonic and cyclic loadings in the  $(q, \varepsilon_a)$ ,  $(\Delta u, \varepsilon_a)$  and  $(p', q)$  planes respectively for a specimen of clean loose Fontainebleau sand having an initial density index  $I_D = 0.10$ , consolidated at 400 kPa and sheared under both monotonic and cyclic loadings.

It is noted that the monotonic behavior forms an envelope limiting the possible states that can be reached in a cyclic test. This is particularly clear for the effective stress paths where it is observed that the cyclic stress paths are totally inscribed within this monotonic envelope. The differences observed in the first cycle (the cyclic path "leaves" slightly out of the monotonic path) are related to a more delicate implementation of the loading point in the cyclic case compared to the monotonous case, which can lead to an imperfection during the loading at the first cycle.

Figure 4.24 and 4.25 present the plot of both monotonic and cyclic tests for the two mixtures of sand-C500 and sand-speswhite respectively. The same behavior is noted concerning the monotonic behavior which forms an envelope limiting the cyclic stress paths. However, it is interesting to note that the cyclic instability line reported for a mixture of sand and C500 presents more pronounced differences (in the range of  $1.1^\circ$ ) than those reported for a clean sand ( $0.5^\circ$ ). This difference becomes more pronounced for the case of sand-speswhite mixture ( $2.6^\circ$ ).

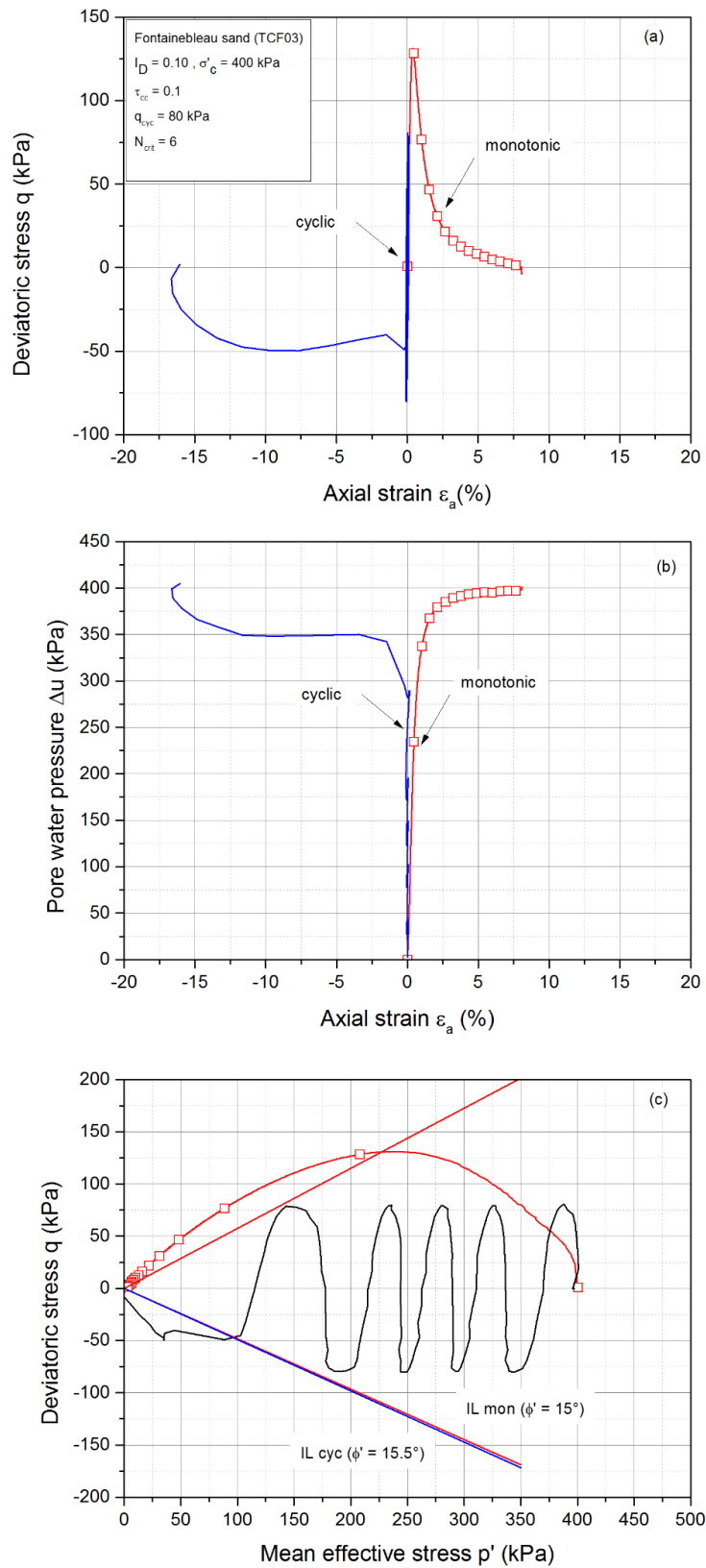


**Figure 4.23: Comparison between monotonic and cyclic shearing of loose Fontainebleau sand**

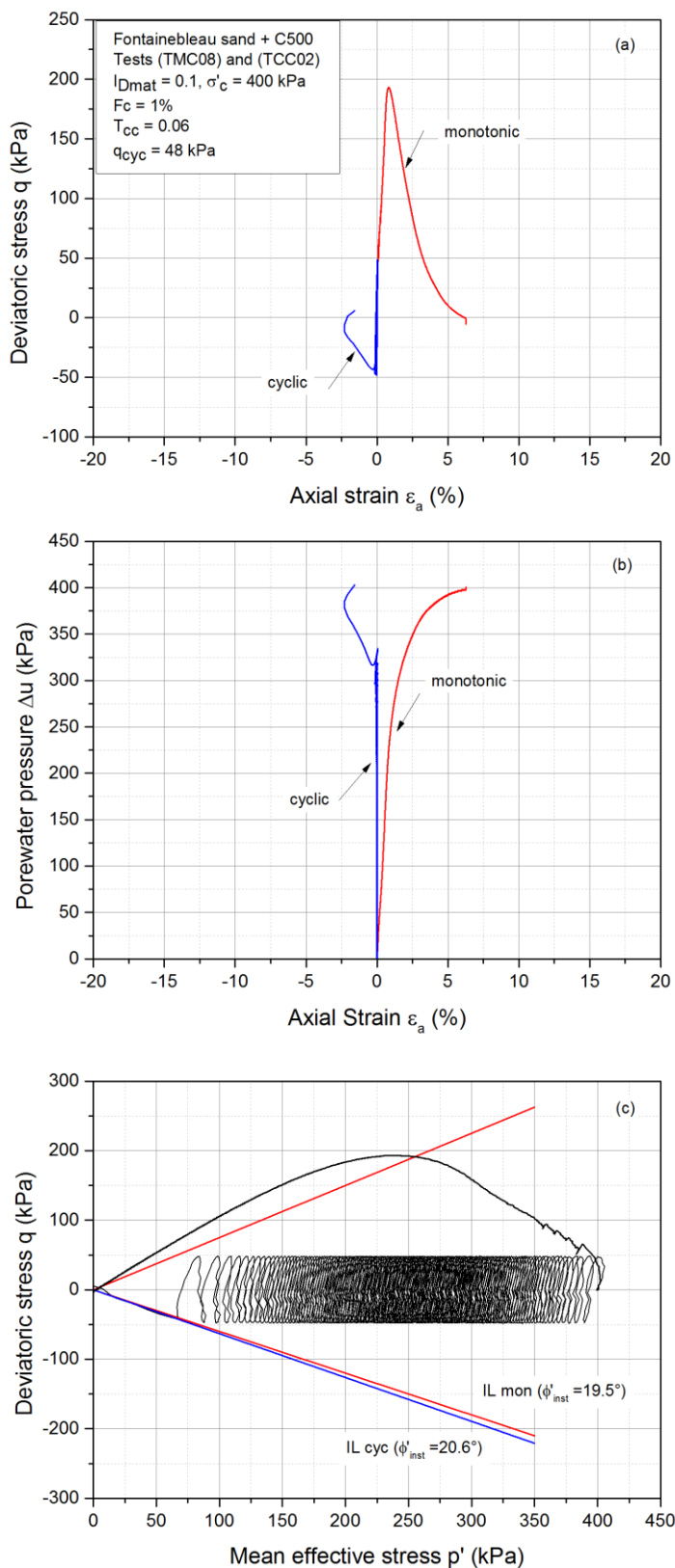


**Figure 4.24: Comparison between monotonic and cyclic shearing of loose sand-C500 mixture**

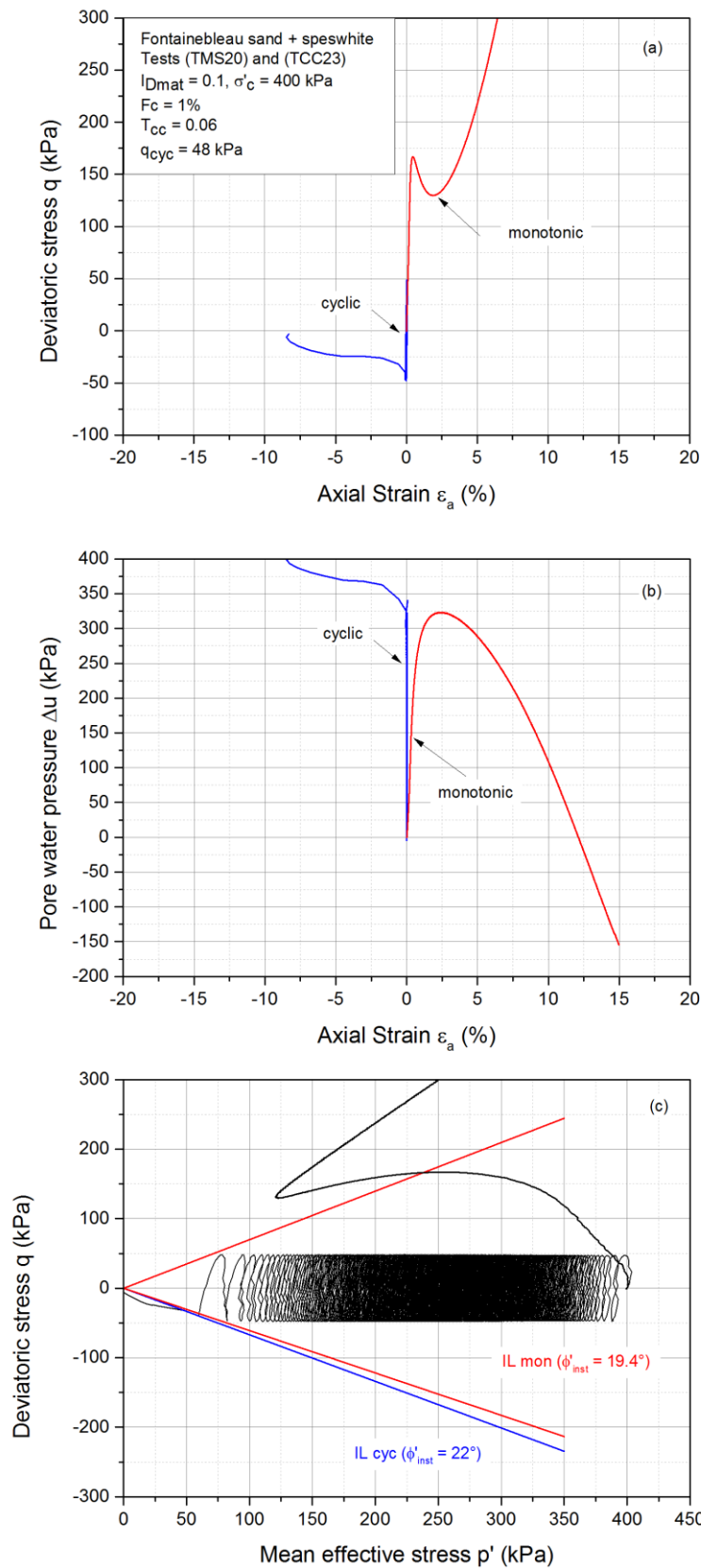
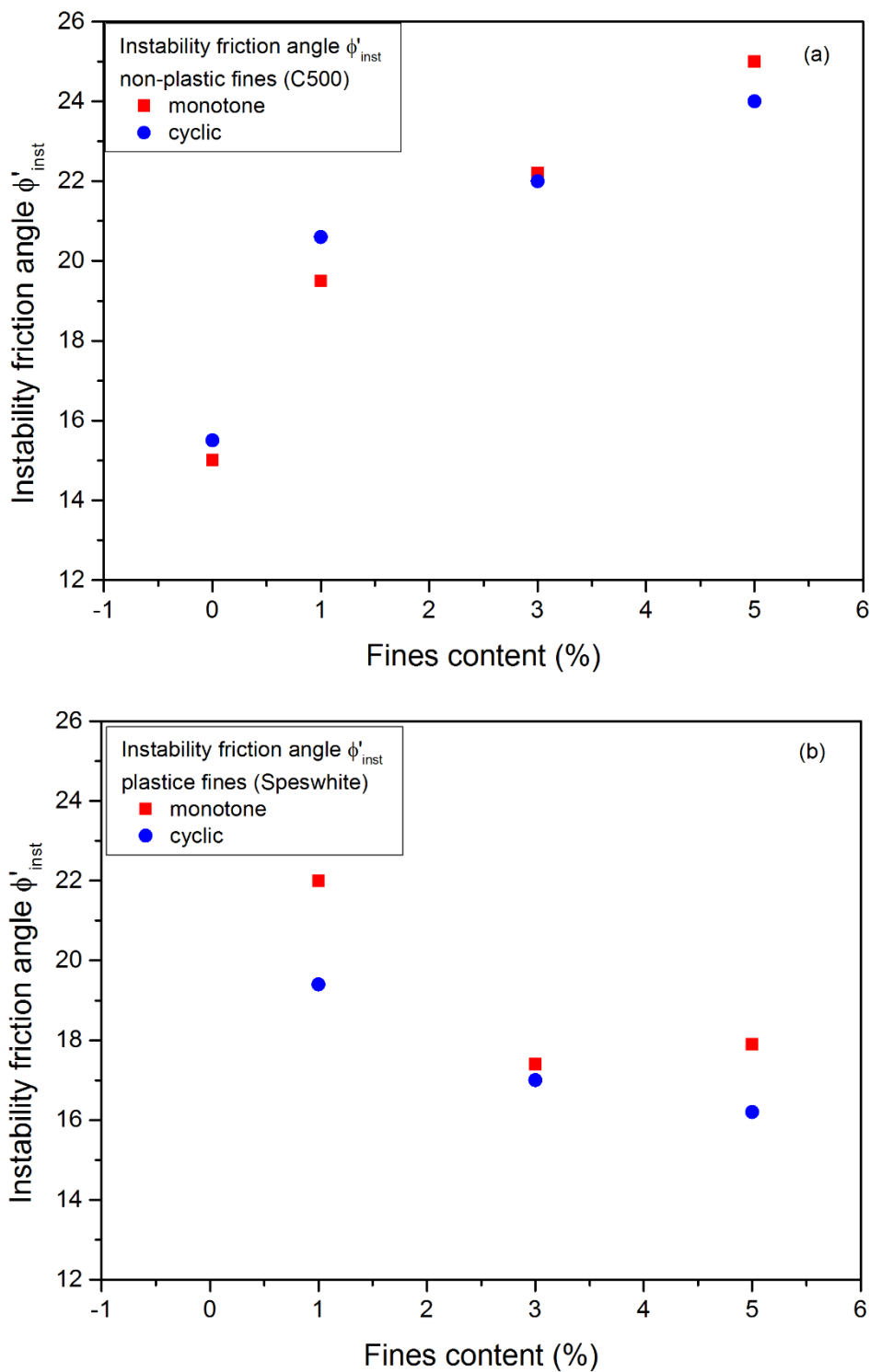


Figure 4.25: Comparison between monotonic and cyclic shearing of loose sand-Speswhite mixture

In order to compare the instability thresholds corresponding to the initiation of liquefaction, obtained under monotonic and cyclic stress, the instability friction angle in both monotonic and cyclic testing as a function of fines content is presented in figure 4.26 in a synthetic manner. It is noted that the mixtures of sand and C500 have closer values of monotonic and cyclic instability angles (figure 4.26a) whereas those of sand and speswhite record more noticeable differences (order of  $2^\circ$ ) that still acceptable (figure 4.26b).

The average values of the evolution of the instability friction angle with the increase in fines content for both mixtures of sand- C500 and sand- speswhite is presented in figure 4.27. A linear relationship has been established to define the evolution of the instability angle with the increase in fines content.



**Figure 4.26: Comparison between the monotonic and cyclic instability lines**

**(a) Non-plastic fines ; (b) plastic fines**

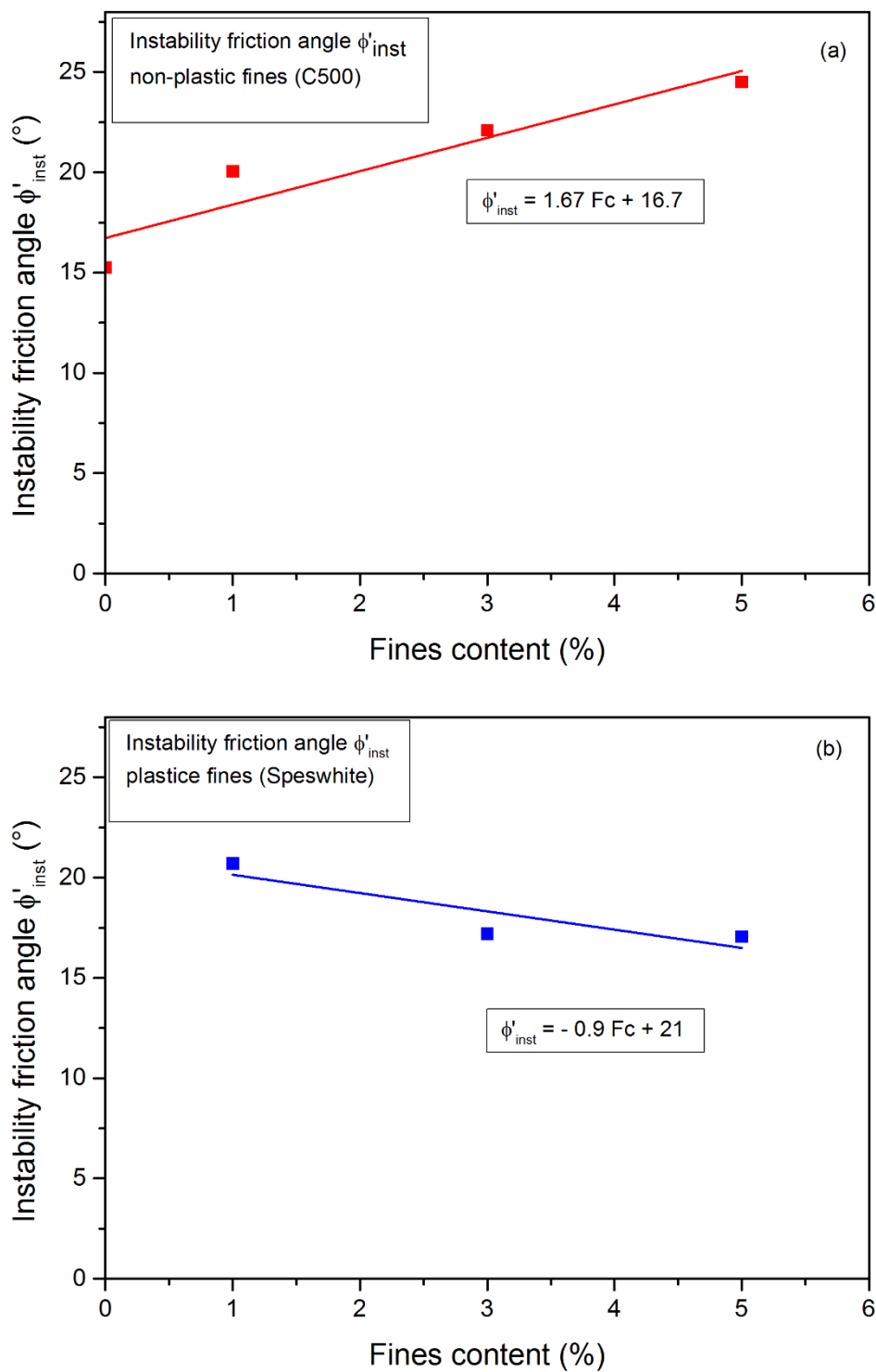


**Figure 4.27: Evolution of instability friction angle with the increase in fines content**

(b) Non-plastic fines ; (b) plastic fines

#### 4.7.2 Cyclic mobility phenomenon (case of dilating mixtures)

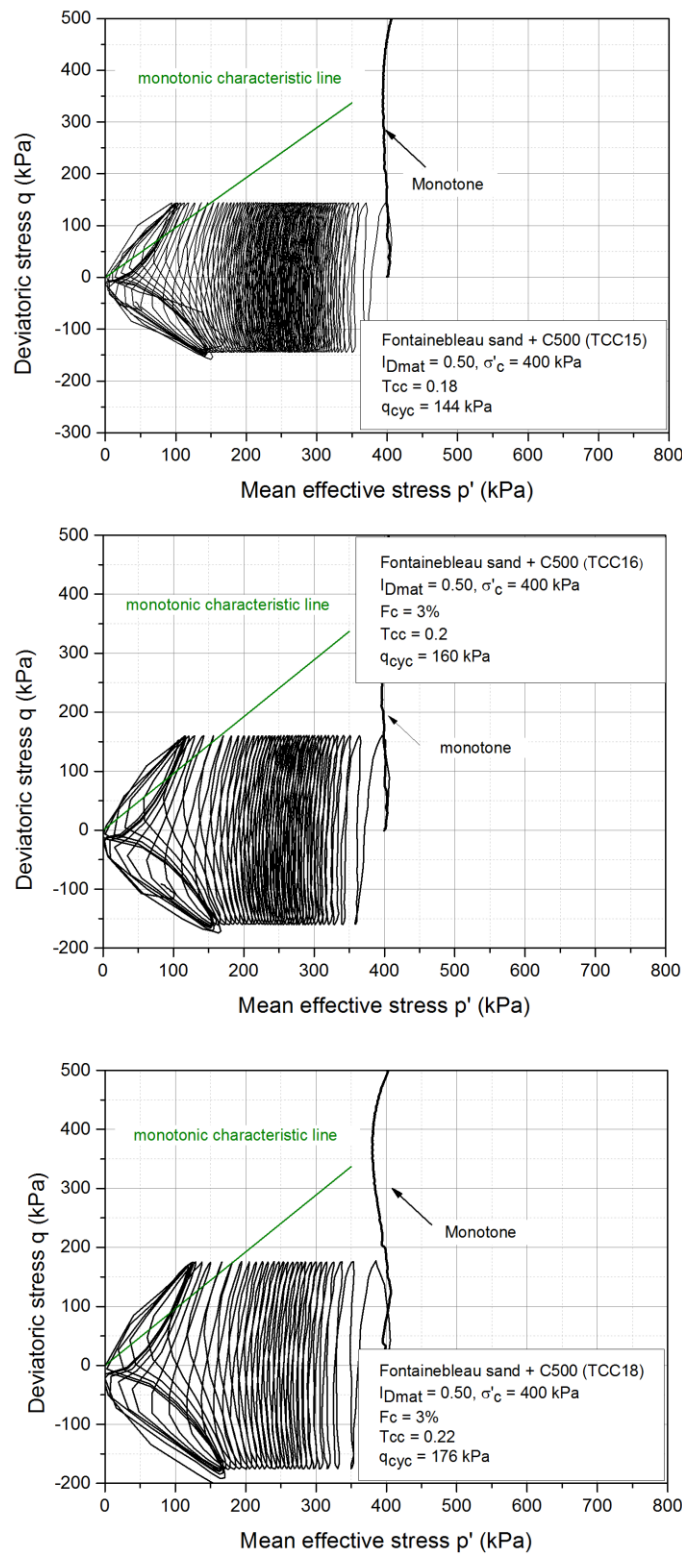
A comparison between the observed behaviors under monotonic and cyclic loading for dilatant states of mixtures is presented in this part in terms of overall behavior described in the  $(q, \epsilon_a)$ ,  $(\Delta u, \epsilon_a)$  and  $(p', q)$  planes and then in terms of the initiation of the cyclic mobility phenomenon.

Figure 4.28 presents a comparison between monotonic and cyclic behaviors observed for identical samples having the same initial conditions ( $I_{Dmat} = 0.50$ ,  $\sigma'_c = 400$  kPa,  $F_c = 3\%$ ) but subjected to different cyclic amplitudes. Unlike the total liquefaction behavior for loose specimens, the cyclic path here doesn't find the monotonic path since the latter is dilatant and therefore it goes up along the rupture line whereas the cyclic path regularly migrates towards the origin due to the progressive accumulation of the excess pore water pressure. However, the monotonic path remains here an envelope that covers the cyclic states that can be reached during a cyclic test.

The examination of the cyclic stress paths clearly shows that the cyclic mobility phenomenon is initiated when the stress paths starts to return, during the loading phases (in compression or extension), in the dilatant domain, that induces later on more contracting discharges that increase the level of the EPWP and deformation (ratchet phenomenon). Luong (1980) and Benahmed (2001) has shown that the transitions between the contracting and dilating behaviors in the cyclic case were governed by the same threshold (characteristic threshold) as that involved in the monotonic behavior. The examination of the effective stress paths in the  $(q, p')$  planes in figure 4.28 where the characteristic threshold corresponding to the monotonic behavior is represented shows that the latter characterizes quite well the place where the dilatant behavior appears on the first cycles having dilatancy loops and leading to the failure by cyclic mobility. For symmetrical alternating loading, the first dilatancy loops appear systematically during the extension phases which is in good agreement with the fact that the characteristic threshold is less inclined towards the horizontal in extension phase rather than compression (non-symmetrical thresholds). The tests carried out on dilatant specimens thus confirm that the characteristic threshold remains valid under cyclic shearing and controls the initiation of the phenomenon of cyclic mobility which appears a few cycles after the first crossing of this threshold.

Concerning the failure envelope, it is also possible to compare both the monotonic rupture envelope and the cyclic one. The trace of the rupture envelope in the cyclic paths for three

specimens of clean sand, sand-C500 and sand-speswhite reveals a quite different rupture line compared to that obtained under monotonic shearing (figure 4.29). It is interesting to note that the friction angle that corresponds to the cyclic rupture presents higher values near the origin than the angle obtained under monotonic loading. This result could be explained due to the fact that the curvature of the failure envelope in the field of low stresses corresponds to higher failure angles which are found here in the cyclic paths. Similar results have been also reported by Benahmed (2001) for the case of clean sand.



**Figure 4.28: Comparison between monotonic and cyclic shearing for dense specimens in terms of the characteristic state**

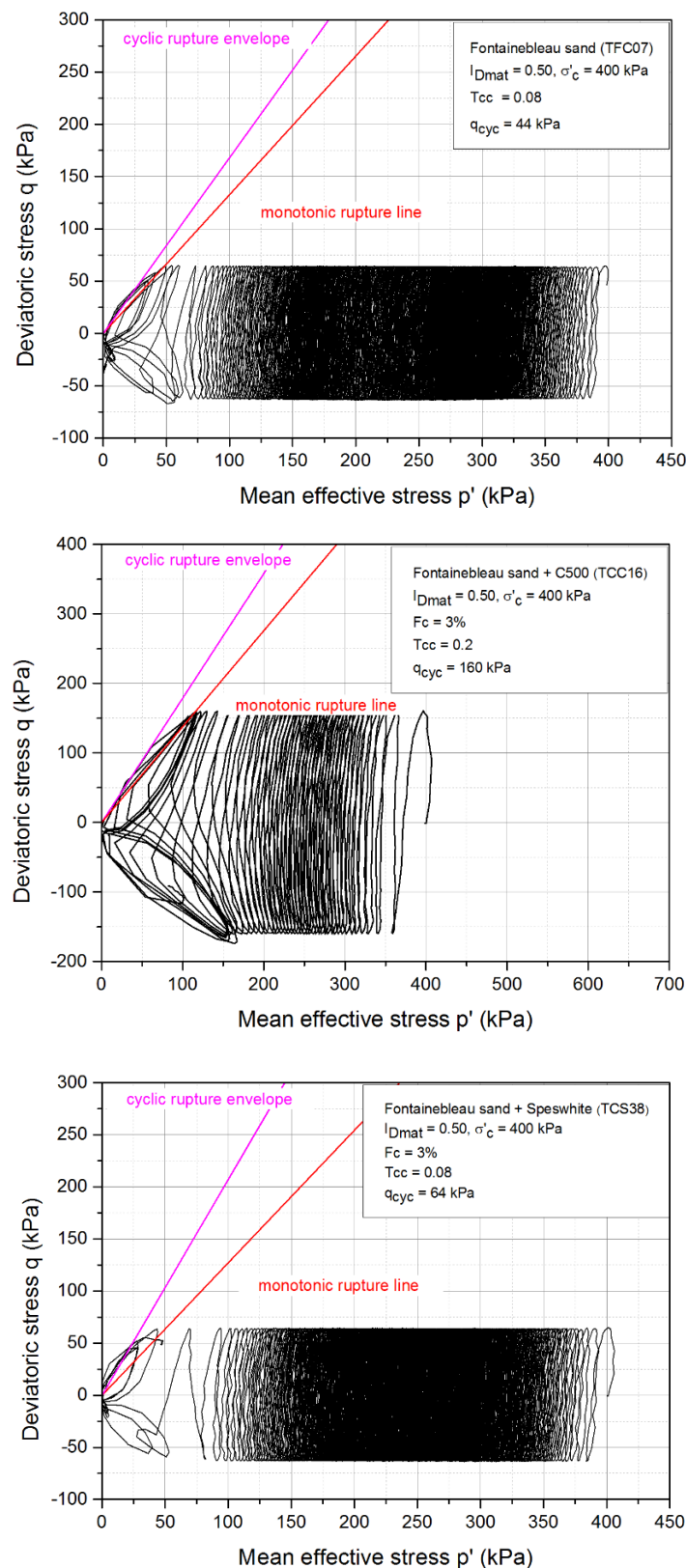


**Figure 4.29: Comparison between monotonic and cyclic shearing for dense specimens in terms of the rupture**

## General conclusions and perspectives

At the end of this work, various conclusions and remarks can be formulated, as well as different lines of research that it would be interesting to deepen or develop and which thus appear as perspectives of extension of this work. Regarding the conclusions:

In general, the experimental approach required to study the mechanical behavior of sands is very difficult to conduct properly and requires a lot of learning, especially for loose structures that have been discussed in this work. The observed behaviors are indeed very sensitive to parameters that are difficult to control with good precision, such as, for example, the initial density index of the material. This study has allowed to develop a testing protocol based on the use of a new servohydraulic triaxial setup ( $\Phi$  100mm) allowing to shear specimens under both monotonic and cyclic loading. We have, in particular, validated this new apparatus.

In terms of initiation of liquefaction instability under undrained monotonic loading, this work has made it possible to clarify the notion of the threshold of instability for sands containing fines and to propose a model of evolution of this threshold of instability (instability line) as a function of the fines content. Also, this study has shown and highlighted the influence of low fines content ( $\leq 5\%$ ) on the mechanical response of sand. In fact, we have also shown the influence of the nature of fines (plastic/non-plastic) where we noted two totally different behaviors in terms of the shear resistance. The increase in non-plastic fines increases the resistance of sand whereas this trend is reversed for the plastic fines.

The evaluation of other parameters such as intergranular void ratio, and equivalent intergranular void ratio has shown relatively constant values with the increase in fine particles. This is explained due to the low percentages of fines and ensure the reliability of the chosen parameter, which is the density index of the sand matrix, for evaluating the liquefaction.

The undrained cyclic tests allowed to plot the cyclic shear resistance curves where we have reported consistent results with monotonic testing translated by an increase of these curves with the non-plastic fines and a decrease in the case of plastic fines. Also, we have presented a model that correlates the CSR curve with the fines content and allows us to predict this curve. Regarding the comparison between the two types of behaviors, we will simply recall the very strong analogies between monotonic behavior and cyclic behavior, and the role of "envelope" played by the monotonic response to the cyclic response. Concerning the initiation of the

## General conclusions and perspectives

---

instability, we noted very consistent results in terms of evaluating the instability lines that were almost identical for the two testing.

In terms of research perspectives, it might be interesting to develop and extend this work. We can mention the following points.

Due to the importance of the structural effects on the observed behaviors, it will undoubtedly be important to pursue research in the field of observation (SEM) in order to identify and clarify the distribution of the fine particles and their localization between the sand grains.

This study has been done on a reference sand (Fontainebleau) and two types of fines for  $F_c \leq 5\%$ . It could also be interesting to test other types of sands such as Hostun sand as well as other types of fines (silt, clay...) and to increase the fines content until 10%.

The specimens tested in this study were all consolidated at an isotropic consolidation stress, it is also interesting to make some cyclic tests at an anisotropic consolidation.

The specimens that were used as part of this work remain reconstituted material of "academic" sands and fines and it is clear that the actual soils encountered in nature are more complex and it will be important to also test natural materials. In fact, it would be interesting to test specimens of real soils in order to validate the proposed model for the prediction of the CSR curves.

## References

- Abedi, M., & Yasrobi, S. S. (2010). Effects of plastic fines on the instability of sand. *Soil Dynamics and Earthquake Engineering*, 30(3), 61–67.
- Amini, F., & Qi, G. Z. (2000). Liquefaction Testing of Stratified Silty Sands. *Journal of Geotechnical and Geoenvironmental Engineering*, 126(3), 208–217.
- Andrews, D. C. A., and Martin, G. R. (2000). Criteria for liquefaction of silty soils. *Proc., 12th World Conf. on Earthquake Engineering, Upper Hutt, New Zealand, NZ Soc. for EQ Engrg.*, Paper No. 0312.
- Bardet JP, Kapuskar M. (1993). Liquefaction sand boils in San Francisco during 1989 Loma Prieta Earthquake. *Journal of Geotechnical Engineering*. 119(3):543–62.
- Been, K., & Jefferies, M. G. (1985). A state parameter for sands. *Géotechnique*, 35(2), 99–112.
- Belkhatir, M., Arab, a., Della, N., Missoum, H., & Schanz, T. (2010). Influence of inter-granular void ratio on monotonic and cyclic undrained shear response of sandy soils. *Comptes Rendus Mécanique*, 338(5), 290–303.
- Benahmed, N., Canou, J., & Dupla, J. C. (2004). Structure initiale et propriétés de liquéfaction statique d'un sable. *Comptes Rendus - Mecanique*, 332(11), 887–894.
- Benahmed, N. (2001). Comportement mécanique d'un sable sous cisaillement monotone et cyclique : application aux phénomènes de liquéfaction et de mobilité cyclique. *Thèse de doctorat, Ecole National des Ponts et Chaussées*.
- Benahmed, N., Nguyen, T. K., Hicher, P. Y., Nicolas, M., Benahmed, N., Nguyen, T. K., & Hicher, P. Y. (2016). An experimental investigation into the effects of low plastic fines content on the behaviour of sand / silt mixtures. *European Journal of Environmental and Civil Engineering* 19:1, 109-128.
- Benghalia, Y., Bouafia, A., & Canou, J. & Dupla, J.C. (2011). Comportement mécanique des sols sableux avec un indice des vides intergranulaire constant. *8ème Colloque National AFPS*.
- Bouferra, R., & Shahrour, I. (2004). Influence of fines on the resistance to liquefaction of a clayey sand. *Ground Improvement*, 8(1), 1–5.
- Boulanger, R., & Idriss, I. (2004). Evaluating the potential for liquefaction or cyclic failure of silts and clays.

## References

---

- Bray, J. D., & Sancio, R. B. (2006). Assessment of the Liquefaction Susceptibility of Fine-Grained Soils. *Journal of geotechnical and geoenvironmental engineering*, 132(9):1165–1177.
- Canou, J., (1989). Contribution a l'étude et a l'évaluation des propriétés de liquefaction d'un sable. *Thèse de Doctorat de l'Ecole Nationale des Ponts et Chaussées, Paris, France*. 172p.
- Carraro, J. a. H., Bandini, P., & Salgado, R. (2003). Liquefaction Resistance of Clean and Nonplastic Silty Sands Based on Cone Penetration Resistance. *Journal of Geotechnical and Geoenvironmental Engineering*, 129(11), 965–976.
- CASAGRANDE, A., (1936). Characteristics of cohesionless soils affecting the stability of slopes and earth fills. *Journal of the Boston Society of Civil Engineers*, January. Reprinted in "Contributions to Soil Mechanics 1925-1940". ASCE, Oct. 1940.
- CASAGRANDE, A., (1975). Liquefaction and cyclic deformation of sands a critical review. *Fifth Panamerican Conference on Soil Mechanics and Foundation Engineering, Buenos Aires, Argentina, Harvard Soil Mechanics*, Series N° 88.
- CASTRO, J., (1969). Liquefaction of sands. Ph.D. Thesis, *Harvard Soil Mechanics Series n°81, Harvard University, Cambridge, MA*, 112 p.
- Chang, N. Y., Yeh, S. T., and Kaufman, L. P. (1982). Liquefaction potential of clean and silty sands. Proc., *3rd Int. Earthquake Microzonation Conf.*, Vol. 2, 1017–1032.
- Chen YC and Liao TS. (1999). Studies of the state parameter and liquefaction resistance of sand. In: *Proceedings of the 2nd international conference on earthquake geotechnical engineering, Lisbon Portugal*. p. 513–18.
- Chu, J., Leong, W. K., Loke, W. L., & Wanatowski, D. (2012). Instability of Loose Sand under Drained Conditions. *Journal of Geotechnical and Geoenvironmental Engineering*, 138(2), 207–216.
- Chu, J., Lo, S. -C. R., & Lee, I. K. (1993). Instability of Granular Soils under Strain Path Testing. *Journal of Geotechnical Engineering*, 119(5), 874–892.
- Daouadji, A., AlGali, H., Darve, F., & Zeghloul, A. (2010). Instability in granular materials: Experimental evidence of diffuse mode of failure for loose sands. *Journal of Engineering Mechanics*, 136(5), 575–588.
- Darve, F., & Laouafa, F. (2000). Instabilities in granular materials and application to landslides. *Mechanics of Cohesive-Frictional Materials*, 627–652.
- Darve, F., Servant, G., Khoa, H. D. V., & Laouafa, F. (2004). Failure in geomaterials: Continuous and discrete analyses. *Computer Methods in Applied Mechanics and Engineering*, 193(27-29).

## References

---

- Darve, F., Sibille, L., Daoudji, A. and Nicot, F. (2007). Bifurcations in granular media: macro- and micro-mechanics approaches. *Comptes Rendu Mécanique*, 335(9-10):496-515.
- Dash, H. K., & Sitharam, T. G. (2011). Undrained monotonic response of sand-silt mixtures: Effect of nonplastic fines. *Geomechanics and Geoengineering*, 6(1), 47–58.
- Derakhshandi, M., Rathje, E. M., Hazirbaba, K., & Mirhosseini, S. M. (2008). The effect of plastic fines on the pore pressure generation characteristics of saturated sands. *Soil Dynamics and Earthquake Engineering*, 28(5), 376–386.
- Desrues J, Viggiani G (2004). Strain localization in sand: an overview of the experimental results obtained in grenoble using stereophotogrammetry. *International Journal for Numerical and Analytical Methods in Geomechanics* ; 28:279–321.
- Dezfulian, H. (1984). “Effects of silt content on dynamic properties of sandy soils.” *Proc., 8th World Conf. on Earthquake Engineering*, Prentice-Hall, Englewood Cliffs, N.J., 63–70.
- Erten, D., & Maher, M. H. (1995). Cyclic undrained behavior of silty sand. *Soil Dynamics and Earthquake Engineering*, 14(2), 115–123.
- Fretti, C., Lo Presti, C.F., Pedroni, S., (1995). A pluvial deposition method to reconstitute well-graded sand specimens. *Geotechnical testing journal*.18 (2), 292–298.
- Frost, J.D., Park, J.-Y., 2003. A critical assessment of the moist tamping technique. *Geotechnical testing journal*. 26 (1), 57–70.
- Gajo, a, Piffer, L., & De Polo, F. (2000). Analysis of certain factors affecting the unstable behaviour of saturated loose sand. *Mechanics of CohesiveFrictional Materials*, 5(October 1998), 215–237.
- Ghahremani, M., & Ghalandarzadeh, A. (2006). Effect of Plastic Fines on Cyclic Resistance of Sands. In *Soil and Rock Behavior and Modeling* (pp. 406–412).
- Ghahremani, M., Ghalandarzadeh, A., & Moradi, M. (2006). Effect of Plastic Fines on the Undrained Behavior of Sands. In *Soil and Rock Behavior and Modeling* (pp. 48–54).
- Habib, P., & Luong, M.P., (1978). Sols pulvérulents sous chargements cycliques. *Séminaire Materiaux et Structures sous Chargement Cyclique*, Ecole Polytechnique, Sept. 28- 29, pp. 49-79.
- Hazirbaba, K., 2005. Pore pressure generation characteristics of sands and silty sands: a strain approach. Dissertation presented for PhD program to the faculty of Graduate School at the University of Texas at Austin.
- Hill, R. (1958). A general theory of uniqueness and stability in elastic-plastic solids. *Journal of the Mechanics and Physics of Solids*, 6(3), 236–249.

## References

---

- Høeg, K., Dyvik, R., & Sandbækken, G. (2000). Strength of Undisturbed versus Reconstituted Silt and Silty Sand Specimens. *Journal of Geotechnical and Geoenvironmental Engineering*, 126(7), 606–617.
- Huang, A. B., & Huang, Y. T. (2007). Undisturbed sampling and laboratory shearing tests on a sand with various fines contents. *Soils and Foundations*, 47(4), 771–781.
- Huang, A.-B., Chang, W.-J., Hsu, H.-H., & Huang, Y.-J. (2015). A mist pluviation method for reconstituting silty sand specimens. *Engineering Geology*, 188, 1–9.
- Huang, Y. T., Huang, A. Bin, Kuo, Y. C., & Tsai, M. D. (2004). A laboratory study on the undrained strength of a silty sand from Central Western Taiwan. *Soil Dynamics and Earthquake Engineering*, 24(9-10), 733–743.
- Ishihara, K. (1993). Liquefaction and flow failure during earthquakes. *Géotechnique*, 43(3), 351–451.
- Ishihara, K., & Yasuda, S., (1975). Sand liquefaction in hollow cylinder torsion under irregular excitation. *Soils and Foundations*. 15(1): 45- 59.
- Juneja, a, & Raghunandan, M. (2010). Effect of Sample Preparation on Strength of Sands. *Indian Geotechnical Conference GEO Trendz, IGS Mumbai*. 16–18.
- Karim, M. E., & Alam, M. J. (2014). Effect of non-plastic silt content on the liquefaction behavior of sand-silt mixture. *Soil Dynamics and Earthquake Engineering*, 65, 142–150.
- Khoa, H. D. V, Georgopoulos, I. O., Darve, F., & Laouafa, F. (2006). Diffuse failure in geomaterials : Experiments and modelling. *Geotechnical*.33, 1–14.
- Kien, N. T. (2014). Etude Expérimentale du comportement instable d'un sable silteux: Application aux digues de protection. *Thèse de Doctorat*.
- Koester, J. P. (1994). The influence of fine type and content on cyclic resistance. Ground failures under seismic conditions, *Geotechnical*. 44, 17–33.
- Koester, J. P. (1992). “The influence of test procedure on correlation of Atterberg limits with liquefaction in fine-grained soils.” *Geotechnical testing journal*.15 (4), 352–361.
- Kuerbis, R., & Vaid, Y. P. (1988). Sand Sample Preparation-the Slurry Deposition Method. *Soils and Foundations*, 28(4), 107–118.
- Ladd, R., (1977). Specimen preparation and cyclic stability of sands. *Journal of the Geotechnical Engineering Division*. 103 (GT6): 535-547.
- Lade, P. V. (1989). Experimental observations of stability, instability, and shear planes in granular materials. *Ingenieur-Archiv*, 59(2), 114–123.

## References

---

- Lade, P. V. (1993). Initiation of static instability in the submarine Nerlerk berm. *Canadian Geotechnical Journal*, 30(6), 895–904.
- Lade, P. V. (1992). Static Instability and Liquefaction of Loose Fine Sandy Slopes. *Journal of Geotechnical Engineering*, 118(1), 51–71.
- Lade, P. V., Nelson, R. B., & Ito, Y. M. (1988). Instability of Granular Materials with Nonassociated Flow. *Journal of Engineering Mechanics*, 114(12), 2173–2191.
- Lade, P. V., Liggio, C. D., Jr., and Yamamuro, J. A. (1998). “Effects of Non-Plastic Fines on Minimum and Maximum Void Ratios of Sand,” *Geotechnical Testing Journal*. 21 (4): 336–347.
- Lambe, T.W., 1951. Soil Testing for Engineers. John Willy & Sons, Inc., New York.
- Lo Presti, D., Pedroni, S., Crippa, V., 1992. Maximum dry density of cohesionless soils by pluviation and by ASTM D 4253-83: a comparative study. *Geotechnical testing journal*. ASTM 15 (2), 180–189.
- Leong, W., Chu, J., and Teh, C.I, (2000)."Liquefaction and Instability of a Granular Fill Material," *Geotechnical Testing Journal*, 23(2): 178-192.
- Luong, P.M., (1980). Phénomènes cycliques dans les sols pulvérulents. *Revue Française de Géotechnique*. 10, 39-53.
- Lyapunov (1907). Problème général de la stabilité des mouvements. *Annales de la Faculté des Sciences de Toulouse*, 9:203-274.
- Maheshwari, B. K., & Patel, A. K. (2010). Effects of non-plastic silts on liquefaction potential of Solani sand. *Geotechnical and Geological Engineering*, 28(5), 559–566.
- Miura, S., & Toki, S. (1982). A Sample Preparation Method and Its Effect on Static and Cyclic Deformation-Strength Properties of Sand. *Soils and Foundations*, 22(1), 61–77.
- Mohammadi, A., & Qadimi, A. (2015). Characterizing the process of liquefaction initiation in Anzali shore sand through critical state soil mechanics. *Soil Dynamics and Earthquake Engineering*, 77, 152–163.
- Monkul, M. M., Gültekin, C., Gülder, M., Akin, Ö., & Eseller-Bayat, E. (2015). Estimation of liquefaction potential from dry and saturated sandy soils under drained constant volume cyclic simple shear loading. *Soil Dynamics and Earthquake Engineering*, 75, 27–36.
- Muhammed, R. (2015). Étude en chambre d'étalementage du frottement sol-pieu sous grands nombres de cycles. Application au calcul des fondations profondes dans les sols fins saturés *Thèse de Doctorat*. Université Pierre et Marie Curie.
- Mulilis, J., Chan, C.K., & Seed, B., (1975). The effects of method of sample preparation on the cyclic stress – strain behavior of sands. Report No. EERC 75-18, *Earthquake Engineering Research Center, University of California, Berkley, California*

## References

---

- Murthy TG, Loukidis D, Carraro JAH, Prezzi M, Salgado R. Undrained mono- tonic response of clean and silty sands (2007). *Geotechnique*, 57(3):273–88.
- Naeini, S. a., & Baziar, M. H. (2004). Effect of fines content on steady-state strength of mixed and layered samples of a sand. *Soil Dynamics and Earthquake Engineering*, 24(3), 181–187.
- Ni, Q., Tan, T. S., Dasari, G. R., & Hight, D. W. (2004). Contribution of fines to the compressive strength of mixed soils. *Géotechnique*, 54(9), 561–569.
- Nicot, F., Darve, F., & Dat Vu Khoa, H. (2007). Bifurcation and second-order work in geomaterials. *International Journal for Numerical and Analytical Methods in Geomechanics*, 31(8), 1007–1032.
- Nicot, F., and Wan, R. (2010). Micromechanics of failure in granular geo- materials, Wiley.
- Oda, M., Koishikawa, I., Higuchi, T., (1978). Experimental study of anisotropic shear strength of sand by plane strain test. *Soils and foundations*. 18 (1), 25–38.
- Okashi, Y. (1970) “Effects Of Sand Compaction On Liquefaction During Tokachioki Earthquake” *Soils and Foundations*. 10 (2): 112-128.
- Papadopoulou A, Tika T. The effect of fines on critical state and liquefaction resistance characteristics of non-plastic silty sands (2008). *Soils and foundations*. 48(5):713–25.
- Pitman, T. D., Robertson, P. K., & Sego, D. C. (1994). Influence of fines on the collapse of loose sands. *Canadian Geotechnical Journal*, 31(5), 728–739.
- Polito, C. (1999). The effects of non-plastic and plastic fines on the liquefaction of sandy soils. *PhD Thesis, Virginia Polytechnic Institute*, (December), 274.
- Polito, C. P., & Martin, J. R. (2003). A Reconciliation of the Effects of Non-Plastic Fines on the Liquefaction Resistance of Sands Reported in the Literature. *Earthquake Spectra*, 19(3), 635–651.
- Polito, C. P., & Martin II, J. R. (2001). Effects of Nonplastic Fines on the Liquefaction Resistance of Sands. *Journal of Geotechnical and Geoenvironmental Engineering*, 127(5), 408–415.
- Qadimi, A., & Mohammadi, A. (2014). Evaluation of state indices in predicting the cyclic and monotonic strength of sands with different fi nes contents. *Soil Dynamics and Earthquake Engineering*, 66, 443–458.
- Rahman, M. M., Lo, S. R., & Gnanendran, C. T. (2008). On equivalent granular void ratio and steady state behaviour of loose sand with fines. *Canadian Geotechnical Journal*, 45(10), 1439–1456.

## References

---

- Rahman, M., Baki, M., & Lo, S. (2014). Prediction of Undrained Monotonic and Cyclic Liquefaction Behaviour of Sand with Fines Based on Equivalent Granular State Parameter. *International Journal of Geomechanics*, 14(2), 254–266.
- Rahman, M. M., Lo, S.-C. R., & Cubrinovski, M. (2010). Equivalent Granular Void Ratio and Behaviour of Loose Sand. *Fifth International Conference on Recent Advances in Geotechnical Earthquake Engineering and Soil Dynamics*, (4), 1–9.
- Rahardjo, P.P., 1989. Evaluation of Liquefaction Potential of Silty Sand Based on Cone Penetration Test. (Ph.D. thesis). Virginia Polytechnic Institute and State University, USA.
- Rice, J. R. (1976). The localization of plastic deformation. In KOITER, W., éditeur : *14<sup>th</sup> International Congress on Theoretical and Applied Mechanics*, pages 207-220, Delft. North-Holland Publishing Co.
- Roscoe, K. H., Schofield, A. N., & Wroth, C. P. (1958). On The Yielding of Soils. *Géotechnique*, 8(1), 22–53.
- Rudnicki, J. W., & Rice, J. R. (1975). Conditions for the localization of deformation in pressure-sensitive dilatant materials. *Journal of the Mechanics and Physics of Solids*, 23(6), 371–394.
- Sadrekarimi, A. (2013). Influence of fines content on liquefied strength of silty sands. *Soil Dynamics and Earthquake Engineering*, 55, 108–119;
- Sawicki, A., & Świdziński, W. (2010). Modelling the pre-failure instabilities of sand. *Computers and Geotechnics*, 37(6), 781–788.
- Seed, H. B., and Idriss, I. M. (1982). “Ground motions and soil liquefaction during earthquakes.” Earthquake Engineering Research Institute, Berkeley, California.
- Seif El Dine, B., Dupla, J. C., Frank, R., Canou, J., & Kazan, Y. (2010). Mechanical characterization of matrix coarse-grained soils with a large-sized triaxial device. *Canadian Geotechnical Journal*, 47(4), 425–438.
- Sladen, J.A., D'hollander, R.D. & Krahn, J., (1985). The liquefaction of sands, a collapse surface approach. *Canadian Geotechnical Journal*. 22, 564-578.
- Stamatopoulos, C. a. (2010). An experimental study of the liquefaction strength of silty sands in terms of the state parameter. *Soil Dynamics and Earthquake Engineering*, 30(8), 662–678.
- Stamatopoulos C, Stamatopoulos A, Balla L. (2004). Cyclic strength of sands in terms of the state parameter. In: *The 11th international conference on soil dynamics and earthquake engineering (11th ICSD) and the third international conference on geotechnical earthquake engineering*, January 7–9.

## References

---

- Tatsouka, F., Ochi, K., Fuji, S., & OKAMOTO, M. (1986). Cyclic undrained triaxial and torsional shear strength of sands for different sample preparation methods. *Soils and Foundations*, 26(3), 23–41.
- Thevanayagam, S., (1998). Effect of fines and confining stress on undrained shear strength of silty sands. *Journal of Geotechnical and Geoenvironmental Engineering*, .124 (6): 479-491.
- Thevanayagam, S., Shethan, T., Mohan, S., & Liang, J. (2002). Undrained Fragility of Clean Sands, Silty Sands, and Sandy Silts. *Journal of Geotechnical and Geoenvironmental Engineering*, 128(10), 849–859.
- Thevanayagam, S., & Martin, G. R. (2002). Liquefaction in silty soils — screening and remediation issues. *Soil Dynamics and Earthquake Engineering*, 22(9), 1035–1042.
- Thevanayagam, S. (2000). Liquefaction potential and undrained fragility of silty soils. *Proceedings of the 12th World Conference on Earthquake Engineering*, 1–8. .
- Tokimatsu, K., & Yoshimi, Y. (1983). Empirical correlation of soil liquefaction based on SPT N-value and fines content. *Japanese Society of Soil Mechanics and Foundation Engineering*, 23(4).
- Ueng, T. S., Sun, C. W., & Chen, C. W. (2004). Definition of fines and liquefaction resistance of Maoluo River soil. *Soil Dynamics and Earthquake Engineering*, 24(9-10), 745–750.
- Vaid VP (1994) Liquefaction of silty soils. Ground failures under seismic conditions, *Geotechnical*. 44, 1–16
- Vaid, Y.P., & Chern, J.C., (1985). Cyclic and monotonic undrained response of saturated sands. *Advances in the Art of Testing Soils Under Cyclic Conditions ASCE, Convention, Detroit, Michigan*, pp. 120-147.
- Vaid, Y.P., Sivathayalan, S. and Stedman, D. (1999). Influence of Specimen-Reconstituting Method on the Undrained Response of Sand, *Geotechnical Testing Journal, ASTM*, 22(3), 187–196.
- Wang, W. (1979). Some findings in soil liquefaction, Water Conservancy and Hydroelectric Power Scientific Research Institute, Beijing, China.
- Wang, K.-L., & Lin, M.-L. (2011). Initiation and displacement of landslide induced by earthquake — a study of shaking table model slope test. *Engineering Geology*, 122(1-2), 106–114.
- Westman, A. E. ., & Hugill, H. (1930). The packing of particles. *Journal of American Ceramic Society*, 13(10): 767–779.
- Xenaki, V. C., & Athanasopoulos, G. a. (2003). Liquefaction resistance of sand-silt mixtures: An experimental investigation of the effect of fines. *Soil Dynamics and Earthquake Engineering*, 23(3), 183–194.

## References

---

- Yamamoto, J. a., & Wood, F. M. (2004). Effect of depositional method on the undrained behavior and microstructure of sand with silt. *Soil Dynamics and Earthquake Engineering*, 24(9-10), 751–760.
- Yamamoto, J. A., & Lade, P. V. (1997). Static liquefaction of very loose sands. *Canadian Geotechnical Journal*. 34, 905-917.
- Yang, S. L., Sandven, R., & Grande, L. (2006a). Steady-state lines of sand–silt mixtures. *Canadian Geotechnical Journal*, 43(11), 1213–1219.
- Yang, S. L., Sandven, R., & Grande, L. (2006b). Instability of sand–silt mixtures. *Soil Dynamics and Earthquake Engineering*, 26(2-4), 183–190.
- Yoshimi, Y., Tokimatsu, K., Kaneko, O., & Makihara, Y. (1984). Undrained cyclic shear strength of a dense Niigata sand. *Soils and Foundations*, 24(4), 131–145.
- Yin, Z., Zhao, J., & Hicher, P. (2014). A micromechanics-based model for sand-silt mixtures. *International Journal of Solids and Structures*, 51, 1350–1363.

## List of figures

Figure 1.1 - Examples of liquefaction phenomena during earthquakes .....	5
Figure 1.2 - Characteristic state (Luong 1985) (a): monotonic behavior; (b) cyclic behavior ...	7
Figure 1.3 - Concept of critical void ratio (Casagrande, 1975).....	9
Figure 1.4 - Diffuse rupture of San Fernando dam, United States 1971 .....	11
Figure 1.5 - Three types of responses in an undrained triaxial test according to Castro (1969)	
.....	13
Figure 1.6 - Data presented by Wang (1979) which led to the development of the Chinese criteria.....	14
Figure 1.7 - Instability zone defined by Vaid et Chern (1985) .....	15
Figure 1.8 - Collapse line and surface according to Sladen (1985).....	16
Figure 1.9 - Instability line and potential instability zone (Lade 1993) .....	17
Figure 1.10 - Pluviator presented by Benahmed (2001) .....	19
Figure 1.11- Schematic layout of the mist pluviation method (Huang <i>et al.</i> 2015).....	21
Figure 1.12 - Configuration of mist pluviation unit and details of pluviator (Huang <i>et al.</i> 2015)	
.....	21
Figure 1.13 - Homogeneity of sample prepared by MP method (Huang 2015).....	22
Figure 1.14 - Repeatability in cyclic undrained triaxial test (Huang 2015) .....	23
Figure 1.15 - Influence of the specimen reconstitution procedure on the observed behavior, for a loose state of the sand: (a) shear curves; (b): effective stress paths (Benahmed <i>et al.</i> 2004)	24
Figure 1.16 - Undrained triaxial test results for medium and low densities showing the effect of reconstitution methods on the specimen behavior (Yamamoto et Wood 2004) .....	25

## List of figures

---

Figure 1.17 - Microphotographies of Hostun sand RF showing two differentiated structures :(a) aggregates and macropores (wet tamping); (b) regular stack (dry pluviation) (Benahmed <i>et al.</i> 2004) .....	26
Figure 1.18 - Comparison of grain contact structure between specimens formed by dry funnel deposition and water sedimentation containing 20% silt (Yamamoto and Wood 2004) .....	26
Figure 1.19 - Schematic Phase Diagrams: (a) silty Sand; (b) silt Matrix ;( c) sand Matrix (Thevanayagam 1998).....	28
Figure 1.20 - Schematic diagram demonstrating particle arrangement of sand-silt mixture with the variation of silt content. (Karim 2014) .....	29
Figure 1.21 - Variation of maximum and minimum void ratios of the sand-silt mixtures. (Belkhatir 2010) .....	30
Figure 1.22 - Different granular structures of sand – fines mixture (Thevayanagam and Martin 2002).....	32
Figure 1.23 - Results from previous studies on the effect of fines content (fc) on cyclic resistance: (a) studies at constant overall void ratio; (b) studies at constant sand skeleton void ratio; and (c) studies at constant relative density (Karim 2014) .....	34
Figure 1.24 - Influence of the fines content on the cyclic liquefaction resistance .....	36
Figure 1.25 - Influence of fines content on the static liquefaction resistance .....	37
Figure 1.26 - Variation in cyclic resistance with relative density (Polito and Martin 2003) ...	38
Figure 1.27 - Variation in cyclic resistance with silt content for Yatesville sand specimens adjusted to 25% soil specific relative density (Polito, 1999) .....	39
Figure 1.28: Variation of cyclic resistance as a function of intergranular void ratio .....	40
Figure 1.29 - Effect of fines content on mechanical behavior of sand at constant intergranular void ratio Benahmed (2015).....	41

## List of figures

---

Figure 1.30 - Influence of fines content on the cyclic shear resistance: (a) $I_D= 0.5$ ; (b) $I_D= 0.15$ (Benghalia 2011) .....	41
Figure 1.31 - Influence of density index on the cyclic shear resistance of sand: (a) $ID= 0.5$ ; (b) $ID= 0.15$ (Benghalia 2011) .....	42
Figure 1.32 - Analysis of the behavior of silty sands in terms of equivalent granular void ratio .....	43
Figure 1.33 - Definition of state parameter $\psi$ (Been and Jefferies 1985) .....	44
Figure 1.34 - Cyclic strength as a function of state parameter (Stamatopoulos 2010) .....	45
Figure 1.35 - Cyclic strength of sand with silt for $f_c < f_{c\text{th}}$ in terms of $\psi$ and $\psi g^*$ (Qadimi 2014) .....	46
Figure 1.36 - Comparison between dry and saturated sands behavior (Monkul 2015) .....	47
Figure 1.37 - Influence of fines content on the friction angle (Huang <i>et al.</i> 2004) .....	49
Figure 1.38 - Influence of fines content on friction angle : (a) 0%, (b) 5%, (c) 10%, (d) 15% (Murthy <i>et. al</i> 2007) .....	50
Figure 1.39 - Influence of fines content on the CSL .....	51
Figure 1.40 - Influence of fines content on resistance to liquefaction of sand–clay mixture (Bouferra and Shahrour 2004) .....	52
Figure 1.41 - Influence of plastic fines content on the generation of excess pore water pressure (Derakhshandi 2008) .....	52
Figure 1.42 - Variation of peak strength as a function of fines content (Abedi and Yasrobi 2010) .....	53
Figure 2.1 - Gradation curve of Fontainebleau sand (Benahmed 2001) .....	55
Figure 2.2 - Gradation curve of Silica flour C500 .....	56
Figure 2.3 - Gradation curve of kaolinite Speswhite (Muhammed, 2015) .....	57
Figure 2.4 - Schematic diagram of the triaxial testing device .....	59

## List of figures

---

Figure 2.5 - Different parts of the triaxial device: (a) triaxial cell and slab; (b) cylindrical metal; (c) confinement enclosure; (d) piston .....	60
Figure 2.6 - Typical monotonic test of clean Fontainebleau sand: (a) ( $q-\varepsilon_a$ ) curve; (b) ( $\Delta u-\varepsilon_a$ ) curve; .....	63
Figure 2.7 - Total collapse of a loose specimen of Fontainebleau sand .....	64
Figure 2.8 - Piston position during a monotonic test .....	66
Figure 2.9 - Results of calibration of the cell .....	67
Figure 2.10 - Schematic diagram of the piston effect .....	67
Figure 2.11- Results of repeated monotonic test with the adopted method: (a) ( $q-\varepsilon_a$ ) curve; (b) ( $\Delta u-\varepsilon_a$ ) curve; (c) ( $q-p'$ ) curve .....	68
Figure 2.12 - View of the laser diffraction analyzer apparatus .....	70
Figure 2.13 - Gradation curve of mixture of Fontainebleau sand and C500 for $F_c = 1\%$ .....	72
Figure 2.14 - Gradation curve of mixture of Fontainebleau sand and C500 for $F_c = 3\%$ .....	73
Figure 2.15 - Gradation curve of mixture of Fontainebleau sand and C500 for $F_c = 5\%$ .....	74
Figure 2.16 - Gradation curve of mixture of Fontainebleau sand and Speswhite for $F_c = 1\%$ .....	75
Figure 2.17 - Gradation curve of mixture of Fontainebleau sand and Speswhite for $F_c = 3\%$ .....	76
Figure 2.18 - Gradation curve of mixture of Fontainebleau sand and Speswhite for $F_c = 5\%$ .....	77
Figure 2.19 - Gradation curves of sand-fines mixture .....	79
Figure 2.20 - Preparation of the sample- placing (a) the porous stone, (b) the membrane, (c) the mold .....	81
Figure 2.21 - Mixture preparation, (a) sand, (b) addition of water, (c) addition of fines, (d) mixing .....	83
Figure 2.22 - Preparation of the specimen by layers, (a) division into 10 layers, (b) compaction .....	83

## List of figures

---

Figure 2.23 - Sample preparation, (a) placing the second porous stone, (b) the upper base, (c) demolding the sample .....	84
Figure 2.24 - Assemblage of the triaxial cell .....	85
Figure 2.25 - Piston position during a monotonic test .....	86
Figure 2.26 - Particular steps for a cyclic test, (a) setting the force to zero, (b) piston-sample contact, (c) unblocking the piston .....	87
Figure 3.1 - Undrained behavior of clean Fontainebleau sand.....	93
Figure 3.2 - Undrained behavior of Fontainebleau sand-C500 mixture (loose state) .....	94
Figure 3.3 - Undrained behavior of Fontainebleau sand-speswhite mixture (loose state) .....	96
Figure 3.4 - Repeatability test of Fontainebleau sand-C500 mixtures (loose state).....	97
<b>Figure 3.5 - Influence of density index on the behavior of Fontainebleau sand-C500 mixtures.....</b>	<b>99</b>
Figure 3.6 - Influence of density index on the behavior of Fontainebleau sand-Speswhite mixtures .....	101
Figure 3.7 - Influence of the density index on the evolution of the peak shear resistance of Fontainebleau sand-C500 mixtures (a) $F_c = 1\%$ ; (b) $F_c = 3\%$ ; (c) $F_c = 5\%$ .....	102
Figure 3.8 - Influence of the density index on the evolution of the peak shear resistance of Fontainebleau sand-speswhite mixtures (a) $F_c = 1\%$ ; (b) $F_c = 3\%$ ; (c) $F_c = 5\%$ .....	103
Figure 3.9 - Influence of the consolidation stress on the undrained behavior of loose and medium dense Fontainebleau sand-C500 mixtures: (a) $(q-\epsilon_a)$ curve; (b) $(\Delta u- \epsilon_a)$ curve; (c) $(q-p')$ curve .....	106
Figure 3.10 - Influence of the consolidation stress on the undrained behavior of loose and medium dense Fontainebleau sand-Speswhite mixtures: (a) $(q-\epsilon_a)$ curve; (b) $(\Delta u- \epsilon_a)$ curve; (c) $(q-p')$ curve.....	107

## List of figures

---

Figure 3.11 - Influence of the consolidation stress on the undrained peak resistance of loose Fontainebleau sand-C500 mixtures .....	108
Figure 3.12 - Influence of the consolidation stress on the undrained peak resistance of loose sand-C500 mixtures.....	108
Figure 3.13 - Influence of non-plastic fines (C500) on the mechanical behavior of loose Fontainebleau sand (a) ( $q-\varepsilon_a$ ) curve ; (b) ( $\Delta u-\varepsilon_a$ ) curve ; (c) ( $q-p'$ ) curve .....	113
Figure 3.14 - Influence of plastic fines (Speswhite) on the mechanical behavior of loose Fontainebleau sand .....	114
Figure 3.15 - Influence of non-plastic fines (C500) on the mechanical behavior of medium dense Fontainebleau sand .....	115
Figure 3.16 - Influence of plastic fines (Speswhite) on the mechanical behavior of loose Fontainebleau sand: (a) ( $q-\varepsilon_a$ ) curve; (b) ( $\Delta u-\varepsilon_a$ ) curve; (c) ( $q-p'$ ) curve.....	116
Figure 3.17 - Influence of fines content on peak shear resistance.....	117
Figure 3.18 - Influence of type of fine (plastic/non-plastic) on the mechanical response of Fontainebleau sand .....	119
Figure 3.19 - Evolution of maximum friction angle as a function of fines content .....	121
Figure 3.20 - Linear correlation of the evolution of maximum friction angle with fines content .....	122
Figure 3.21 - Evolution of characteristic friction angle as a function of fines content .....	123
Figure 3.22 - Plot of the instability line in the ( $p',q$ ) plane for Fontainebleau sand-C500 mixtures .....	125
Figure 3.23 - Evolution of the instability line for Fontainebleau sand-C500 mixtures.....	126
Figure 3.24 - Plot of the instability line in the ( $p',q$ ) plane for Fontainebleau sand-Speswhite mixtures .....	126
Figure 3.25 - Evolution of the instability line Fontainebleau sand-Speswhite mixtures.....	127

## List of figures

---

Figure 3.26 - Evolution of instability friction angle with fines content .....	127
<b>Figure 3.27: Conceptual models explaining particle shape effects in mixed soils .....</b>	<b>130</b>
Figure 3.28- Influence of fines content in terms of intergranular void ratio.....	133
Figure 3.29 - Westman and Hugill diagram (1930) .....	135
Figure 3.30 - Estimation of the critical fines content using the Westman diagram .....	136
<b>Figure 4.1- Phenomenon of cyclic liquefaction of Fontainebleau sand (loose specimen)</b>	<b>144</b>
Figure 4.2 - Phenomenon of cyclic mobility of Fontainebleau sand (medium dense specimen) .....	147
Figure 4.3 - Phenomenon of liquefaction for Fontainebleau sand and non-plastic fine mixture (loose specimen) .....	151
Figure 4.4 -Phenomenon of cyclic mobility for Fontainebleau sand and non-plastic fine mixture (medium dense specimen).....	152
Figure 4.5 - Initiation of the cyclic mobility phenomenon for sand and non-plastic fines (medium-dense specimen).....	154
Figure 4.6 - Initiation of total liquefaction phenomenon at a critical cycle (loose specimen)	155
Figure 4.7: Repeatability test of a cyclic total liquefaction phenomenon .....	156
Figure 4.8: Stabilization of the behavior of the specimen at a small loading amplitude .....	158
Figure 4.9: Influence of the density index on the cyclic behavior of Fontainebleau sand- Speswhite mixtures.....	160
Figure 4.10: Influence of loading amplitude on the cyclic shear resistance of loose Fontainebleau sand-C500 mixtures .....	162
Figure 4.11: Influence of loading amplitude on the cyclic shear resistance of dense Fontainebleau sand-C500 mixtures .....	164
Figure 4.12: Influence of fines content on the cyclic shear resistance of loose Fontainebleau sand-C500 mixtures .....	166
	208

## List of figures

---

Figure 4.13: Cyclic shear resistance curve for Fontainebleau sand .....	168
Figure 4.14: Influence of the non-plastic fines content (C500) on the cyclic shear resistance curves (loose state) .....	169
Figure 4.15: Influence of the plastic fines content (Speswhite) on the Evolution of cyclic shear resistance curves (loose state) .....	170
Figure 4.16: Influence of the non-plastic fines (C500) content on the evolution of cyclic shear resistance curves (dense state).....	172
Figure 4.17: Influence of the plastic fines (Speswhite) content on the Evolution of cyclic shear resistance curves (dense state).....	173
Figure 4.18: Comparison of the cyclic shear resistance curves of Fontainebleau sand and plastic fines (Speswhite) with literature results.....	174
Figure 4.19: Influence of fines content on the number of cycles to liquefaction of loose specimens .....	175
Figure 4.20: Influence of fines content on the number of cycles to liquefaction of dense specimens .....	176
Figure 4.21 : Evolution of the parameter « a » with the increase in fines content .....	179
Figure 4.22: Evaluation of the proposed method .....	180
Figure 4.23: Comparison between monotonic and cyclic shearing of loose Fontainebleau sand .....	182
Figure 4.24: Comparison between monotonic and cyclic shearing of loose sand-C500 mixture .....	183
Figure 4.25: Comparison between monotonic and cyclic shearing of loose sand-speswhite mi xtur .....	184
Figure 4.26: Comparison between the monotonic and cyclic instability lines .....	186
Figure 4.27: Evolution of instability friction angle with the increase in fines content .....	187
	209

## List of figures

---

Figure 4.28: Comparison between monotonic and cyclic shearing for dense specimens in terms of the characteristic state ..... 190

Figure 4.29: Comparison between monotonic and cyclic shearing for dense specimens in terms of the rupture ..... 191

## List of tables

Table 2.1 - Characteristics of Fontainebleau sand (Benahmed 2001) .....	54
Table 2.2 - Characteristics of kaolinite Speswhite (Muhammed 2015) .....	57
Table 2.3 - Characteristics of mixtures .....	80
Table 3.1- Testing program for clean Fontainebleau sand .....	91
Table 3.2 - Testing program for sand-fines mixtures .....	91
Table 3.3 - Characteristics of the undrained monotonic tests of Fontainebleau sand and fines .....	128
Table 3.4 : Characteristics of the undrained monotonic tests of Fontainebleau sand and fines .....	138
Table 4.1 - Clean sand cyclic testing program .....	140
Table 4.2 - Sand-fines mixtures cyclic testing program.....	141
Table 4.3 - Values of a and b for sand-C500 mixtures.....	177
Table 4.4 - Values of a and b for Fontainebleau sand-Speswhite mixtures .....	177